

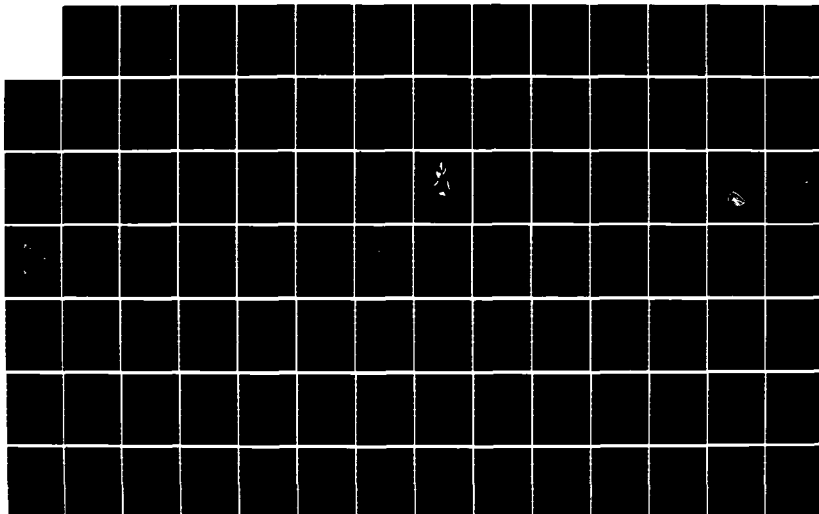
NO-A164 516

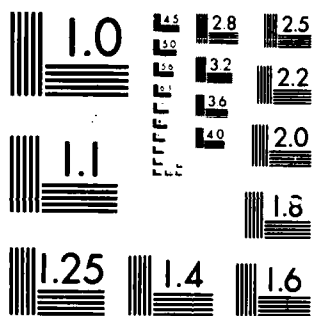
MULTIVARIABLE OUTPUT CONTROL LAW DESIGN FOR THE STOL
(SHORT TAKEOFF AND L..(U) AIR FORCE INST OF TECH
WRIGHT-PATTERSON AFB OH SCHOOL OF ENGI.. B H ACKER
DEC 85 AFIT/GE/ENG/85D-1 F/G 1/2

1/4

UNCLASSIFIED

NL





MICROCOPY RESOLUTION TEST CHART
NATIONAL BUREAU OF STANDARDS 1963-A

AD-A164 516



MULTIVARIABLE OUTPUT CONTROL LAW
DESIGN FOR THE STOL F-15 IN
LANDING CONFIGURATION

THESIS

Bruce H. Acker
Captain, USAF

AFIT/GE/ENG/85D-1

DTIC FILE COPY

DTIC
ELECTE
FEB 13 1986
S D E

DEPARTMENT OF THE AIR FORCE
AIR UNIVERSITY
AIR FORCE INSTITUTE OF TECHNOLOGY

Wright-Patterson Air Force Base, Ohio

This document has been approved
for public release and sale; its
distribution is unlimited.

86 2 12 028

AFIT/GE/ENG/85D-1

MULTIVARIABLE OUTPUT CONTROL LAW
DESIGN FOR THE STOL F-15 IN
LANDING CONFIGURATION

THESIS

Bruce H. Acker
Captain, USAF

AFIT/GE/ENG/85D-1

DTIC
S
D

Approved for public release; distribution unlimited

AFIT/GE/ENG/85D-1

MULTIVARIABLE OUTPUT CONTROL LAW DESIGN FOR THE STOL F-15 IN LANDING CONFIGURATION

THESIS

Presented to the Faculty of the School of Engineering
of the Air Force Institute of Technology

Air University

In Partial Fulfillment of the
Requirements for the Degree of
Master of Science in Guidance and Control

Bruce H. Acker, B.S.

Captain, USAF

December 1985

Accession For	
NTIS GRA&I	<input checked="" type="checkbox"/>
DTIC TAB	<input type="checkbox"/>
Unannounced	<input type="checkbox"/>
Justification	

Approved for public release; distribution unlimited



Preface

This thesis investigates the development of preliminary designs for the longitudinal flight control laws for the STOL/F-15 aircraft in the landing configuration using the multivariable output feedback techniques of Professor Brian Porter from the University of Salford, England.

I wish to thank the sponsor of this effort, Captain Greg Mandt of the Flight Dynamics Laboratory, for his guidance and assistance in obtaining modeling data for the STOL/F-15.

My special thanks are extended to the AFIT faculty members who patiently and expertly guided me through this research effort. The technical knowledge, suggestions, and dedication of my thesis advisor Professor John J. D'Azzo and my two readers, Professors Delmar W. Breuer and Peter S. Maybeck, were instrumental in the success of this thesis.

Finally, I wish to express my respect and appreciation to the four fellow students who also studied the STOL/F-15. The many stimulating and enlightening discussions with Captains Greg Gross and Kevin Sheehan, and Lieutenants Bruce Clough and Bob Houston were enjoyable

and an invaluable addition to the thesis. I especially thank Kevin Sheehan for his motivation, friendship, and leadership in both our academic and recreational pursuits.

— Captain Bruce H. Acker

Table of Contents

	Page
Preface	ii
List of Figures	vii
List of Tables	xvi
List of Symbols	xviii
Abstract	xxiii
I. Introduction	1
1.1 Background	1
1.2 Problem	4
1.3 Scope	4
1.4 Overview	5
II. The STOL F-15 Aircraft	7
2.1 Introduction	7
2.2 General Description	9
2.3 Canards	11
2.4 Two-Dimensional Nozzle and Thrust Reversing Vanes	12
2.5 Summary	17
III. Aircraft Model	18
3.1 Introduction	18
3.2 Fundamental Assumptions	18
3.3 Linearized Longitudinal Equations	19
3.4 Flight Conditions	20
3.5 Representative Plant	23
Introduction	23
Plant Matrix	23
Input Matrix	25
Output Matrix	27
3.6 Actuator Dynamics	27
3.7 Computational Time Delay	28
3.8 Sensor Dynamics and Noise	30
3.9 Control Surface Nonlinearity	31

	Page
IV. Design Procedure	35
4.1 Introduction	35
4.2 Mathematical Considerations	37
Controllability and Observability	37
Porter Design Requirements	38
4.3 Design Process	41
General	41
Design Variables	41
Design for the Basic Plant	42
Actuator Dynamics and	
Computational Time Delay	54
Sensor Dynamics	70
Control Surface Nonlinearity	70
Parameter Variation	70
Sensor Noise	73
Additional Maneuvers	73
4.4 Summary	75
V. Results	76
5.1 Introduction	76
5.2 Format of the Results	76
Commanded Input	76
Plotted Data	78
Tabular Data	78
5.3 Plant Plus Actuators and	
Computational Delay	80
5.4 Plant Plus Actuators Delay	
and Sensors	89
5.5 Plant Actuators, Delay, Sensors,	
and Surface Nonlinearity	98
5.6 Addition of Sensor Noise	107
5.7 Parameter Variation	135
5.8 Special Maneuvers	149
5.9 Summary	154
VI. Conclusions and Recommendations	155
6.1 Design Results	155
6.2 Comments on the Design Method	155
6.3 Improvements to MULTI	156
6.4 Proposed Future Work	158

	Page
Index for Appendix A	160
Appendix A: Additions to Multi	162
Appendix B: Multivariable Control Theory	223
Appendix C: Actuator and Sensor Data	236
Appendix D: Aircraft Data	245
Bibliography	265
Vita	267

List of Figures

Figure	Page
2.1 STOL F-15	8
2.2 STOL F-15 Dimensions	10
2.3 Nozzle Design	13
2.4 Primary Jet Vectoring	14
2.5 Rotating Vane Vectoring	15
3.1 STOL F-15 Sign Conventions	21
3.2 Open Loop State Space Model, Flight Condition 1	24
3.3 Open Loop Block Diagram	29
4.1 Discrete Closed Loop Block Diagram	45
4.2 Step Response $\Gamma(1,1)$, $g = 40, 80, \infty$	59
4.3 Step Response $\Gamma(1,2)$, $g = 40, 80$	49
4.4 Step Response $\Gamma(1,3)$, $g = 40, 80$	50
4.5 Step Response $\Gamma(2,1)$, $g = 40, 80$	50
4.6 Step Response $\Gamma(2,2)$, $g = 40, 80, \infty$	51
4.7 Step Response $\Gamma(2,3)$, $g = 40, 80$	51
4.8 Step Response $\Gamma(3,1)$, $g = 40, 80$	51
4.9 Step Response $\Gamma(3,2)$, $g = 40, 80$	52
4.10 Step Response $\Gamma(3,3)$, $g = 40, 80, \infty$	53
4.11 Outputs, $\sigma_1 = 1$	57
4.12 Surface Deflection, $\sigma_1 = 1$	57
4.13 Outputs, $\sigma_1 = 15$	58

Figure		Page
4.14	Outputs, $\sigma_1 = 15$	58
4.15	Outputs, $\sigma_2 = .1$	60
4.16	Outputs, $\sigma_2 = .25$	61
4.17	Outputs, $\sigma_2 = .40$	61
4.18	Flight Path Angle, $\bar{\alpha} = .01, .10, 1.0$	62
4.19	Outputs, $K_s = 1$	64
4.20	Surface Deflection, $K_s = 1$	64
4.21	Outputs, $K_s = 1.25$	65
4.22	Surface Deflection, $K_s = 1.25$	65
4.23	Outputs, $K_s = 1.5$	66
4.24	Surface Deflection, $K_s = 1.5$	66
4.25	Outputs, $K_q = .1$	67
4.26	Surface Deflection, $K_q = .1$	67
4.27	Outputs, $K_q = .25$	68
4.28	Surface Deflection $K_q = .25$	68
4.29	Outputs, $K_q = .35$	69
4.30	Surface Deflection, $K_q = .35$	69
4.31	Outputs, $\sigma_1 = 15, \sigma_2 = .4, \sigma_3 = .4$	71
4.32	Surface Deflections, $\sigma_1 = 15, \sigma_2 = .4$ $\sigma_3 = .4$	71
4.33	Outputs, $\sigma_1 = 10, \sigma_2 = .55, \sigma_3 = .55$	72
5.34	Surface Deflections, $\sigma_1 = 10, \sigma_2 = .55$ $\sigma_3 = .55$	72
5.1	Landing Flight Path Command Input	77
5.2	Outputs with Actuators and Computational Delay, Flight Condition 1	83

Figure		Page
5.3	Surface Deflections with Actuators and Computational Delay, Flight Condition 1	83
5.4	Outputs with Actuators and Computational Delay, Flight Condition 2	84
5.5	Surface Deflections with Actuators and Computational Delay, Flight Condition 2	84
5.6	Outputs with Actuators and Computational Delay, Flight Condition 3	85
5.7	Surface Deflections with Actuators and Computational Delay, Flight Condition 3	85
5.8	Outputs with Actuators and Computational Delay, Flight Condition 4	86
5.9	Surface Deflections with Actuators and Computational Delay, Flight Condition 4	86
5.10	Outputs with Actuators and Computational Delay, Flight Condition 5	87
5.11	Surface Deflections with Actuators and Computational Delay, Flight Condition 5	87
5.12	Outputs with Actuators and Computational Delay, Flight Condition 6	88
5.13	Surface Deflections with Actuators and Computational Delay, Flight Condition 6	88
5.14	Outputs, Including Sensor Dynamics, Flight Condition 1	92
5.15	Surface Deflections, Including Sensor Dynamics, Flight Condition 1	92
5.16	Outputs, Including Sensor Dynamics, Flight Condition 2	93
5.17	Surface Deflections, Including Sensor Dynamics, Flight Condition 2	93
5.18	Outputs, Including Sensor Dynamics, Flight Condition 3	94

Figure		Page
5.19	Surface Deflections, Including Sensor Dynamics, Flight Condition 3	94
5.20	Outputs, Including Sensor Dynamics, Flight Condition 4	95
5.21	Surface Deflections, Including Sensor Dynamics, Flight Condition 4	95
5.22	Outputs, Including Sensor Dynamics, Flight Condition 5	96
5.23	Surface Deflections, Including Sensor Dynamics, Flight Condition 5	96
5.24	Outputs, Including Sensor Dynamics, Flight Condition 6	97
5.25	Surface Deflections, Including Sensor Dynamics, Flight Condition 6	97
5.26	Outputs, Including Surface Nonlinearity, Flight Condition 1	101
5.27	Surface Deflections, Including Surface Nonlinearity, Flight Condition 1	101
5.28	Outputs, Including Surface Nonlinearity, Flight Condition 2	102
5.29	Surface Deflections, Including Surface Nonlinearity, Flight Condition 2	102
5.30	Outputs, Including Surface Nonlinearity, Flight Condition 3	103
5.31	Surface Deflections, Including Surface Nonlinearity, Flight Condition 3	103
5.32	Outputs, Including Surface Nonlinearity, Flight Condition 4	104
5.33	Surface Deflections, Including Surface Nonlinearity, Flight Condition 4	104
5.34	Outputs, Including Surface Nonlinearity, Flight Condition 5	105

Figure		Page
5.35	Surface Deflections, Including Surface Nonlinearity, Flight Condition 5	105
5.36	Outputs, Including Surface Nonlinearity, Flight Condition 6	106
5.37	Surface Deflections, Including Surface Nonlinearity, Flight Condition 6	106
5.38	Outputs, Realistic Noise, Simulation 1	109
5.39	Surface Deflections, Realistic Noise, Simulation 1	109
5.40	Outputs, Realistic Noise, Simulation 2	110
5.41	Surface Deflections, Realistic Noise, Simulation 2	110
5.42	Outputs, Realistic Noise, Simulation 3	111
5.43	Surface Deflections, Realistic Noise, Simulation 3	111
5.44	Outputs, Realistic Noise, Simulation 4	112
5.45	Surface Deflections, Realistic Noise, Simulation 4	112
5.46	Outputs, Realistic Noise, Simulation Mean	113
5.47	Surface Deflections, Realistic Noise, Simulation Mean	113
5.48	Outputs, Velocity Noise, Simulation 1	115
5.49	Surface Deflections, Velocity Noise, Simulation 1	115
5.50	Outputs, Velocity Noise, Simulation 2	116
5.51	Surface Deflections, Velocity Noise, Simulation 2	116
5.52	Outputs, Velocity Noise, Simulation 3	117
5.53	Surface Deflections, Velocity Noise, Simulation 3	117

Figure		Page
5.54	Outputs, Velocity Noise, Simulation 4	118
5.55	Surface Deflections, Velocity Noise, Simulation 4	118
5.56	Outputs, Velocity Noise, Simulation Mean . . .	119
5.57	Surface Deflections, Velocity Noise, Simulation Mean	119
5.58	Outputs, Angle of Attack Noise, Simulation 1	120
5.59	Surface Deflections, Angle of Attack Noise, Simulation 1	120
5.60	Outputs, Angle of Attack Noise, Simulation 2	121
5.61	Surface Deflections, Angle of Attack Noise, Simulation 2	121
6.62	Outputs, Angle of Attack Noise, Simulation 3	122
6.63	Surface Deflections, Angle of Attack Noise, Simulation 3	122
5.64	Outputs, Angle of Attack Noise, Simulation 4	123
5.65	Surface Deflections, Angle of Attack Noise, Simulation 4	123
5.66	Outputs, Angle of Attack Noise, Simulation Mean	124
5.67	Surface Deflections, Angle of Attack Noise, Simulation Mean	124
5.68	Outputs, Flight Path Noise, Simulation 1 . . .	125
5.69	Surface Deflections, Flight Path Noise, Simulation 1	125
5.70	Outputs, Flight Path Noise, Simulation 2 . . .	126
5.71	Surface Deflections, Flight Path Noise, Simulation 2	126

Figure		Page
5.72	Outputs, Flight Path Noise, Simulation 3 . . .	127
5.73	Surface Deflections, Flight Path Noise, Simulation 3	127
5.74	Outputs, Flight Path Noise, Simulation 4 . . .	128
5.75	Surface Deflections, Flight Path Noise, Simulation 4	128
5.76	Outputs, Flight Path Noise, Simulation Mean . .	129
5.77	Surface Deflections, Flight Path Noise, Simulation Mean	129
5.78	Outputs, Pitch Rate Noise, Simulation 1	130
5.79	Surface Deflections, Pitch Rate Noise, Simulation 1	130
5.80	Outputs, Pitch Rate Noise, Simulation 2	131
5.81	Surface Deflections, Pitch Rate Noise, Simulation 2	131
5.82	Outputs, Pitch Rate Noise, Simulation 3	132
5.83	Surface Deflections, Pitch Rate Noise, Simulation 3	132
5.84	Outputs, Pitch Rate Noise, Simulation 4	133
5.85	Surface Deflections, Pitch Rate Noise, Simulation 4	133
5.86	Outputs, Pitch Rate Noise, Simulation Mean . .	134
5.87	Surface Deflections, Pitch Rate Noise, Simulation Mean	134
5.88	Outputs, Controller 1, Flight Condition 2 . . .	136
5.89	Surface Deflections, Controller 1, Flight Condition 2	136
5.90	Outputs, Controller 1, Flight Condition 3 . . .	137
5.91	Surface Deflections, Controller 1, Flight Condition 3	137

Figure		Page
5.92	Outputs, Controller 1, Flight Condition 4 . .	138
5.93	Surface Deflections, Controller 1, Flight Condition 4	138
5.94	Outputs, Controller 1, Flight Condition 6 . .	139
5.95	Surface Deflections, Controller 1, Flight Condition 6	139
5.96	Outputs, Controller 2, Flight Condition 1 . .	140
5.97	Surface Deflections, Controller 2, Flight Condition 1	140
5.98	Outputs, Controller 2, Flight Condition 3 . .	141
5.99	Surface Deflections, Controller 2, Flight Condition 3	141
5.100	Outputs, Controller 2, Flight Condition 4 . .	142
5.101	Surface Deflections, Controller 2, Flight Condition 4	142
5.102	Outputs, Controller 3, Flight Condition 4 . .	143
5.103	Surface Deflections, Controller 3, Flight Condition 4	143
5.104	Outputs, Controller 6, Flight Condition 1 . .	144
5.105	Surface Deflections, Controller 6, Flight Condition 1	144
5.106	Outputs, Controller 6, Flight Condition 2 . .	145
5.107	Surface Deflections, Controller 6, Flight Condition 2	145
5.108	Outputs, Controller 6, Flight Condition 3 . .	146
5.109	Surface Deflections, Controller 6, Flight Condition 3	146
5.110	Outputs, Controller 6, Flight Condition 4 . .	147
5.111	Surface Deflections, Controller 6, Flight Condition 4	147

Figure		Page
5.112	Flare Command Input	150
5.113	Attitude for Flare Maneuver	150
5.114	Outputs for Flare Maneuver	151
5.115	Surface Deflections for Flare Maneuver . . .	151
5.116	Flight Path Command Input	152
5.117	Outputs for Flight Path Change	153
5.118	Surface Deflections for Flight Path Change .	153
A.1	Sample Custom Input--Unsmoothed	183
A.2	Sample Custom Input--Smoothed	183
A.3	Option #22 Algorithm Outline	184
B.1	System Block Diagram--Continuous Case	226
B.2	System Block Diagram--Discrete Case	228
C.1	Second and Third Order Canard Actuator Frequency Response	238
C.2	Second and Third Order Canard Actuator Step Response	238
C.3	Second and Third Order Aileron Actuator Frequency Response	239
C.4	Second and Third Order Aileron Actuator Step Response	239
C.5	Second and Third Order Angle of Attack Sensor Step Response	242
C.6	Second and Third Order Angle of Attack Sensory Frequency Response	242

List of Tables

Table		Page
3.1	Flight Conditions	22
4.1	A Comparison of Asymptotic and Finite System Roots	47
4.2	Maximum Steady State Maneuver	56
5.1	Design Parameters for the Plant Plus Actuators and Computational Time Delay	81
5.2	Figures of Merit for Plant Plus Actuators and Computational Time Delay	82
5.3	Design Parameters for the Plant Plus Actuators, Computational Time Delay and Sensor Dynamics	90
5.4	Figures of Merit for Plant Plus Actuators, Computational Time Delay and Sensor Dynamics	91
5.5	Design Parameters for the Plant Plus Actuators, Computational Time Delay, Sensor Dynamics and Surface Nonlinearities	99
5.6	Figures of Merit for Plant Plus Actuators, Computational Time Delay Sensors and Surface Nonlinearity	100
5.7	Sensor Noise Data	108
5.8	Threshold Noise Levels	114
5.9	Parameter Variation Results	148
B.1	Asymptotic Equations for Zero- B_2 Form	231
C.1	Realistic Noise Values	243
D.1	Flight Condition 1 Aero Data	246
D.2	Flight Condition 2 Aero Data	247
D.3	Flight Condition 3 Aero Data	248

Table		Page
D.4	Flight Condition 4 Aero Data	249
D.5	Flight Condition 5 Aero Data	250
D.6	Flight Condition 6 Aero Data	251
D.7	Flight Condition 1 State Model	253
D.8	Flight Condition 2 State Model	254
D.9	Flight Condition 3 State Model	255
D.10	Flight Condition 4 State Model	256
D.11	Flight Condition 5 State Model	257
D.12	Flight Condition 6 State Model	258
D.13	Flight Condition 1 Transfer Functions	259
D.14	Flight Condition 2 Transfer Functions	260
D.15	Flight Condition 3 Transfer Functions	261
D.16	Flight Condition 4 Transfer Functions	262
D.17	Flight Condition 5 Transfer Functions	263
D.18	Flight Condition 6 Transfer Functions	264

List of Symbols

<u>A</u>	Continuous-time Plant matrix
α	Angle of attack, perturbation angle of attack in perturbation equations
$\bar{\alpha}$	Ratio of proportional to integral feedback
<u>B</u>	Continuous-time plant matrix
<u>C</u>	Continuous-time Output Matrix
CG,cg	Center of gravity
C_m	Nondimensional coefficient of pitching moment
C_{m_α}	Nondimensional variation of pitching moment with angle of attack
C_{m_δ}	Nondimensional variation of pitching moment with stabilator (δ_H), canard (δ_C) or stab-nozzle (δ_{HN})
C_{m_q}	Nondimensional variation of pitching moment with pitch rate
C_{m_u}	Nondimensional variation of pitching moment with forward velocity perturbations
C_x	Nondimensional x-force coefficient
C_{x_α}	Nondimensional variation of x-force with angle of attack
C_{x_δ}	Nondimensional variation of x-force with stabilator (δ_H), canard (δ_C), throttle (δ_T), or stab-nozzle (δ_{HN})
C_{x_q}	Nondimensional variation of x-force with pitch rate
C_{x_u}	Nondimensional variation of x-force with forward velocity perturbation
C_z	Nondimensional z-force coefficient

C_{z_α}	Nondimensional variation of z-force with angle of attack
$C_{z_{\dot{\alpha}}}$	Nondimensional variation of z-force with the rate of change of angle of attack
C_{z_δ}	Nondimensional variation of z-force with stabilator (δ_H), canard (δ_C), or stab-nozzle (δ_{HN})
C_{z_q}	Nondimensional variation of z-force with pitch rate
C_{z_u}	Nondimensional variation of z-force with forward velocity perturbation
deg	Degree
δ_C	Canard deflection
δ_C	Combined canard, aileron, flap deflection
δ_S	Stabilator deflection
δ_T	Nozzle deflection vane deflection
$e(t), \underline{e}$	Error vector
$\underline{e}(kT)$	Discrete error vector
ϵ	Epsilon scalar multiplier
ft	Feet
f	Sampling frequency
g	Gravity, type of pilot command, gain constant
$\underline{G}(s)$	Transfer function matrix
I_{xx}	Moment of inertia about x-axis
I_{yy}	Moment of inertia about y-axis
I_{zz}	Moment of inertial about z-axis
I_{xz}	Product of inertia about xz-axes
\underline{I}	Identity matrix
\underline{K}_0	Proportional control law feedback matrix

\underline{K}_1	Integral control law feedback matrix
K_q	Pitch rate feedback gain
K_s	Stabilator actuator gain
lbs	pounds
ℓ	Number of system outputs
\underline{M}	Measurement matrix
m	Aircraft mass, number of inputs
M_α	Dimensional variation of pitching moment with angle of attack
M_α	Dimensional variation of pitching moment with the rate of change of angle of attack
M_q	Dimensional variation of pitching moment with pitch rate
M_θ	Dimensional variation of pitching moment with pitch angle
M_x	Moment about the x-axis
n	Number of states
p	Number of outputs, roll rate
q	Pitch rate
rad	Radians
S	Surface area
s	Laplace operator
sec	Seconds
σ	Elements of the Sigma (Σ) matrix
Σ	Sigma Gain Weighting matrix
\underline{T}	Transformation matrix
T	Sampling period, Thrust

U	Velocity along x-axis
u	Perturbation velocity along x-axis
\underline{u}	Input vector
\underline{v}	Command input vector
V_T	Forward Velocity
\underline{w}	Controller output vector
\underline{x}	State vector
X_α	Dimensional variation of x-force with angle of attack
\dot{X}_α	Dimensional variation of x-force with the rate of change of angle of attack
X_δ	Dimensional variation of x-force with stabilator (δ_H), canard (δ_C), throttle (δ_T), or stab-nozzle (δ_{HN})
X_q	Dimensional variation of x-force with pitch rate
X_u	Dimensional variation of x-force with forward velocity perturbation
\underline{y}	Output vector
$\underline{z}(t), \underline{z}$	Integral of error vector
$\underline{z}(kT)$	Discrete Integral of error vector
Z_α	Dimensional variation of z-force with angle of attack
\dot{Z}_α	Dimensional variation of z-force with the rate of change of angle of attack
Z_δ	Dimensional variation of z-force with stabilator (δ_H), canard (δ_C), or stab-nozzle (δ_{HN})
Z_q	Dimensional variation of z-force with pitch rate
Z_u	Dimensional variation of z-force with forward velocity perturbation
Z_t	Transmission zeros

$z_{1,2}$	Finite system roots
z_3	Infinite system roots
θ	Pitch angle
$\Gamma(\lambda)$	Asymptotic transfer function matrix
$\hat{\Gamma}(\lambda)$	Asymptotic transfer function matrix (fast roots)
$\tilde{\Gamma}(\lambda)$	Asymptotic transfer function matrix (slow roots)

Abstract

Multivariable, output feedback digital control laws are designed for the short take-off and landing F-15 aircraft in the landing configuration. The design is based on the methods developed by Professor Brian Porter of the University of Salford, England, and was accomplished using a computer-aided design and simulation program called MULTI.

The STOL F-15 landing configuration includes canards and reversible thrust in addition to the conventional F-15 control surfaces. The additional controls allow decoupling of the output variables in the longitudinal plane. Longitudinal aircraft dynamics are derived from data provided by McDonnell-Douglas, the prime contractor for the STOL F-15, and are presented in linearized state space form for the design procedure.

Control laws are developed to stabilize the aircraft to perform longitudinal landing maneuvers (flight path control and flare) at six flight conditions. The design encompasses actuator dynamics, computational delay, sensor dynamics, sensor noise, and plant nonlinearities. Proportional plus integral controller designs for each of the flight conditions demonstrate good time response characteristics. The designs of two of the flight conditions

are sufficiently insensitive to plant variations to be used at all but one of the remaining flight conditions.

The technique of multivariable output feedback, through the use of the program MULTI, is shown to provide good robust designs for the STOL F-15. Additional areas of research on this aircraft are discussed as well as suggested enhancements to the MULTI program.

MULTIVARIABLE OUTPUT CONTROL LAW DESIGN FOR THE STOL F-15 IN LANDING CONFIGURATION

I. Introduction

1.1 Background

Short takeoff and landing (STOL) and thrust vectoring technology are not new concepts in the aerospace industry. STOL techniques such as high lift devices or wing flaps have long been employed on aircraft of all types and sizes. In the past few decades even more sophisticated STOL devices have been developed for special purpose aircraft both in the civilian and military aviation field. Vectored thrust and, more commonly, thrust reversing are routinely used on commercial airliners to facilitate shorter landing rolls. Thrust reversing propellers on the Lockheed C-130 Hercules provide excellent short field characteristics for that nineteen-fifties vintage aircraft. It was not until the late sixties and early seventies, however, that these techniques proved successful on a fighter aircraft. The British Aerospace Harrier aircraft design allowed not only short field operations, but also vertical takeoff capability. That design features moveable engine nozzles that can be pointed backward for normal takeoff and flight, downward for hover or vertical flight, and even

forward for rapid deceleration. Deployed by the United Kingdom to the Falkland Island conflict in 1982, the Harrier proved itself in aerial combat against the Argentine air forces. The maneuverability and operational flexibility of operating from short landing facilities proved invaluable to the success of the air war in the Falklands (4:38). Despite the successes of the Harrier, it is fairly slow for a fighter and lacks the range, payload, and sophisticated avionics of modern fighter aircraft. The United States Air Force recognizes the advantages of STOL/thrust vectoring technology and in September 1983 issued a "request for proposal" for advanced development of a STOL demonstrator fighter aircraft. Plans call for an aircraft capable of takeoff and landing in 1500 feet or less in all weather conditions. Furthermore, the Air Force seeks an aircraft with supersonic capability and advanced maneuvering technology, including thrust vectoring and integrated flight and propulsion controls (11:30).

Current technology fighters require extremely long runway surfaces, particularly for landing. The McDonnell Douglas F-15, the premier air superiority aircraft in the Air Force inventory, requires 8000 feet to safely land in an all weather environment. Runways are easily targetable facilities and it is merely prudent to assume that substantial battle damage will be incurred in a conflict. A runway requires little damage to reduce its usable length to

just a few thousand feet, rendering the fighter force useless if on the ground, and unrecoverable if in the air. Moveable barrier cables similar to the fixed barrier currently used by the Air Force and Navy have been proposed as a simple solution to the landing problem. However, such systems detract from an aircraft's autonomy by increasing its dependence on ground support equipment. Reducing the aircraft's runway requirements opens up a number of reasonable alternatives. Fighter aircraft could operate from usable portions of battle damaged military runways, smaller civilian fields, or even stretches of unobstructed highway. In general, three factors drive the amount of runway required by an aircraft: approach velocity, touchdown dispersion and braking capability. STOL and thrust vectoring technology can reduce the approach speed and provide more precise flight path control. Most importantly, thrust reversing substantially decreases the stopping distance of a high speed fighter regardless of runway braking coefficients. The benefits extend to shorter takeoff rolls as well, although, as is the case with most high thrust aircraft like the F-15, takeoff distance is generally much shorter than landing.

The design of an aircraft that has these capabilities often requires destabilizing aerodynamic surfaces, and almost without exception a greater number of controllable surfaces. It has been shown in numerous previous papers

and theses, as well as in experimental aircraft like the General Dynamics AFTI/F-16 and the Grumman X-29, that on-board flight control computers are capable of compensating for instability and efficiently controlling additional control surfaces to achieve precise decoupled control. This thesis investigates the design of flight control laws for the STOL/F-15 as a preliminary determination of the ability to achieve precise, decoupled, low speed flight path control.

1.2 Problem

The objective of this thesis is to design longitudinal control laws for the STOL/F-15, based on a well developed mathematical model, that provide stabilization as well as precise decoupled flight path control at landing airspeed. Using the multivariable output feedback control law design techniques of Professor Brian Porter of the University of Salford, England, control laws are developed to perform longitudinal landing maneuvers at six flight conditions. A build-up design approach is used, starting with the basic aircraft and then including in succession the actuator dynamics, computational time delay, sensor dynamics, plant nonlinearities, and sensor noise.

1.3 Scope

This thesis accomplishes the following objectives toward the ultimate goal of practical control of the STOL/F-15:

1. Successful control of the linear aircraft model including actuator dynamics, sensor dynamics, and computational time delay.

2. Identification, simulation, and successful compensation of a specific nonlinearity arising from large control surface deflections.

3. Simulation of output measurement noise and its effects on the performance of the closed loop performance of the aircraft.

4. Numerous enhancements to the computer aided design and simulation program MULTI (9).

1.4 Overview

A general description of the aircraft used for this study is presented in Chapter II, followed in Chapter III by a more detailed discussion of the mathematical representation and the simplifying assumptions made to obtain the model used for design and simulation. Having defined the mathematical model, the details of the design procedure are covered in Chapter IV, including some preliminary results that demonstrate the effects of each of the design variables. Chapter V contains the results of applying the design procedure of Chapter IV to the various flight conditions and levels of model complexity presented in Chapter III, culminating in a simulation of the aircraft with actuator dynamics, sensor dynamics, computational

time delay, control surface nonlinearity, and sensor noise. The chapter also presents a demonstration of controller robustness to plant parameter variations. Finally, Chapter VI summarizes these results and recommends potential improvements and recommended topics for future study. Four appendices are included as supplementary material to augment the material presented in the body of the thesis. Appendix A details the revisions and additions made to MULTI in the course of the thesis, Appendix B presents a brief overview of the theory behind the Porter method, and Appendices C and D contain modeling data for the actuators, sensors and aircraft in general.

II. The STOL F-15 Aircraft

2.1 Introduction

The STOL F-15, illustrated in Figure 2.1, is a technology demonstrator aircraft and is the object of a program to investigate, develop, and validate several technological developments related to STOL capability for fighter aircraft. There are two principal objectives of this program: to demonstrate the use of two-dimensional thrust vectoring/reversing nozzles, integrated flight/propulsion control, rough field STOL Landing Gear, and an advanced pilot/vehicle interface; and to provide design options for future fighter aircraft, specifically the Advanced Tactical Fighter (ATF). In pursuit of these objectives the McDonnell-Douglas Aircraft Corporation (MCAIR) developed the demonstrator aircraft with the following design features:

1. Additional control surfaces (canards)
2. Two-dimensional engine nozzles
3. Thrust reversing vanes
4. Improved landing gear
5. Advanced avionics and cockpit instrumentation

This chapter is devoted to describing the basic airframe and the first three items on this list in detail and

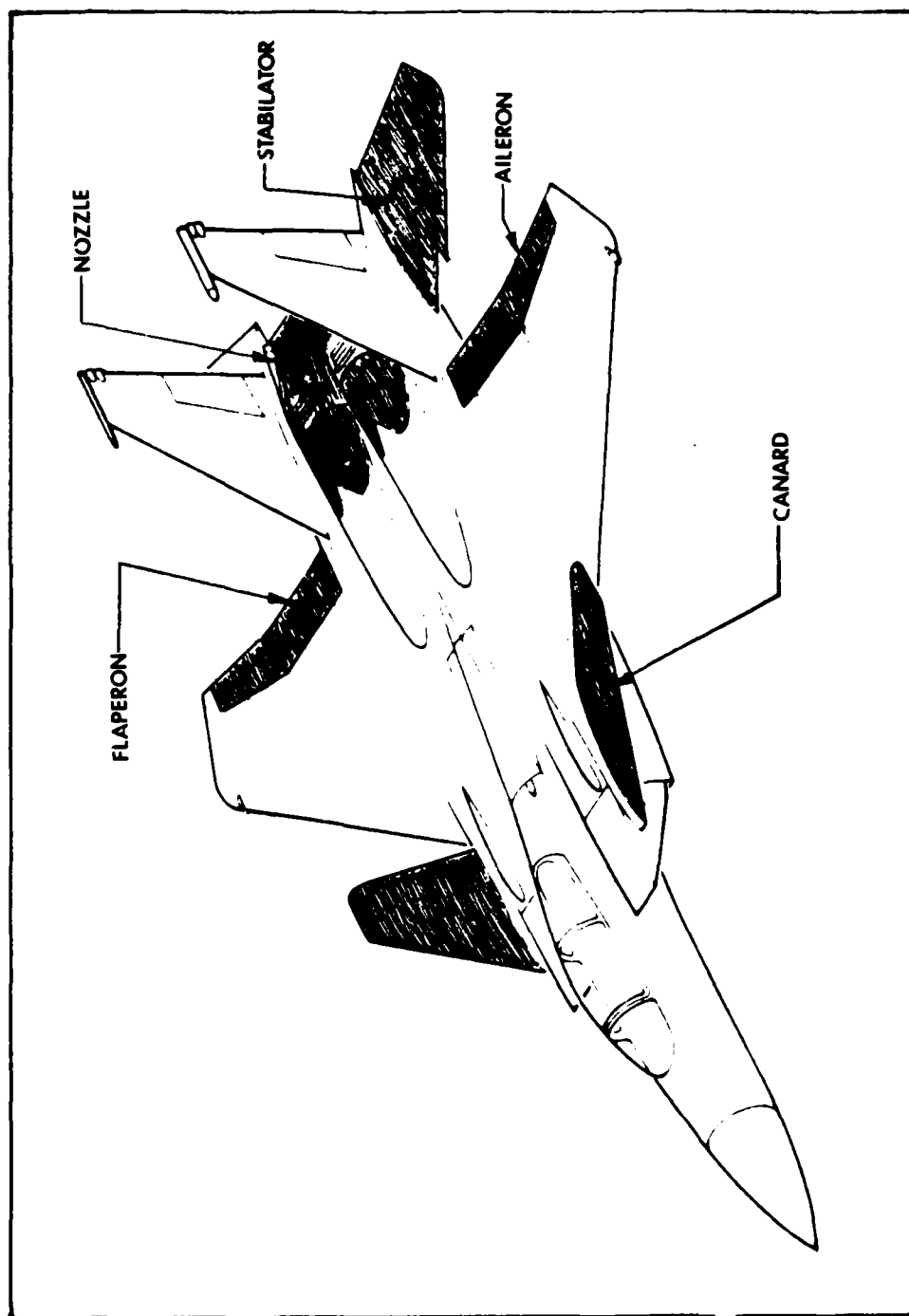


Fig. 2.1. STOL F-15

discussing their effect on the control of the aircraft. Since this thesis is an investigation of the physical control of this vehicle in the approach phase of flight, the improved avionics and landing gear are not relevant topics for further discussion.

2.2 General Description

The original F-15 aircraft, a modern and sophisticated airframe, has been proven by more than a decade of safe and reliable peacetime and combat service. MCAIR took advantage of this by using the same basic airframe as a baseline for the demonstrator aircraft design. The outward appearance and dimensions of the STOL aircraft (Figure 2.2) are very similar to that of the F-15B (tandem seat version) except for the addition of the canards on the engine inlets. Structurally, the airframe is essentially unchanged other than the canard torque shaft and fairings for both the canard and nozzles. Internally, the flight control system has been replaced by an integrated digital fly by wire control system. The STOL F-15 features all of the same control surfaces as the original aircraft. These include ailerons, trailing-edge flaps, horizontal stabilators, two rudders, and a speed brake. In general, the basic F-15 is a two-engine fighter aircraft characterized by an unusually high thrust to weight ratio (greater than 1.0 in certain conditions) and exceptional

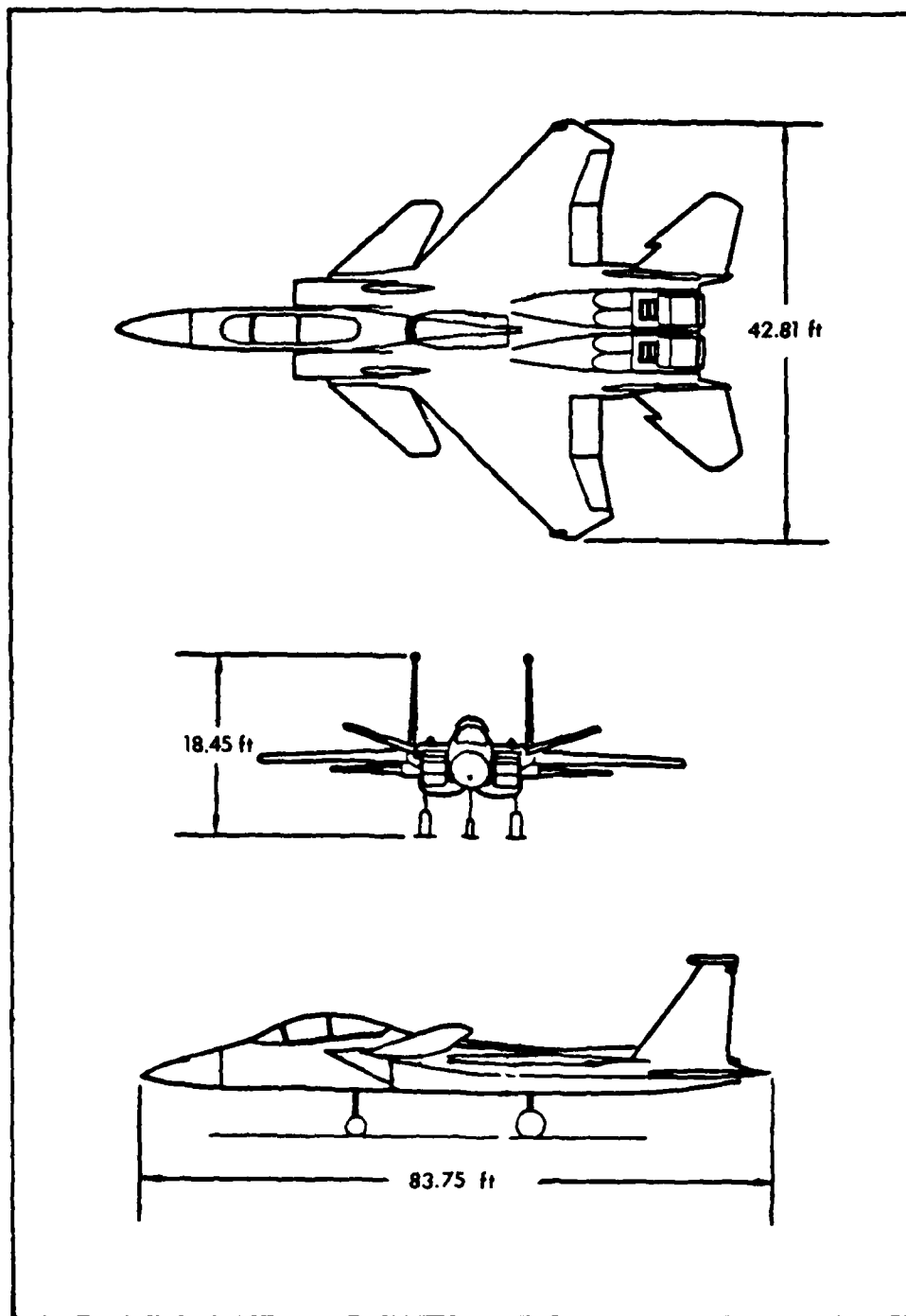


Fig. 2.2. STOL F-15 Dimensions

maneuverability. Although untested in flight, MCAIR anticipates substantial improvement in the STOL F-15 in both performance and maneuverability based on their calculations and wind tunnel tests.

2.3 Canards

Rather than design and manufacture a canard, MCAIR chose to adapt the stabilator of the F-18 aircraft, an airplane smaller than the F-15 but of comparable performance and sophistication. The canards are located on the engine intakes (Figure 2.1) just aft of the variable inlets. As is often the case with the addition of canards, the destabilizing effect of the surfaces forward of the center of gravity results in static instability in some flight conditions. Although this situation requires active control of the aircraft, zero or negative static stability is often desirable to improve the maneuvering capability of the aircraft. Instability is of no advantage in the landing phase of flight and of course requires effective, reliable stability augmentation. Even though the canard is a relatively fast surface, MCAIR plans to schedule the canard with angle of attack, accomplishing the bulk of the stability augmentation through the use of the stabilators. For the purposes of this thesis, however, the canard will be treated as a fully controllable surface. Like the stabilators, the left and right canards can be actuated

either together or independently, allowing their use in both longitudinal and lateral control of the aircraft. The canards are installed with fifteen degrees of dihedral, enhancing lateral stability as well as affording additional control in the lateral mode. Deflection of the canard is limited to +15 degrees (leading edge up), and -35 degrees, at a rate of 23 degrees per second.

2.4 Two-Dimensional Nozzle and Thrust Reversing Vanes

The conventional nozzles of the F-15 have been replaced with the two-dimensional nozzles depicted in Figures 2.3, 2.4, and 2.5. Each nozzle features four flaps and ten vanes to control the thrust of the jet engine exhaust. As shown in these figures, the nozzles have two modes of operation, primary jet vectoring and rotating vane vectoring. In the primary jet vectoring mode the ten rotating vanes remain closed and the direction of the primary jet is turned as much as 20 degrees with four hydraulically actuated flaps. The four flaps (two convergent and two divergent) produce the desired force and moment while simultaneously maintaining the required pressure gradient and area ratio for the nozzle. In this mode, the principal means for controlling the magnitude of the thrust is through fuel flow to the engine as in a conventional aircraft. The two nozzles (left and right) can be controlled symmetrically and/or differentially, influencing both the

Nozzle Design

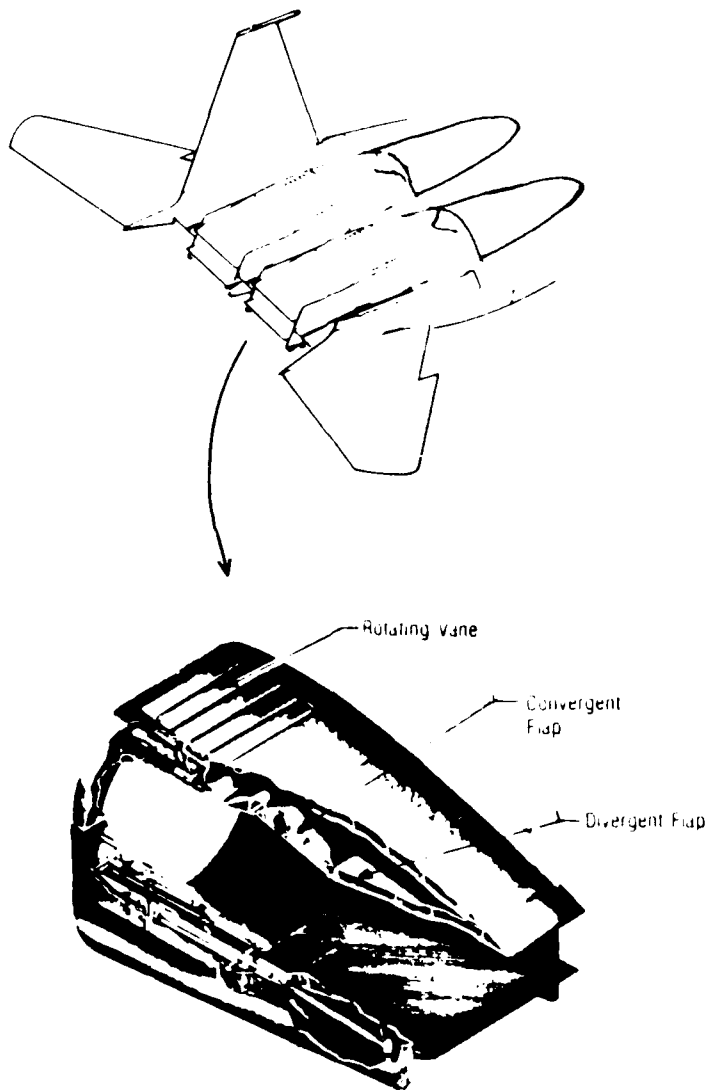
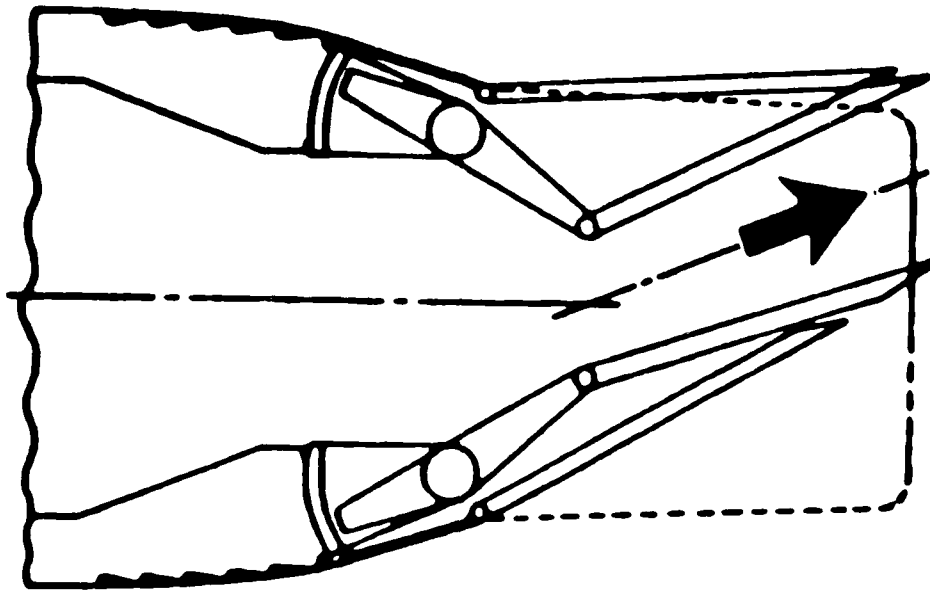


Fig. 2.3. Nozzle Design

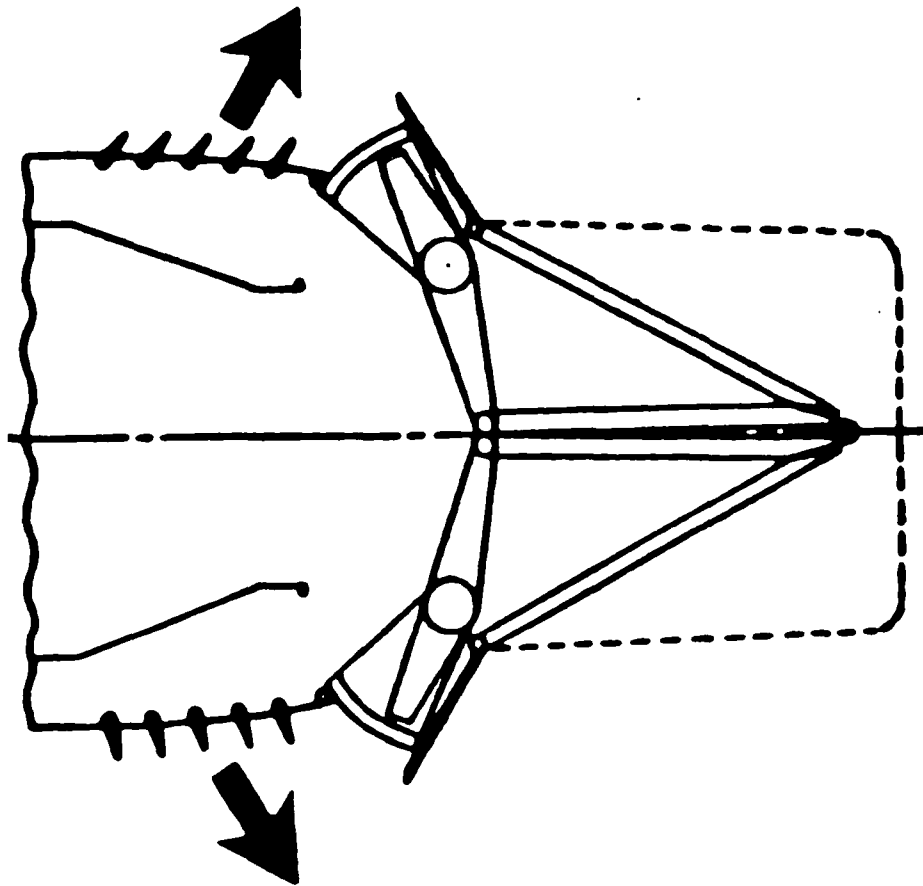
Primary Jet Vectoring



In-Flight Maneuvering/Takeoff

Fig. 2.4. Primary Jet Vectoring

Rotating Vane Vectoring



Landing Approach Control

Fig. 2.5. Rotating Vane Vectoring

longitudinal and lateral motion of the aircraft. In the rotating vane vectoring mode, the ducting for the primary jet exhaust closes down entirely, diverting the flow through the rotating vanes. The vanes are also hydraulically controlled and their variable deflection angle produces controllable forces and moments. Of the ten vanes (five each top and bottom) eight are dedicated to vectoring the thrust in the desired direction with deflection limits of 45 degrees to 135 degrees at a rate of 180 degrees per second. The remaining two (one each, top and bottom) are deflected independently to maintain the equivalent nozzle throat area at the optimal value. The top and bottom vanes are controlled independently except for the two vanes reserved for throat area control. In this mode, the resultant force produced can be controlled without changing the RPM of the engines, reducing wear and tear on the engine and allowing rapid transition to a full thrust landing abort. Also, since the vanes are significantly faster than the engine response time, much more precise thrust control is possible. Like the nozzles, the left and right engine vanes are independent and contribute to both the longitudinal and lateral motion. As a result, the available thrust ranges from 70 percent of its maximum military thrust aft (the afterburner is disabled in this mode) to the same amount of thrust reversal, with an infinite range of control in between. The precise thrust control and

thrust reversal of this mode are well suited to the requirements of landing, so it is the principal mode of operation for approach and landing flight conditions. Since this thesis is limited to the study of the landing performance of this aircraft, it is always assumed that the aircraft is in the rotating vane vectoring mode.

2.5 Summary

The STOL F-15 is a demonstrator aircraft design derived from an operational, high performance fighter aircraft. The addition of canards and thrust vectoring/reversing affords the STOL F-15 enhanced control authority and projected improvements in performance. This thesis is a study of one control law design technique to make use of the STOL F-15's unique capabilities in the landing configuration.

III. Aircraft Model

3.1 Introduction

The Porter method of multivariable output feedback control is founded in the principals of linear control theory and requires that the system to be controlled be expressed in linear state space form. Like all physical systems, airplanes are not linear, but in most cases their equations of motion are adequately approximated by a linear system of perturbation equations around a trim operating point. This chapter describes the linear aircraft model, beginning with the fundamental assumptions and developing the longitudinal equations for six flight conditions. In addition, the equations for modeling the dynamics of the surface actuators, output sensors and noise, and computational time delay are defined. Finally, a limitation to the linearized equations is identified, and a nonlinear approximation of the solution is presented.

3.2 Fundamental Assumptions

In the development of linear, time-invariant equations of motion for aircraft, a number of assumptions have been adopted as standard and are found in nearly every text that develops these equations. Following is a summary of

the results of the rigorous descriptions of these assumptions found in Etkin (7:121-189).

1. The surface of the earth is flat and is a stationary inertial reference frame.

2. The air is stationary with respect to the earth's surface.

3. The physical dimensions of the aircraft do not change in time, neglecting changes in mass, and any bending of the airframe.

4. The aerodynamic characteristics of the aircraft are fixed for a given flight condition.

5. Airflow variations that result from the aircraft's maneuvers occur instantaneously.

6. Perturbation of the aircraft from equilibrium is sufficiently small to use the first order Taylor series approximation to the sine and cosine of perturbation angles.

7. The motion is constrained to the longitudinal plane and is assumed to be uncoupled from all lateral motion. This requires the existence of a plane of symmetry and no gyroscopic effects.

3.3 Linearized Longitudinal Equations

The application of the preceding assumptions to the generalized equations of motion result in a system of four linear, time-invariant differential equations (7:163). These equations are expressed in terms of the dimensional

aerodynamic stability derivatives in the stability axis system (X axis aligned with relative wind at equilibrium). Although these equations are useful for determining the effects of specific derivatives on the motion of the aircraft, it is more convenient for controller design purposes to express the relationships in the principal (body) axis system (Figure 3.1) and in dimensional state space for (2:37). The STOL F-15 data provided by MCAIR are expressed in nondimensional stability axis coefficient form, which necessitates computation of the matrix elements and rotation through the angle of attack to obtain a body axis system of linear equations. These computations and results are contained in Appendix D. The sign conventions for control surface deflections are also shown in Figure 3.1.

3.4 Flight Conditions

One of the drawbacks of linearized aircraft equations is that their validity is entirely dependent on the assumption that a number of quantities remain constant, even though they are in fact variables. The process of linearization is therefore valid at only one particular design condition and must be reaccomplished whenever the conditions are changed. This suggests that the equations may be time variant, which is true, but in the case of the conditions of flight it is assumed that the quantities change slowly enough in time that they are constant over

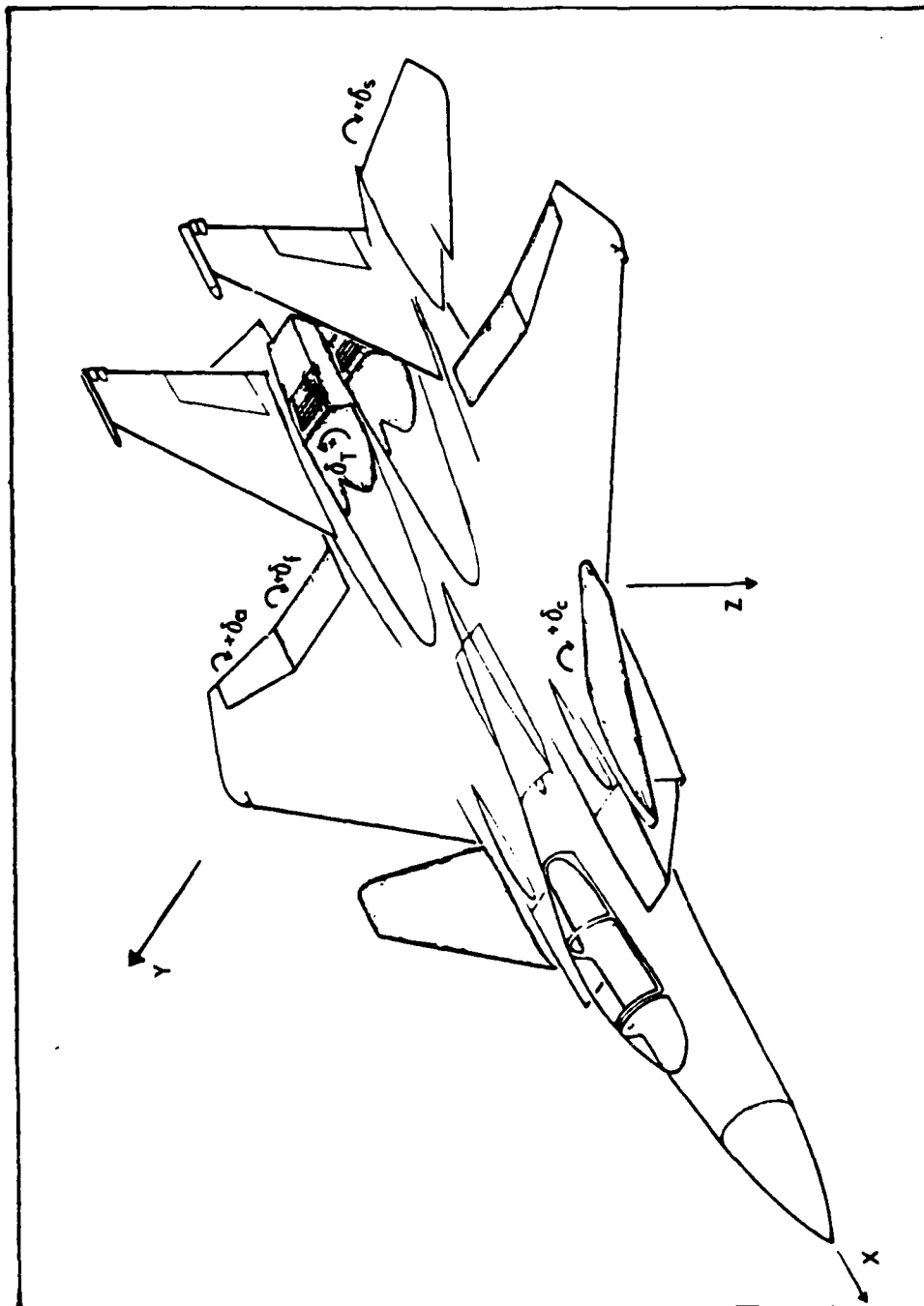


Fig. 3.1.1. STOL F-15 Sign Conventions

the time period of interest. To perform a thorough controller design it is necessary to determine the extent of the variability of these pseudo-constants and linearize at flight conditions throughout the parameter space. For this thesis, six landing flight conditions, listed in Table 3.1, are chosen from the available data. All of these flight conditions are in landing configuration (gear down, flaps 20 degrees). With 1500 lbs of fuel remaining, the aircraft weighs 33576 lbs, a condition approximating a landing at the end of a mission. At this weight and at sea level on a standard day, the recommended landing speed is 200 ft/sec (condition 1), 20 percent higher than the stall speed of 168 ft/sec (condition 2). With 11435 lbs internal fuel, the gross weight is 43511 lbs, a simulated heavy-weight landing.

TABLE 3.1
FLIGHT CONDITIONS

Flight Condition	Altitude (Ft)	Aircraft Weight (lbs)	True Velocity (Ft/Sec)
1	0	33576	200
2	0	33576	168
3	0	43511	200
4	0	43511	304
5	10000	43511	304
6	10000	33576	200

The velocities chosen in flight conditions 3, 4, 5, and 6 are not chosen for any particular significance other than that the data are available and represent reasonable landing conditions.

3.5 Representative Plant

Introduction. In the course of this thesis, sample calculations and examples are included to illustrate the concepts and techniques used throughout the design process. For consistency and brevity, one plant model is chosen as a representative plant for this purpose. The plant model of flight condition 1 is chosen because it represents the conditions most commonly encountered in an approach and landing situation. The remainder of this section details the development of each of the plant models using the representative plant as an example.

Plant Matrix. The plant matrix, also referred to as the "A" matrix, is calculated as described in Section 3.3 of Appendix D. The result for flight condition 1 is shown in Figure 3.2. The states in this model, as with all the models of this thesis are pitch angle (θ), X-axis component of velocity (u), pitch rate (q), and the angle of attack (α). Note that the first state (θ) is chosen such that the kinematic equation is at the top of the A matrix. This is a requirement of the computer program MULTI.

$$\dot{x} = \underline{A}x + \underline{B}u$$

$$y = \underline{C}x$$

$$x = \begin{bmatrix} \theta \\ u \\ q \\ \alpha \end{bmatrix} \quad u = \begin{bmatrix} \delta_C \\ \delta_S \\ \delta_T \end{bmatrix} \quad y = \begin{bmatrix} u \\ \alpha \\ \gamma \end{bmatrix}$$

$$\underline{A} = \begin{bmatrix} 0 & 0 & 1 & 0 \\ -31.54 & -0.06909 & -40.16 & 0.3350 \\ 0 & -3.603 \times 10^{-4} & -0.9912 & 1.366 \\ -0.03232 & 0.9925 \times 10^{-5} & 0.9796 & -0.6392 \end{bmatrix}$$

$$\underline{B} = \begin{bmatrix} 0 & 0 & 0 \\ -2.546 & -3.237 & -21.80 \\ 0.8407 & -1.578 & -0.0250 \\ -0.02060 & -0.07660 & 0 \end{bmatrix}$$

$$\underline{C} = \begin{bmatrix} 0 & 1 & 0 & 0 \\ 0 & 0 & 0 & 1 \\ 1 & 0 & 0 & -1 \end{bmatrix}$$

Fig. 3.2. Open Loop State Space Model, Flight Condition 1

Input Matrix. The input ("B") matrix is also calculated according to the procedure of Section 3.3 except that some additional manipulation is required to put it in a usable form. The STOL F-15 has nine independently actuated longitudinal control surfaces. They are the canard, the stabilator, the trailing edge flaps, the ailerons (actuated together like the flaps), each of the four rotating vanes, and the speed brake. Since it is a fundamental requirement of multivariable control system theory that there be a unique solution to the equations, the inputs must be mathematically independent and there can be no more inputs than there are independent states. Pitch rate is simply the time derivative of pitch angle, leaving only three independent states. It should also be obvious that with only two force equations and a moment equation in the longitudinal plane, a fourth input would clearly be a linear combination of the other three. Without additional equations only three independent inputs are possible. Optimal control theory allows the definition of cost functions that weight the inputs according to user definable optimality criteria. These cost functions can provide the necessary additional equations to use extra inputs; however, the current capabilities of the Porter method do not include their use. The first simplification is made by eliminating the speed brake for consideration. Although the rotating vanes, when operating independently, provide significant

independent contributions to all three equations, their utility is best realized as an input into the horizontal force equation. By summing the contributions of all four vanes, their combined effect can be treated as a single input. This same mathematical effect could be achieved by physically prohibiting independent actuation of the rotating vanes. The two remaining excess inputs are removed by summing the effects of the flaps, ailerons, and canards. To make maximum use of each of these surfaces they are weighted prior to the summation such that they reach maximum surface deflection simultaneously. Weighting the surfaces in this manner is in effect a type of cost function that is invariant and can be evaluated in advance. The weighting process is described in Appendix C. There are now three inputs and they are labeled in Figure 3.2 as the combined canard, flaps, and ailerons acting as one equivalent surface (δ_C), the stabilator (δ_S), and the rotating vanes (δ_T). The "B" matrix is composed of partial derivatives of the state equations with respect to control surface deflections, and as such are accurate only for small deflections of the surface away from the equilibrium position. In certain circumstances it is necessary to modify the "B" matrix as control surface deflections become large to account for the inaccuracies of linearization. Paragraph 3.9 of this chapter describes these circumstances and the modifications made for this thesis.

Output Matrix. The output matrix ("C") combines and weights the states to obtain the output variables which are to be controlled. With three independent inputs, three outputs can be controlled. Since any three independent outputs can be used, the designer must choose the desired outputs based on the type of maneuver to be accomplished and the accessibility of the states that must be measured. The key objective of a landing maneuver is to control the flight path of the aircraft. Since the flight path angle is simply the difference of the pitch angle and the angle of attack, this is a readily measured quantity as well. Control of velocity and angle of attack is also important since landing is usually at critically slow airspeed and maximum angle of attack. Pitch angle, although important as visual feedback to the pilot, is subordinate to angle of attack in this flight condition and must be controlled indirectly using flight path angle and angle of attack. The result of these considerations is the "C" matrix of Figure 3.2 and is the same for all of the flight conditions of this thesis. The variables are velocity (u), angle of attack (α), and flight path angle (γ).

3.6 Actuator Dynamics

The equations of Figure 3.2 relate the motion of the aircraft to the deflections of the control surfaces. Since the control input quantities are signals generated

from the measurement of the outputs, the dynamic response of the actuators (converting electrical signals to surface movement) must be considered. The data provided by MCAIR (Appendix C) specifies the actuator dynamics for each surface as LaPlace domain transfer functions, most of which have third order characteristic equations. The program MULTI allows entry of actuator transfer functions without augmenting the plant matrix but is limited to second order characteristic equations and zero order numerators. Since the surfaces have been combined as described in paragraph 3.5, the actuator data provided by MCAIR must be altered to satisfy these constraints. Appendix C demonstrates that in all cases the dynamics are well modeled by second order transfer functions with no zeros, even after combining surfaces. Figure 3.3 contains the results of these calculations and illustrates the placement of the actuator dynamics in block diagram form. The actuator dynamics are constant and independent of flight condition. Note that for each actuator a variable gain is included for potential design enhancement. The use of these gains is demonstrated in the following chapter.

3.7 Computational Time Delay

The program MULTI features an option of including a delay of one or more sample periods to simulate the delay in computing the control inputs from the measurements of

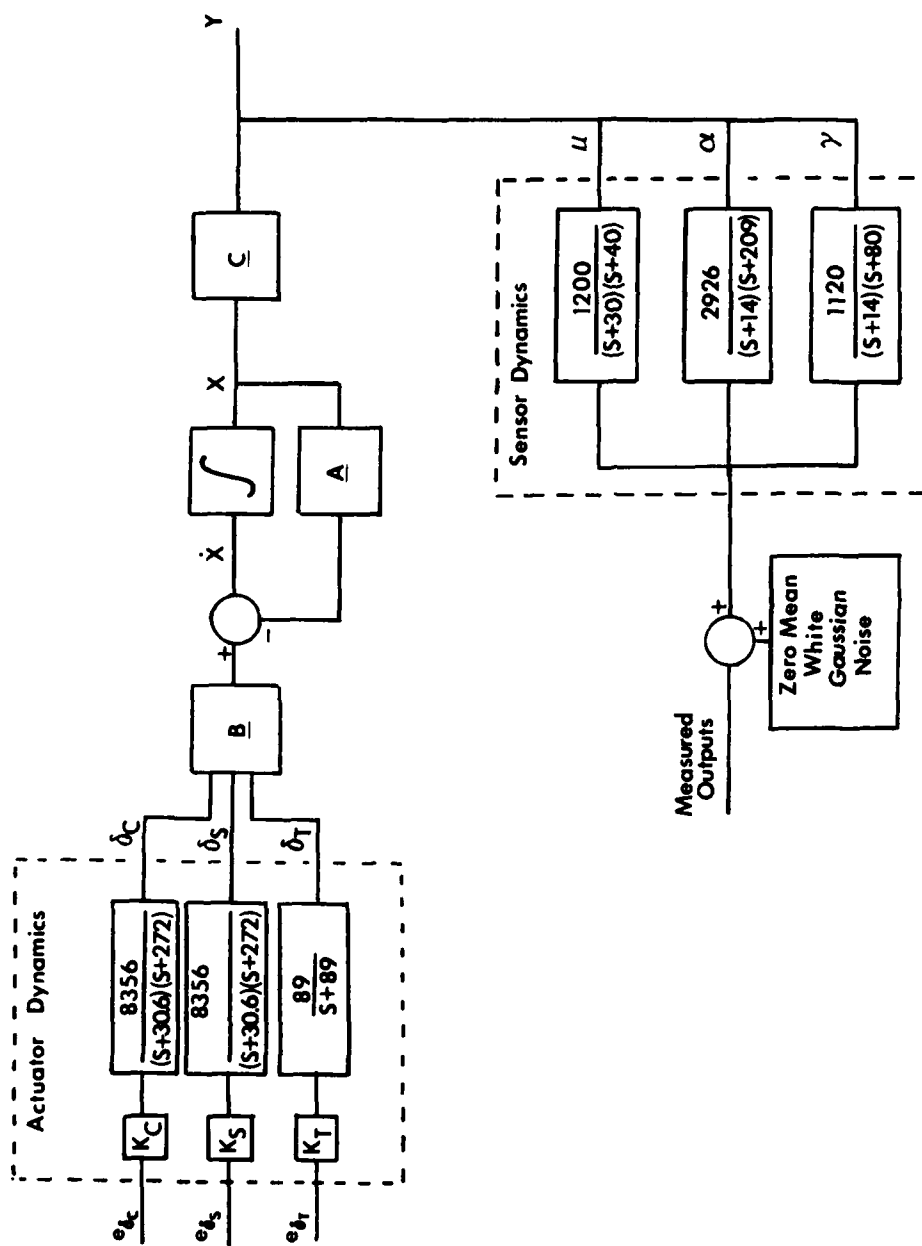


Fig. 3.3. Open Loop Block Diagram

the outputs. The computational time delay for this thesis is chosen to be one sample period (0.025 sec) and its incorporation into the controller design is discussed in Chapter IV.

3.8 Sensor Dynamics and Noise

In the design of aircraft controllers, output quantities being fed back must be measured and as a result the feedback signals are subject to the limitations of imperfect measurement. Two of these limitations are considered in this thesis; sensor dynamics and measurement noise. Like any physical system, sensors are incapable of responding instantaneously to an input (the quantity being measured) but their response is usually well modeled with linear transfer functions similar to actuator dynamics. As with the actuator dynamics, transfer functions for the sensors are entered into the MULTI program independent of the plant, input, or output matrices and are also limited to second order dynamics with no zeros. The data provided by MCAIR again must be altered (Appendix C) to conform to these constraints and the results are shown in Figure 3.3. Measurement noise arises from a variety of sources, each with its own stochastic characteristics. The simplest model, and the one used in this thesis, is a zero-mean, white, Gaussian noise model. Each measured output is corrupted with independent noise, added immediately after the

sensor dynamics, resulting in a vector of measured outputs as shown in Figure 3.3. As with the actuators, the sensor dynamics and noise are constant over all flight conditions.

3.9 Control Surface Nonlinearity

In the derivation of the linear perturbation equations for the aircraft, it is assumed that the deviations from equilibrium are small enough for the forces and moments generated to be linear functions of the deviation. For most of the parameters the deviations can be quite large (as much as 20 degrees) before significant error results. One particular exception is the drag (force in the longitudinal direction) resulting from changes in the angle of attack on the various aerodynamic surfaces. Drag variation with angle of attack is usually dominated by the induced drag, particularly at high angles of attack (5:149). Induced drag varies with the square of the lift coefficient, generally considered a linear function of the angle of attack. The change in drag of a lifting surface at high angles of attack (like the wing of an aircraft in a landing situation) is therefore a parabolic function of the angle of attack. Since the angle of attack of the wing and fuselage of the aircraft varies at most only a few degrees from the equilibrium value (see Chapter V) it is reasonable to treat the wing/body drag as a linear function of angle of attack. At angles of attack near zero

(like control surfaces nearly aligned with the relative wind) the slope of the function is rapidly changing and the function is no longer accurately modeled as linear unless only a very small range of values is considered. The control surfaces, however, can vary as much as 50 degrees in some cases. Of particular importance is that the minimum value of induced drag occurs at zero angle of attack (symmetric airfoil) and in no case is the drag less than zero (it is important to note that this discussion is dealing with the absolute drag and angle of attack, not perturbation values). A linear model results in negative drag (thrust) at negative angles of attack, a situation that grossly misrepresents the physical system. This phenomenon requires an accurate model to have "B" matrix elements that are a function of each surface's angle of attack. From a design perspective a time dependent B matrix would be impractical since the Porter method is dependent upon linear constant coefficient equations. However, it is possible to recreate this phenomenon during the simulation of the aircraft's performance with a controller designed using linear methods. If the data were available, one method of simulating this effect would be to have a table of values for the drag coefficients at various angles of attack for each of the aerodynamic control surfaces. The simulation program could then use the appropriate entry in such a table as the current value of that element of the

"B" matrix. Since the data are not available from MCAIR at this time, an alternative solution is required. The principal objection to the linear model is the apparent creation of thrust by aerodynamic surfaces. In reality, an aerodynamic surface has the capability of reducing drag by decreasing its angle of attack to zero. However, the linear approximation allows the mathematical equivalent of thrust to result from large surface deflections in the opposite direction of the equilibrium deflection for which the linear derivative is accurate. Observing that the derivative of a parabolic drag function is positive for positive angles of attack and negative for negative angles of attack suggests a simple solution to this error. By testing the position of the surface at each step in the simulation, the angle of attack is determined and if necessary the sign of the appropriate control surface derivative is reversed to insure that the drag is always positive. This results in an absolute value function with slopes of plus or minus the equilibrium control surface derivative. This is a crude approximation to the parabolic function, but precludes the erroneous results possible with the linear model. Since drag is defined to be parallel to the relative wind, this force should technically be rotated through the angle of attack for the aircraft prior to being included in a body axis representation of the aircraft equations of motion. This would result in a modification of every element

of the "B" matrix and would require knowledge of equilibrium parameters not currently needed in the simulation. For simplicity, the effects of this phenomenon are assumed to be limited to the elements of the "B" matrix that influence the longitudinal velocity of the aircraft (u). Since the rotation angle (α) is small, this is a reasonable approximation of reality. This approach to the problem is used for this thesis and its implementation is described in Appendix A.

IV. Design Procedure

4.1 Introduction

In the preceding chapters, the background and motivation for this thesis effort and the physical and mathematical characteristics of the STOL F-15 are presented as introductory material for the design procedure, results, and conclusions. This chapter is the first of three chapters that deal with the key elements of the thesis and is devoted to the detailed description of the procedure used to design the longitudinal controllers for the STOL F-15 during landing operations.

The techniques developed by Professor Porter, outlined in Appendix B, although founded in the deterministic mathematics of linear algebra, require considerable trial and error and qualitative assessment of the system response to achieve a satisfactory controller design. The deterministic portion of the design technique is accomplished through use of the computer program MULTI. MULTI is an indispensable tool in the design process, but like any computer program, the quality of the output is merely a reflection of the quality of the input. There are a number of design parameters in the Porter method that are left to the user to define, based on theoretical insight and experience gained during the trial and error process. As the designer

becomes more familiar with this method, the program MULTI, and the characteristics of the system to be controlled, trends can be identified during design parameter selection that lead to a satisfactory design. This chapter describes the design procedure used for this thesis, and an attempt is made to justify design decisions based on quantitative results. Past thesis efforts have suggested that their subjective design procedures can be applied to a general class of problems, presenting a generalized approach (2; 5). Many of the observations contained in these theses prove valuable in this design effort, but in general the design procedures are found to be unique to the system being controlled and the logical thought processes of the designer. As a result, the approach of this thesis is intended to be a description of the route followed in obtaining the specific results of Chapter V.

This chapter begins with mathematical discussions intended to supplement the information in Appendix B, as well as to further justify the choice of output vectors. The design process is then covered in detail, beginning with the basic plant and expanding the design to account for the actuator dynamics, computational delay, sensor dynamics, and control surface nonlinearities. Finally, a demonstration of the controller's sensitivity to parameter variation and output measurement noise is presented.

4.2 Mathematical Considerations

Controllability and Observability. It is a fundamental requirement of any method that the system be completely controllable and observable. Complete controllability implies that every state in the state vector can be driven to any finite value, in a finite time, with a control input of finite magnitude. Controllability is a function of the system plant and input matrix and can be determined by evaluating the system zeros (6:443). If there are no input-decoupling zeros the system is completely controllable. The program ZERO is used to determine the system zeros for this thesis and reveals that there are no input-decoupling zeros for any flight condition. Thus, all of the aircraft models are completely controllable systems. Complete observability requires that every mode of each state appear in at least one element of the output vector. Like controllability, observability is also determined from the system zeros and the absence of output-decoupling zeros indicates complete observability. Output-decoupling zeros are a function of the plant and output matrices. Observability is influenced by the choice of the output vector elements and it is imperative to establish the existence of elements that result in a completely observable system. Fortunately, ZERO shows that there are no output-decoupling zeros regardless of the choice of physically meaningful outputs. Therefore, all of the states

include each of the system modes and the output vector is not restricted due to observability considerations. Porter and Bradshaw have shown that the addition of proportional plus integral feedback control does not change the system controllability and observability provided that some well defined conditions are satisfied (13).

Porter Design Requirements. Although a number of output vectors may be chosen without causing an unobservable mode, the principals of multivariable output feedback control in general and specifically the Porter method place additional restrictions on the desired output variables. Transmission zeros, defined as zeros of the equivalent transfer function representation that block transmission of a particular exponential input, are regions to which some of the slow roots of a system migrate as the gain approaches infinity. Although transmission zeros in the left hand "s" plane do not guarantee stability at all gains, transmission zeros in the right half plane always result in a region of a gain for which the system is unstable. Since determination of gain boundaries in multivariable control is difficult, it is desirable to have all transmission zeros in the left half plane. The existence of a transmission zero at the origin, a condition that results from including pitch rate in the output vector, is a situation that can complicate the search for a satisfactory

design since this may cause a region of gain for which the system is unstable. The location of the transmission zeros affects only the migration pattern of certain roots as a function of gain. At any particular gain the roots of the system are fixed and unaffected by asymptotic properties of the system. Therefore, the location of transmission zeros (slow closed-loop system roots) and asymptotes (fast roots) are significant only during the design process while choosing the various gains (Appendix B). When the number of outputs is equal to the number of inputs (a requirement of the program MULTI) the number of transmission zeros is given by (8):

$$\#Z_t = (n - m) - r \quad (4-1)$$

where

$\#Z_t$ = number of transmission zeros

n = number of states

m = number of outputs

r = rank defect of $\underline{C}_2 \underline{B}_2$

The use of pitch rate as an output results in one transmission zero (at the origin) because $\underline{C}_2 \underline{B}_2$ is of full rank. Failure to feed back pitch rate results in no transmission zeros. However, without pitch rate in the output vector, $\underline{C}_2 \underline{B}_2$ has a rank deficiency of one, and a measurement matrix is required to use Porter's method of determining the

controller gain matrices. The use of a measurement matrix introduces transmission zeros whose locations are dependent on the matrix elements chosen by the designer. It is interesting to note that when the minimum measurement matrix is chosen, the result is equivalent to a minor loop pitch rate feedback with the feedback gain determined by the one measurement matrix entry required. The measurement matrix in this case introduces one transmission zero, located at the negative reciprocal of the pitch rate feedback gain. These findings demonstrate two important facts. First, pitch rate feedback is required for the design method, but pitch rate need not be actively controlled. Second, there must be an additional transmission zero, but its location can be chosen by the designer. Chapter III outlines the practical reasoning for choosing velocity, angle of attack, and flight path as controlled quantities. This section also reveals that feeding pitch rate back in a minor loop, rather than as an output, affords additional control over the asymptotic properties of the system. It is important to realize that changing the gain of the pitch rate feedback affects not only system response to high gain, but also affects the transient response of the system at finite gain. For this reason the designer does not have unlimited authority to arbitrarily choose the location of the transmission zero.

4.3 Design Process

General. The generalized procedure for designing a control law for the most realistic STOL F-15 model (actuators, time delay, sensors, noise, and nonlinear surfaces all included) is to begin with the basic model as a baseline design and to redesign for each of these additional factors one at a time. The effects of actuators and computational time delay with respect to the Porter method have been investigated in the past and are demonstrated in several documents (2; 5). Therefore, the simplest model used for design in this thesis is that of the plant with actuators and computational time delay. However, the basic plant is used for computation of open loop transfer functions and demonstration of the asymptotic characteristics. Unfortunately, once the actuators and computational time delay are included in the simulation, the roots of the complete system are not easily calculated. From that point onward, the design process relies on evaluation of the simulated time response of the system to determine the requirements for changes in the design parameters.

Design Variables. Following is a list of the variables that are available for assigning the asymptotic properties of the system. These variables are defined in Appendix B.

1. Sigma (Σ) matrix diagonal elements.
2. Epsilon (ϵ), the sigma matrix multiplier.
3. Alpha (α), ratio of integral to proportional control.
4. K_g , measurement matrix element (pitch rate feedback gain).

An additional parameter, stabilator actuator gain (K_S), is used as a design variable even though actuator dynamics are actually plant parameters.

Design for the Basic Plant. The state space model of Figure 3.2 (flight condition 1) results in the following LaPlace transfer functions:

$$CE = (s - .3468)(s + 1.998)(s + .02428 - j.07015)(s + .02428 + j.07015) \quad (4-2)$$

$$u(s)/\delta_C(s) = (s + 31.76)(s + .6421 - j.1493)(s + .6421 + j.1493) / CE \quad (4-3)$$

$$u(s)/\delta_S(s) = (s + 15.35)(s + .03081)(s - .06574) / CE \quad (4-4)$$

$$u(s)/\delta_T(s) = (s + .06900)(s + .6661 - j3.068)(s + .6661 + j3.068) / CE \quad (4-5)$$

$$\alpha(s)/\delta_C(s) = (s - 19.49)(s + .9976)(s + .5559) / CE \quad (4-6)$$

$$\alpha(s)/\delta_S(s) = (s + 21.21)(s - .03936)(s + .07535) / CE \quad (4-7)$$

$$\alpha(s)/\delta_T(s) = (s + 4.198)(s - 3.627)(s + .06949) / CE \quad (4-8)$$

$$\gamma(s)/\delta_C(s) = (s + 1.979)(s - .3659)(s - .02897) / CE \quad (4-9)$$

$$\gamma(s)/\delta_S(s) = (s - .2343)(s - .03284) / CE \quad (4-10)$$

$$\gamma(s)/\delta_T(s) = (s + 53.59)(s - .2307) / CE \quad (4-11)$$

These transfer functions are typical of a statically unstable aircraft, characterized by a lightly damped complex pair (phugoid) and two real roots (short period), one of which is positive. Naturally, the first objective of the controller is to stabilize the aircraft, and then the controller is tailored to obtain an acceptable response.

Porter and Bradshaw (13) have shown that the roots of the closed loop system approach very predictable values as the gain approaches infinity. Specifically, in the four state, three output system of this thesis, there are seven closed loop roots divided into two categories, fast roots and slow roots. The fast roots (Z_3) depend on the value of gain and are a function of the elements of diagonal sigma matrix which are selected by the designer.

$$Z_3 = \{\lambda: |\lambda I - g\Sigma| = 0\} \quad (4-12)$$

where $\Sigma = FBK_0$.

The slow roots of the system consist of the union of two sets of roots (Z_1 Z_2), defined by Equations (4-13) and (4-14):

$$Z_2 = \{\lambda: (\lambda + K_q^{-1}) = 0\} \quad (4-13)$$

$$Z_1 = \{\lambda: |\lambda K_0 + K_1| = 0\} \quad (4-14)$$

Selecting the controller matrices K_0 and K_1 so that they differ only by a constant ($\bar{\alpha}$), Equation (4-14) reduces to:

$$z_1 = \{\lambda: (\lambda - \bar{\alpha})^3 = 0\} \quad (4-15)$$

By trial and error, and the observations of Courtheyn (5:51) relating the steady state transfer function, $G(0)$, to the sigma matrix, the following design parameters are found to provide a satisfactory time response to a step input. As described in Appendix B, these parameters define controller matrices, and they result in the system illustrated in Figure 4.1.

$$\underline{\alpha} = .01$$

$$\epsilon = .05$$

$$\Sigma = \begin{bmatrix} 15 & 0 & 0 \\ 0 & .4 & 0 \\ 0 & 0 & .4 \end{bmatrix}$$

$$K_q = .25$$

$$\underline{M} = [0 \quad K_q \quad 0]^T$$

These parameters result in the following asymptotic roots:

Fast Roots

$$z_3 = \{-.75g, -.02g, -.02g\}$$

Slow Roots

$$z_2 = \{-4.0\}$$

$$z_1 = \{-.01, -.01, -.01\}$$

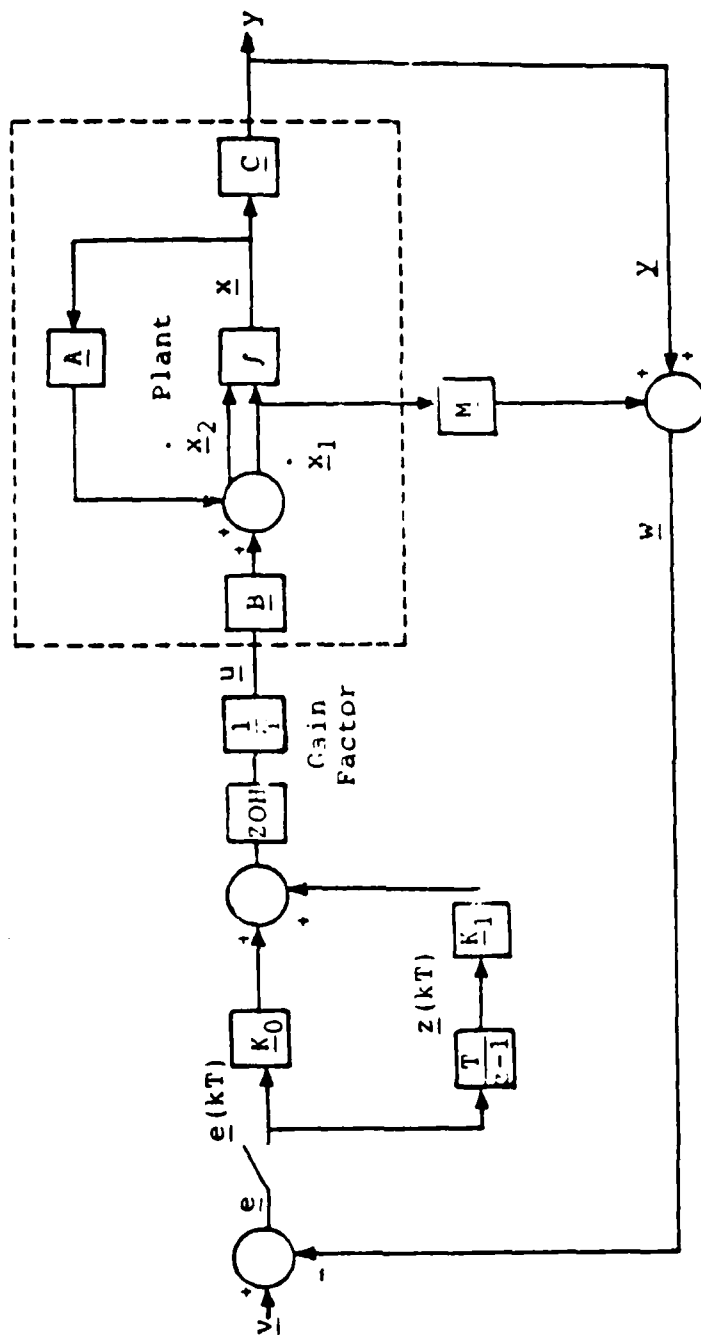


Fig. 4.1. Discrete Closed Loop Block Diagram

Although the gain (g) is fixed for the STOL F-15 model by the reciprocal of the sampling time (40.0), using gain as a variable in this discussion allows demonstration of the asymptotic properties of the system. Table 4.1 compares the asymptotic roots to the actual roots at two different gains to show the progression with higher gain.

Porter and Bradshaw have also shown that as the gain approaches infinity, the input/output transfer function matrix asymptotically approaches a diagonal or near diagonal form, depending on the measurement matrix and choice of output variables (13). If no measurement matrix is used (pitch rate in the output vector) this matrix is always diagonal and contains only the fast roots of the system, thereby exhibiting increasingly tight and decoupled control with increasing gain. However, with a measurement matrix the asymptotic transfer function may not be diagonal, and always includes the transmission zero as a mode that dominates one of the output responses. This results in at least one transfer function that does not exhibit increasingly tight control, and if it is not diagonal, the off-diagonal terms define coupling terms that also contain the transmission zero as a mode, a situation that does not change with increasing gain. It is important to note that if the transmission zero is not due to a measurement matrix, the asymptotic transfer function matrix is diagonal and the mode associated with the transmission zero does not appear

TABLE 4.1

A COMPARISON OF ASYMPTOTIC AND FINITE SYSTEM ROOTS

Gain	Asymptotic Roots	System Roots
40	$-.01 (\bar{\alpha})$	$-.00776 + .001839j$
	$-.01 (\bar{\alpha})$	$-.00776 - .001839j$
	$-.01 (\bar{\alpha})$	$-.01154$
	$-4.0 (K_q^{-1})$	-1.873
	$-.80 (.02g)$	$-.6700 + 1.200j$
	$-.80 (.02g)$	$-.6700 - 1.200j$
	$-30.0 (.75g)$	-30.06
80	$-.01 (\bar{\alpha})$	$-.0120 + .00436j$
	$-.01 (\bar{\alpha})$	$-.0120 - .00436j$
	$-.01 (\bar{\alpha})$	$-.004388$
	$-4.0 (K_q^{-1})$	-2.417
	$-1.6 (.02g)$	$-1.197 + 1.893j$
	$-1.6 (.02g)$	$-1.197 - 1.893j$
	$-60.0 (.75g)$	-60.06

in the matrix. Since the controller integrates the feedback error, the off-diagonal elements have the characteristics of a disturbance rejection transfer function and a final value of zero. Using the procedure of Reference 13, the asymptotic transfer function matrix (Γ) is computed for the design parameters listed previously.

$$\Gamma(\lambda) = \begin{bmatrix} .75g/(\lambda + .75g) & 0 & 0 \\ 0 & 4.0/(\lambda + 4.0) & -\lambda/(\lambda + 4.0) \\ 0 & 0 & .02g/(\lambda + .02g) \end{bmatrix} \quad (4-16)$$

It is evident from (4-16) that the cross-coupling term is not affected by gain and is present regardless of the choice of design variables, although its location can be changed with the pitch rate feedback gain. The significance of this element is that regardless of design parameters chosen, there is coupling of flight path angle and angle of attack. At less than infinite gain this element has an additional term that is a function of gain and the third diagonal element of the sigma matrix (σ_3).

$$\Gamma_{2,3}(\lambda) = (4 - \varepsilon\sigma_3 g)\lambda / (\lambda + 4)(\lambda + \varepsilon\sigma_3 g) \quad (4-17)$$

Judicious selection of σ_3 may help to reduce the coupling but might also degrade the desired tracking response. Of course, the actual system cannot operate with infinite gain, and Figures 4.2 through 4.10 are the step responses

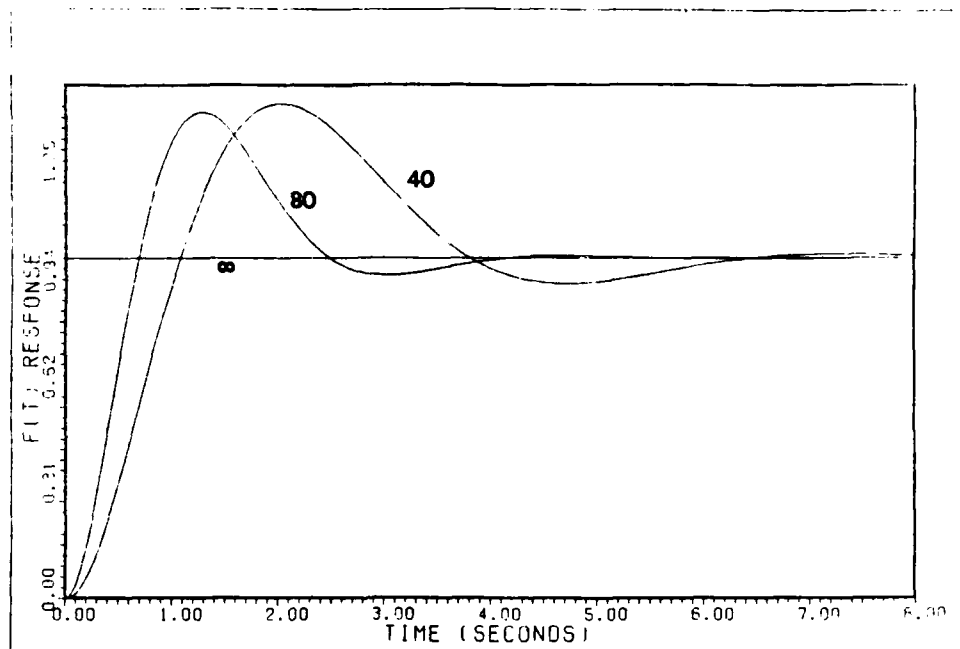


Fig. 4.2. Step Response $\Gamma(1,1)$, $g = 40, 80, \infty$

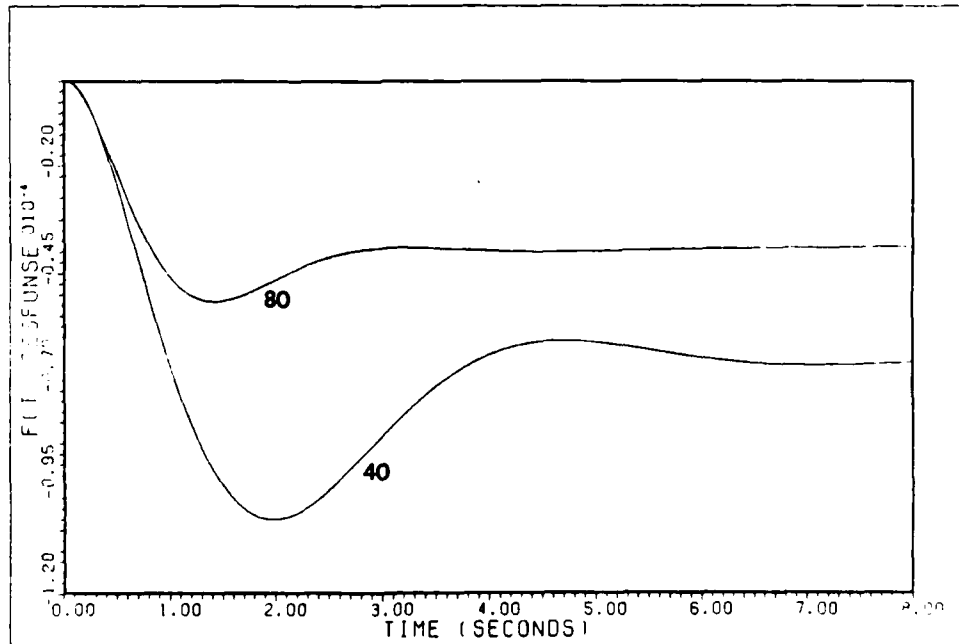


Fig. 4.3. Step Response $\Gamma(1,2)$, $g = 40, 80$

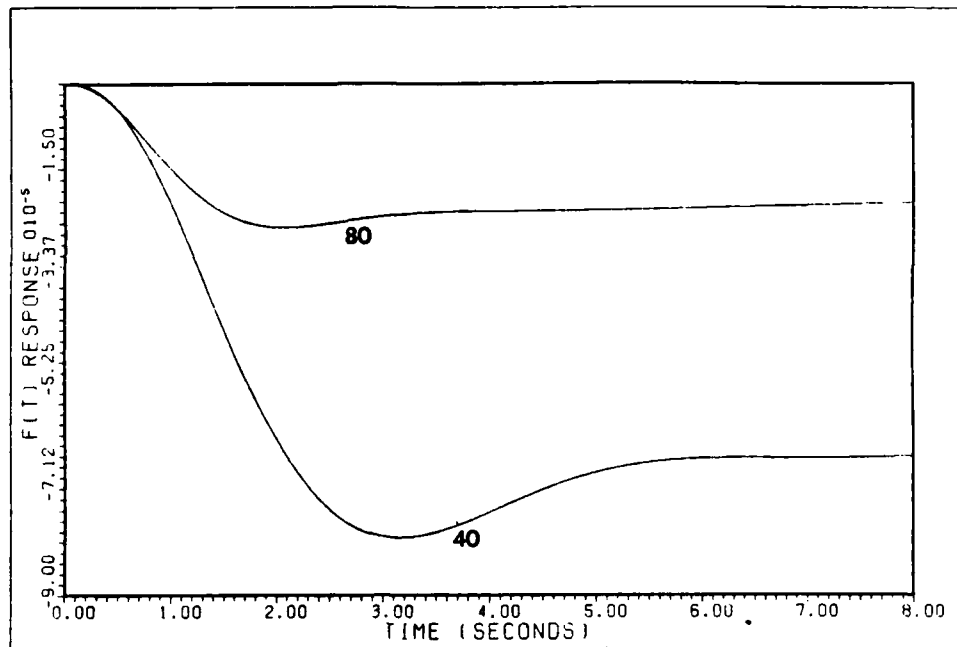


Fig. 4.4. Step Response $\Gamma(1,3)$, $g = 40, 80$

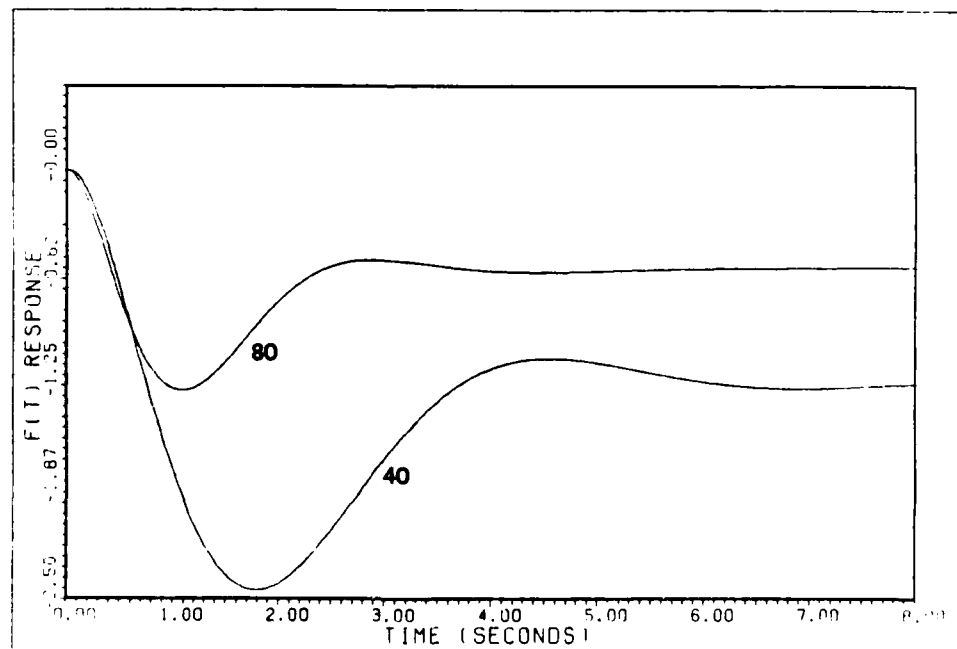


Fig. 4.5. Step Response $\Gamma(2,1)$, $g = 40, 80$

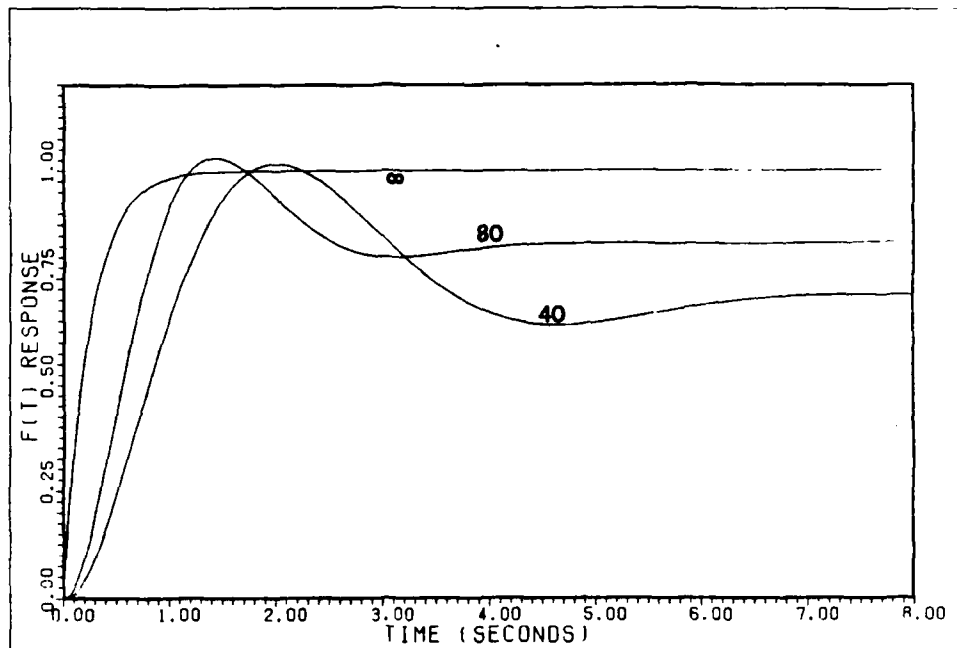


Fig. 4.6. Step Response, $\Gamma(2,2)$, $g = 40, 80, \infty$

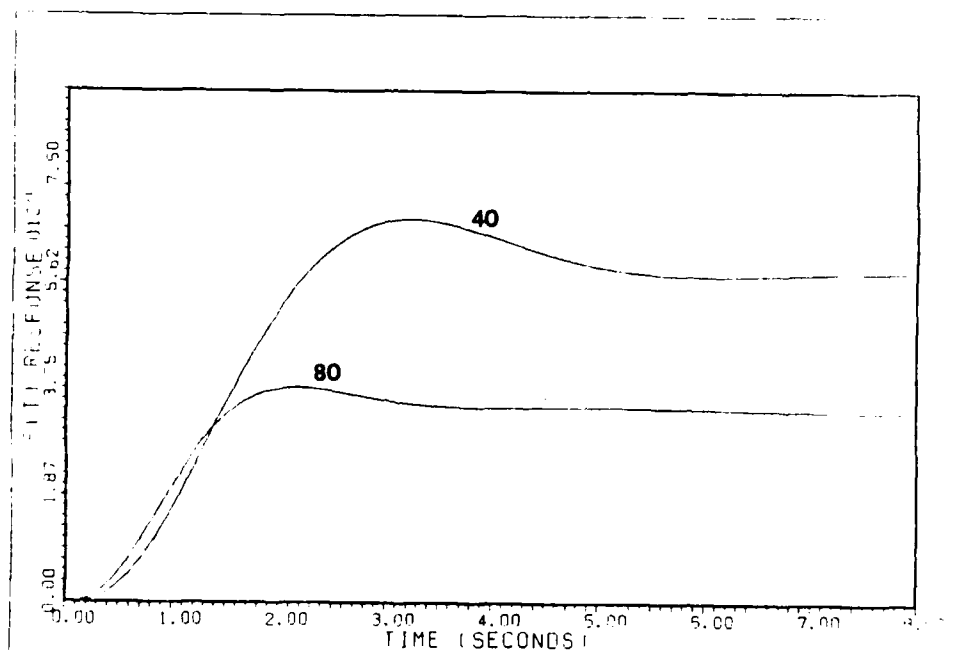


Fig. 4.7. Step Response, $\Gamma(2,3)$, $g = 40, 80$

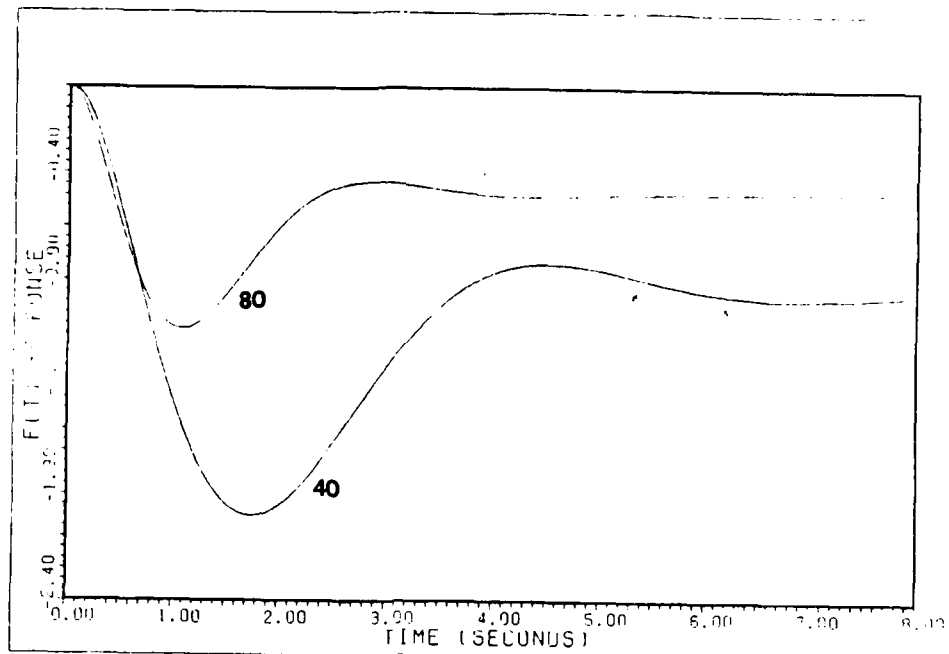


Fig. 4.8. Step Response $\Gamma(3,1)$, $g = 40, 80$

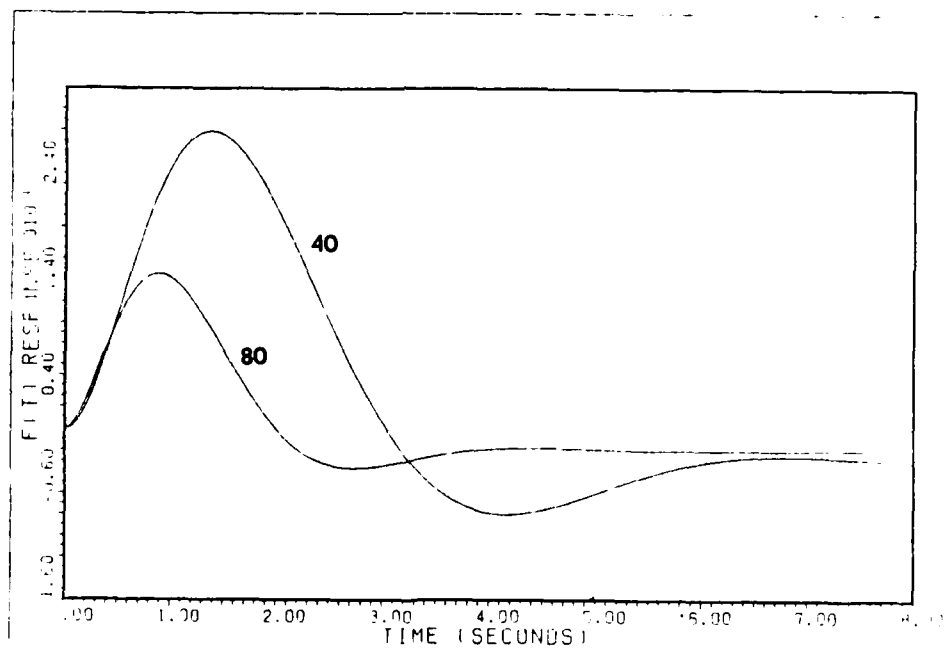


Fig. 4.9. Step Response $\Gamma(3,2)$, $g = 40, 80$

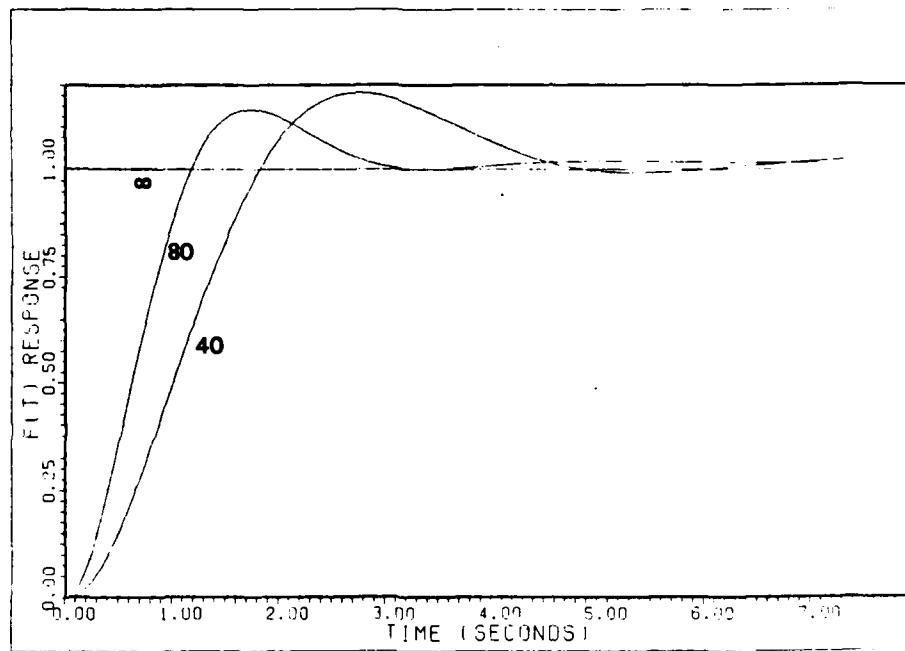


Fig. 4.10. Step Response $\Gamma(3,3)$, $g = 40, 80, \infty$

for the actual transfer functions and show that at finite gains the system exhibits reasonably tight tracking in the diagonal elements. Also, that there is significant coupling that is not predicted by the asymptotic properties, particularly in the output responses corresponding to the velocity input command.

Actuator Dynamics and Computational Time Delay.

Once actuators and time delay are included in the system simulation, the program does not compute all of the closed-loop system roots. To design a controller under these and all subsequent considerations, the linear characteristics of the system are used to estimate an acceptable control law, and then a complete simulation is performed. An iterative technique is used to find a controller that results in an acceptable time response. Rather than discuss the results of each step in the iterative process, this thesis presents examples of the effects of the principal parameters used to achieve the desired results. Since the inclusion of the various "real world" effects does modify the performance, it is important to consider the practical aspects of aircraft flight control systems. The first of these practical aspects to limit the flexibility of controller design is control surface saturation. The previous section shows the possible methods of influencing the transient response by manipulating the system's

asymptotic properties. However, the control surface authority limits the choice of design variables dramatically. In fact, after stabilizing the aircraft, the most difficult problem encountered is obtaining a reasonably fast, critically damped response without surface deflections that exceed the physical limits. In all design cases, the input to the system is that of a six degree decrease in flight path angle from level flight, and the desired output is a smooth and non-oscillatory flight path response with little or no change in angle of attack and velocity. This input, although not the maximum possible based on the steady-state transfer function, is chosen as a reasonably challenging input command for a jet aircraft. Table 4.2 lists the maximum steady-state flight path change and the limiting surface for each flight condition. The maximum possible command input for this aircraft is not limited by the steady state control surface requirements but by the transient overshoot in the control surfaces. Although not shown in Table 4.2, the transient control surface deflections for the maximum maneuver at any flight condition must not exceed the deflection limits. To assist in minimizing initial control surface overshoot the commanded input is slightly ramped (0.8 seconds) and smoothed. Two additional inputs are considered to simulate an aborted landing situation and the final roundout/flare for touchdown. The designs are not altered for these maneuvers, rather the adaptability of

TABLE 4.2
MAXIMUM STEADY STATE MANEUVER

Flight Condition*	Maximum Flight Path Change	Limiting Surface
1	48.7 degrees	rotating vanes
2	25.7 degrees	stabilator
3	14.3 degrees	stabilator
4	15.5 degrees	canard
5	17.2 degrees	canard
6	11.5 degrees	canard

*See page 22 for flight conditions.

landing approach designs to other maneuvers appropriate to the flight condition is demonstrated.

1. Sigma Weighting Matrix. It is difficult to identify one parameter to use to achieve a particular effect, but several trends are evident from analysis of the system response. The following paragraphs describe these trends and present graphical justification. Analysis of the asymptotic transfer function indicates that at high gain the first output (velocity) should be uncoupled from the other two and the principal control variable is the corresponding sigma matrix element. The velocity can be controlled relatively independently of the other two outputs as is demonstrated in Figures 4.11 through 4.14.

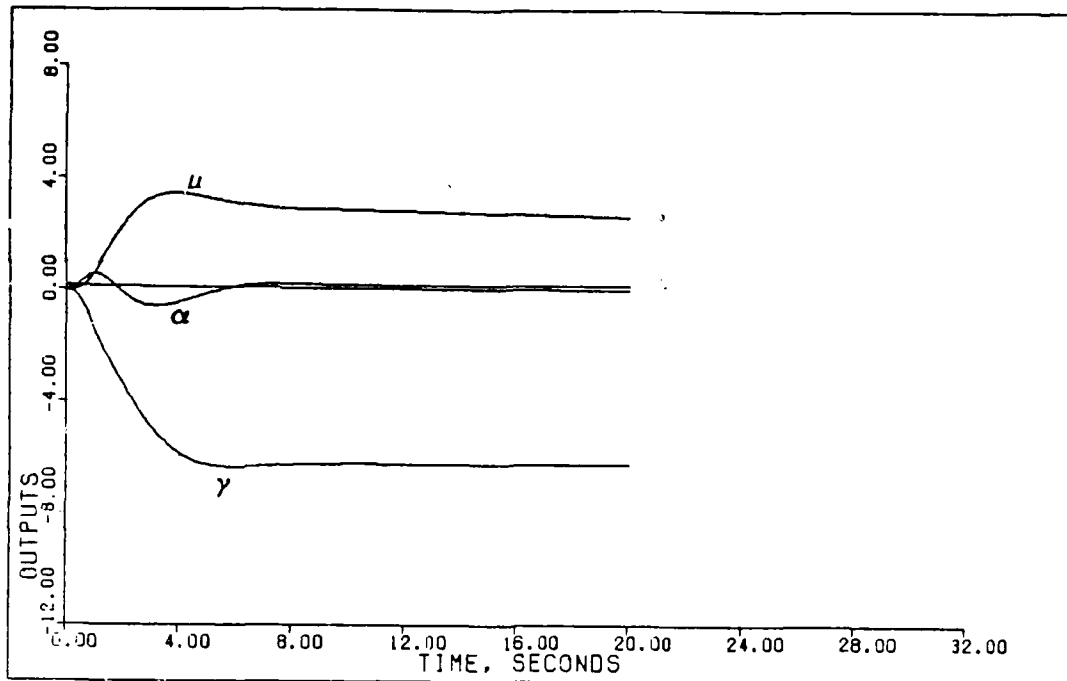


Fig. 4.11. Outputs, $\sigma_1 = 1$

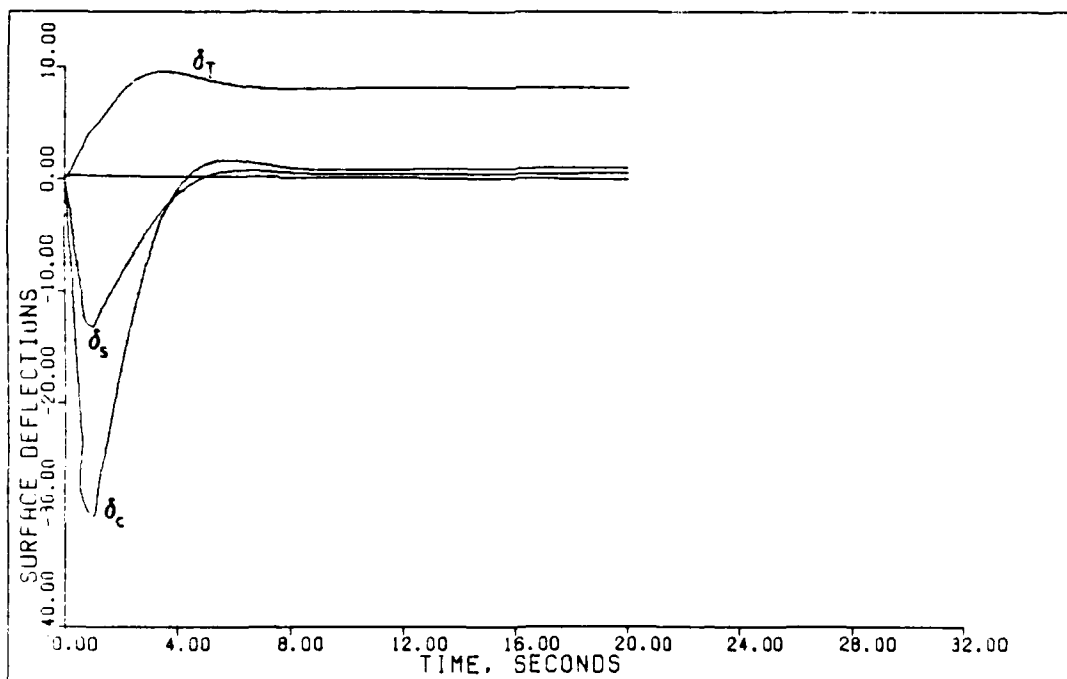


Fig. 4.12. Surface Deflection, $\sigma_1 = 1$

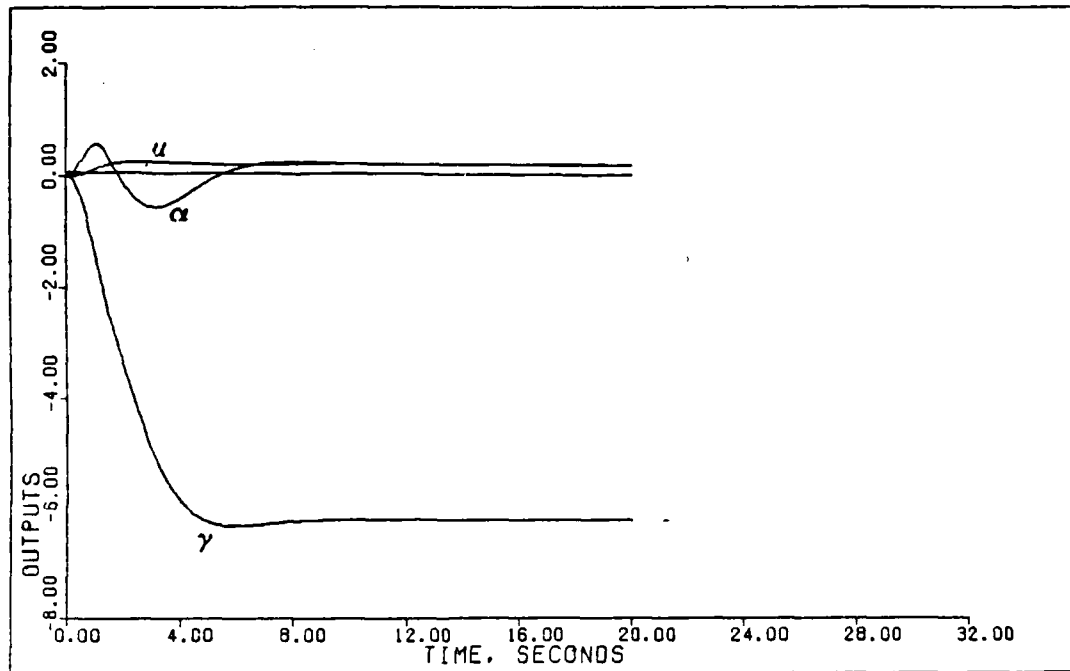


Fig. 4.13. Outputs, $\sigma_1 = 15$

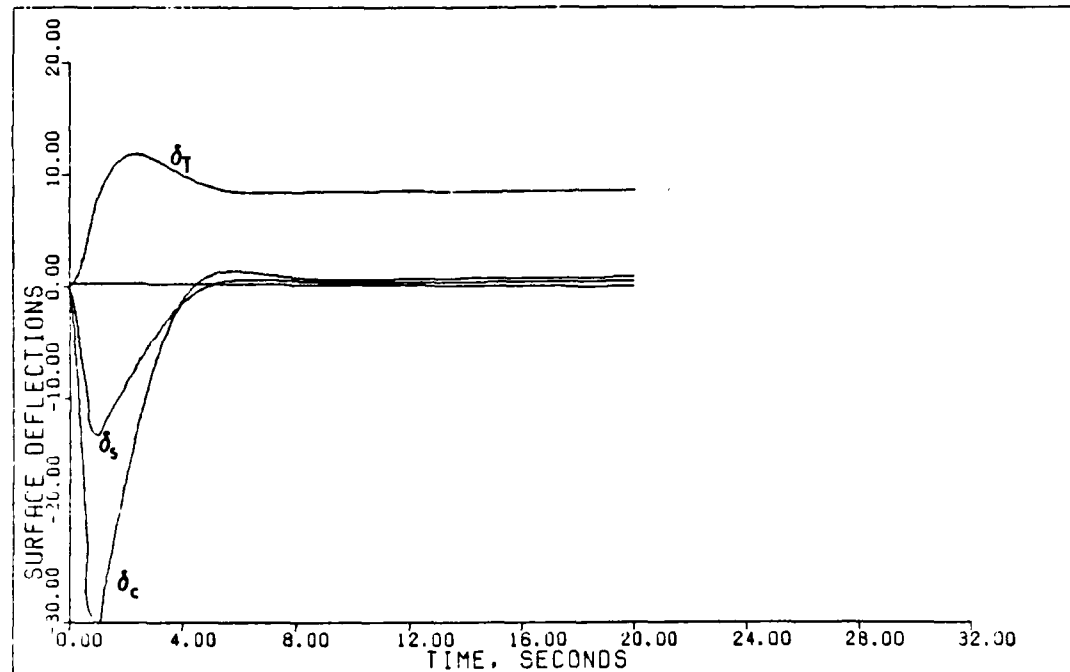


Fig. 4.14. Outputs, $\sigma_1 = 15$

As the sigma element corresponding to velocity is increased, the velocity transient diminishes without significantly changing the other two outputs. As the asymptotic transfer function matrix suggests, the angle of attack and flight path are not decoupled and changing either of the two corresponding sigma elements influences both outputs (Figures 4.15, 4.16, and 4.17). Changing the σ_3 element to minimize coupling (Equation (4-17)) proves to be impractical due to the control surface deflection and rate requirements. Thus, choosing $\sigma_3 = 2$ theoretically eliminates coupling but is prohibitive from a practical standpoint as it results in system instability. Obviously, roots that do not appear in an asymptotic analysis do influence the system response.

2. Integrator Gain. As discussed earlier, the ratio of integral to proportional control defines three slow roots that do not appear in any of the asymptotic transfer functions. However, at finite gains, the slow roots are observable and significantly influence the outputs. Figure 4.18 shows how increasing integral gain causes overshoot in the commanded output. This situation can cause considerable variation in the apparent steady state response of the system as flight conditions change, since the step response may not settle within the time period of interest. This phenomenon is not shown here but can be seen in the following chapter. It is important to

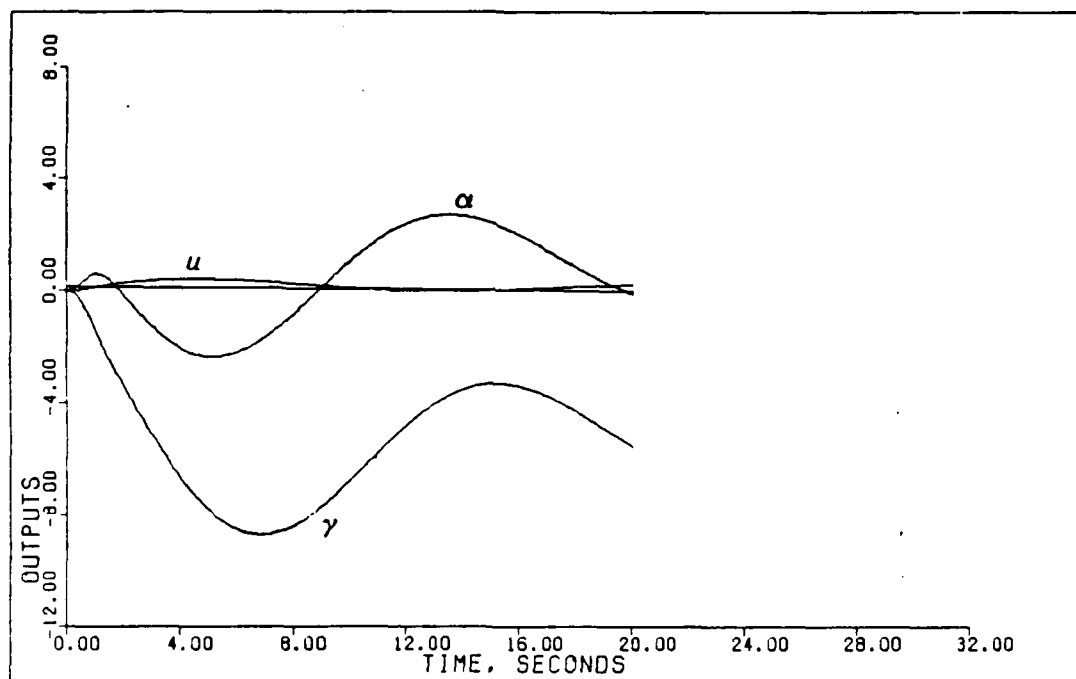


Fig. 4.15. Outputs, $\sigma_2 = .1$

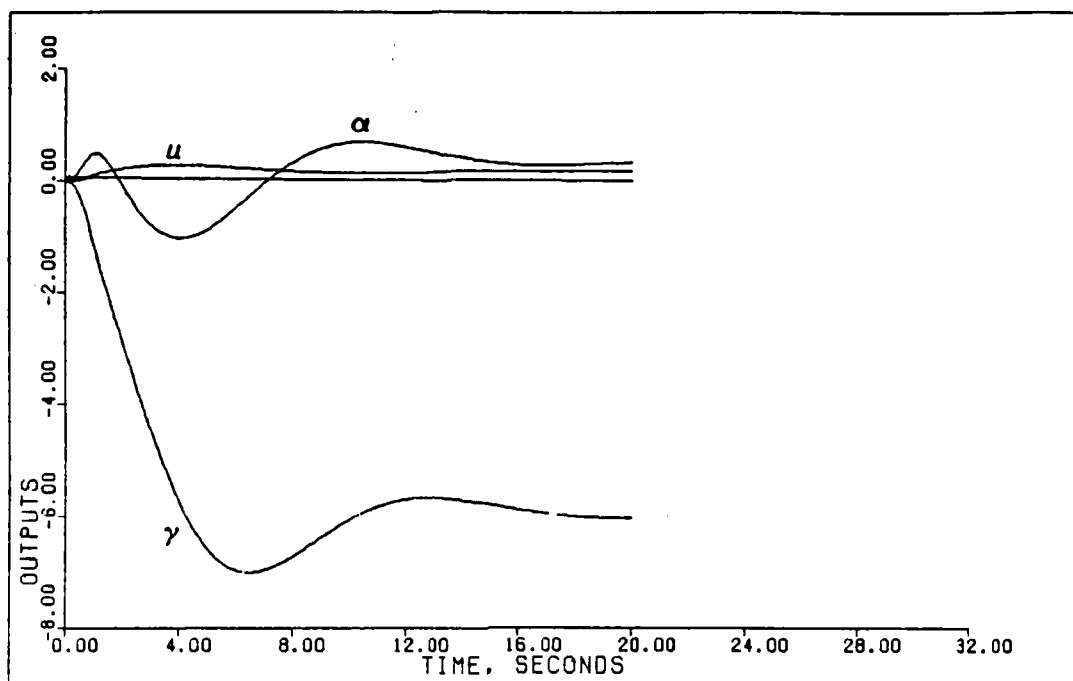


Fig. 4.16. Outputs, $\sigma_2 = .25$

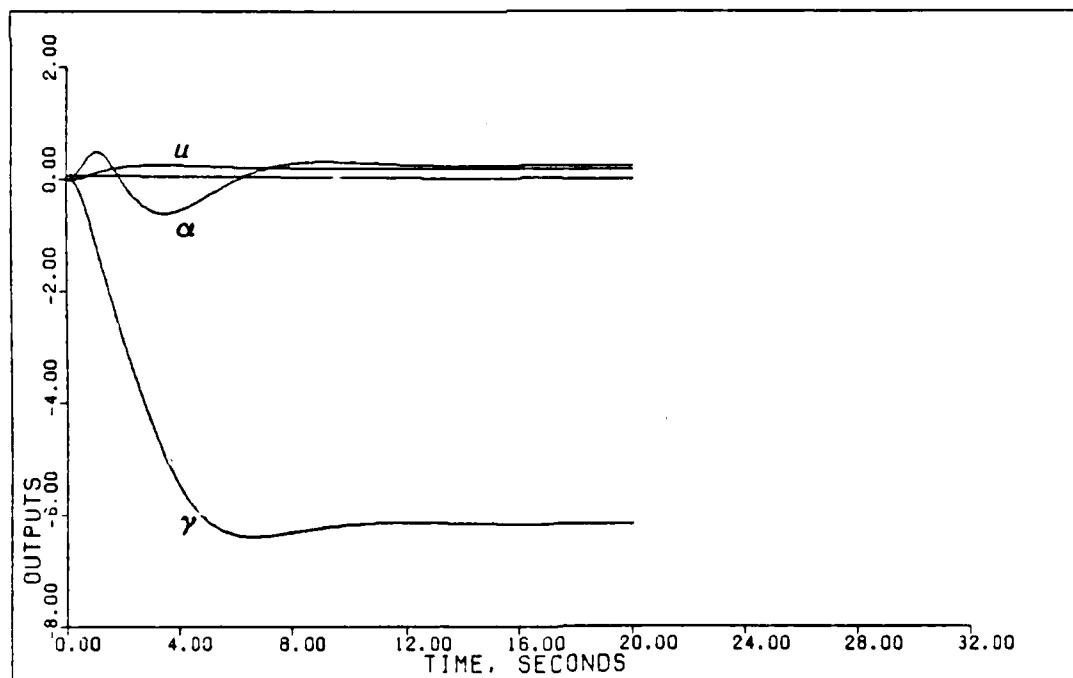


Fig. 4.17. Outputs, $\sigma_2 = .40$

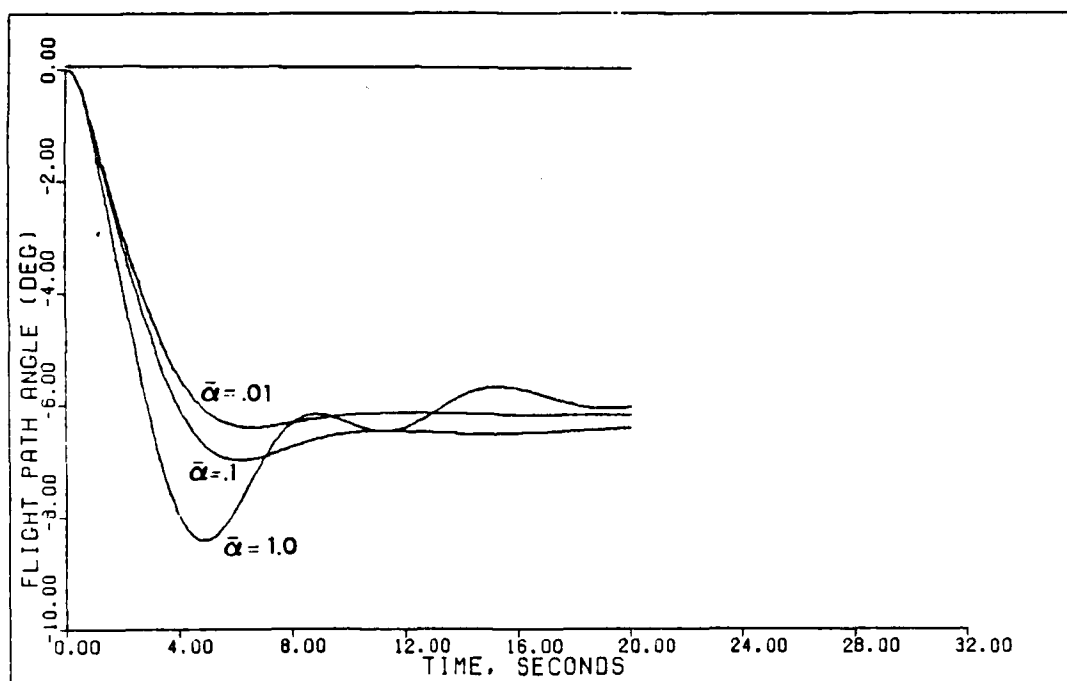


Fig. 4.18. Flight Path Angle, $\bar{\alpha} = .01, .10, 1.0$

realize that pilots expect changes in the response of their aircraft with changing airspeed, altitude, and gross weight, and it is a fundamental aspect of learning to fly a particular aircraft.

3. Actuator Gain. The gain of each of the surface actuators may also be adjusted and, in particular, the stabilator actuator gain (K_s) proves useful in reducing surface and output oscillations. Figures 4.19 through 4.24 show that increasing the stabilator actuator gain by 25 percent ($K_s = 1.25$) damps the oscillation and further increase results in an overdamped response.

4. Pitch Rate Feedback. As discussed previously in this chapter, the measurement matrix results in a minor loop feedback of the pitch rate. It is important to point out that this is not pitch rate or pitch damping control because the pitch rate is not compared to a commanded pitch rate or pitch angle. It is included as a signal to augment the angle of attack feedback signal. Therefore, the pitch rate feedback gain should not be expected to affect primarily pitch damping as predicted by conventional methods (10:59). However, it is obvious from Figures 4.25 through 4.30 that the pitch rate feedback gain most definitely influences the system's oscillation, and increasing gain results in increased damping.

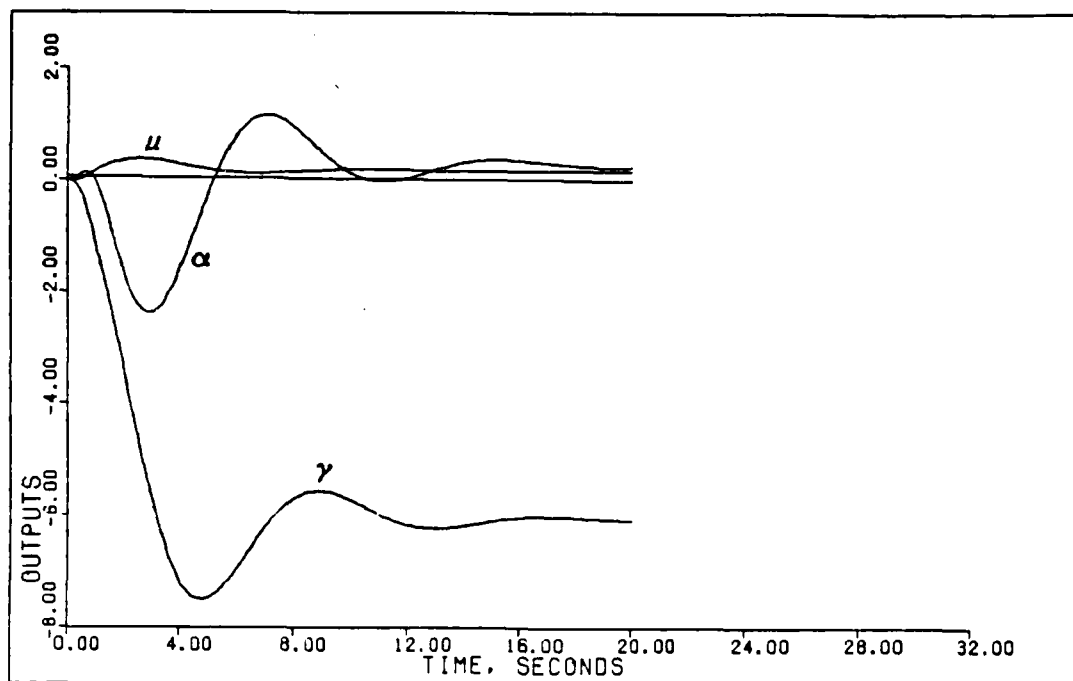


Fig. 4.19. Outputs, $K_s = 1$

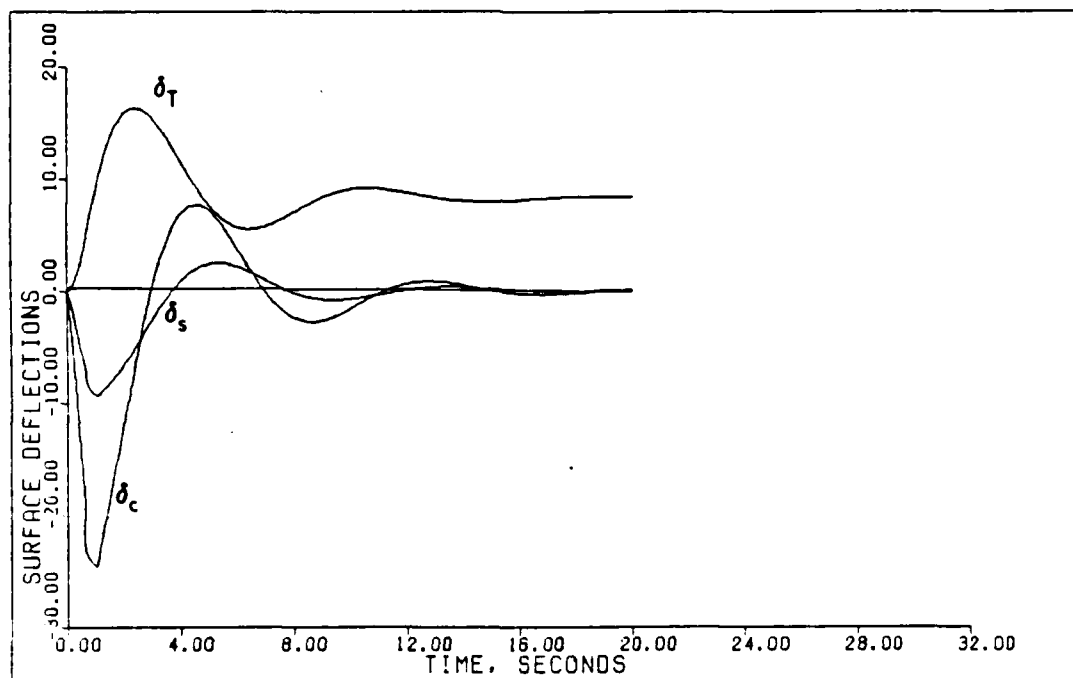


Fig. 4.20. Surface Deflection, $K_s = 1$

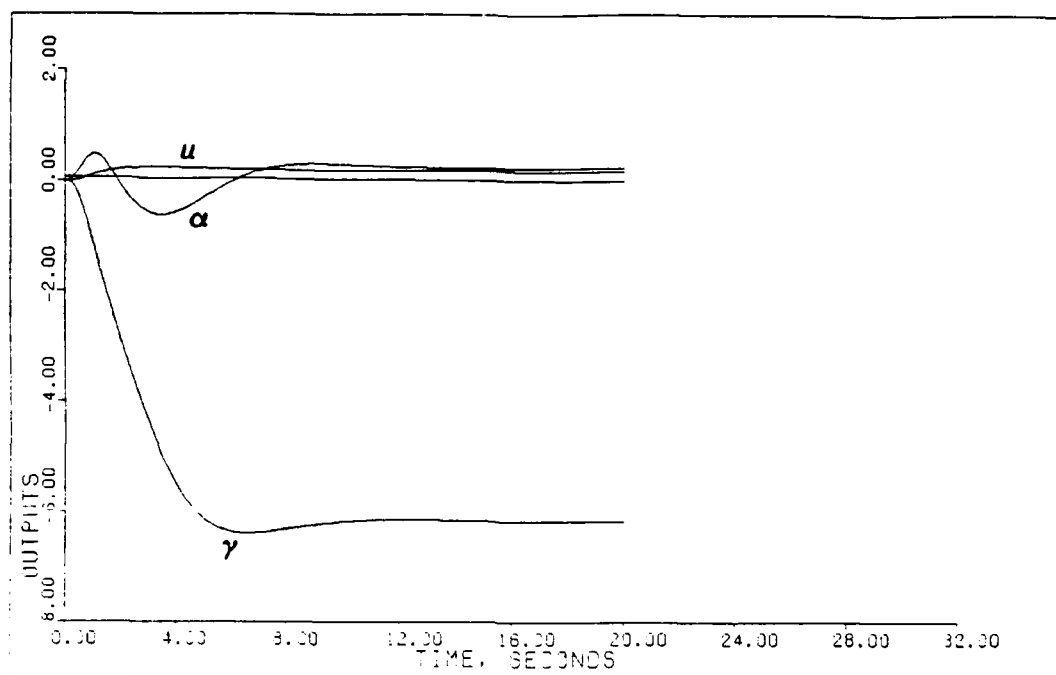


Fig. 4.21. Outputs, $K_s = 1.25$

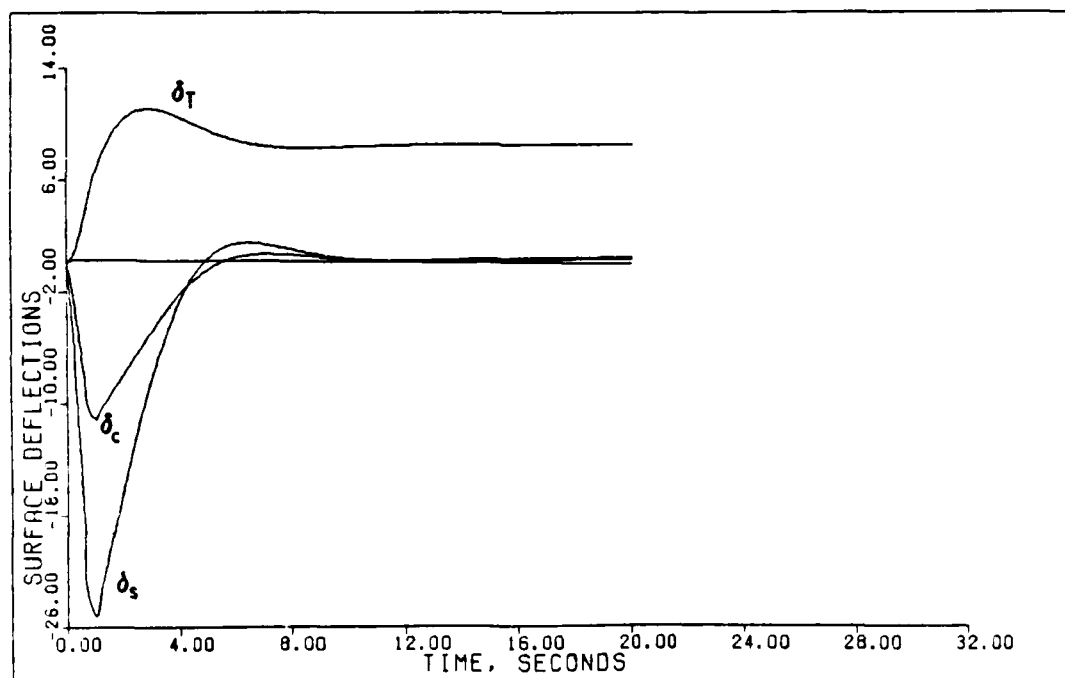


Fig. 4.22. Surface Deflection, $K_s = 1.25$

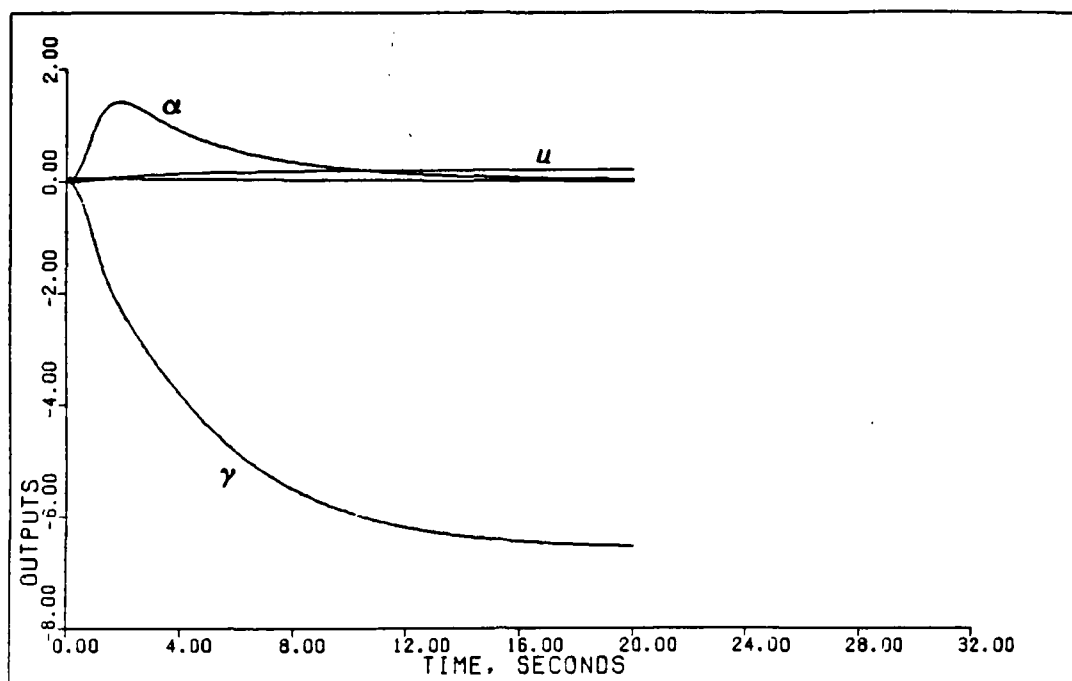


Fig. 4.23. Outputs, $K_s = 1.5$

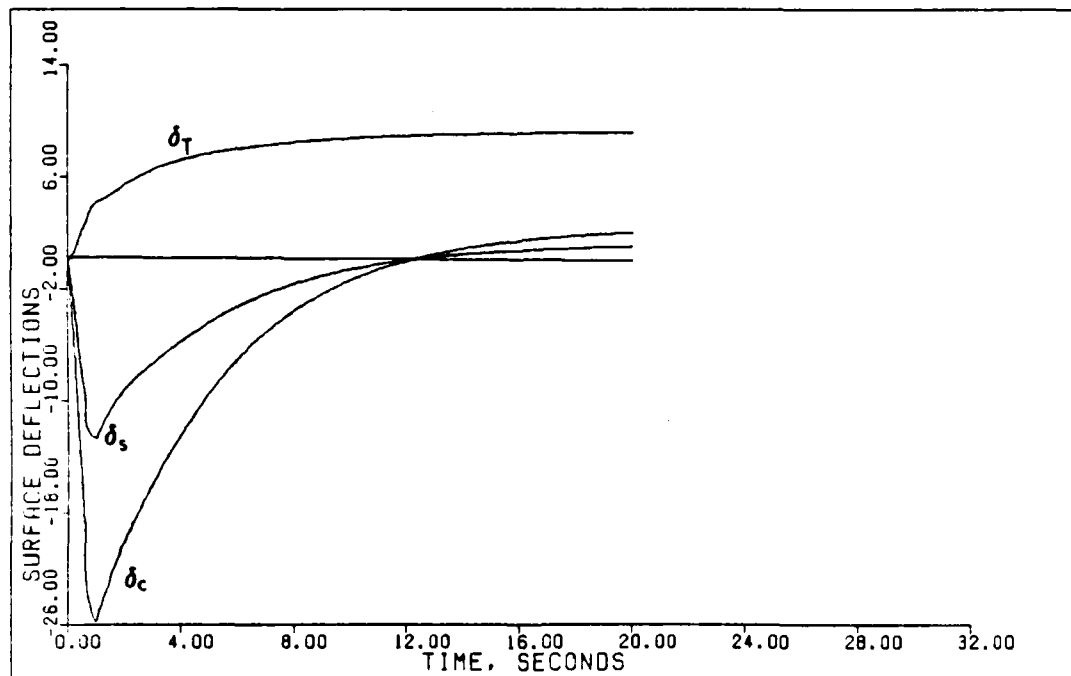


Fig. 4.24. Surface Deflection, $K_s = 1.5$

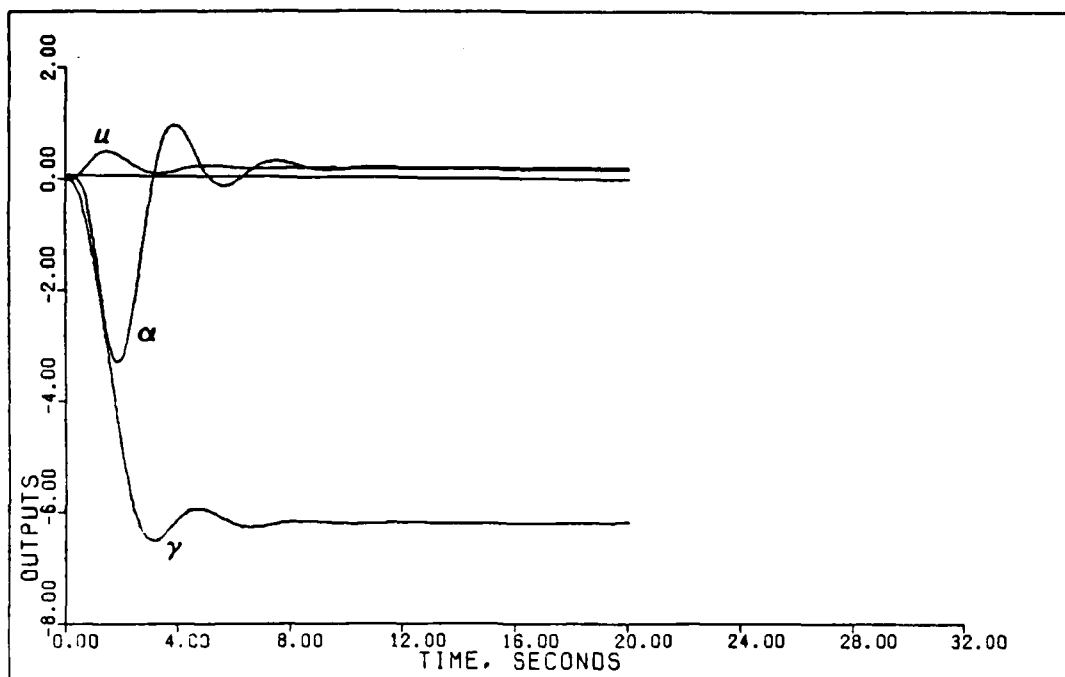


Fig. 4.25. Outputs, $K_q = .1$

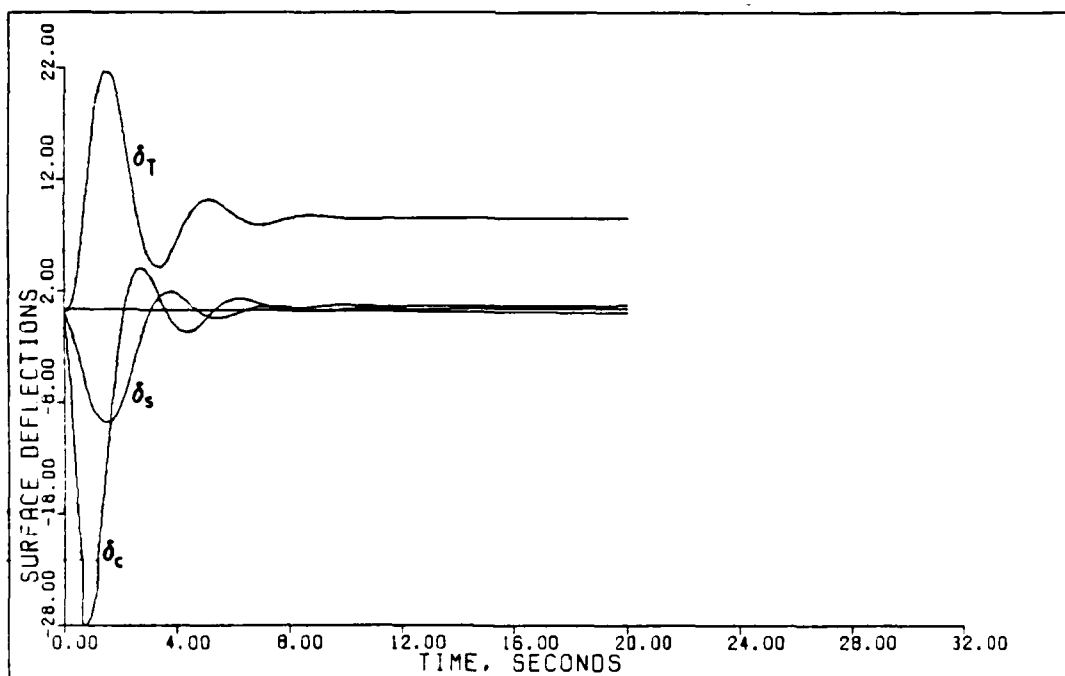


Fig. 4.26. Surface Deflection, $K_q = .1$

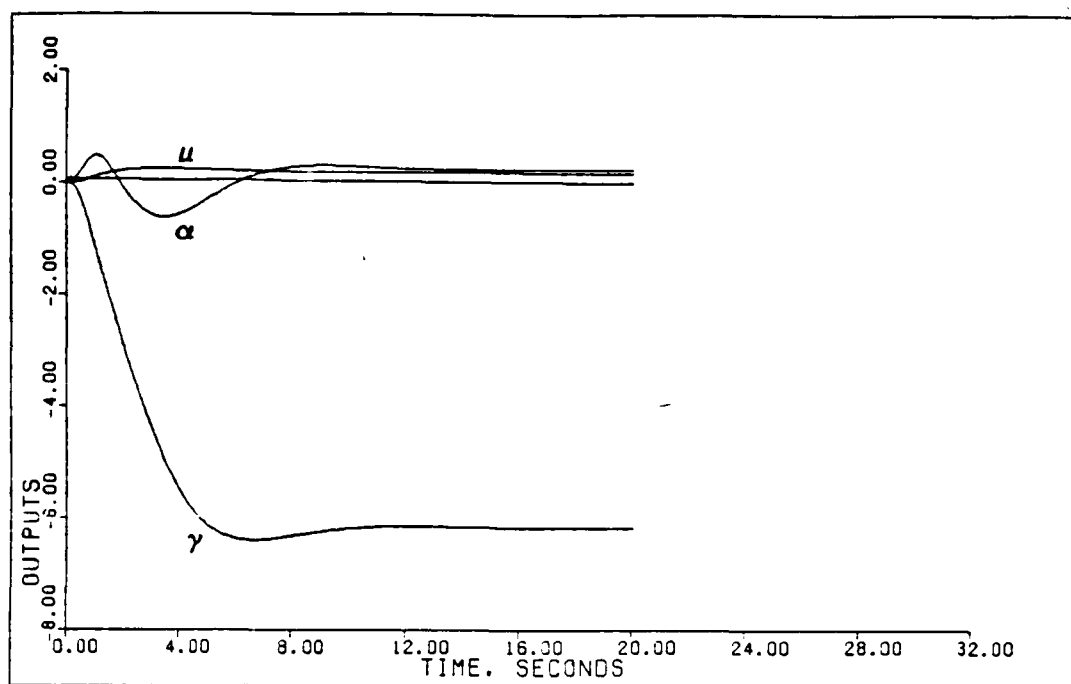


Fig. 4.27. Outputs, $K_q = .25$

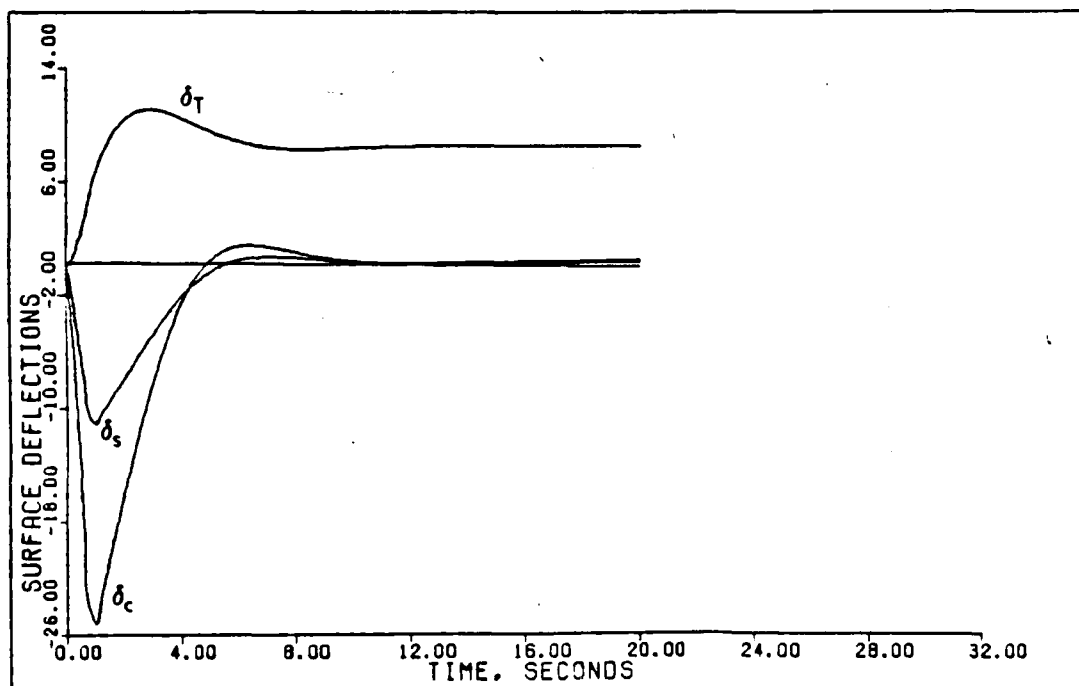


Fig. 4.28. Surface Deflection, $K_q = .25$

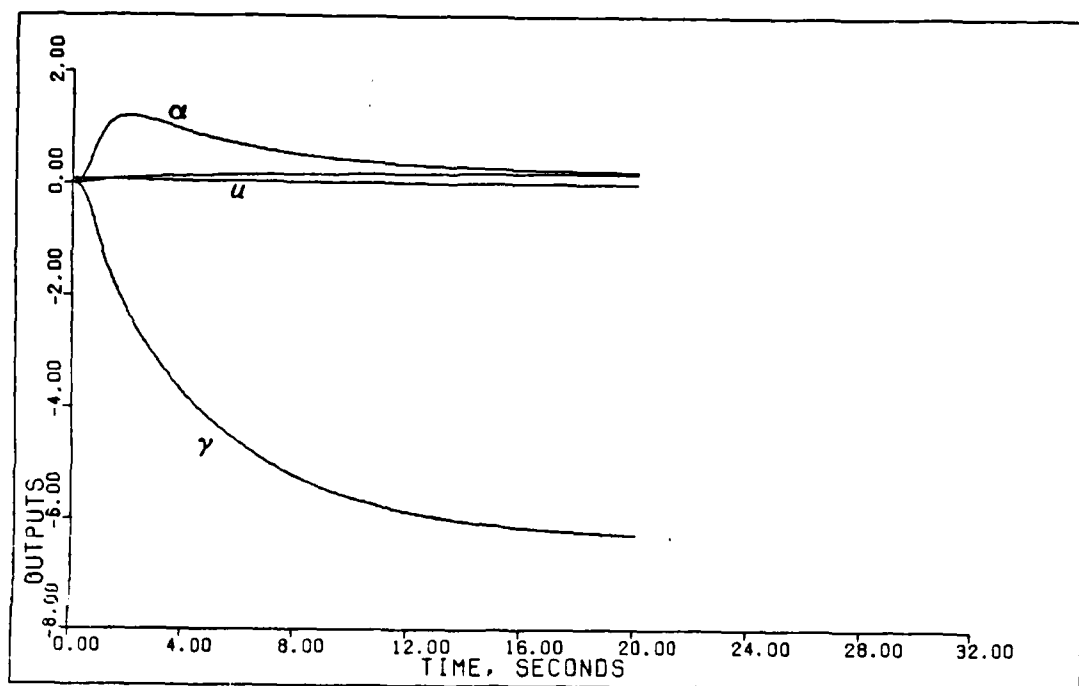


Fig. 4.29. Outputs, $K_q = .35$

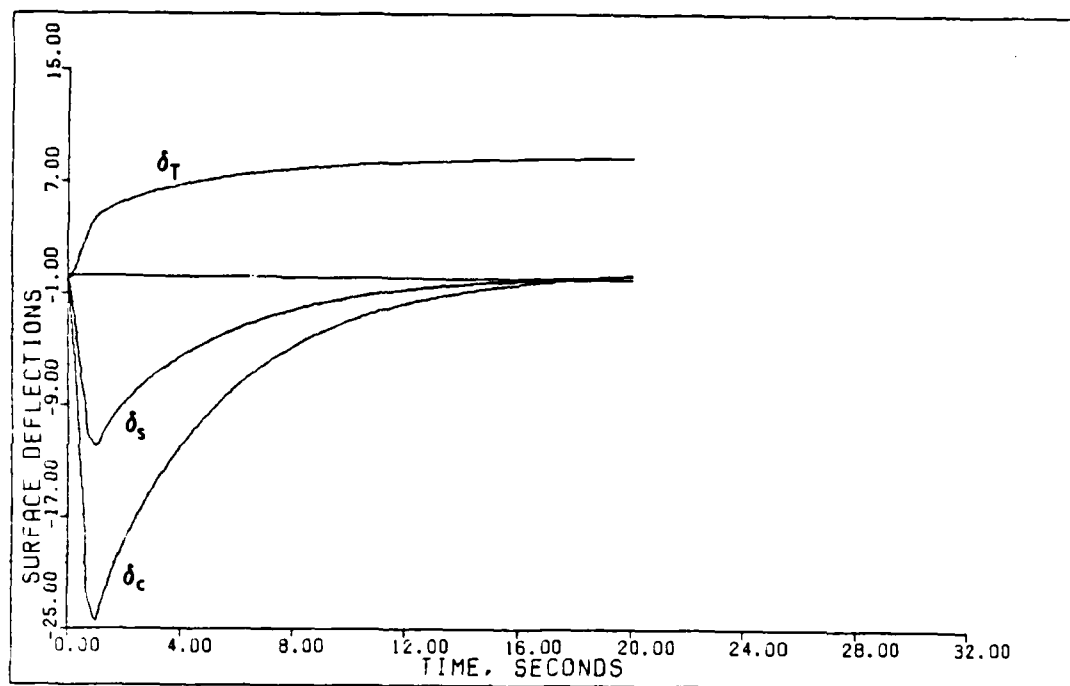


Fig. 4.30. Surface Deflection, $K_q = .35$

Sensor Dynamics. The addition of sensor dynamics tends to destabilize the system response and is generally compensated for by reduction of the gain (sigma matrix multiplier) and minor modification of the sigma weighting elements. The same qualitative trends observed in the design of the basic plant with actuators and time delay hold true with the addition of sensors but usually changing other parameters is not required. A complete presentation of the results of applying these observations are contained in Chapter V.

Control Surface Nonlinearity. Simulating the control surface nonlinearity described in the preceding chapter also produces some mild instability in some cases. The situation is easily remedied by a reduction in either the first sigma matrix element or epsilon. The source of this instability is probably the point discontinuity in the control surface derivatives as they pass through zero angle of attack. In reality, the function is a smooth parabolic arc and should not cause the erratic behavior of Figure 4.32. Even with the discontinuity of the surfaces, the outputs (Figure 4.31) are not significantly affected. Figures 4.33 and 4.34 show the surface deflections and outputs after the sigma elements are adjusted.

Parameter Variation. To demonstrate the ability of the design method to provide satisfactory control in the

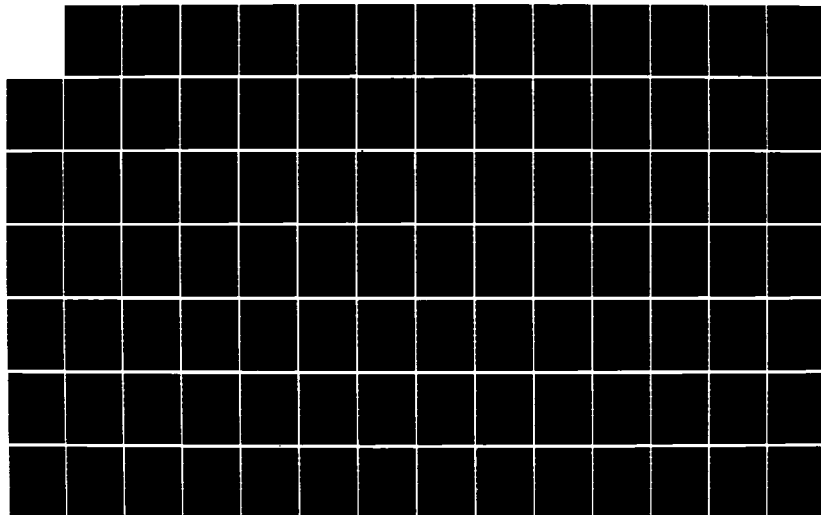
AD-A164 516

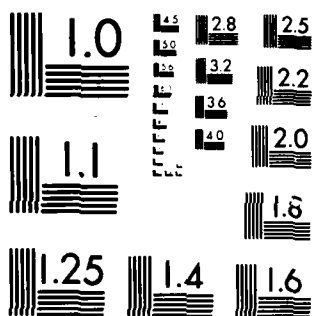
MULTIVARIABLE OUTPUT CONTROL LAW DESIGN FOR THE STOL
(SHORT TAKEOFF AND L. (U) AIR FORCE INST OF TECH
WRIGHT-PATTERSON AFB OH SCHOOL OF ENGI.. B H ACKER
DEC 85 AFIT/GE/ENG/85D-1 F/G 1/2

2/4

UNCLASSIFIED

NL





MICROCOPY RESOLUTION TEST CHART
NATIONAL BUREAU OF STANDARDS-1963-A

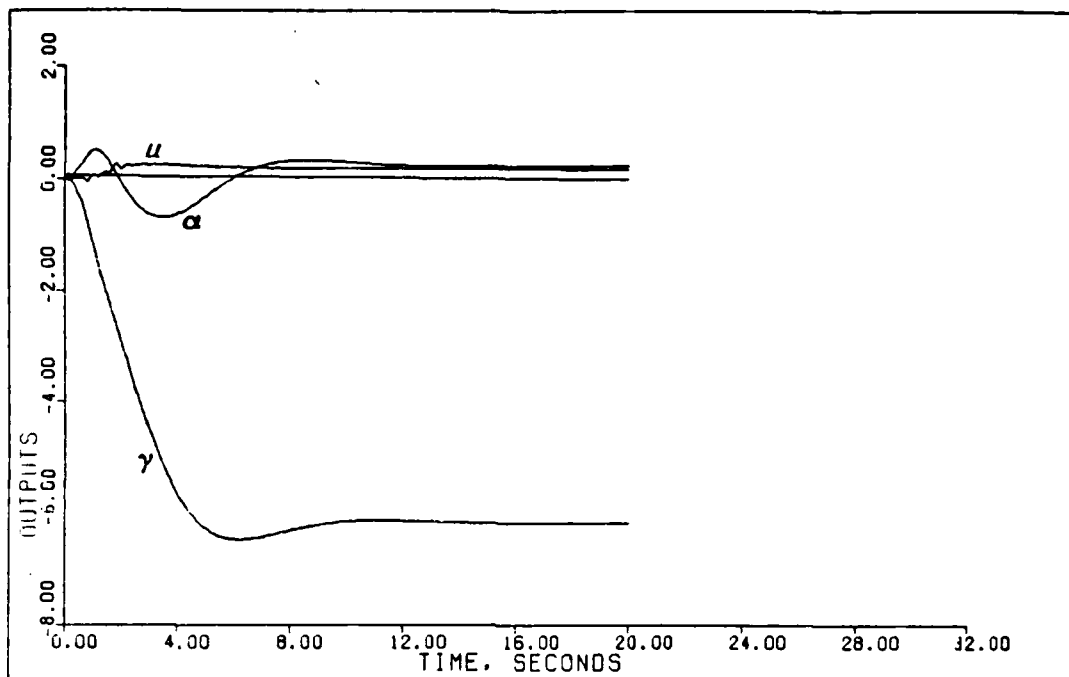


Fig. 4.31. Outputs, $\sigma_1 = 15$, $\sigma_2 = .4$, $\sigma_3 = .4$

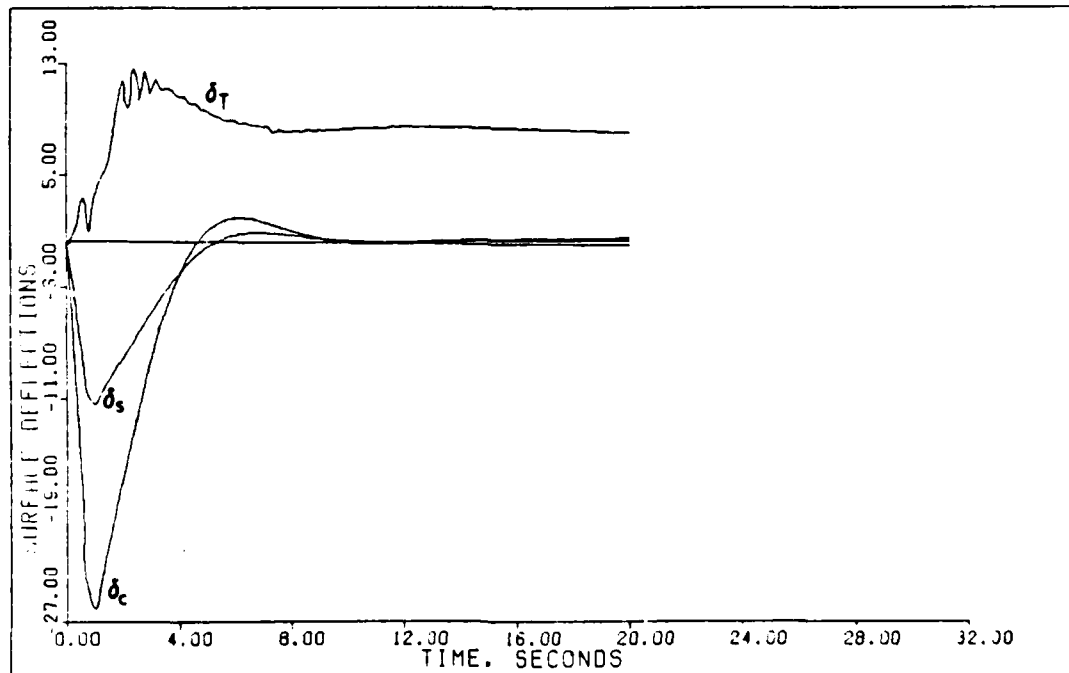


Fig. 4.32. Surface Deflections, $\sigma_1 = 15$, $\sigma_2 = .4$, $\sigma_3 = .4$

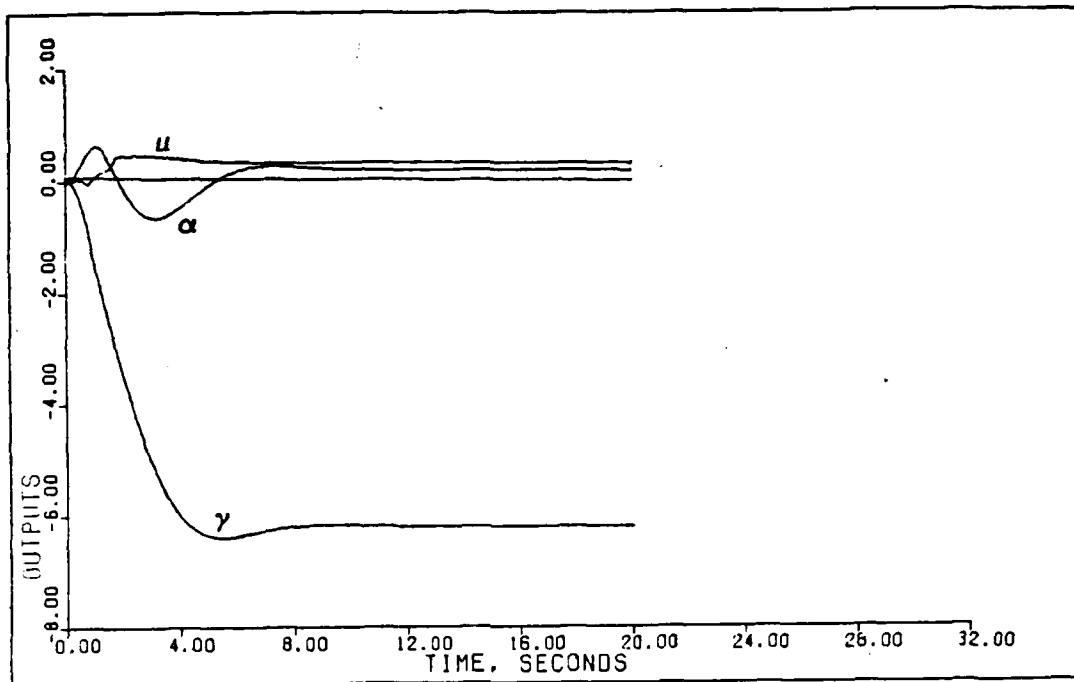


Fig. 4.33. Outputs, $\sigma_1 = 10$, $\sigma_2 = .55$, $\sigma_3 = .55$

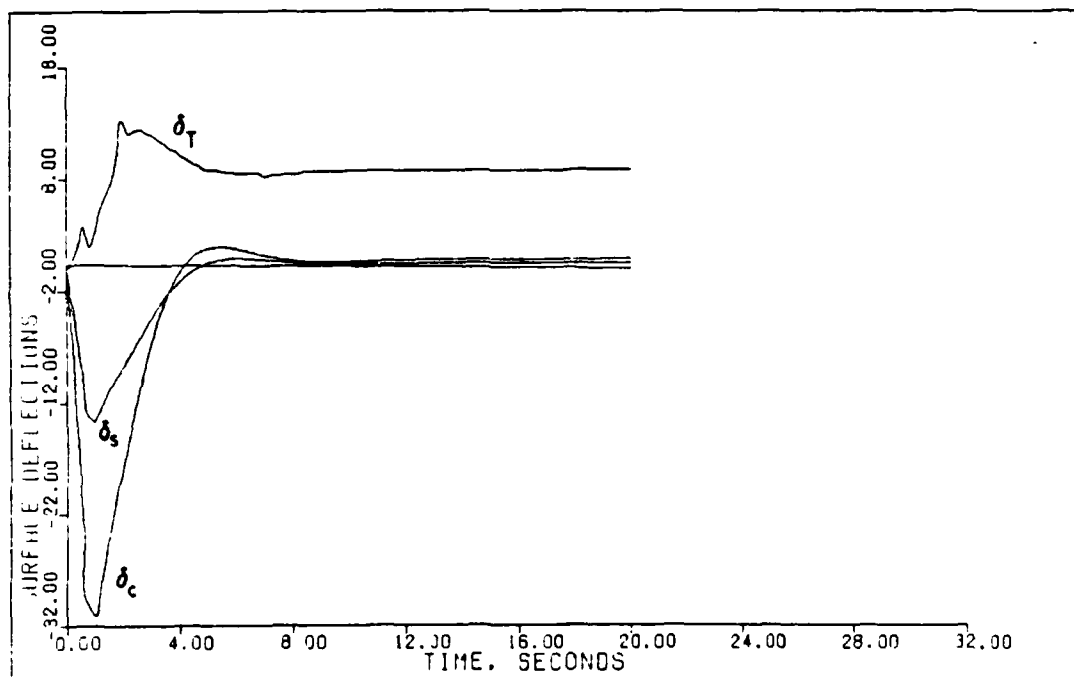


Fig. 4.34. Surface Deflections, $\sigma_1 = 10$, $\sigma_2 = .55$, $\sigma_3 = .55$

presence of plant uncertainty, each controller, tailored for one particular flight condition, is tested at each of the remaining five flight conditions. No changes are made to any of the controllers during this analysis since the objectives are strictly demonstrative.

Sensor Noise. To demonstrate the influence of sensor noise, the noise values of Appendix C are added to the simulation. In addition, each noise value is increased individually to its threshold level, defined as the level above which the system diverges beyond control surface limits within the twenty second simulation period. A Monte Carlo analysis, consisting of five independent simulations, is conducted for each of the noise configurations to obtain a mean response. MULTI does not currently include the capability to calculate the variance for a Monte Carlo simulation. As a result, the variance must be inferred from the qualitative analysis of each of the five simulations. All noise analysis is conducted at flight condition 1 and no changes are made to the controller design. The results of this analysis are contained in the following chapter.

Additional Maneuvers. Two additional maneuvers are performed at flight condition 1 to demonstrate that the controllers are not tuned to just this one maneuver, and they are capable of performing other maneuvers that must be

considered in the landing phase of flight. Assuming that the aircraft can establish a steady state descent on a desired flight path in preparation for landing (the result of the first maneuver studied), there are basically two possible follow-on maneuvers: a roundout and flare to touchdown, and a go-around or aborted landing. The first maneuver entails a smooth return to a level flight attitude just as the landing gear touch down. It is necessary to insure that there is a significant nose high pitch attitude at touchdown to prevent nose wheel damage, and the velocity should be minimized to reduce the landing roll and touchdown dispersion. At the velocity of flight condition 1 (120 knots) the level flight pitch attitude is already more than eleven degrees nose high. This is more than sufficient for the flare and no increase in angle of attack is commanded. It is also assumed that the equilibrium velocity will be maintained, rather than commanding it to a level dangerously close to a stall condition. The maneuver is thereby simplified to a commanded return to zero flight path angle with no input to either the angle of attack or flight path. The second maneuver assumes that for some reason the landing is refused and the descent must be immediately terminated. It is further assumed that after stabilizing briefly at a level or near level condition the landing is resumed. The purpose of this maneuver is twofold; to demonstrate that the aircraft will smoothly and

quickly return to near equilibrium conditions, and that despite the relatively long theoretical settling time resulting from low integral gain, the aircraft can be rapidly maneuvered without inducing unacceptable flight characteristics. This analysis is conducted with the model of flight condition 1 with actuators, computational time delay, sensor dynamics and surface nonlinearities included in the simulation. No changes are made to the controller design during this demonstration and the results are presented in Chapter V.

4.4 Summary

In general, it is very difficult to describe one's thought processes as he proceeds through a design of a complex system by a method that requires some trial and error. There are a number of clues contained in the theory used to develop the design method, but often these relationships are not apparent until after successful results are achieved. This chapter is an attempt to present systematically the abstract procedures that are personal to an individual and peculiar to a specific mathematical model in a quantitative and objective manner that may be useful to future users of the Porter method of multivariable output feedback control.

V. Results

5.1 Introduction

This chapter presents the results of applying the design procedure of Chapter IV to the STOL F-15 aircraft model. The chapter begins with a discussion of the general format of the data presented and then proceeds to the specific results, starting with the plant plus actuators and computational delay, and progressing to a simulation of the plant with actuators, computational time delay, sensor dynamics, nonlinear control surface effects and sensor noise. Next, simulations of the response of each controller to plant parameter variation are presented to establish the robustness of the controllers designed at each flight condition. Finally, two additional maneuvers are simulated, demonstrating the controlled aircraft's ability to perform other essential maneuvers characteristic of a landing situation.

5.2 Format of the Results

Commanded Input. Except for the results of Section 5.8 of this chapter, all simulations represent the response of the complete closed-loop system to a smoothed, ramped, step command input to the flight path angle channel of the controller (Figure 5.1). The commanded flight path angle

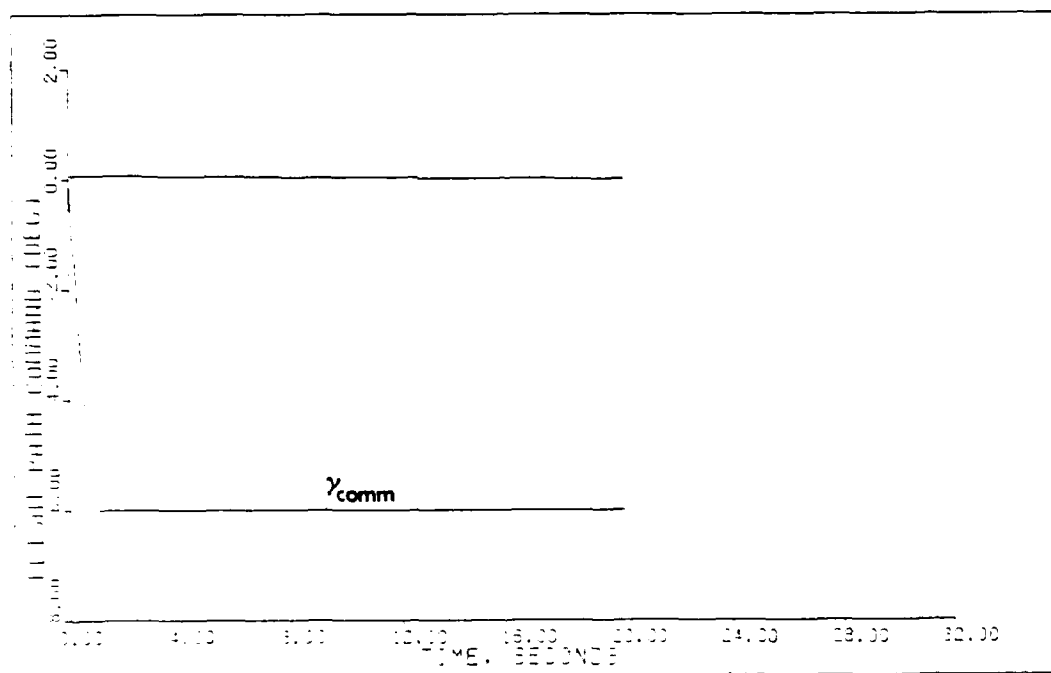


Fig. 5.1. Landing Flight Path Command Input

input is ramped over 0.8 seconds and has a final constant value of -6.0 degrees. This input, along with a commanded input of zero in the other two channels, represents a constant velocity, constant angle of attack descent command at an angle of six degrees to the horizontal. Section 5.8 presents two additional maneuvers described in detail in that section.

Plotted Data. The graphical data presented consists of two plots for each simulation. The first plot is a time history of the three output variables (u , α , and γ) expressed in units of degrees. The second plot is a time history of the deflection of each of the control surfaces (δ_C , δ_S , and δ_T) also expressed in degrees. All variables plotted are perturbation values and the magnitude plotted represents the deviation from an equilibrium value.

Tabular Data. In addition to graphical data, the result of the design procedure at each flight condition and the corresponding time responses are presented in tabular form. The design data tables (Tables 5.1, 5.3, and 5.5) contain the pertinent design parameters and resulting controller matrix at each flight condition. There are two intentional omissions from these tables. First, since the integral control matrix (K_I) is simply equal to the product of the proportional control matrix (K_P) and \bar{a} , K_I is not presented. Also, the sigma weighting matrix

multiplier (ϵ) is merely a design tool and the true sigma weighting matrix is the product of " ϵ " and the diagonal sigma matrix (Σ). The resulting diagonal sigma matrix elements are included in the tables. Presenting the sigma elements in this manner allows direct comparison between flight conditions without regard to " ϵ ." The simulation results tables (Tables 5.2, 5.4, and 5.6) contain the figures of merit calculated by MULTI for each of the outputs at the various flight conditions. The tables include figures for the final value of the flight path angle. With integral control the system is guaranteed to have zero steady state error and therefore the final value is the same as the commanded input. However, since the gain of the integral control is so low (one hundredth of the proportional gain), the simulation may not reach steady state within the simulation time. The final value is therefore taken to be the value at the end of the simulation. The settling time is also computed with respect to this final value. These values are presented to indicate the quasi-steady state response of the system within the time period of interest. Provided the system's transient response is essentially completed in the simulation time these values provide reasonable quantification of the settling time of the response.

5.3 Plant Plus Actuators and Computational Delay

The design parameters obtained for the six flight conditions are shown in Table 5.1. In general, the sigma element corresponding to velocity is at least one order of magnitude higher than the other two elements. The ratio of integral to proportional control is 0.01 for all flight conditions. The simulation results using these controllers are contained in Table 5.2, and Figures 5.2 through 5.13.

The rise times and settling times of Table 5.2 clearly indicate that the slowest responses are for the flight conditions in which the aircraft weight is the highest. This is an expected result since the higher mass and pitch moment of inertia certainly affects the open loop bandwidth of the plant. These results are substantiated by qualitative inspection of the corresponding figures as well. The speed of the response is also apparently affected by dynamic pressure as the response at a particular weight is the slowest at the lowest dynamic pressure (flight conditions 3 and 6). This is no surprise either, since the controlling forces generated by the aerodynamic surfaces are directly proportional to the dynamic pressure. It is important to keep in mind that these comparisons are made between different controllers at different flight conditions. Each controller is chosen subjectively as the best one found for that given flight condition.

TABLE 5.1

DESIGN PARAMETERS FOR THE PLANT PLUS ACTUATORS
AND COMPUTATIONAL TIME DELAY

Flight Condition	$\bar{\alpha}$	Sigma	\underline{K}_0 Matrix		
1	0.01	1.25	-7.401E-4	5.146E-2	3.160E-1
		0.025	5.033E-4	-3.500E-2	1.115E-1
		0.025	-5.740E-2	2.569E-3	-3.273E-2
2	0.01	1.25	6.656E-4	6.049E-2	2.923E-1
		0.025	-1.262E-1	-4.040E-2	8.379E-1
		0.025	-5.210E-2	-1.067E-3	-2.701E-2
3	0.01	1.11	-1.647E-3	5.737E-2	3.044E-1
		0.027	-1.777E-2	-4.333E-2	1.138E-1
		0.018	-6.869E-2	-2.599E-3	-2.082E-2
4	0.01	1.20	-1.472E-4	5.141E-2	3.312E-1
		0.056	-1.075E-2	-4.743E-2	1.543E-1
		0.034	-6.635E-2	-3.995E-3	-2.887E-2
5	0.01	1.313	-2.194E-2	4.866E-2	2.768E-1
		0.0338	-1.487E-3	-2.677E-2	1.579E-1
		0.0188	-9.024E-2	-3.434E-3	-4.028E-2
6	0.01	1.000	-1.042E-2	5.418E-2	2.975E-1
		0.015	-5.522E-3	-2.020E-2	1.078E-1
		0.015	-6.397E-2	-4.620E-3	-3.201E-2

$$K_q = .25$$

$$K_s = 1.25$$

TABLE 5.2

FIGURES OF MERIT FOR PLANT PLUS ACTUATORS
AND COMPUTATIONAL TIME DELAY

Flight Condition	Output	Peak Value	Time To Peak	Final Value*	Settling Time
1	u	0.158	2.60	**	**
	α	-0.558	3.20	**	**
	γ	-6.305	6.00	-6.196	4.60
2	u	0.196	2.00	**	**
	α	-1.287	2.80	**	**
	γ	-6.746	5.20	-6.491	6.60
3	u	0.177	4.60	**	**
	α	-0.426	3.80	**	**
	γ	-7.631	11.2	-7.437	14.4
4	u	0.210	7.60	**	**
	α	1.376	1.20	**	**
	γ	-7.162	12.2	-7.055	7.40
5	u	0.123	4.00	**	**
	α	0.479	1.20	**	**
	γ	-6.209	17.4	-6.209	7.60
6	u	0.194	3.40	**	**
	α	-8.876	4.20	**	**
	γ	-6.812	8.80	-6.711	6.60

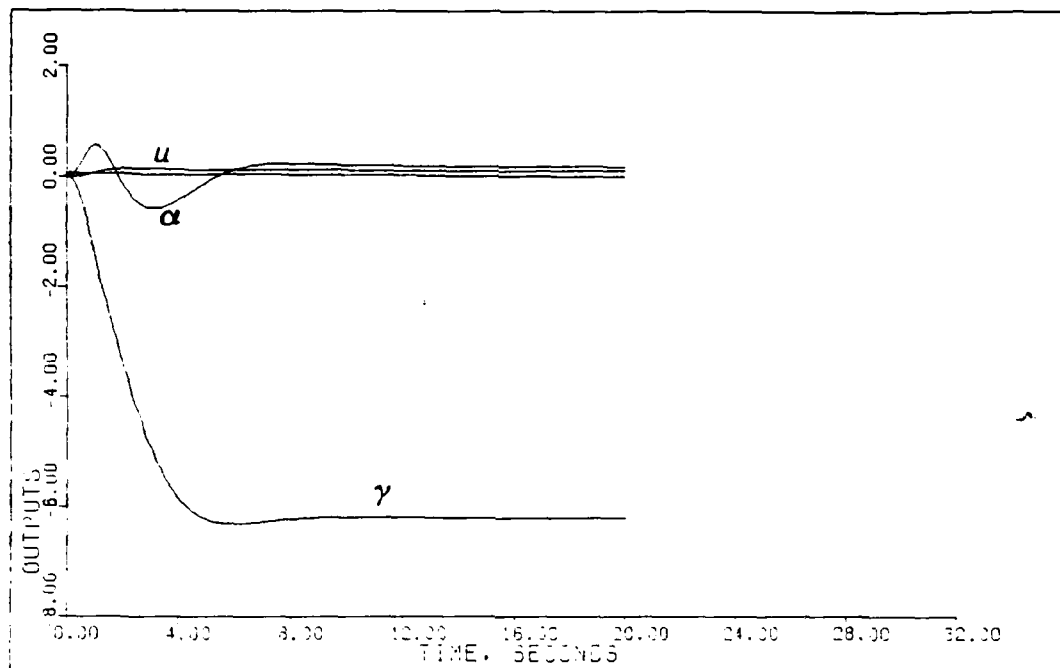


Fig. 5.2. Outputs with Actuators and Computational Delay, Flight Condition 1

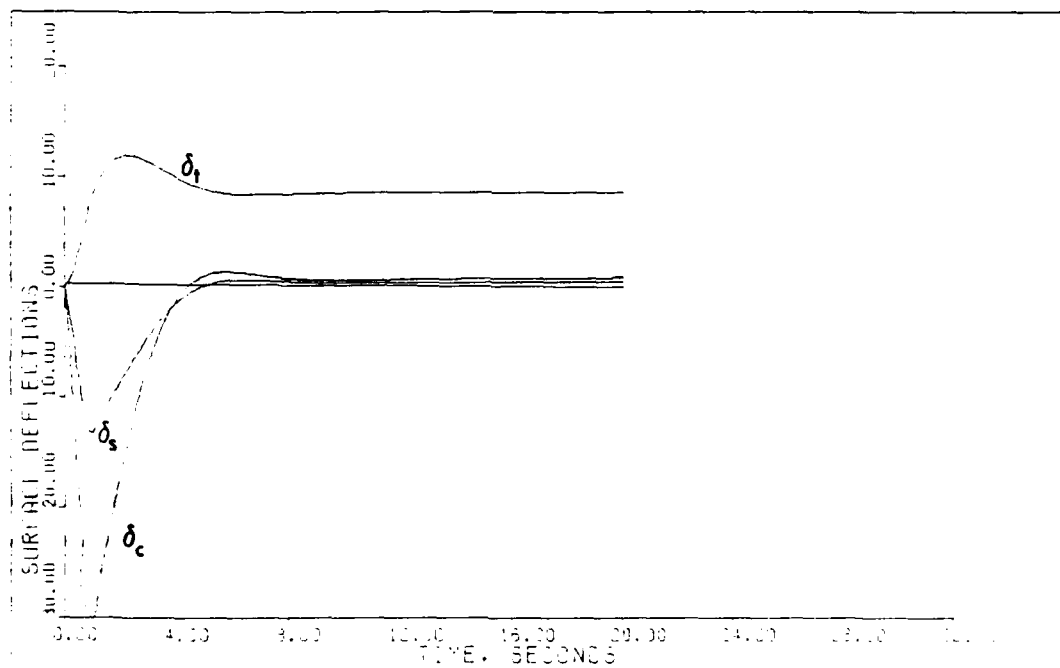


Fig. 5.3. Surface Deflections with Actuators and Computational Delay, Flight Condition 1

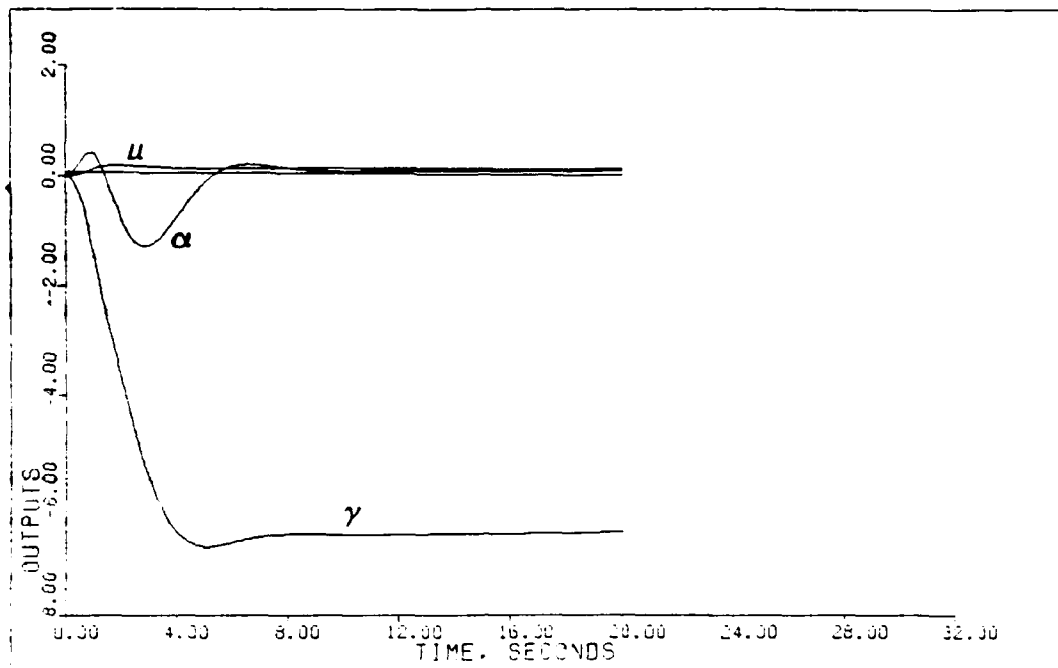


Fig. 5.4. Outputs with Actuators and Computational Delay, Flight Condition 2

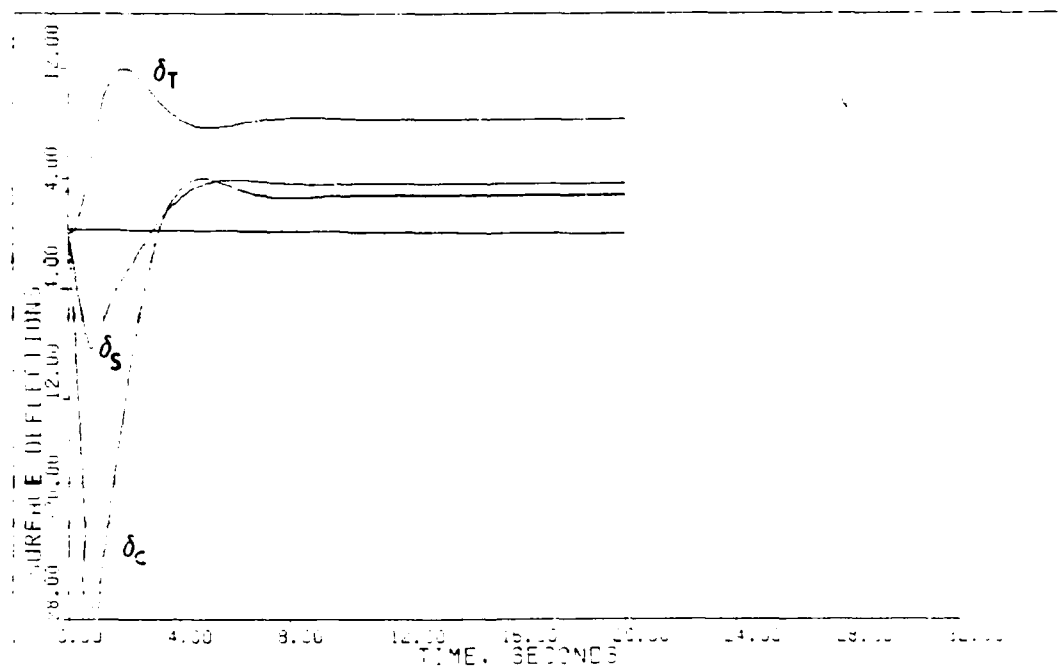


Fig. 5.5. Surface Deflections with Actuators and Computational Delay, Flight Condition 2

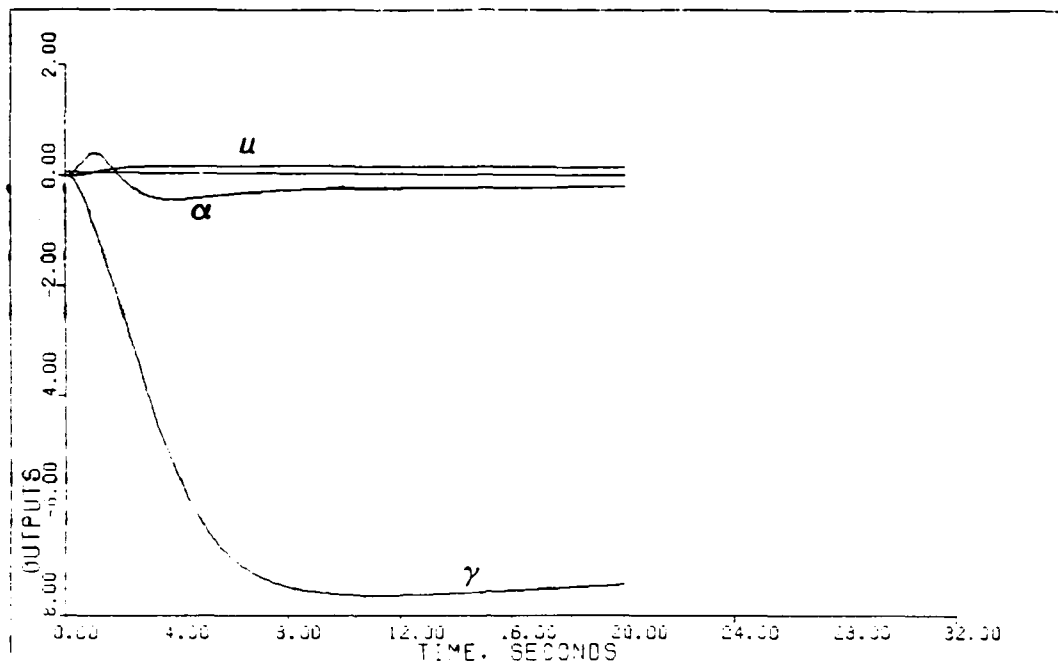


Fig. 5.6. Outputs with Actuators and Computational Delay, Flight Condition 3

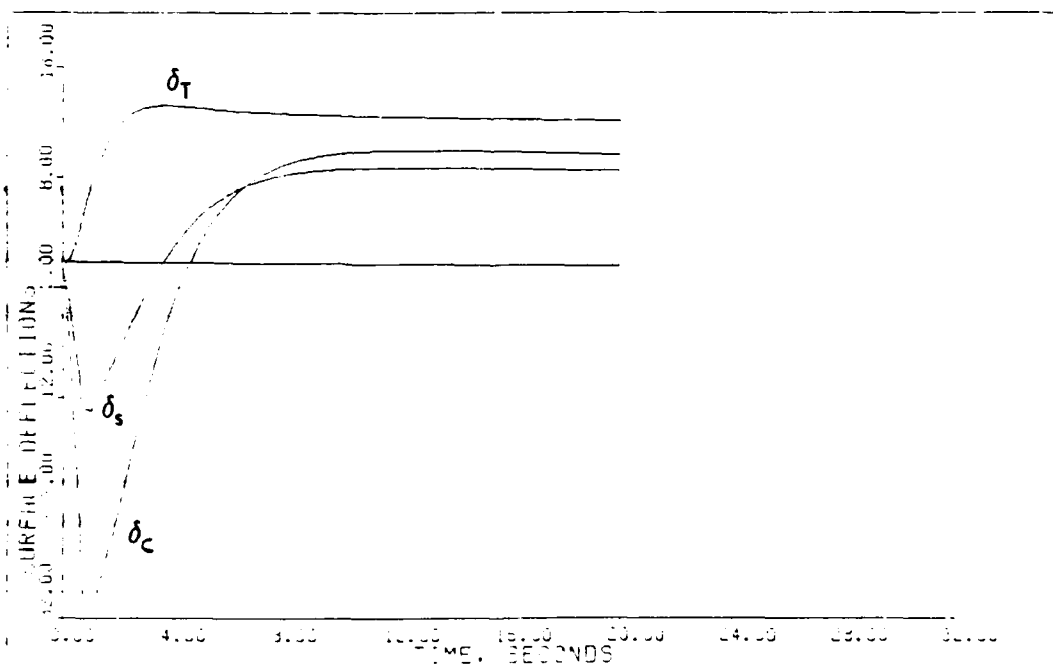


Fig. 5.7. Surface Deflections with Actuator and Computational Delay, Flight Condition 3

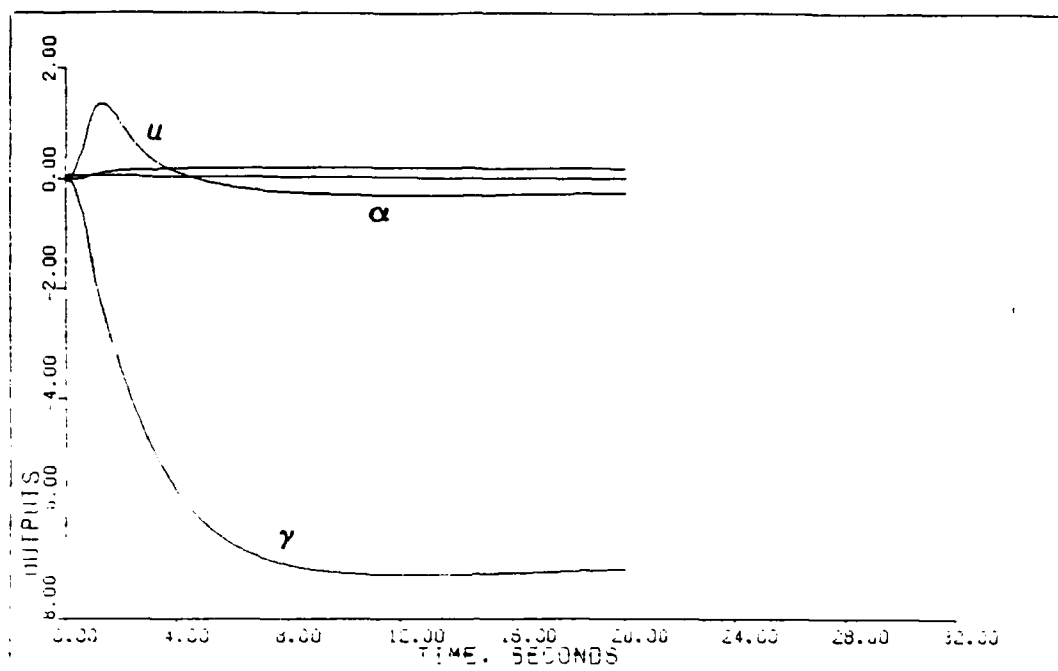


Fig. 5.8. Outputs with Actuators and Computational Delay, Flight Condition 4

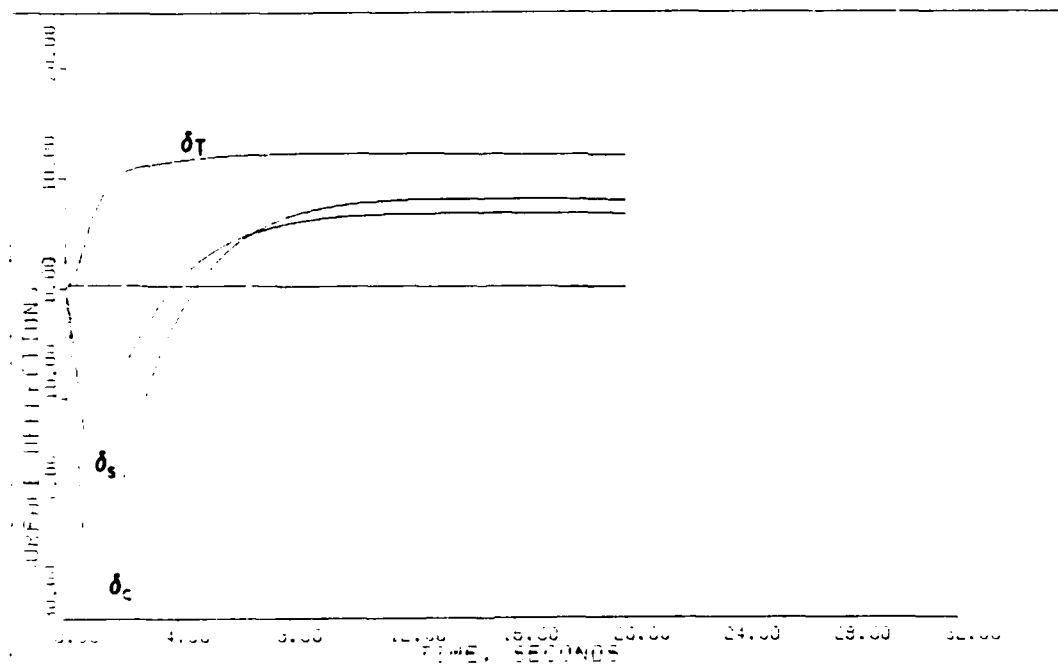


Fig. 5.9. Surface Deflections with Actuators and Computational Delay, Flight Condition 4

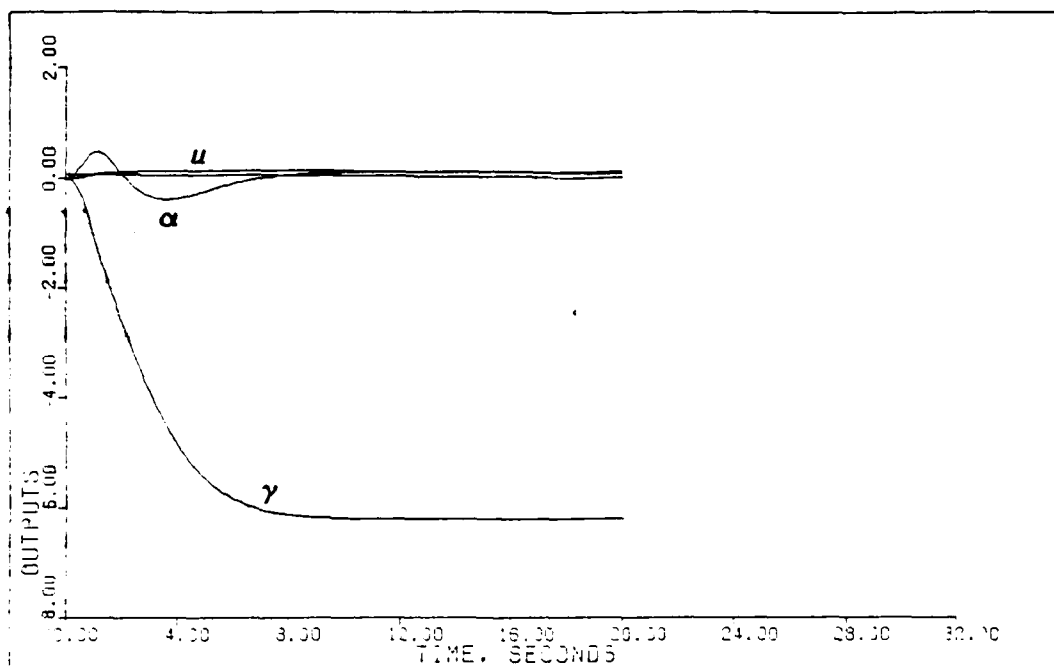


Fig. 5.10. Outputs with Actuators and Computational Delay, Flight Condition 5

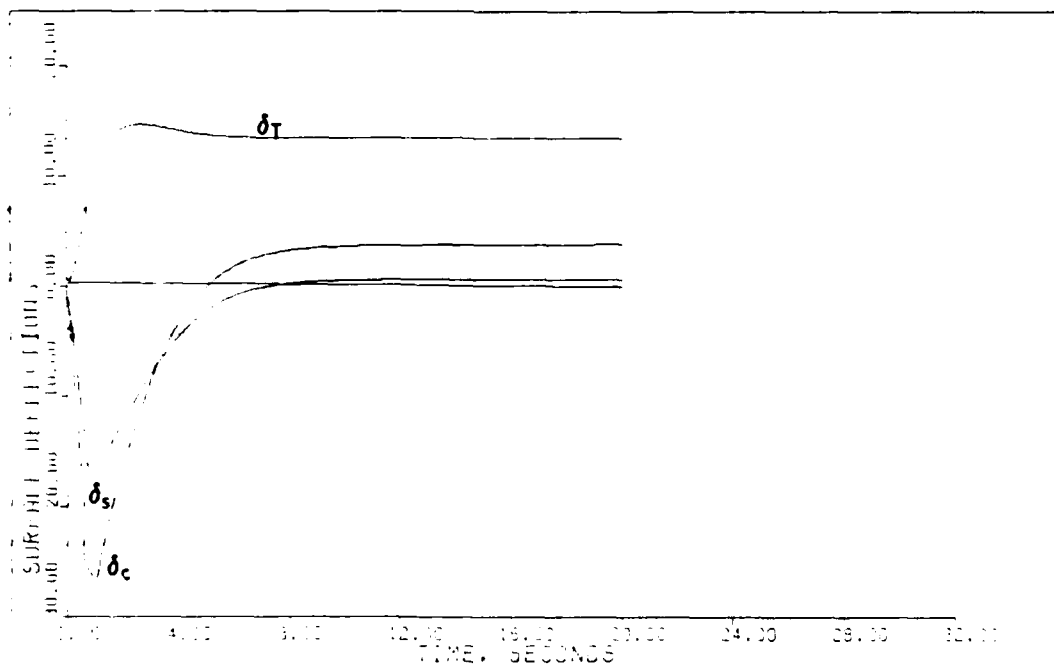


Fig. 5.11. Surface Deflections with Actuators and Computational Delay, Flight Condition 5

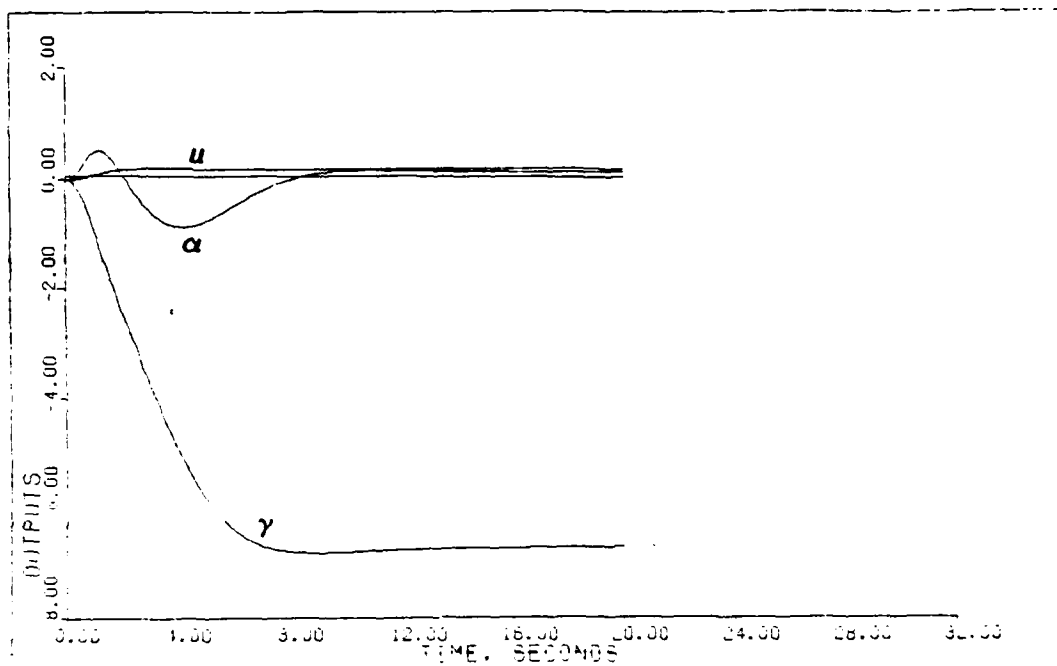


Fig. 5.12. Outputs with Actuators and Computational Delay, Flight Condition 6

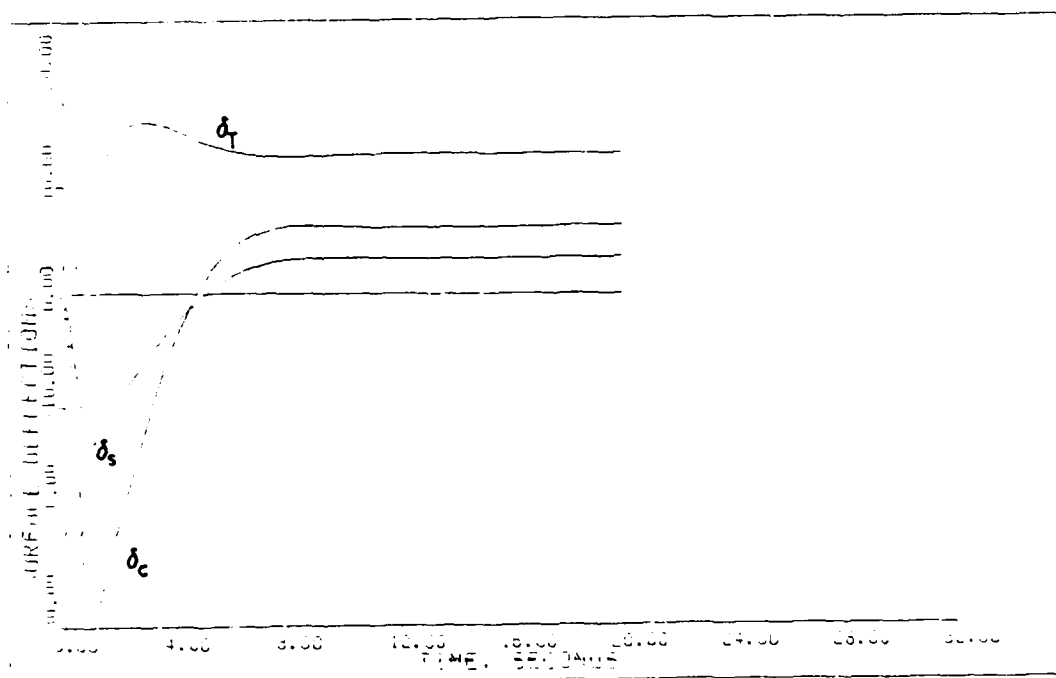


Fig. 5.13. Surface Deflections with Actuators and Computational Delay, Flight Condition 6

The plots at each flight condition demonstrate relatively good decoupling of the outputs at all flight conditions, with the greatest coupling occurring at low weight and low dynamic pressure (Figures 5.4 and 5.12). In general, the responses are smooth, non-oscillatory, and reasonably fast. In most of the surface deflection plots it is evident that the canard deflects almost to its deflection limit (-35 degrees). This is by design to achieve the maximum performance of the system. However, in the performance of the maneuver the canard also is at the limit of and sometimes exceeds its maximum deflection rate (23 degrees per second). This is a characteristic of high gain controllers. Future design efforts with this aircraft should consider implementing rate limits in the MULTI simulation to account for this realistic limitation.

5.4 Plant Plus Actuators Delay and Sensors

The addition of sensor dynamics tends to destabilize the system response using the controllers of Section 5.3. Therefore, the controllers are tailored to optimize the response including the sensors and the results of this adjustment are tabulated in Table 5.3. The new controllers generally feature a reduction in the sigma element corresponding to velocity and minor adjustments to the other two channels. The simulation results are contained in Table 5.4 and Figures 5.14 through 5.25.

TABLE 5.3

DESIGN PARAMETERS FOR THE PLANT PLUS ACTUATORS,
COMPUTATIONAL TIME DELAY AND SENSOR DYNAMICS

Flight Condition	$\bar{\alpha}$	Sigma	K_0 Matrix		
1	0.01	0.75	-4.441E-4	4.117E-2	2.528E-1
		0.02	3.020E-4	-2.800E-2	8.921E-2
		0.02	-3.444E-2	2.055E-3	-2.618E-1
2	0.01	0.750	3.994E-4	7.259E-2	2.923E-1
		0.030	-7.575E-3	-4.848E-2	8.379E-2
		0.025	-3.126E-2	-1.280E-3	-2.701E-3
3	0.01	0.809	-1.138E-3	4.909E-2	2.511E-1
		0.023	-1.228E-2	-3.707E-2	9.386E-2
		0.015	-4.746E-2	-2.224E-3	-1.718E-2
4	0.01	0.900	-1.104E-4	5.141E-2	3.214E-1
		0.056	-8.066E-3	-4.743E-2	1.497E-1
		0.033	-4.976E-2	-3.995E-3	-2.802E-2
5	0.01	0.825	-1.379E-2	3.224E-2	2.584E-1
		0.023	-9.344E-4	-1.784E-2	1.474E-1
		0.018	-5.672E-2	-2.289E-3	-3.759E-1
6	0.01	1.200	1.476E-4	5.143E-2	3.313E-1
		0.056	1.078E-2	-4.614E-2	1.637E-1
		0.034	6.652E-2	4.006E-3	2.894E-2

$$K_q = .25$$

$$K_s = 1.25$$

TABLE 5.4

FIGURES OF MERIT FOR PLANT PLUS ACTUATORS, COMPUTATIONAL
TIME DELAY AND SENSOR DYNAMICS

Condition	Output	Peak Value	Time To Peak	Final Value*	Settling Time
1	u	0.264	3.20	**	**
	α	-0.677	3.40	**	**
	γ	-6.467	6.20	-6.175	8.20
2	u	0.335	1.80	**	**
	α	-1.195	2.80	**	**
	γ	-6.619	4.80	-6.495	3.80
3	u	0.272	6.40	**	**
	α	-0.488	4.20	**	**
	γ	-8.239	12.0	-7.993	16.0
4	u	0.213	7.00	**	**
	α	1.536	1.40	**	**
	γ	-7.213	11.6	-7.089	7.00
5	u	0.206	6.40	**	**
	α	0.722	1.40	**	**
	γ	-6.372	10.2	-6.156	13.4
6	u	0.395	3.20	**	**
	α	-0.966	4.20	**	**
	γ	-6.823	8.20	-6.684	8.60

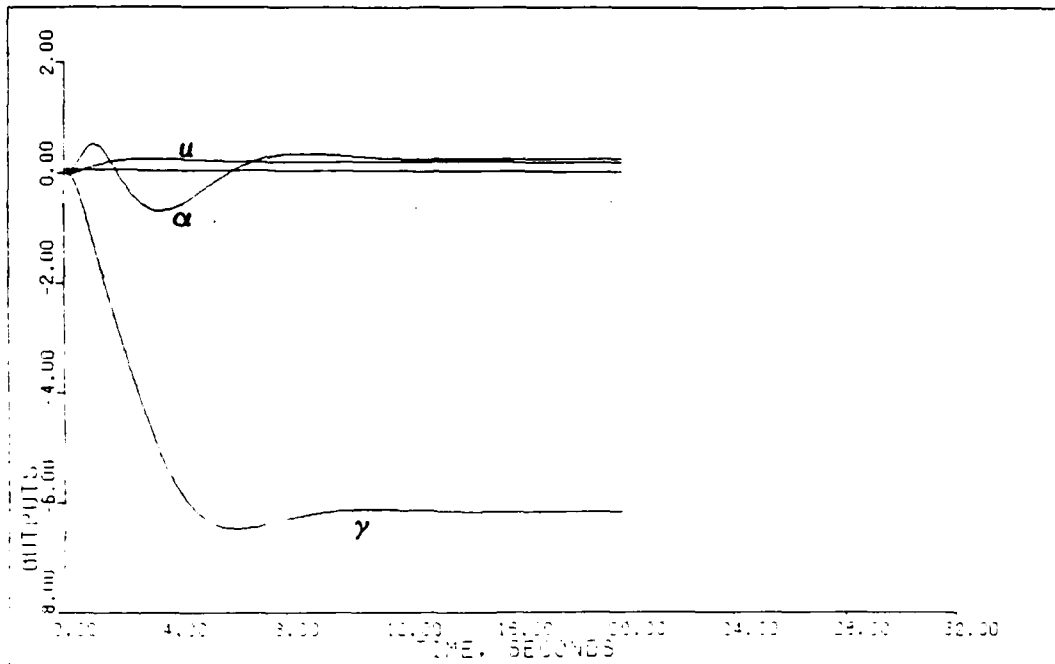


Fig. 5.14. Outputs, Including Sensor Dynamics, Flight Condition 1

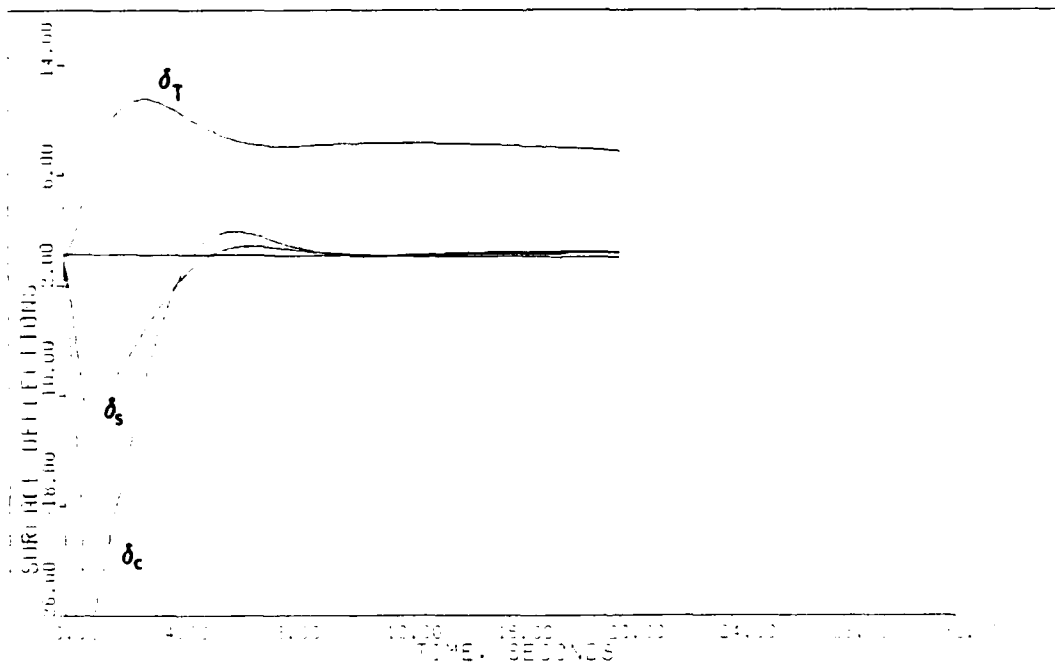


Fig. 5.15. Surface Deflections, Including Sensor Dynamics, Flight Condition 1

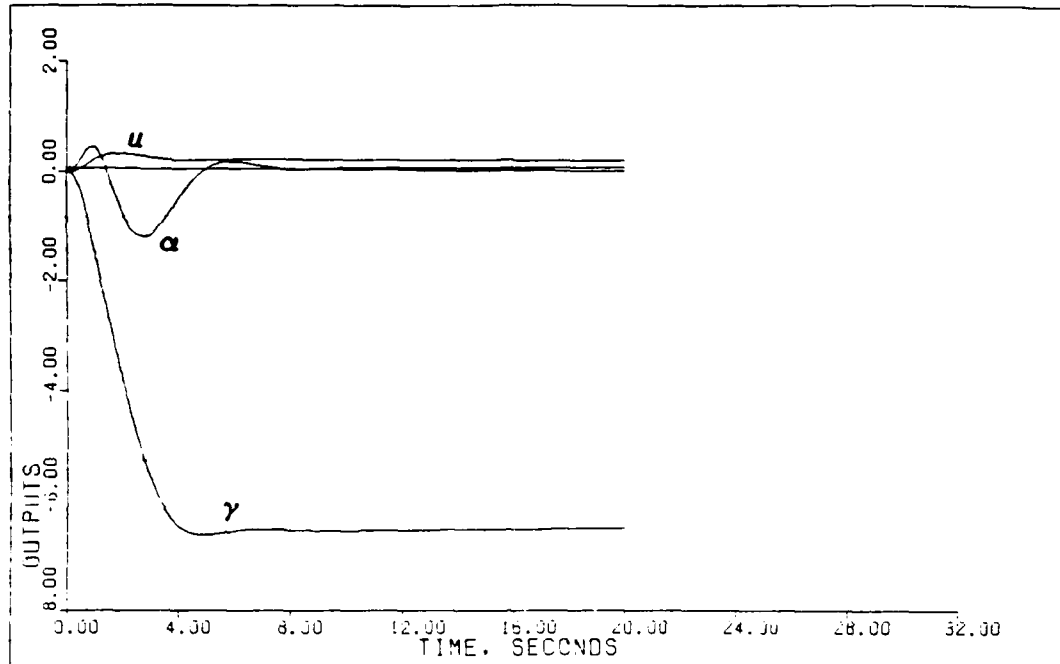


Fig. 5.16. Outputs, Including Sensor Dynamics, Flight Condition 2

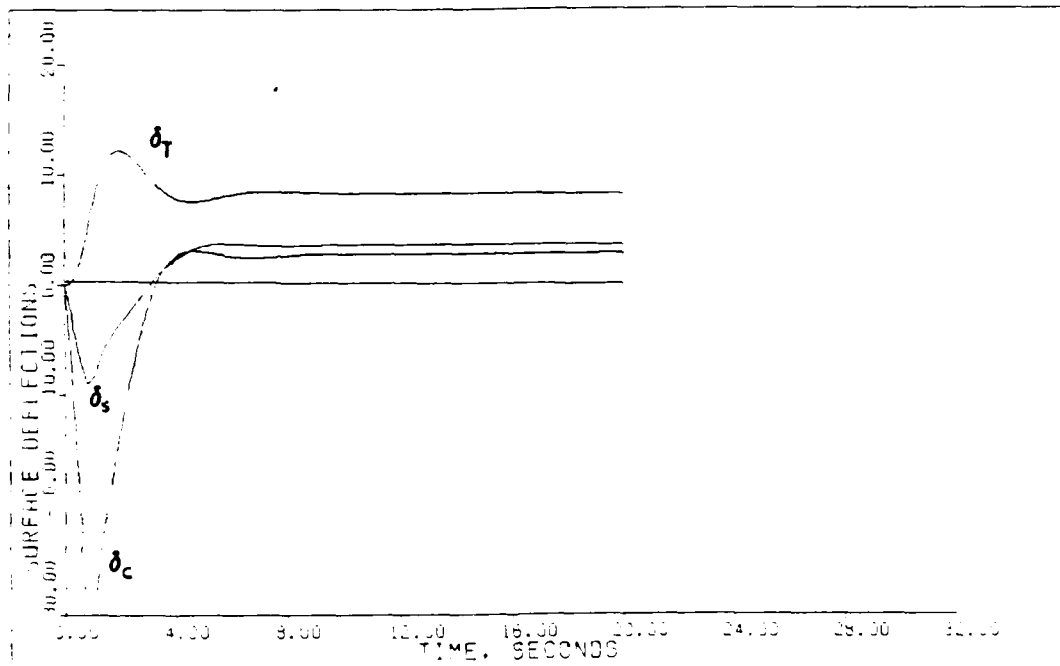


Fig. 5.17. Surface Deflections, Including Sensor Dynamics, Flight Condition 2

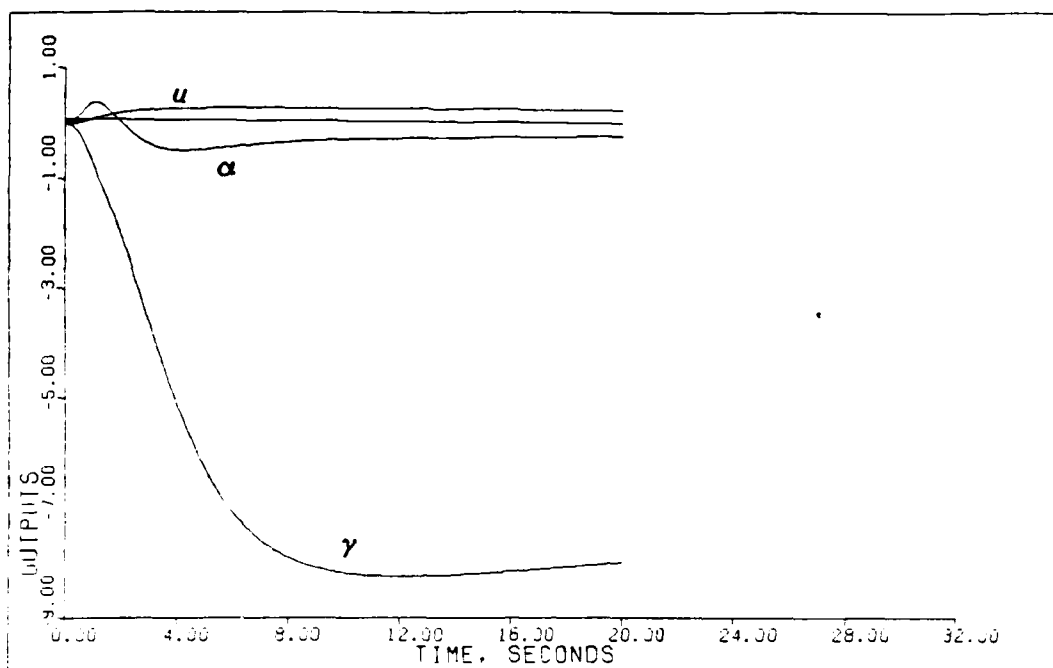


Fig. 5.18. Outputs, Including Sensor Dynamics, Flight Condition 3

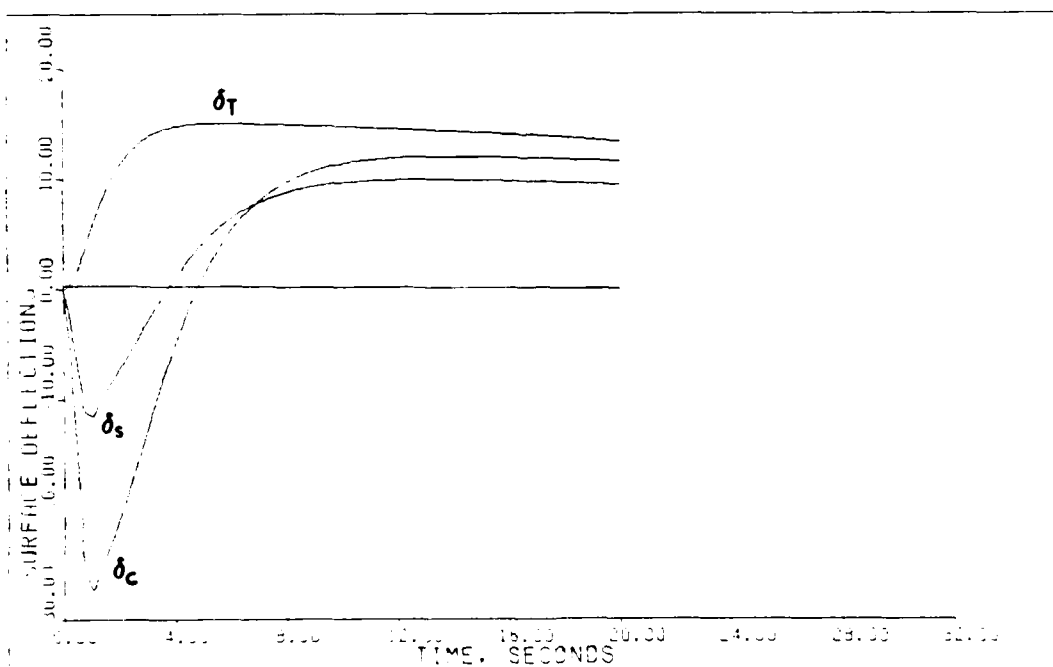


Fig. 5.19. Surface Deflections, Including Sensor Dynamics, Flight Condition 3

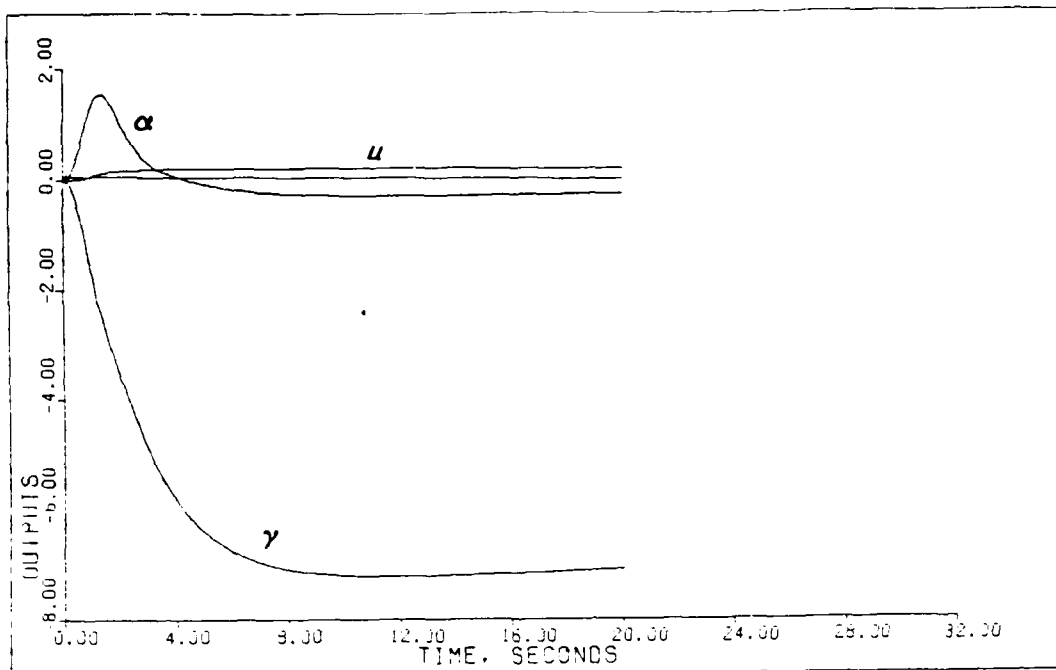


Fig. 5.20. Outputs, Including Sensor Dynamics, Flight Condition 4

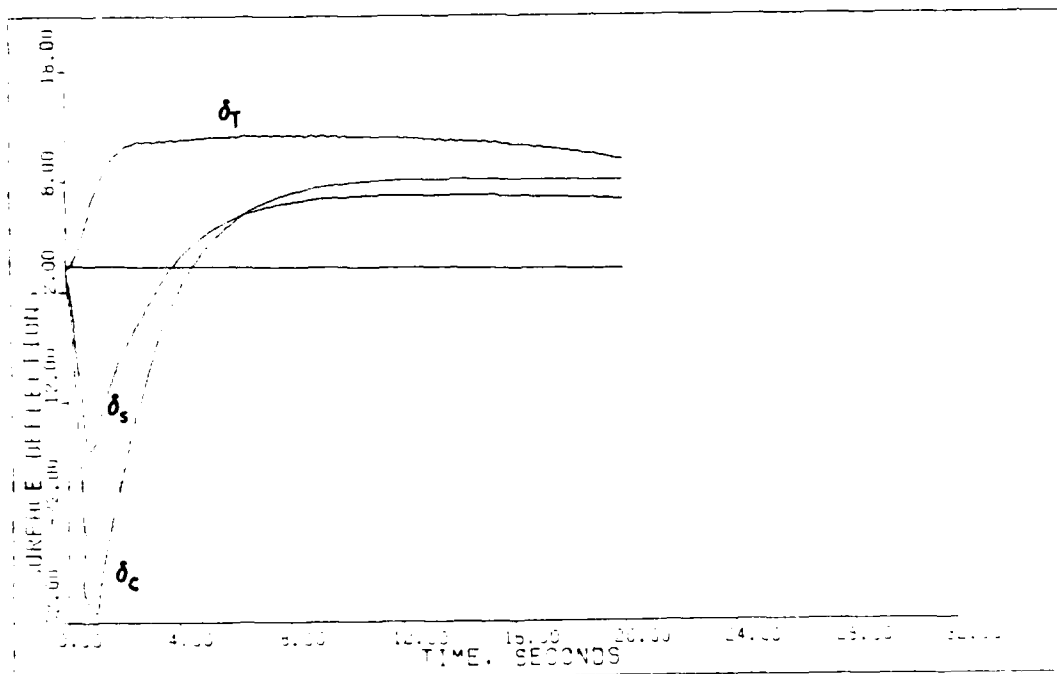


Fig. 5.21. Surface Deflections, Including Sensor Dynamics, Flight Condition 4

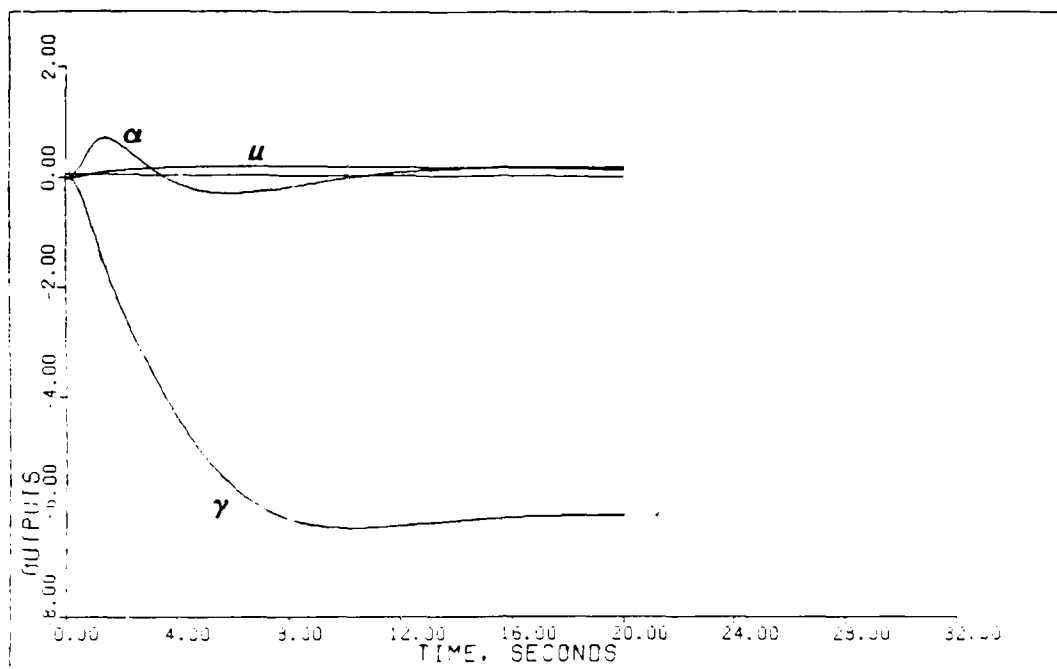


Fig. 5.22. Outputs, Including Sensor Dynamics, Flight Condition 5

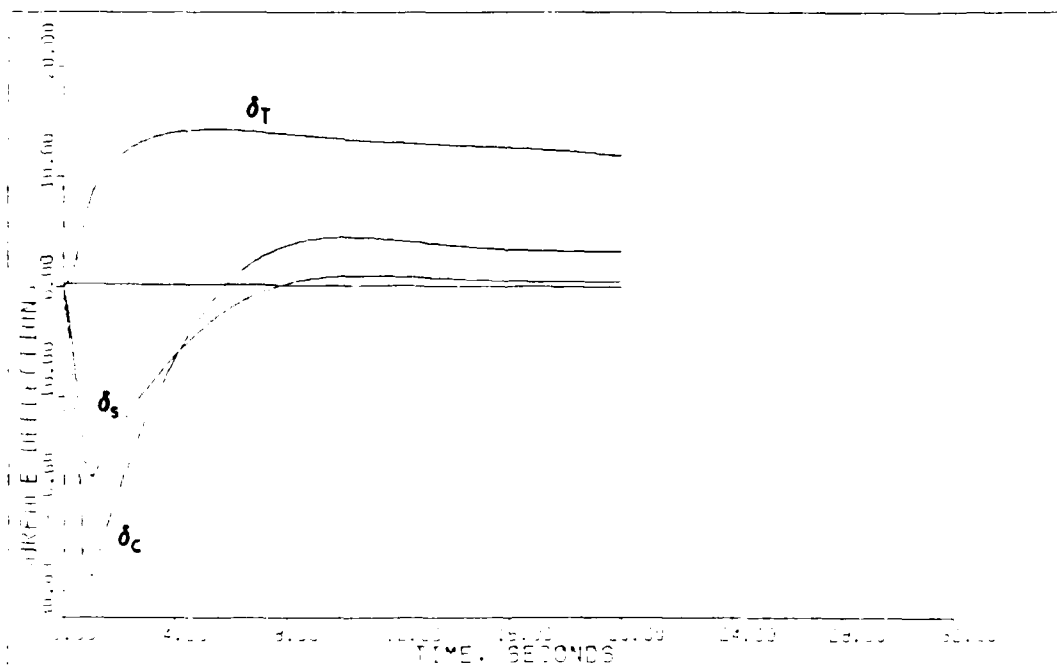


Fig. 5.23. Surface Deflections, Including Sensor Dynamics, Flight Condition 5

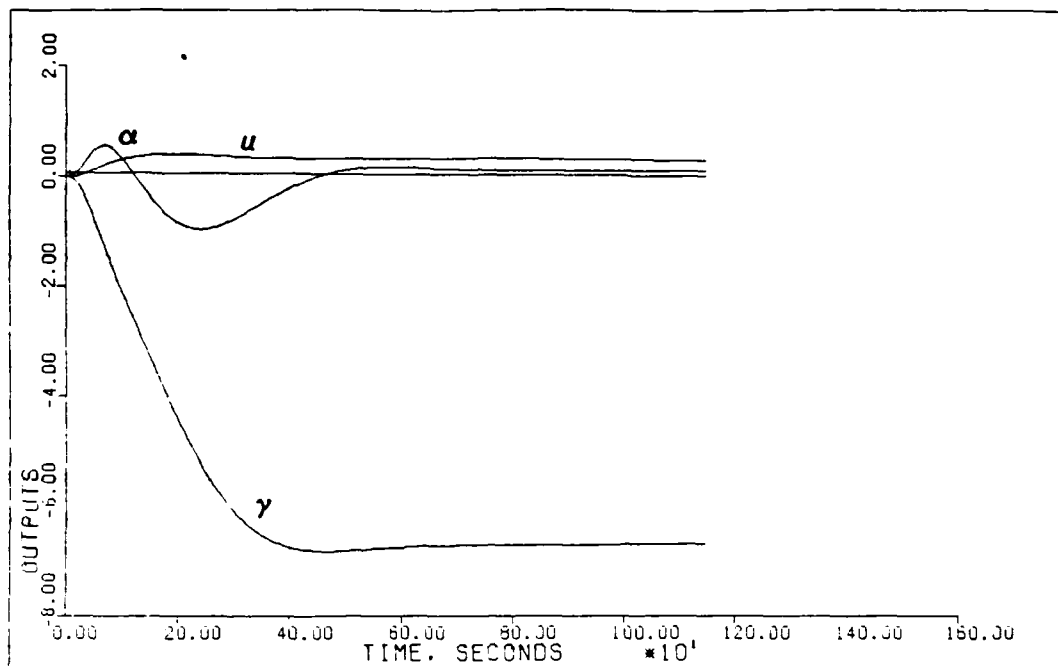


Fig. 5.24. Outputs, Including Sensor Dynamics, Flight Condition 6

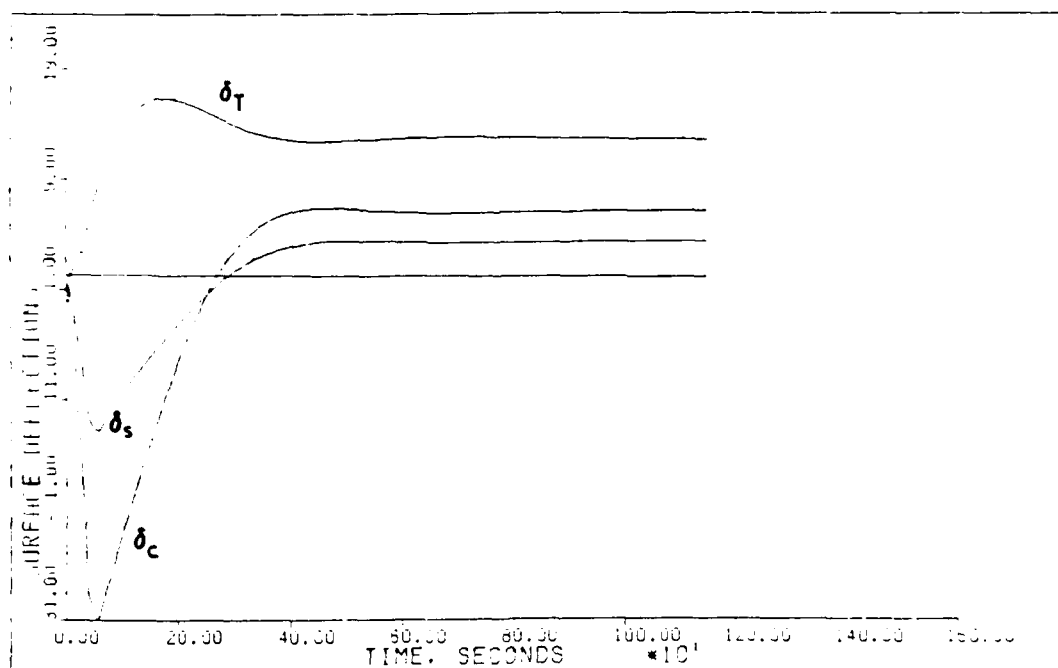


Fig. 5.25. Surface Deflections, Including Sensor Dynamics, Flight Condition 6

The same observations that are discussed in the preceding section regarding aircraft weight and dynamic pressure apply when sensor dynamics are included. Comparing the peak values of the angle of attack and velocity from Tables 5.2 and 5.4, it is evident that the addition of sensor dynamics tends to increase coupling between the input/output channels. The increase is relatively small and appears to be within acceptable limits. Overall, it is possible to obtain responses nearly as fast as without sensors at the expense of a slight increase of coupling and increased overshoot of the commanded input. The responses are still smooth and non-oscillatory.

5.5 Plant Actuators, Delay, Sensors, and Surface Nonlinearity

The nonlinearity of the drag on the control surface as modeled in this thesis induces a slightly erratic behavior of the control surfaces as the surface passes through zero angle of attack. This is most likely caused by the discontinuity in the modeled drag derivative that does not exist in nature. However, this problem is largely resolved by a reduction in one or more of the sigma elements as necessary. The resulting controller designs are shown in Table 5.5. The simulation results with the modeled surface nonlinearities included are contained in Table 5.6 and Figures 5.26 through 5.37.

TABLE 5.5

DESIGN PARAMETERS FOR THE PLANT PLUS ACTUATORS,
COMPUTATIONAL TIME DELAY, SENSOR DYNAMICS
AND SURFACE NONLINEARITIES

Flight Condition	$\bar{\alpha}$	Sigma	K_0 Matrix		
1	.01	0.450	-2.665E-4	5.095E-2	3.128E-1
		0.025	1.812E-4	-3.465E-2	1.104E-1
		0.025	-2.066E-2	2.543E-3	-3.240E-2
2	.01	0.750	3.994E-4	7.259E-2	2.923E-1
		0.030	-7.575E-3	-4.848E-2	8.379E-2
		0.025	-3.126E-2	-1.280E-3	-2.701E-3
3	.01	0.578	-8.129E-4	4.909E-2	2.511E-1
		0.023	-8.877E-3	-3.707E-2	9.386E-2
		0.015	-3.390E-2	-2.224E-3	-1.718E-2
4	.01	0.750	-9.200E-6	5.141E-2	3.214E-1
		0.056	-6.721E-4	-4.743E-2	1.497E-1
		0.033	-4.147E-3	-3.995E-3	-2.802E-2
5	.01	0.600	-1.003E-2	3.244E-2	2.584E-1
		0.025	-6.796E-4	-1.784E-2	1.474E-1
		0.017	-4.125E-2	-2.289E-3	-3.759E-2
6	.01	1.200	1.476E-4	5.143E-4	3.313E-3
		0.056	1.078E-2	-4.614E-2	1.637E-1
		0.034	6.652E-2	4.006E-3	2.894E-2

$$K_q = .25$$

$$K_s = 1.25$$

TABLE 5.6
FIGURES OF MERIT FOR PLANT PLUS ACTUATORS,
COMPUTATIONAL TIME DELAY SENSORS AND
SURFACE NONLINEARITY

Flight Condition	Output	Peak Value	Time To Peak	Final Value*	Settling Time
1	u	0.467	0.80	**	**
	α	-0.651	3.20	**	**
	γ	-6.388	5.40	-6.197	6.60
2	u	0.338	1.80	**	**
	α	-1.190	2.80	**	**
	γ	-6.619	4.80	-6.494	3.80
3	u	0.432	9.80	**	**
	α	-0.484	4.20	**	**
	γ	-8.521	13.6	-8.323	15.8
4	u	2.732	9.80	**	**
	α	1.589	1.40	**	**
	γ	-7.103	12.6	-7.015	7.60
5	u	0.284	6.40	**	**
	α	0.729	1.40	**	**
	γ	-6.366	10.2	-6.152	13.4
6	u	0.387	3.40	**	**
	α	-0.952	4.20	**	**
	γ	-6.820	8.20	-6.686	8.60

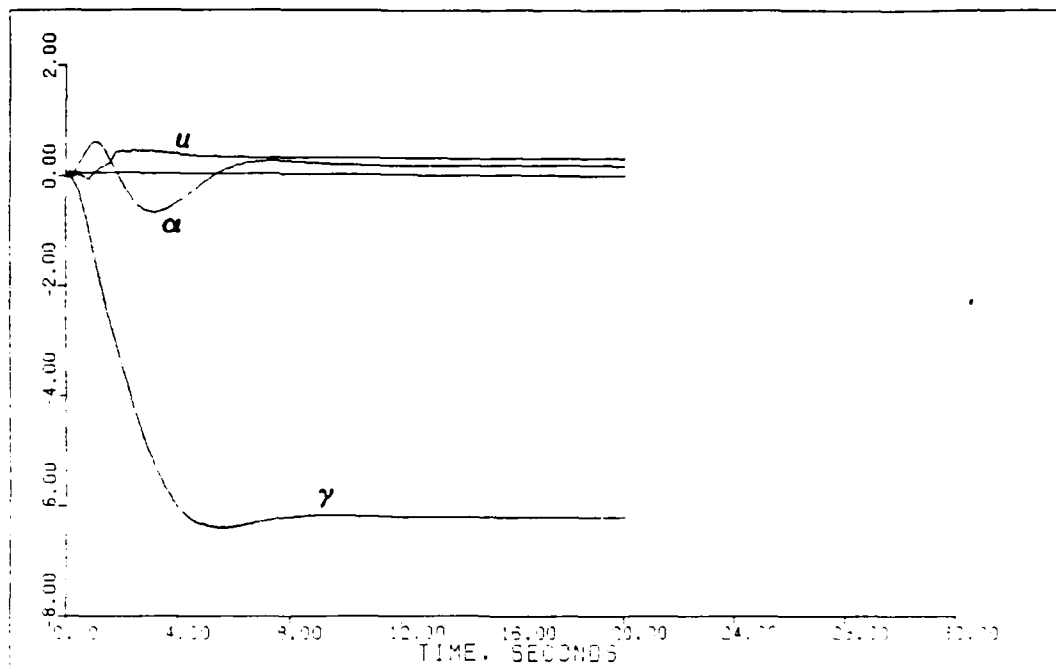


Fig. 5.26. Outputs, Including Surface Nonlinearity, Flight Condition 1

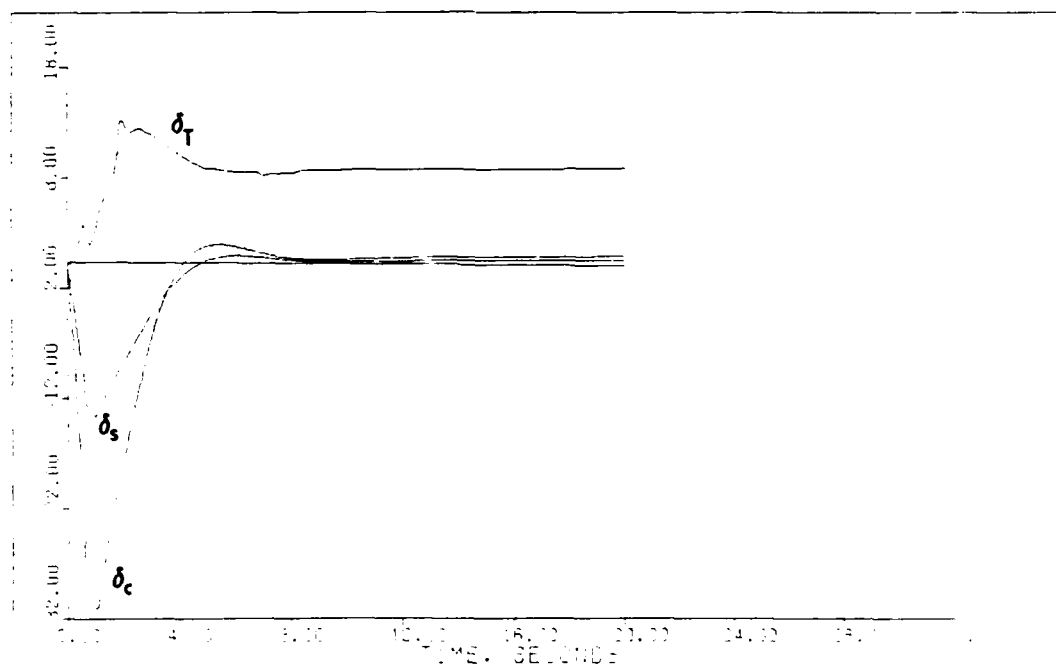


Fig. 5.27. Surface Deflections, Including Surface Nonlinearity, Flight Condition 1

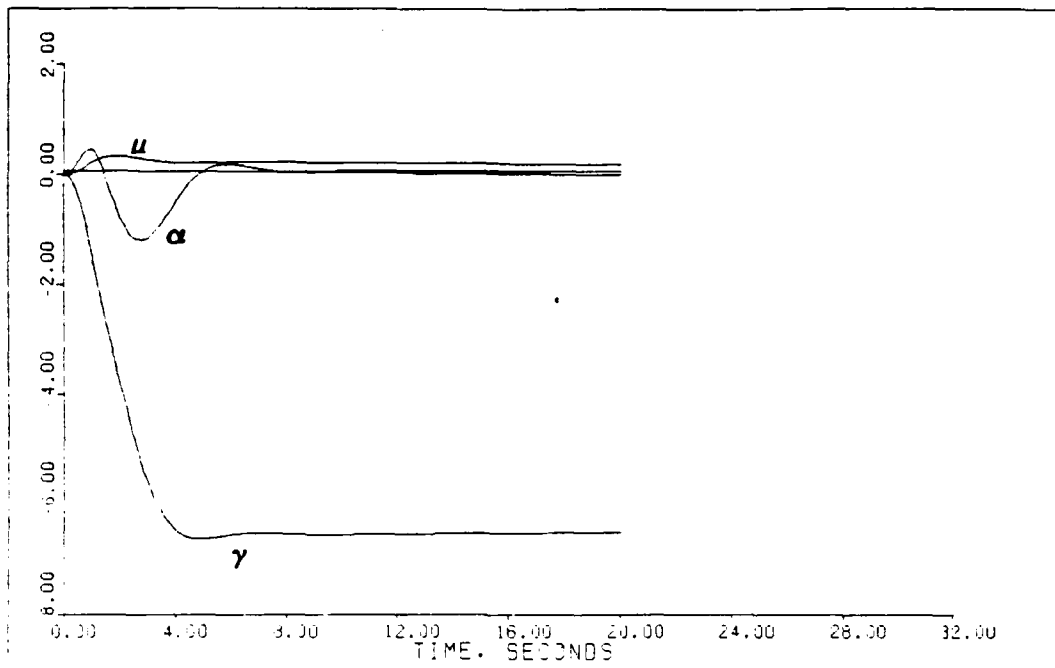


Fig. 5.28. Outputs, Including Surface Nonlinearity, Flight Condition 2

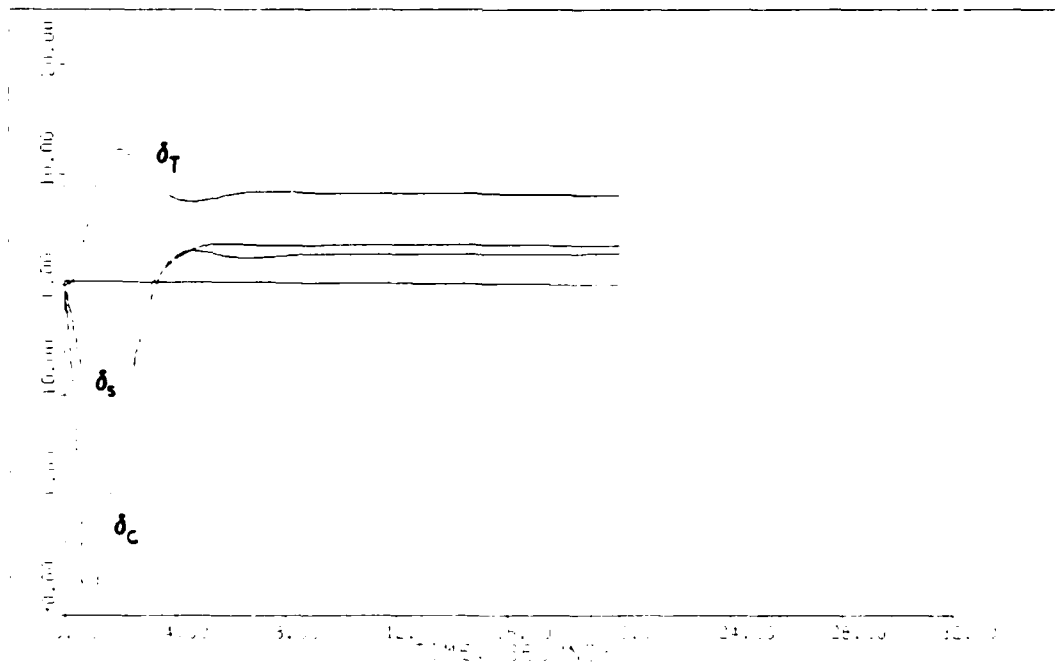


Fig. 5.29. Surface Deflections, Including Surface Nonlinearity, Flight Condition 2

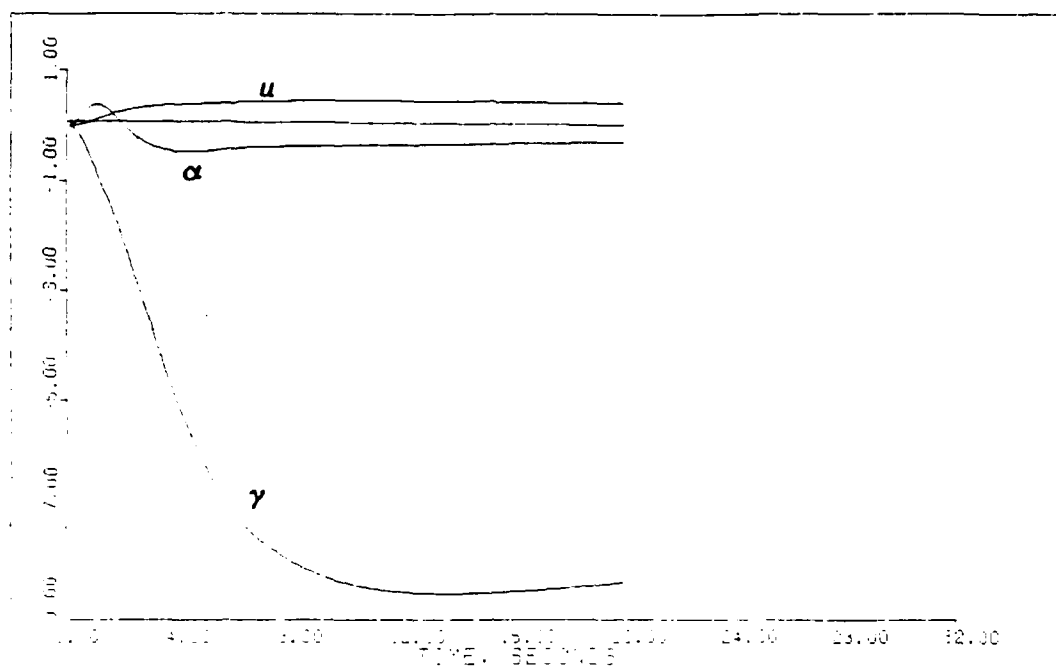


Fig. 5.30. Outputs, Including Surface Nonlinearity, Flight Condition 3

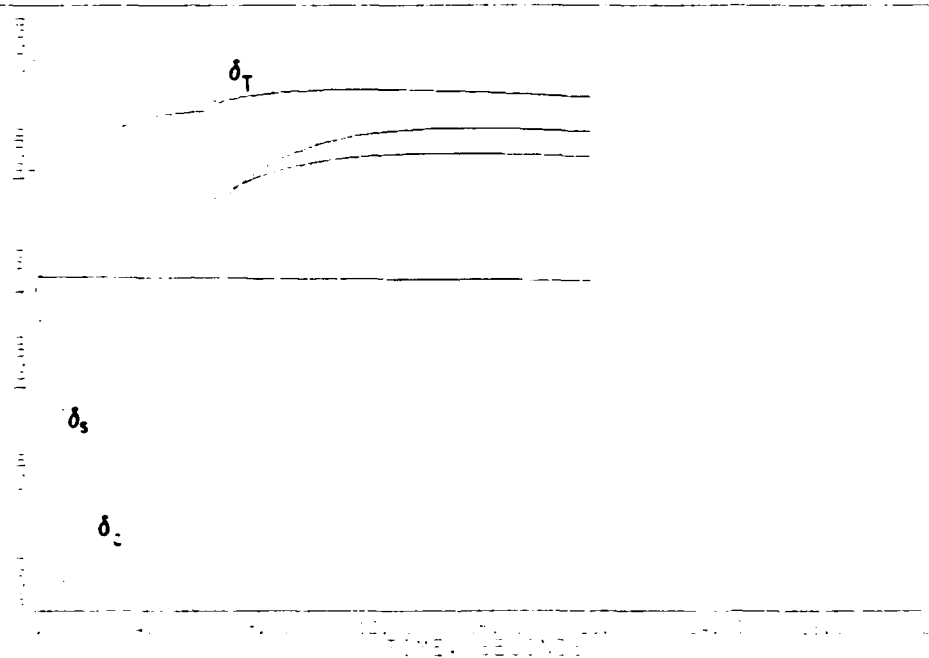


Fig. 5.31. Surface Deflections, Including Surface Nonlinearity, Flight Condition 3

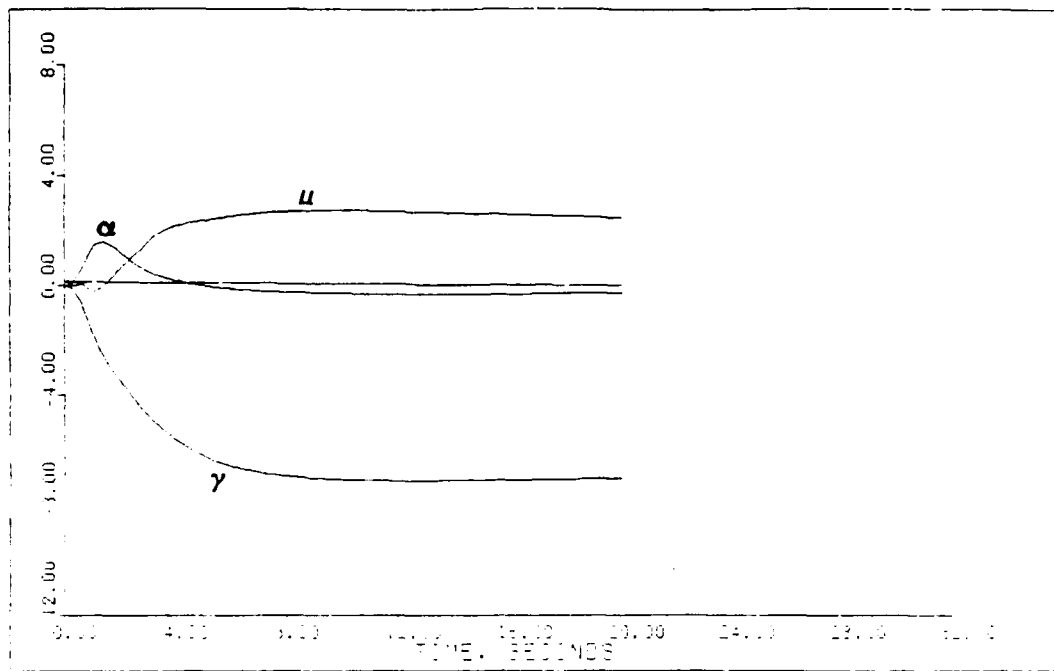


Fig. 5.32. Outputs, Including Surface Nonlinearity, Flight Condition 4

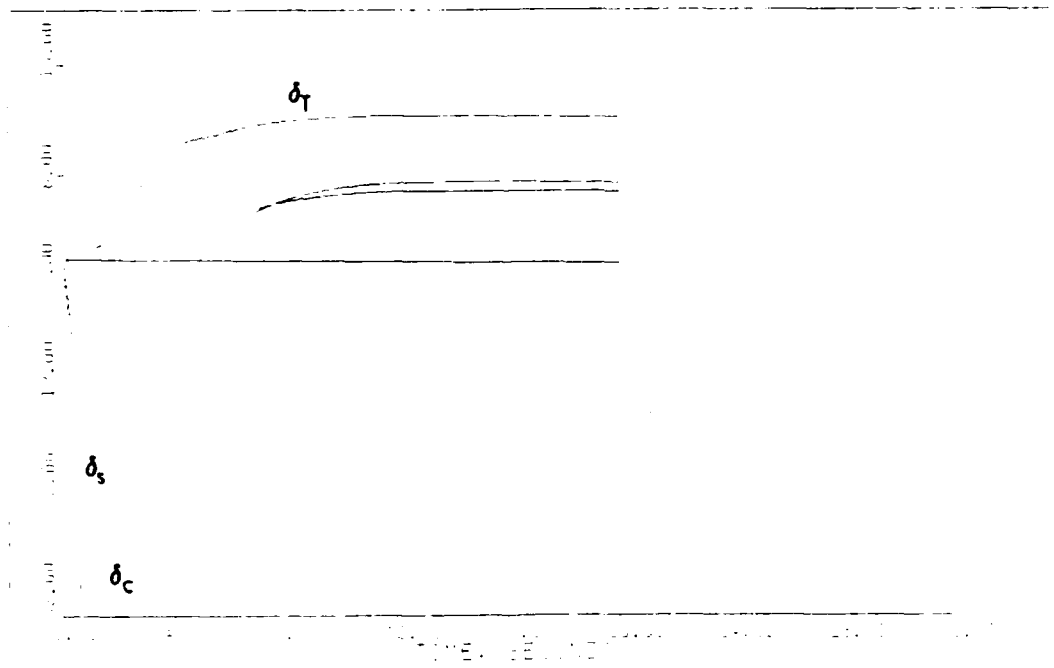


Fig. 5.33. Surface Deflections, Including Surface Nonlinearity, Flight Condition 4

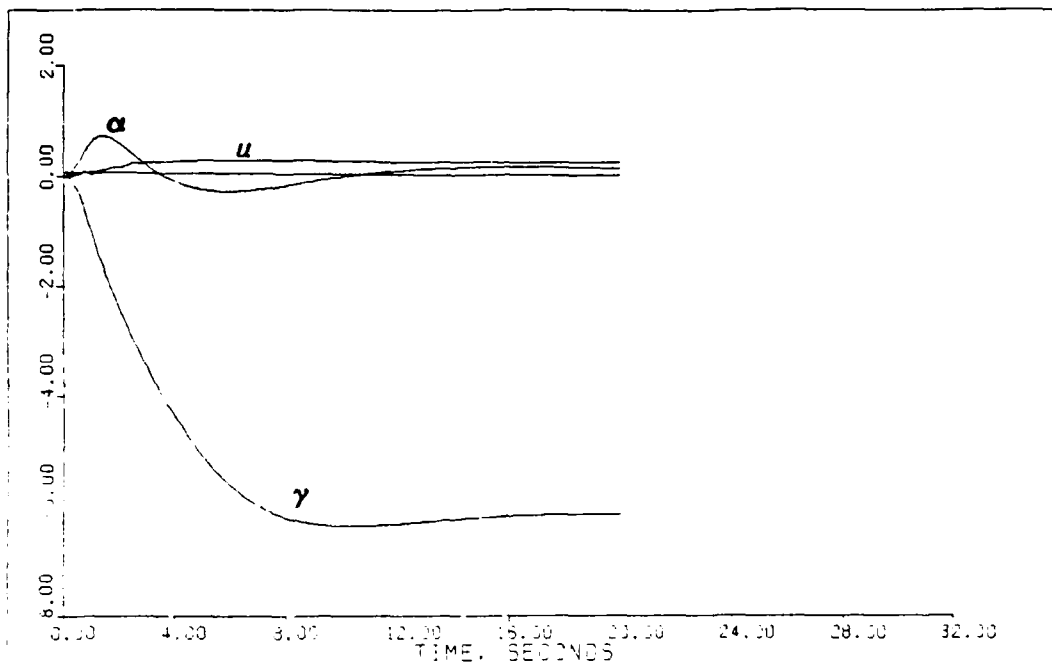


Fig. 5.34. Outputs, Including Surface Nonlinearity, Flight Condition 5

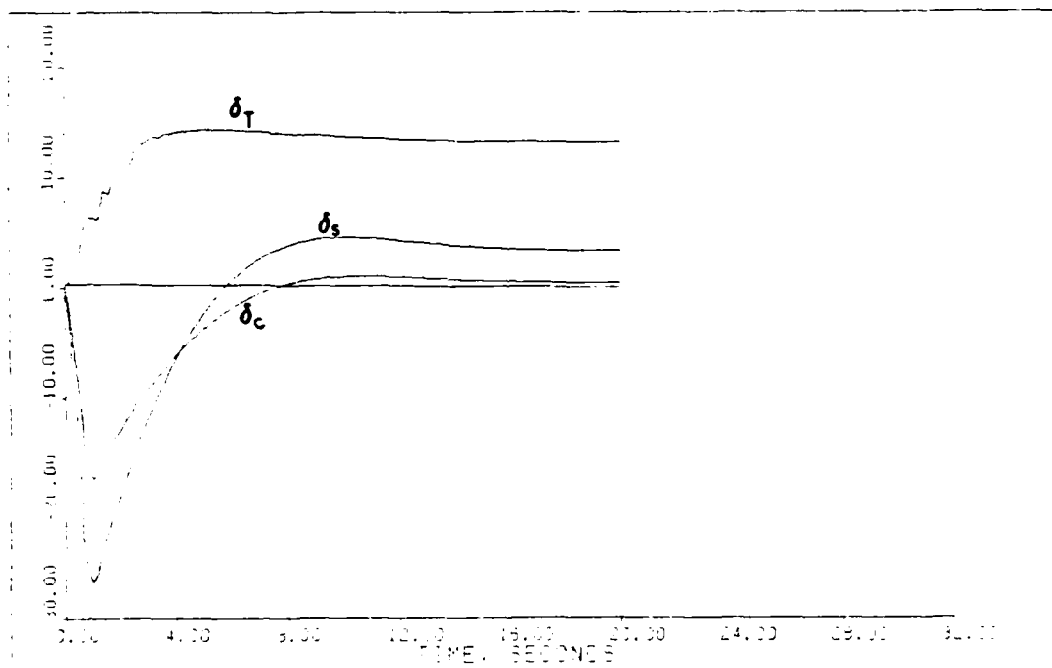


Fig. 5.35. Surface Deflections, Including Surface Nonlinearity, Flight Condition 5

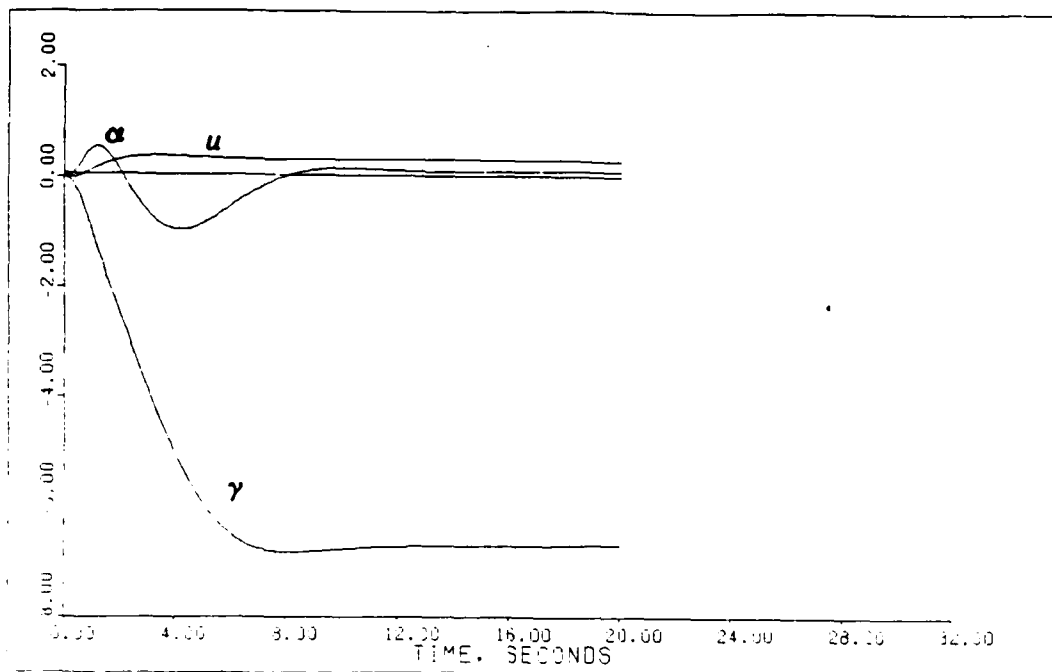


Fig. 5.36. Outputs, Including Surface Nonlinearity, Flight Condition 6

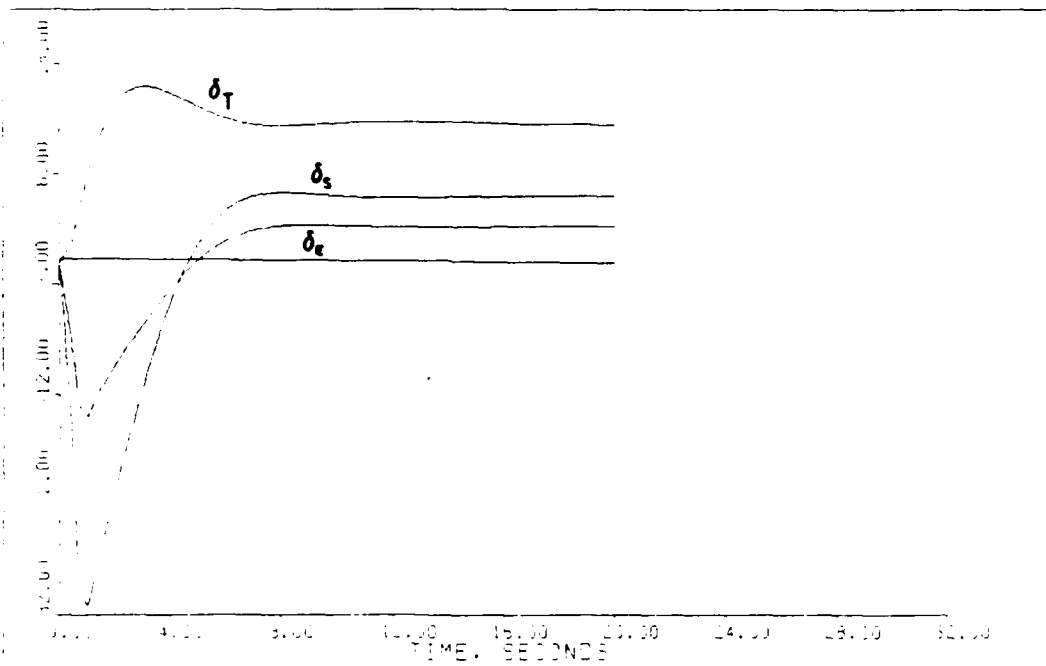


Fig. 5.37. Surface Deflections, Including Surface Nonlinearity, Flight Condition 6

The output responses are basically unaffected by the surface nonlinearities other than the expected result of altered sigma matrix elements. Increased coupling, particularly with respect to velocity, is evident from the reduction in the corresponding sigma elements for flight conditions 1, 3, 4, and 5. The flight path angle response is not significantly degraded from the adjustments for the surface nonlinearity. Control surface deflections, however, still exhibit a slight jump (particularly the rotating vanes) that cannot be avoided without further reduction of the velocity sigma element or possibly a smoothing of the surface drag derivative at angles of attack near zero. This erratic behavior does not appear in the outputs with sufficient magnitude to warrant redesign to attempt to remove it.

5.6 Addition of Sensor Noise

The controller design of Section 5.5 for flight condition 1 is next subjected to simulations in which independent white, gaussian noise is injected into each of the four measured quantities (u , α , γ , and q). The first simulation includes realistic noise levels for a comparable aircraft (Grumman F-14 Tomcat, Reference 12). This data is presented in Table 5.7 as derived in Appendix C (units are radians). Note that no realistic values of velocity measurement noise are provided and it is therefore omitted from the

TABLE 5.7
SENSOR NOISE DATA

Measured Quantity	Noise Mean	Variance
α	0.0	1.220E-5
γ	0.0	1.309E-5
q	0.0	3.220E-5

simulation. To establish statistical validity, the simulation is performed five times with a different random noise seed. The results of the first four simulations and a mean response are shown in Figures 5.38 through 5.47. Comparing these results to Figures 5.26 and 5.27, the response is indistinguishable from the simulation without noise. Although this is a satisfying result, it does not yield any information on the system's response to higher noise levels. Therefore, the noise levels are increased individually to a value that appears to be the threshold that the system can withstand. The threshold is defined in this case as the highest noise level that does not result in divergence beyond control surface limits within the twenty-second simulation time. Table 5.8 contains the threshold values of noise, expressed in units of radians (velocity noise units are feet per second). Comparing the threshold variance on the basis of signal to noise ratio, the system is most sensitive to noise in the velocity measurement and least

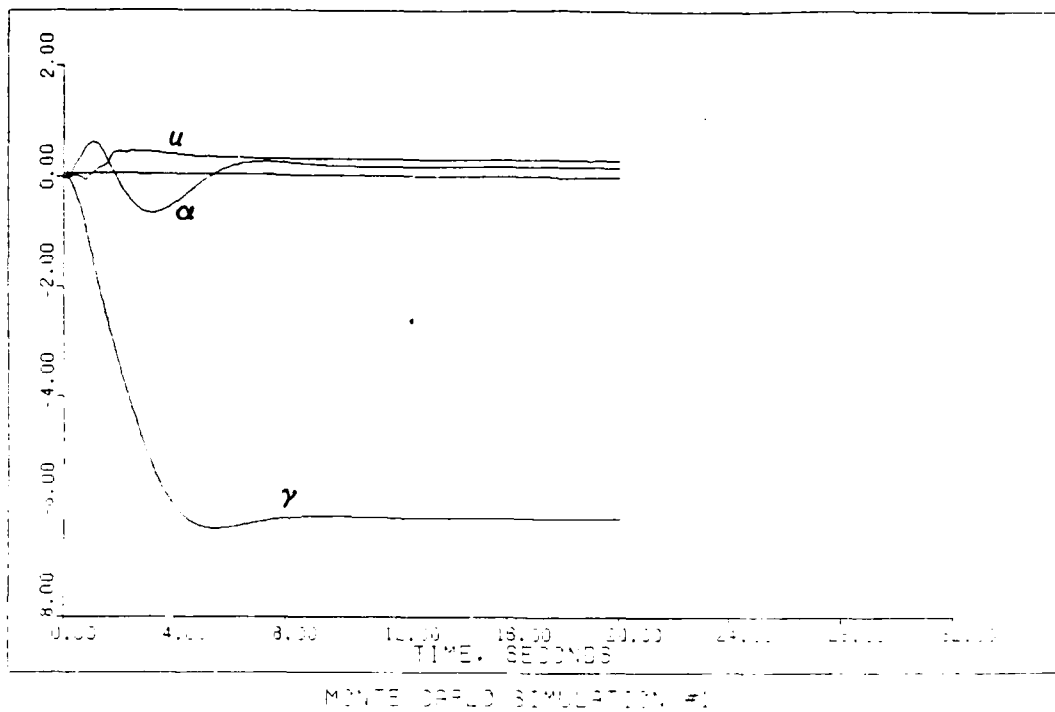


Fig. 5.38. Outputs, Realistic Noise, Simulation 1

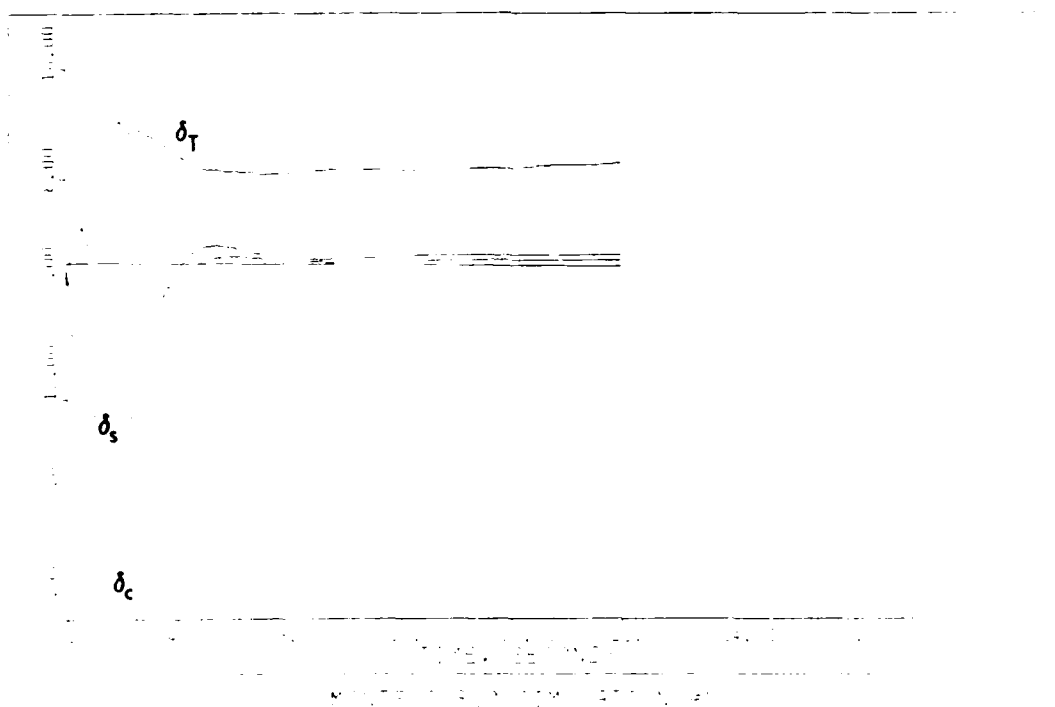


Fig. 5.39. Surface Deflections, Realistic Noise, Simulation 1

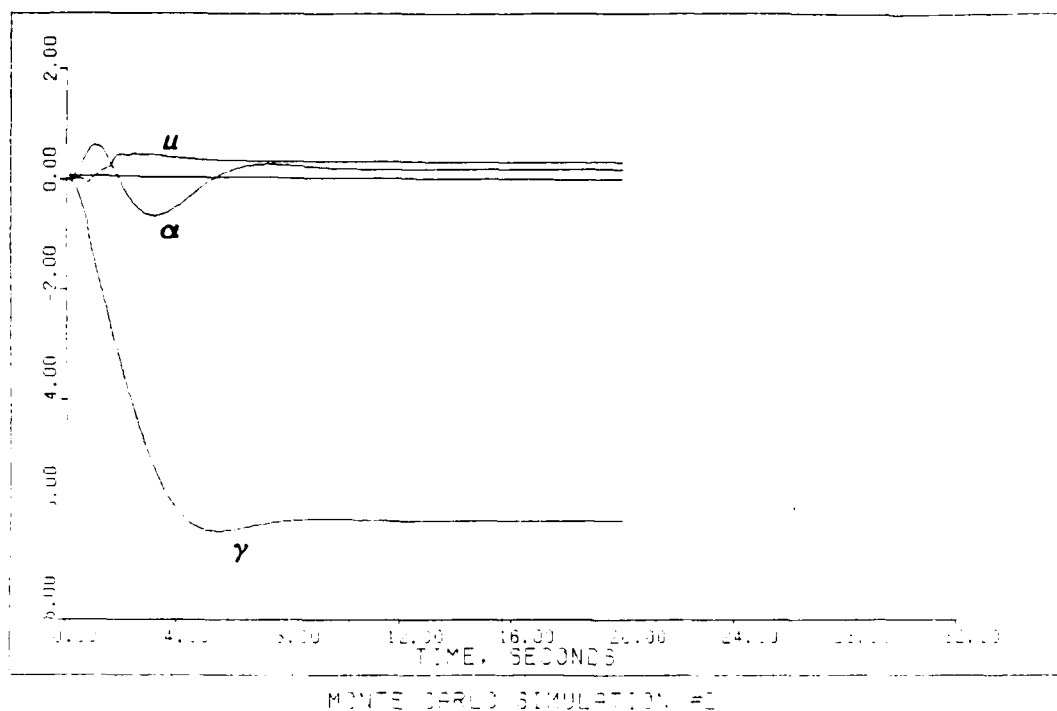


Fig. 5.40. Outputs, Realistic Noise, Simulation 2

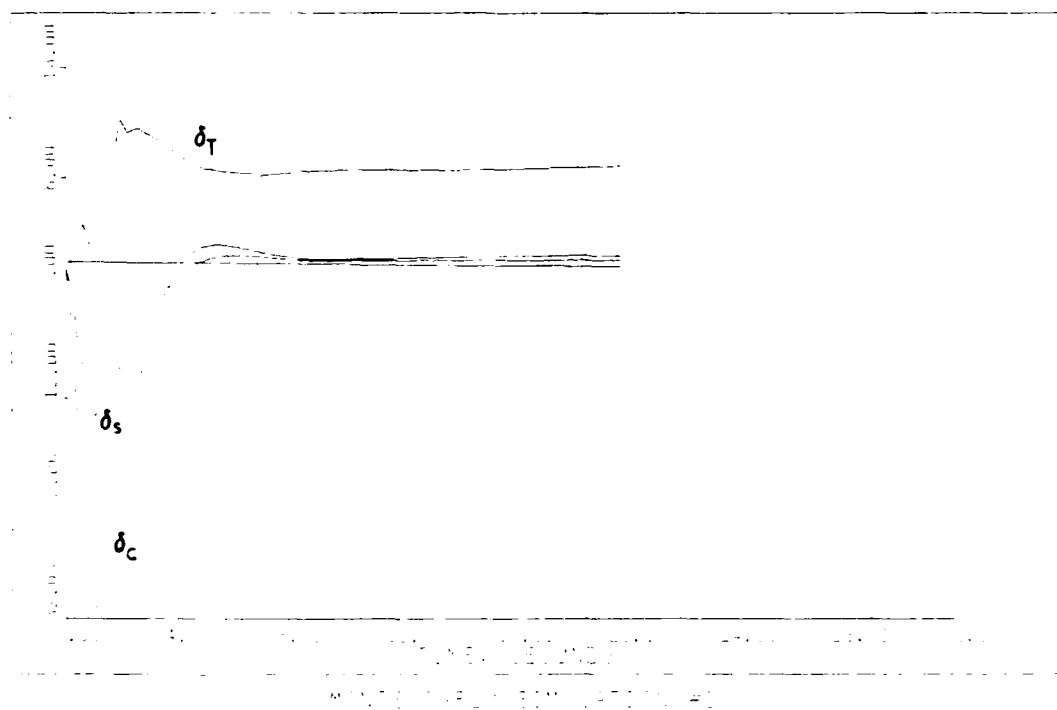


Fig. 5.41. Surface Deflections, Realistic Noise, Simulation 2

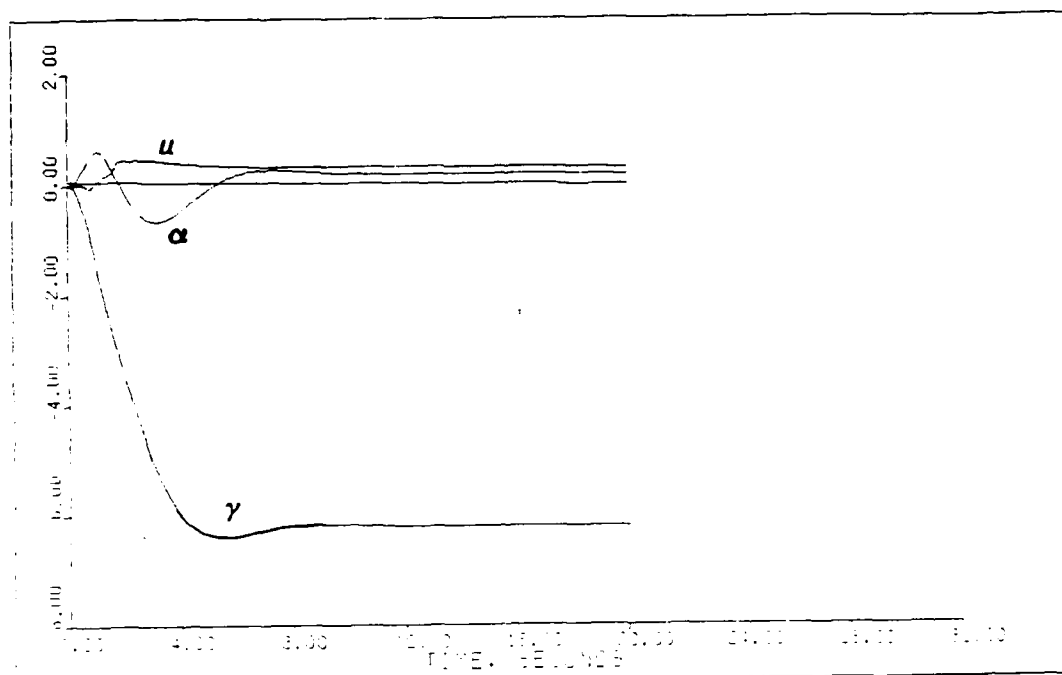


Fig. 5.42. Outputs, Realistic Noise, Simulation 3

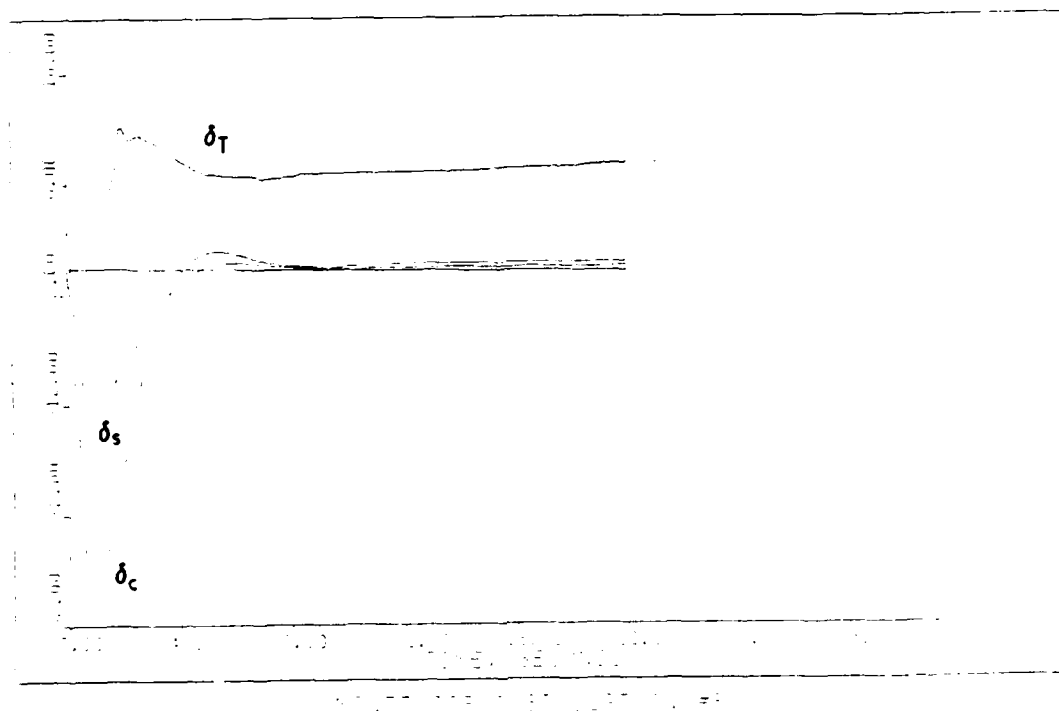
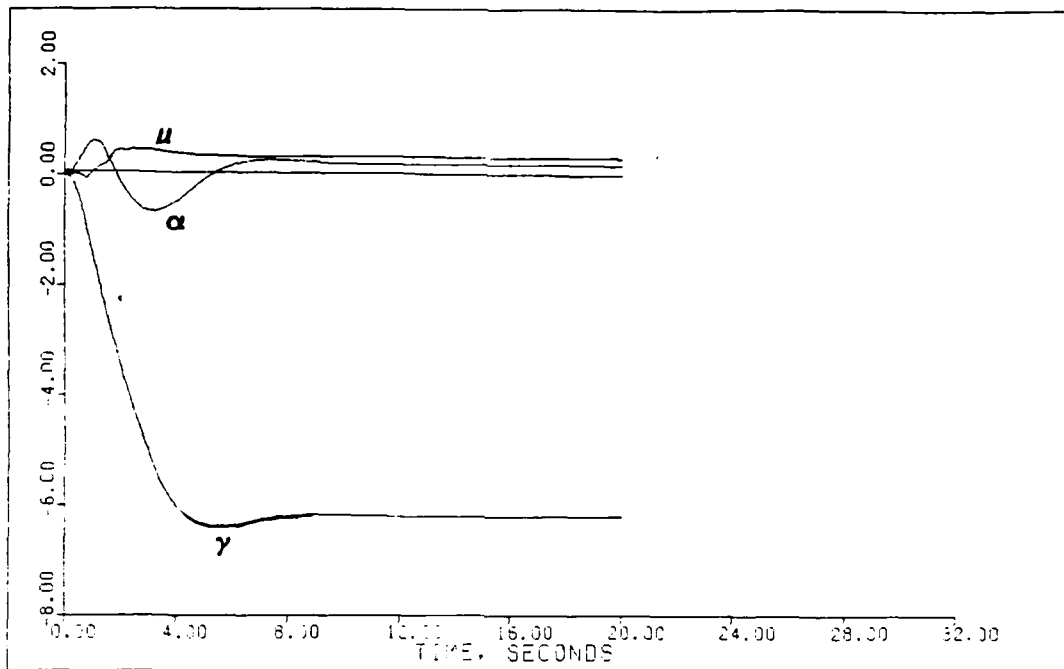
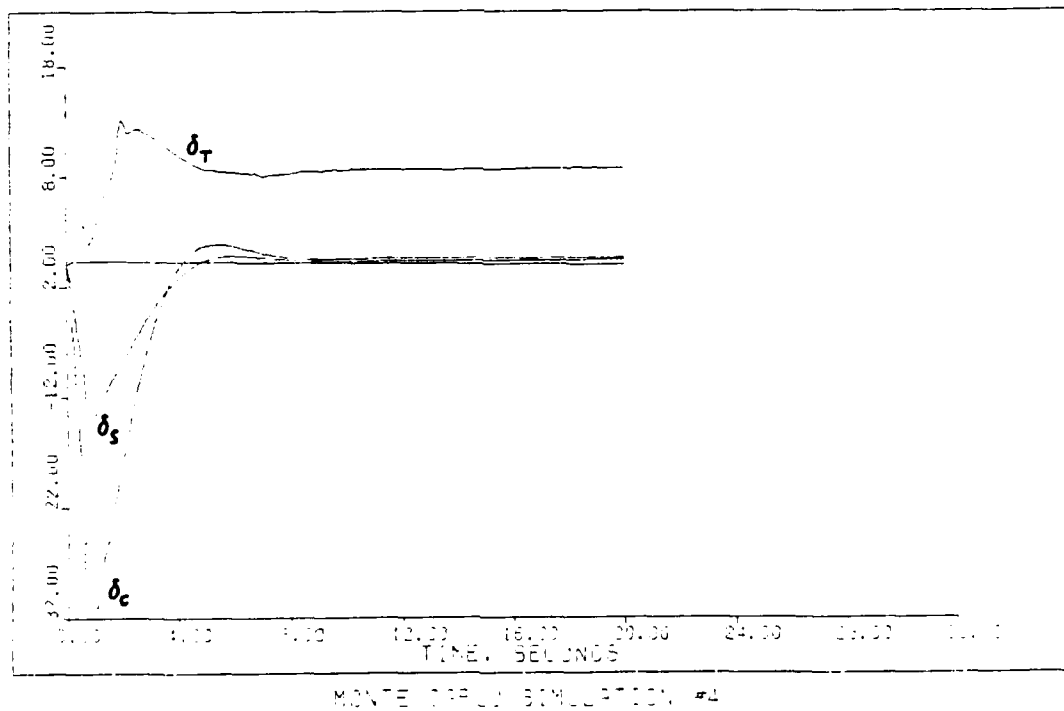


Fig. 5.43. Surface Deflections, Realistic Noise, Simulation 3



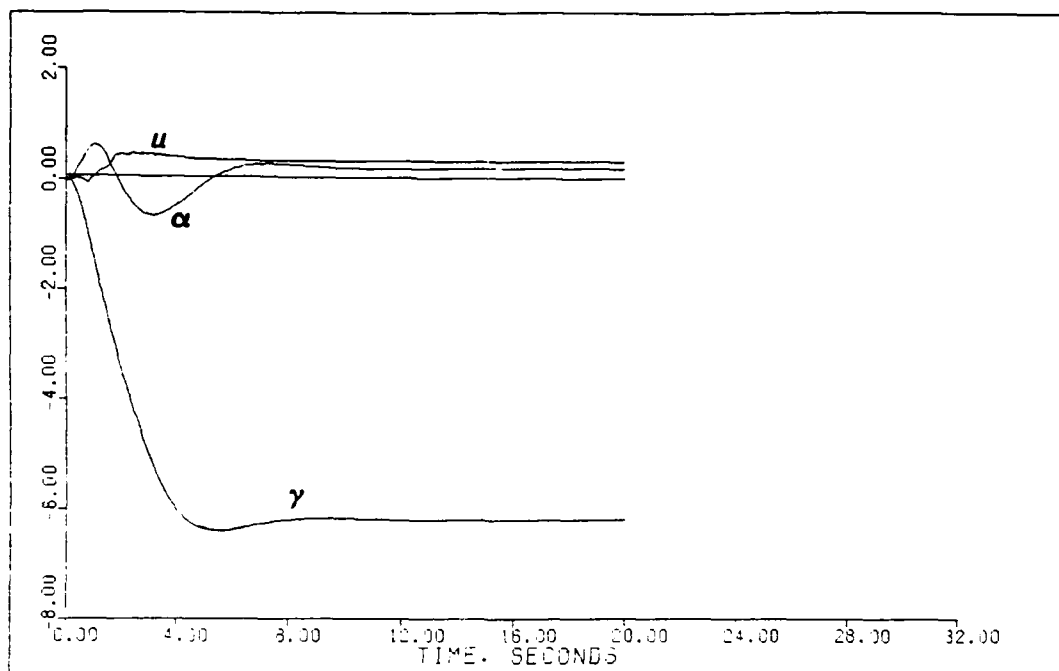
MONTE CARLO SIMULATION #4

Fig. 5.44. Outputs, Realistic Noise, Simulation 4



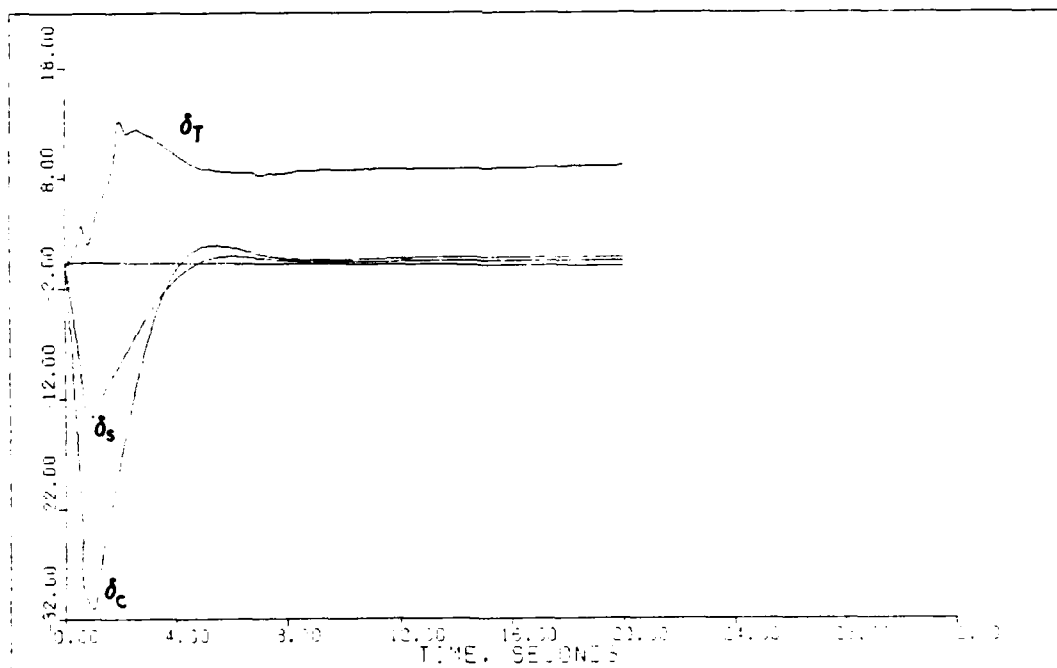
MONTE CARLO SIMULATION #4

Fig. 5.45. Surface Deflections, Realistic Noise, Simulation 4



MONTÉ CARLO SIMULATION MEAN

Fig. 5.46. Outputs, Realistic Noise, Simulation Mean



MONTÉ CARLO SIMULATION MEAN

Fig. 5.47. Surface Deflections, Realistic Noise, Simulation Mean

TABLE 5.8
THRESHOLD NOISE LEVELS

Measured Quantity	Threshold Variance	Signal to Noise Ratio
u	0.010	86 db
α	0.010	26 db
γ	0.005	25 db
q	0.010	8 db

sensitive to measurement of the pitch rate. Since the velocity feedback channel has the highest gain (diagonal sigma element) it is to be expected that the system would be most sensitive to noise in that channel. The signal to noise ratios presented here are calculated based on the maximum absolute value of the signal of interest encountered during the simulation. As with the realistic noise, five independent simulations are accomplished at each threshold value to obtain a statistically valid sample of the responses. Figures 5.48 through 5.87 contain the first four responses and a mean response for each of the four types of noise. It is apparent in many of the individual and mean simulations that the noise causes the control surfaces to gradually diverge in time. This result is predictable since the white gaussian noise input is being integrated by the controller, resulting in Brownian motion or random walk (10:154). This divergence tends to be hidden

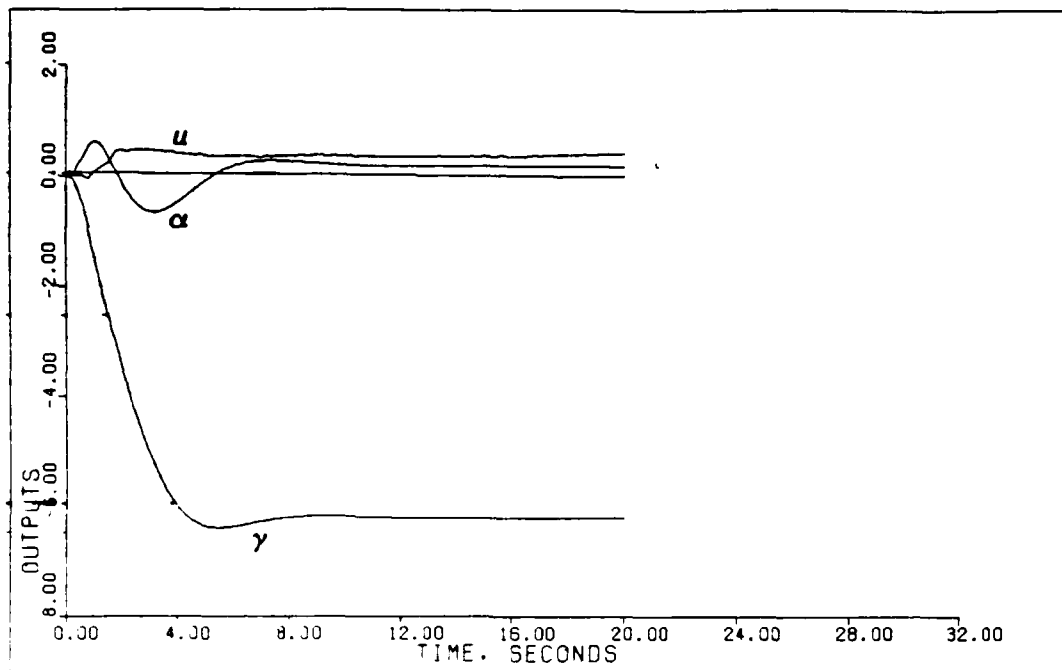


Fig. 5.48. Outputs, Velocity Noise, Simulation 1

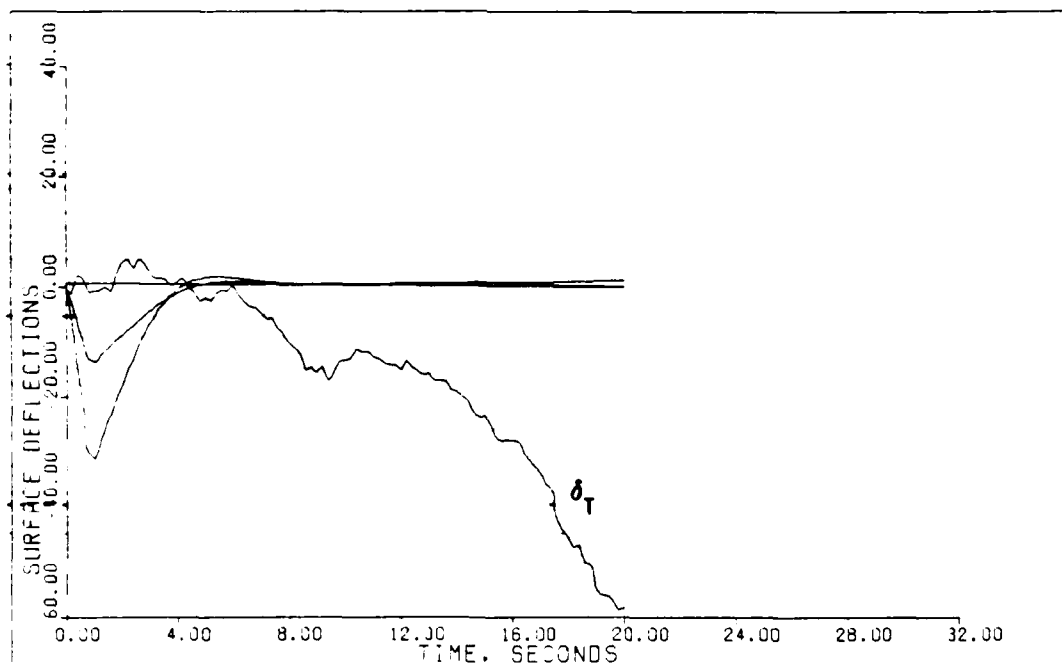


Fig. 5.49. Surface Deflections, Velocity Noise, Simulation 1

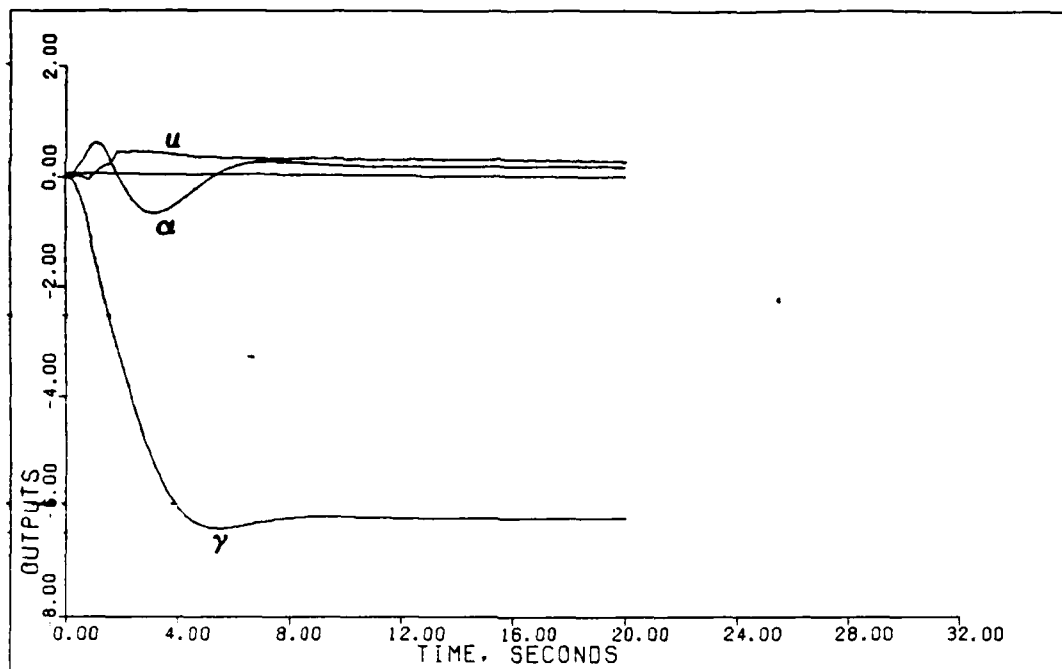


Fig. 5.50. Outputs, Velocity Noise, Simulation 2

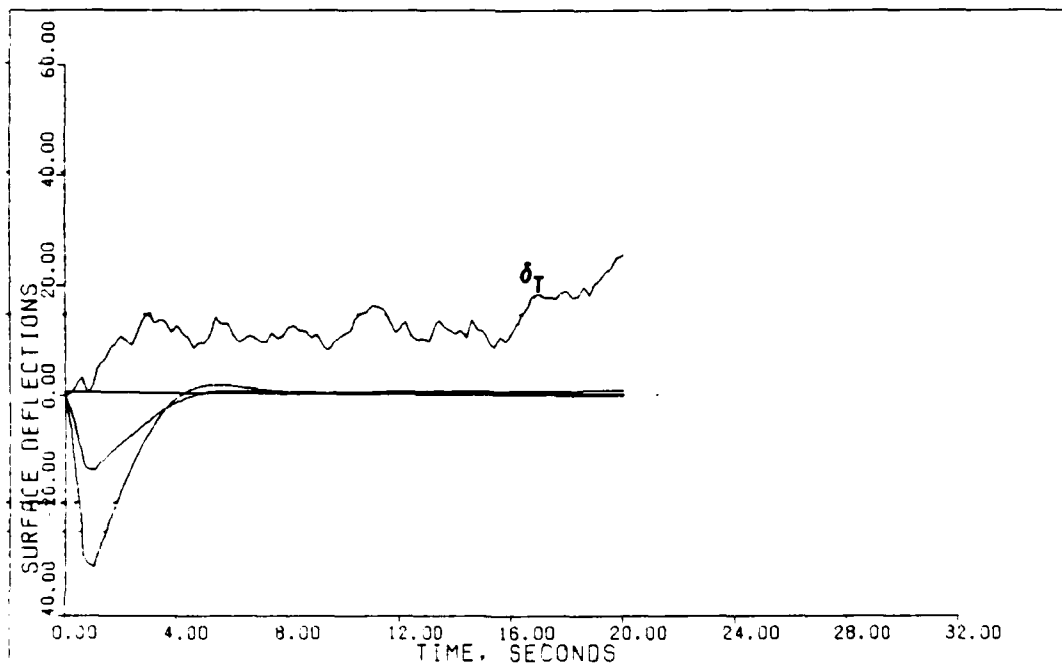


Fig. 5.51. Surface Deflections, Velocity Noise, Simulation 2

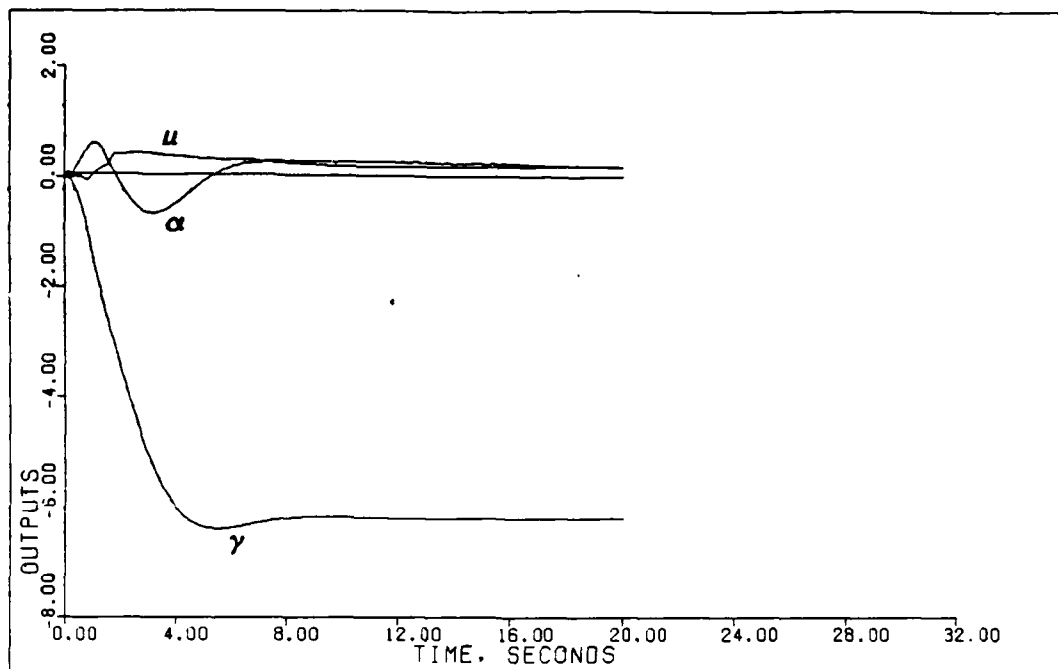


Fig. 5.52. Outputs, Velocity Noise, Simulation 3

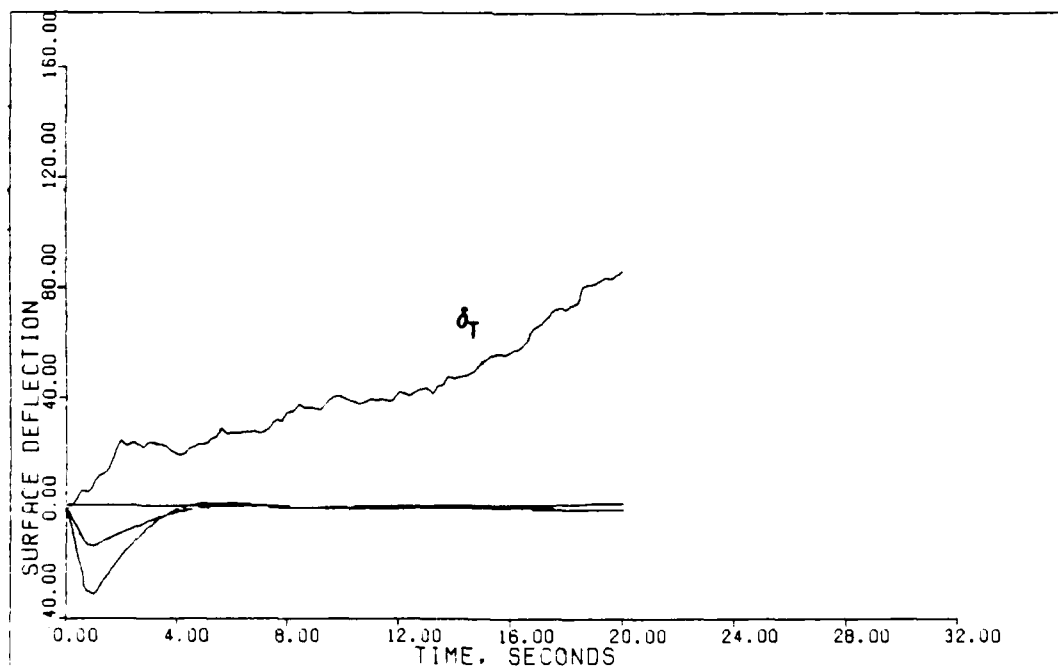


Fig. 5.53. Surface Deflections, Velocity Noise, Simulation 3

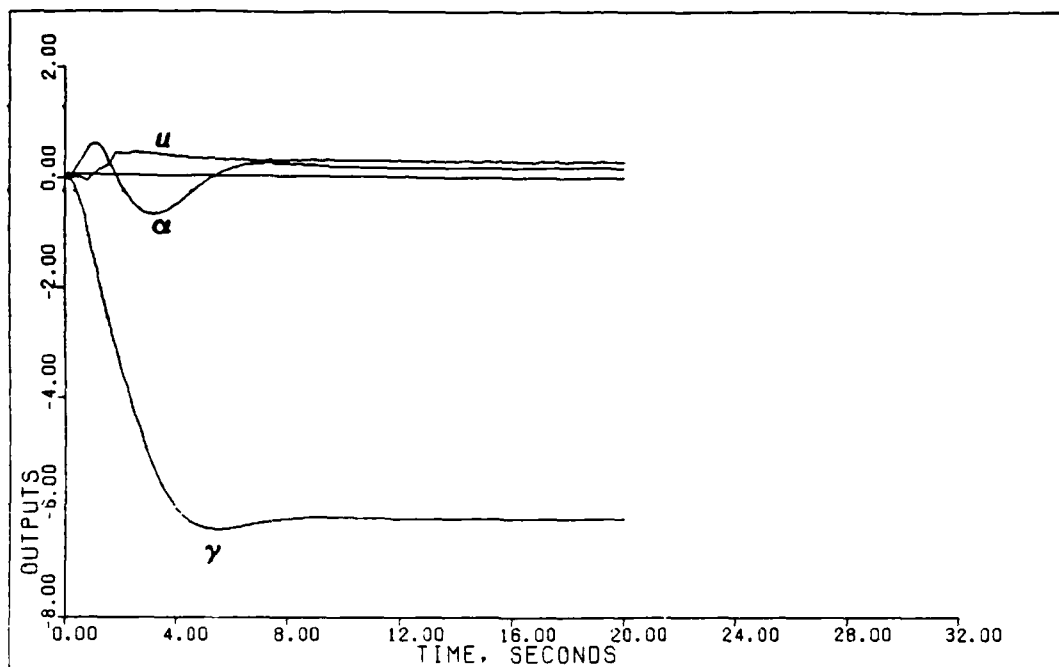


Fig. 5.54. Outputs, Velocity Noise, Simulation 4

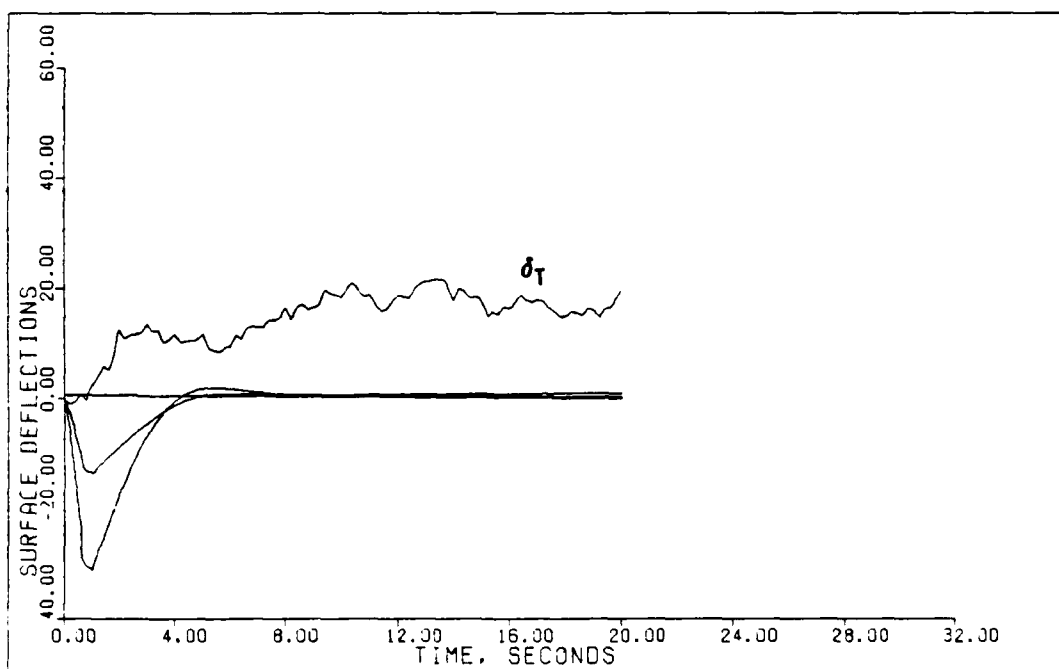


Fig. 5.55. Surface Deflections, Velocity Noise, Simulation 4

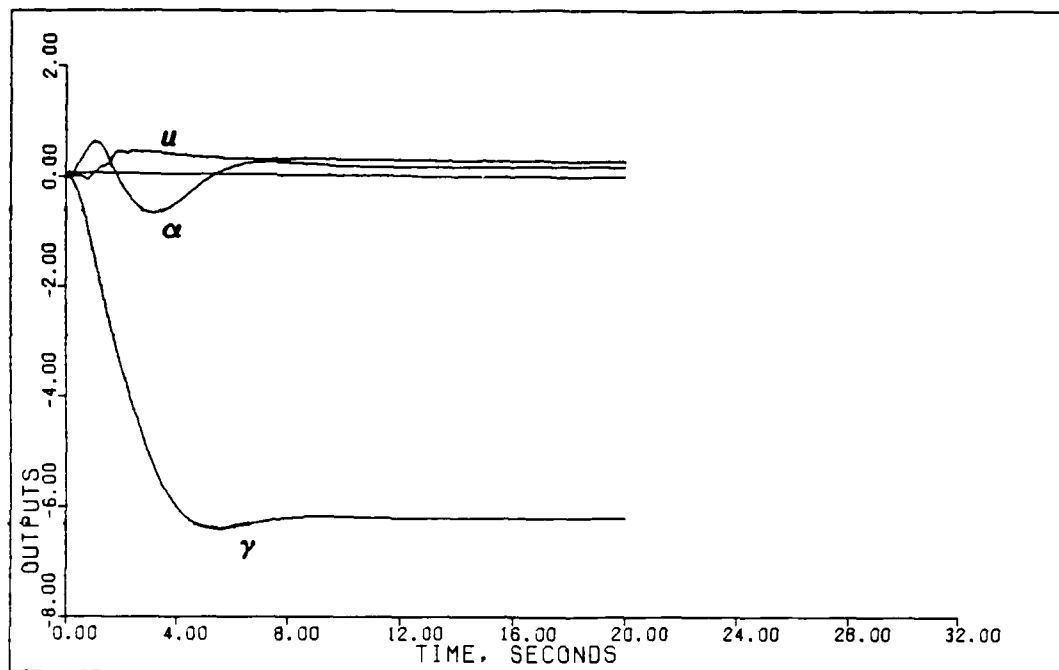


Fig. 5.56. Outputs, Velocity Noise, Simulation Mean

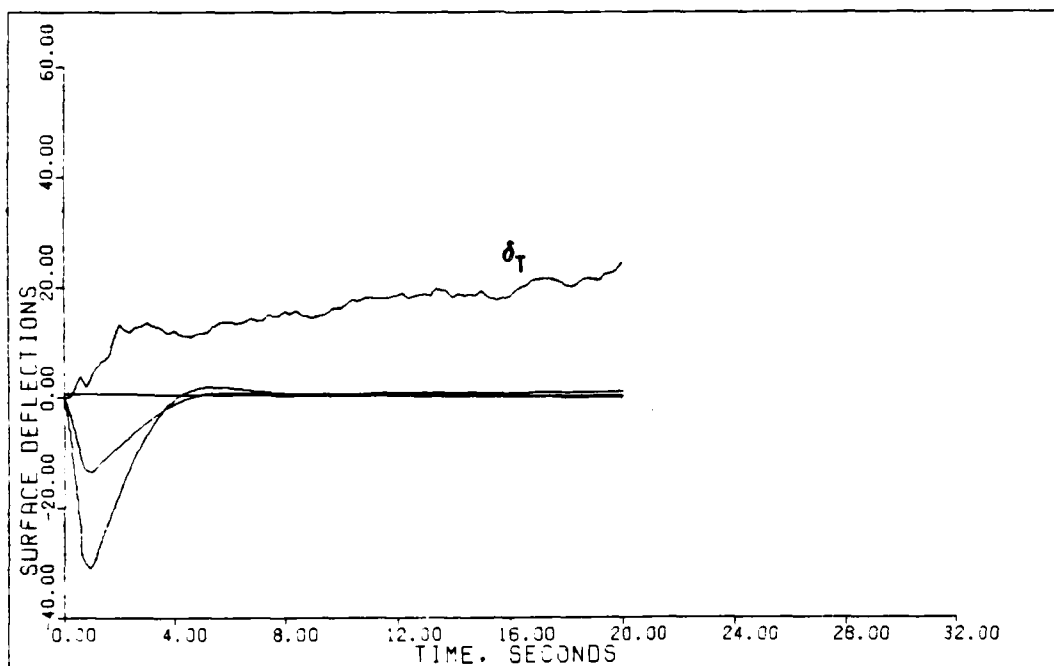


Fig. 5.57. Surface Deflections, Velocity Noise, Simulation Mean

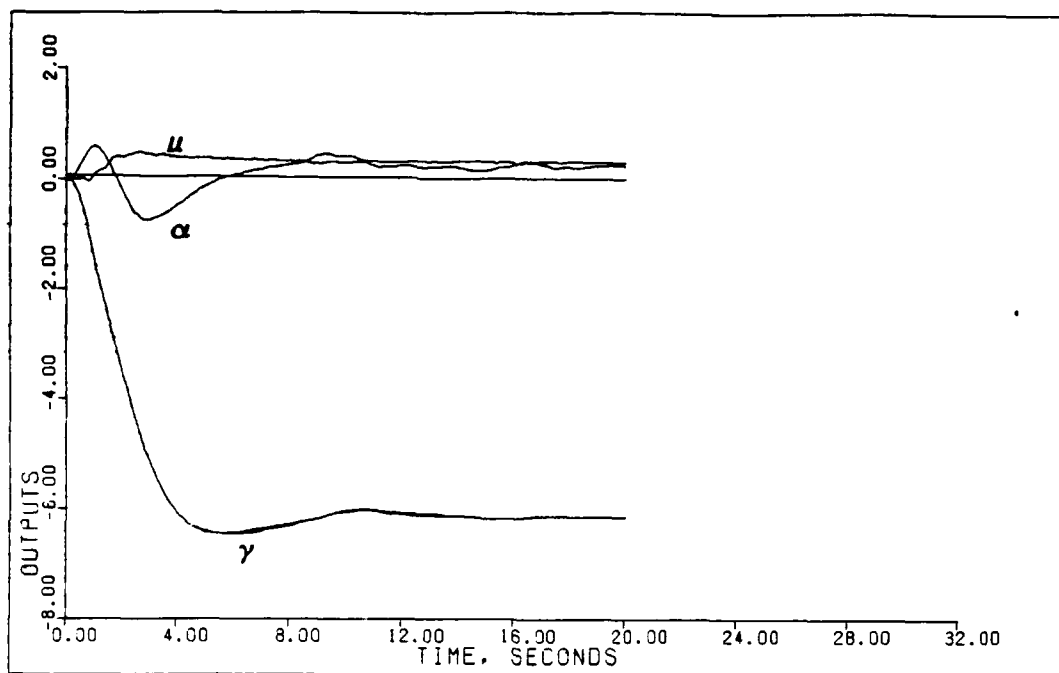


Fig. 5.58. Outputs, Angle of Attack Noise, Simulation 1

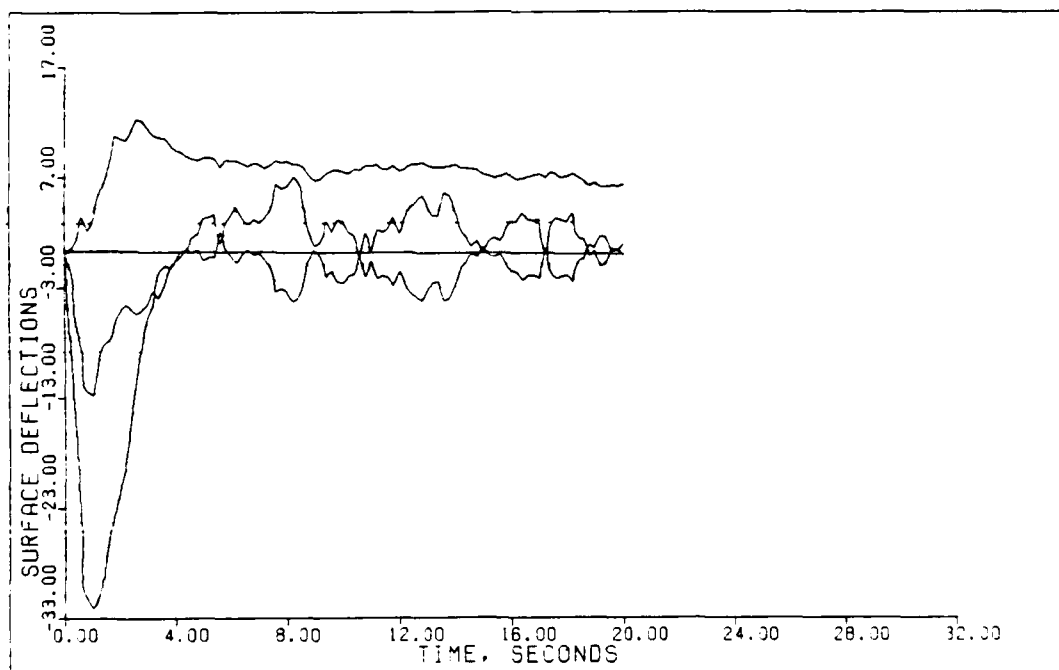


Fig. 5.59. Surface Deflections, Angle of Attack Noise, Simulation 1

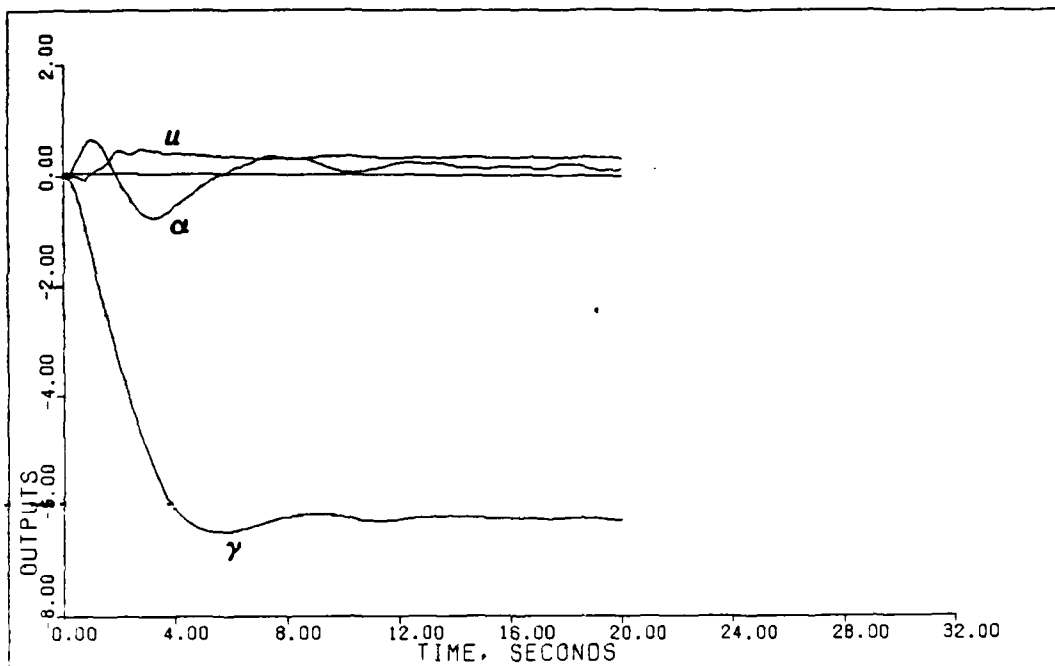


Fig. 5.60. Outputs, Angle of Attack Noise, Simulation 2

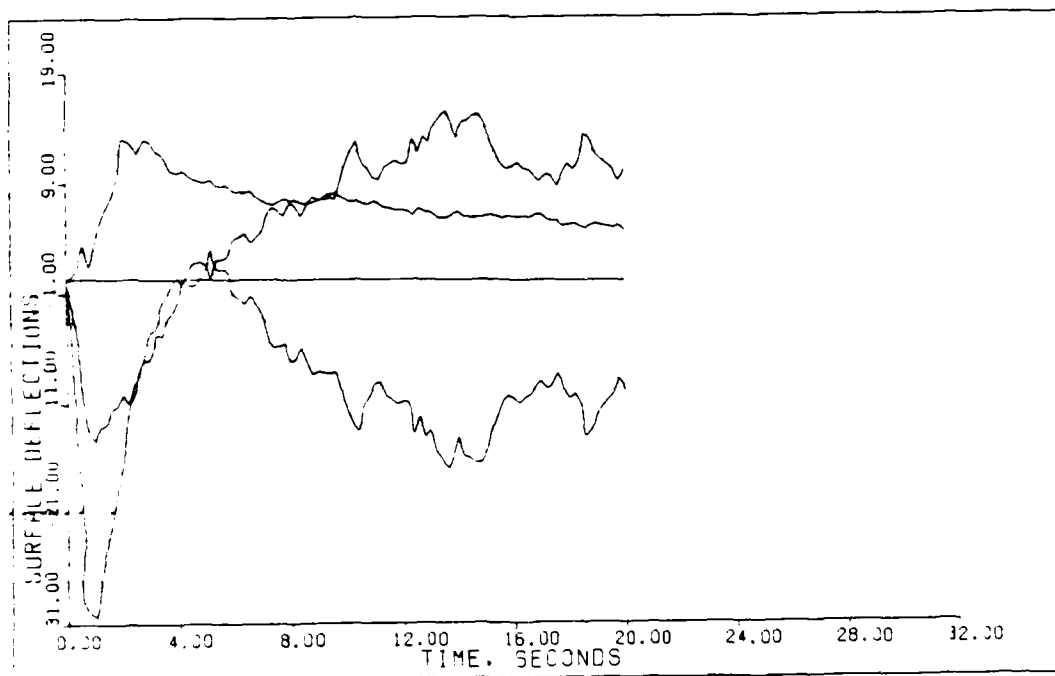


Fig. 5.61. Surface Deflections, Angle of Attack Noise, Simulation 2

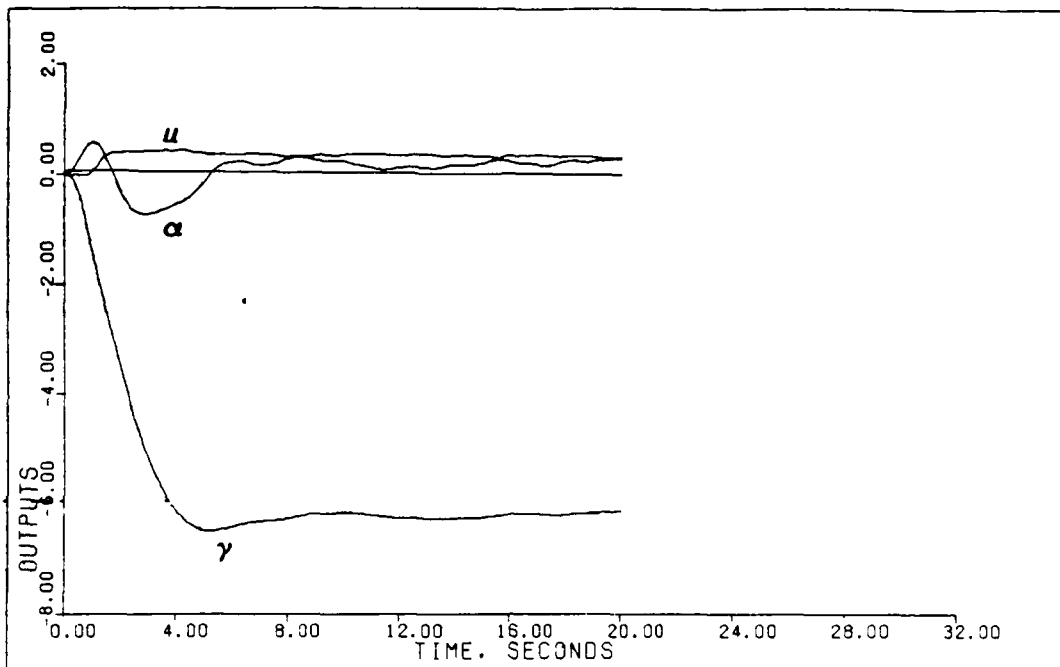


Fig. 5.62. Outputs, Angle of Attack Noise, Simulation 3

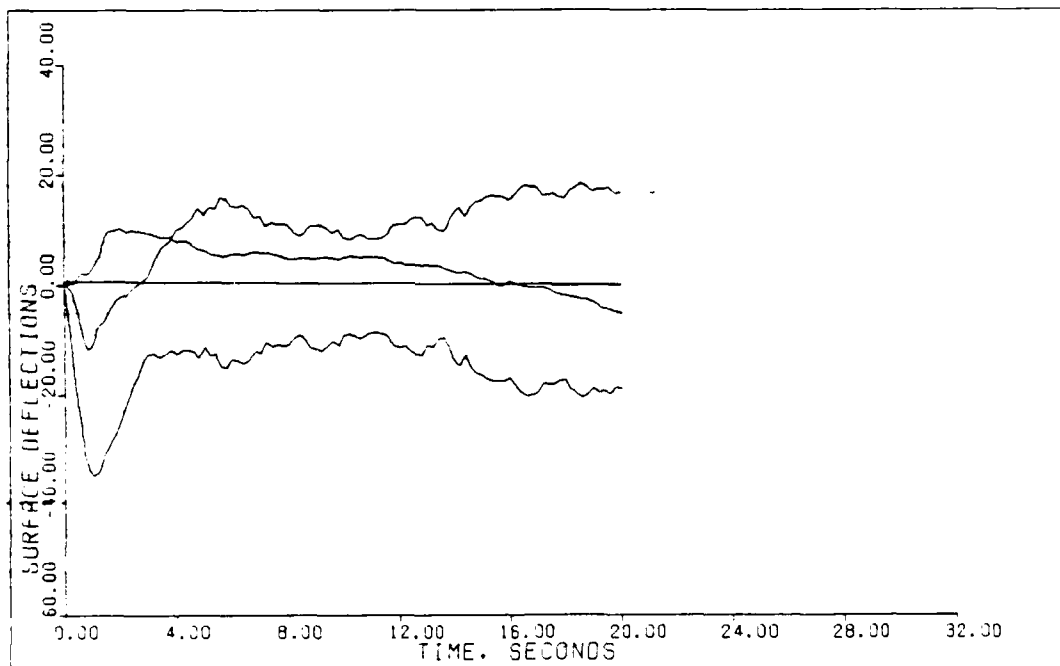


Fig. 5.63. Surface Deflections, Angle of Attack Noise, Simulation 3

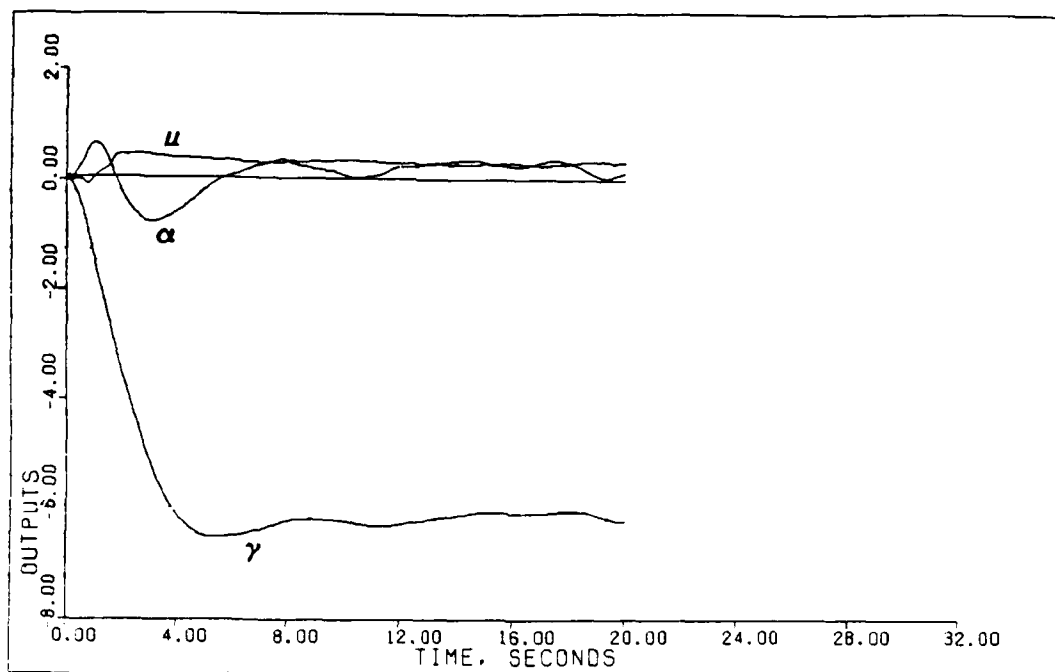


Fig. 5.64. Outputs, Angle of Attack Noise, Simulation 4

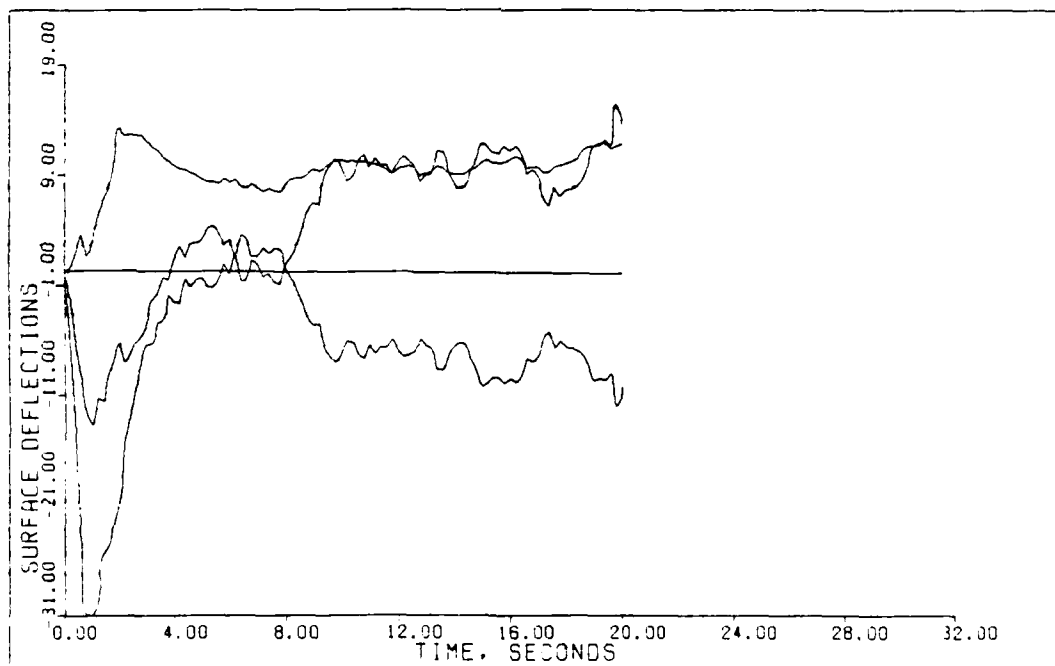


Fig. 5.65. Surface Deflections, Angle of Attack Noise, Simulation 4

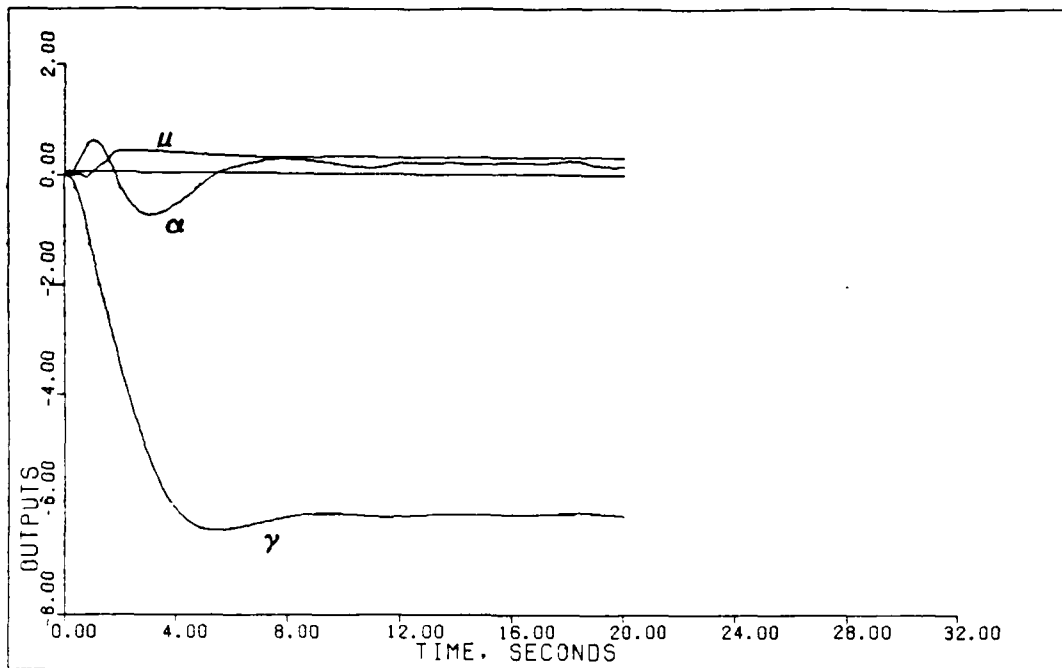


Fig. 5.66. Outputs, Angle of Attack Noise, Simulation Mean

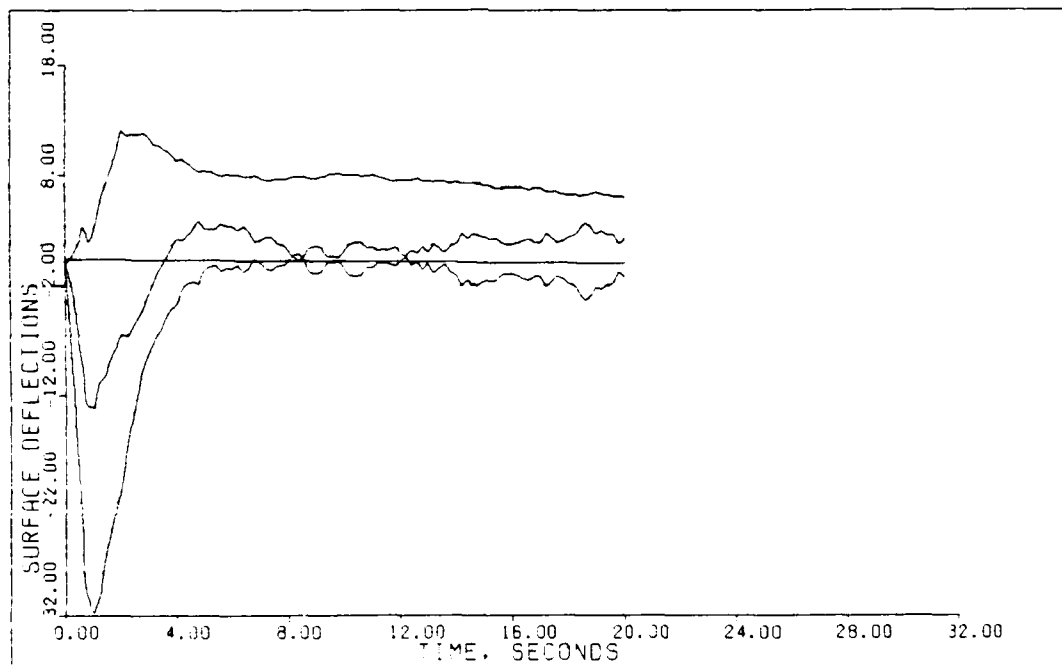


Fig. 5.67. Surface Deflections, Angle of Attack Noise, Simulation Mean

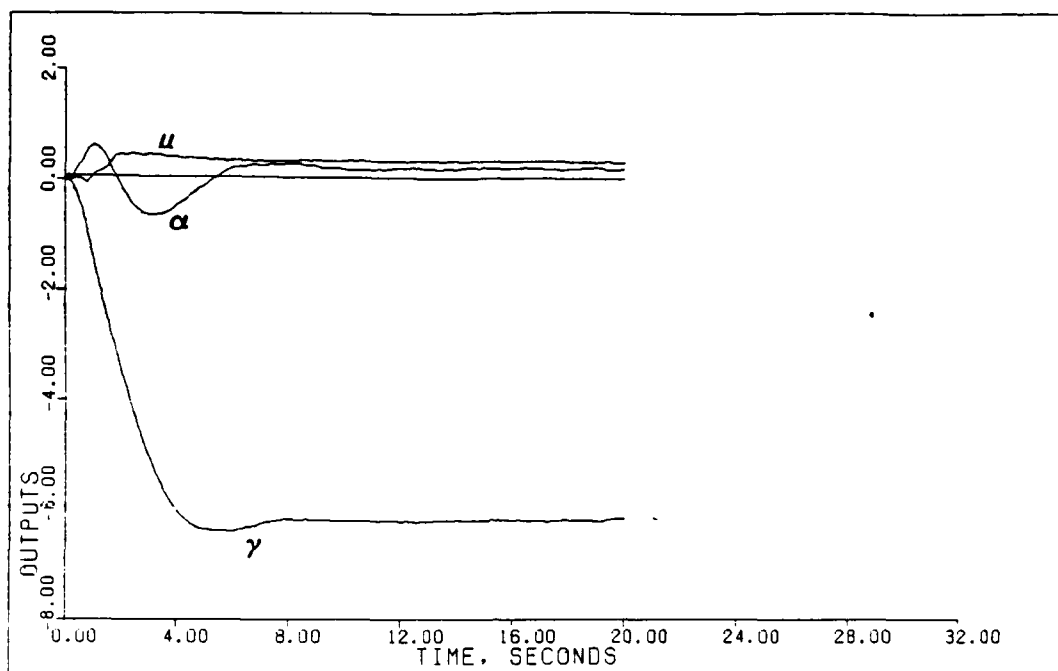


Fig. 5.68. Outputs, Flight Path Noise, Simulation 1

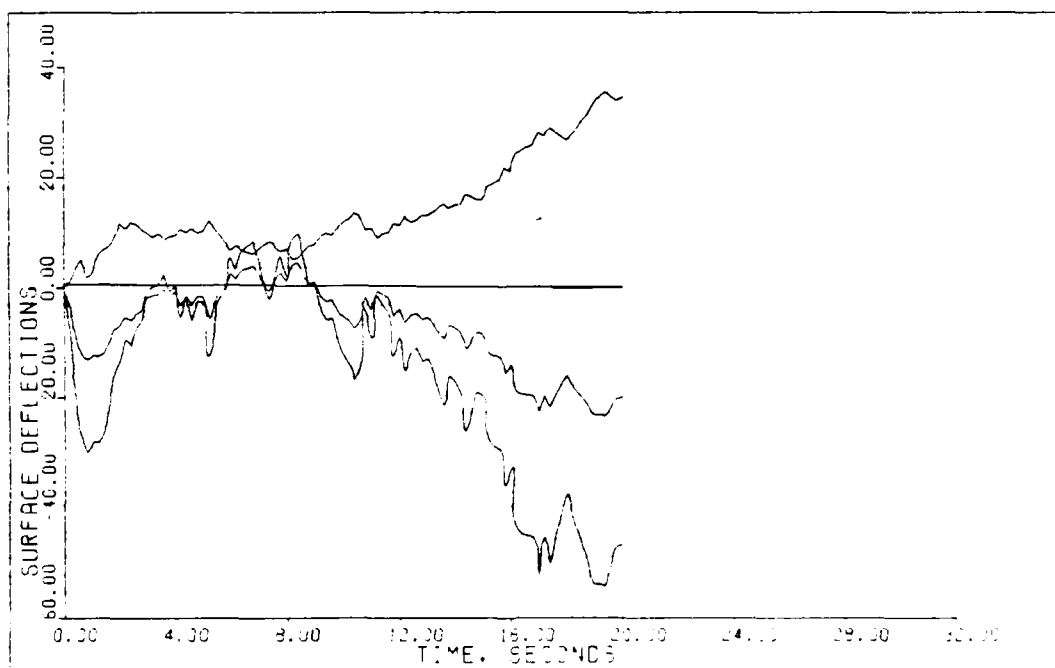


Fig. 5.69. Surface Deflections, Flight Path Noise, Simulation 1

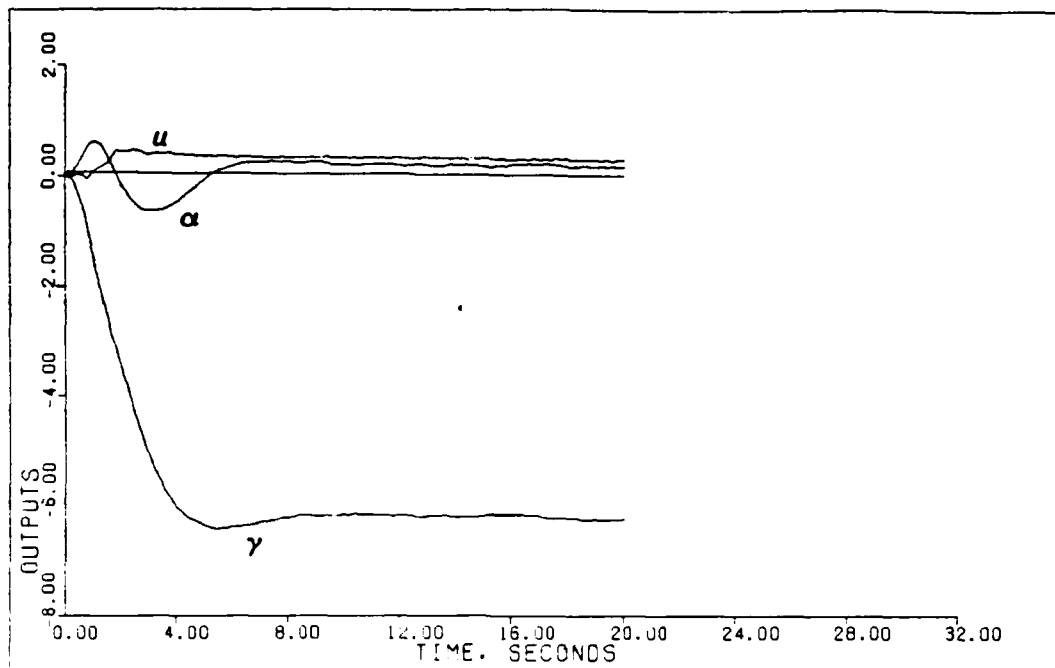


Fig. 5.70. Outputs, Flight Path Noise, Simulation 2

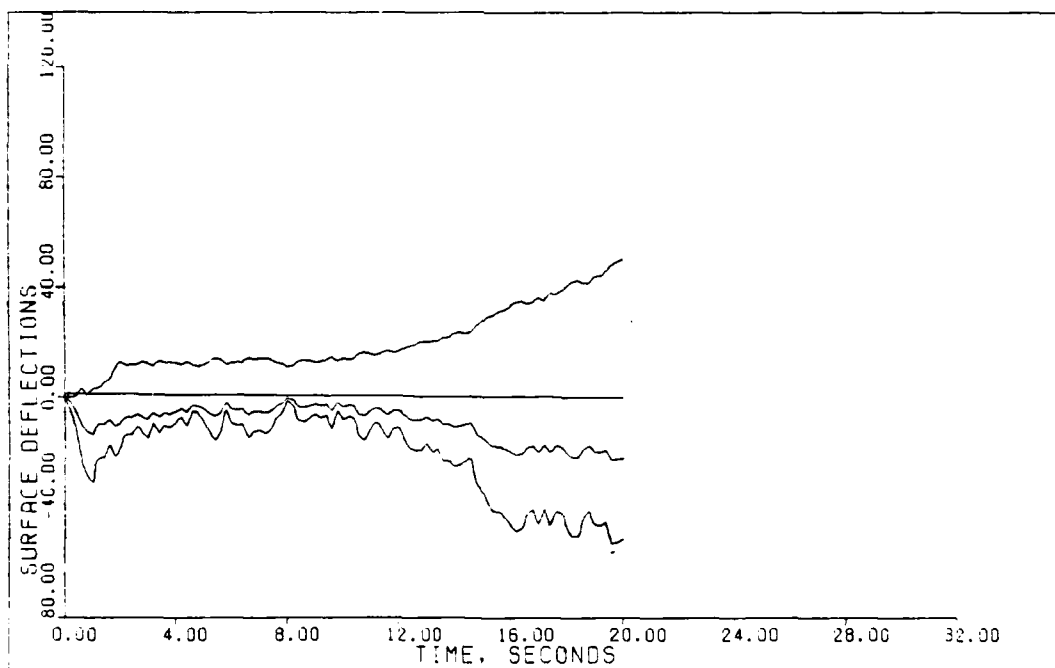


Fig. 5.71. Surface Deflections, Flight Path Noise, Simulation 2

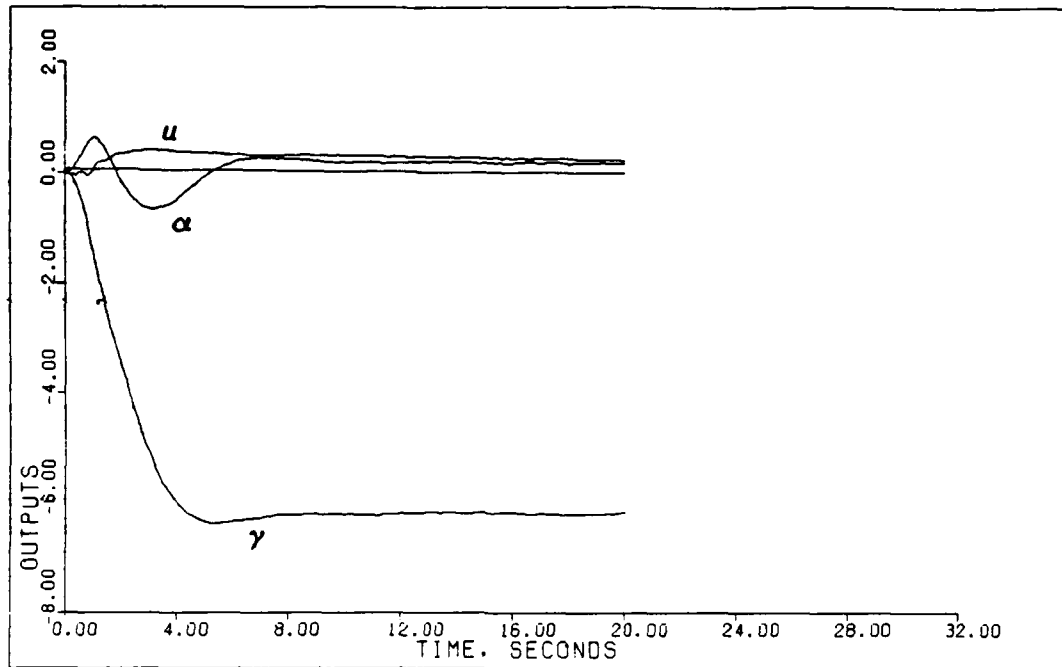


Fig. 5.72. Outputs, Flight Path Noise, Simulation 3

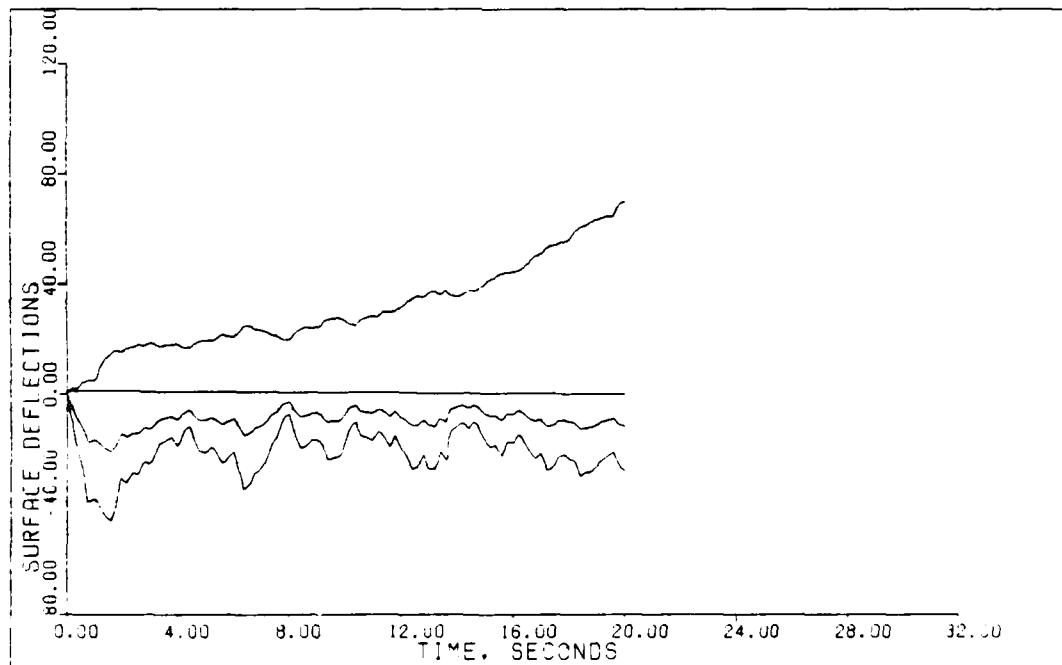


Fig. 5.73. Surface Deflections, Flight Path Noise, Simulation 3

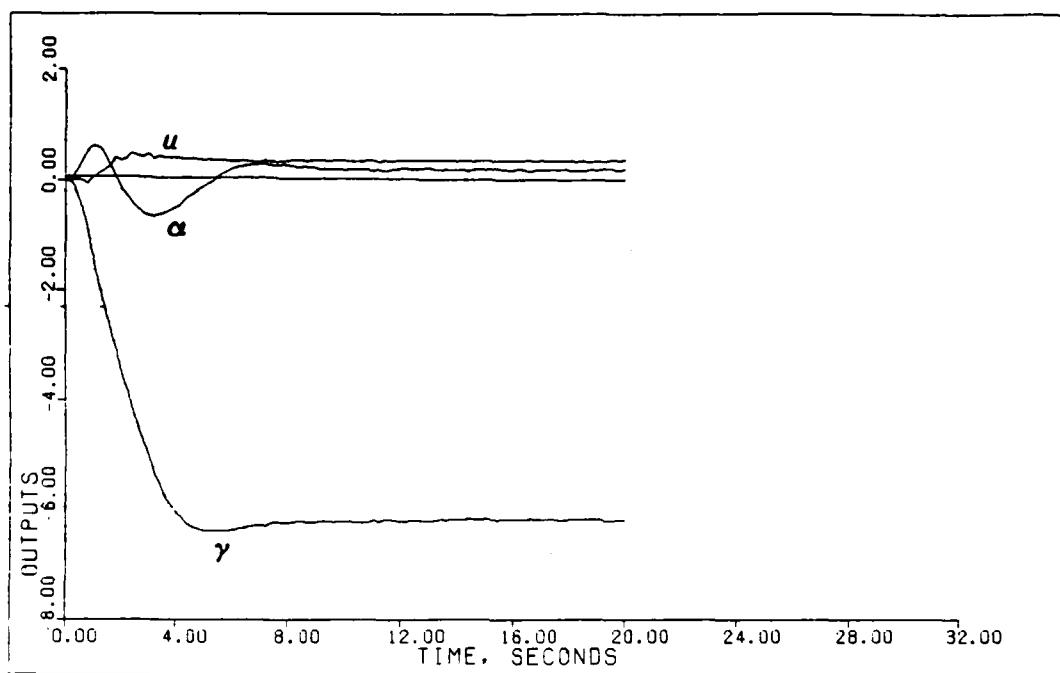


Fig. 5.74. Outputs, Flight Path Noise, Simulation 4

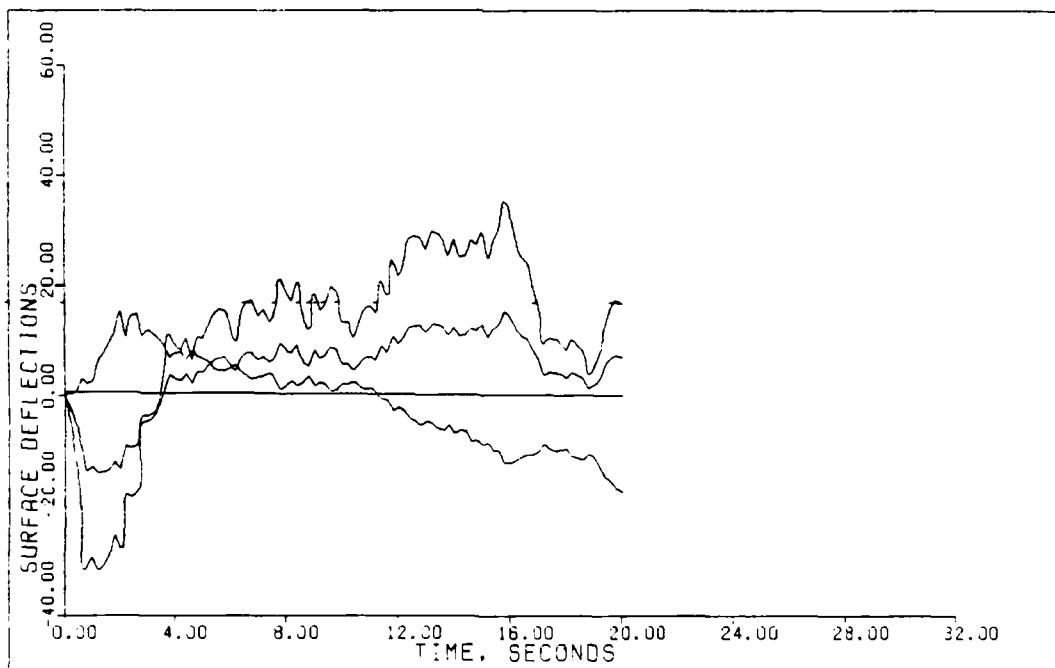


Fig. 5.75. Surface Deflections, Flight Path Noise, Simulation 4

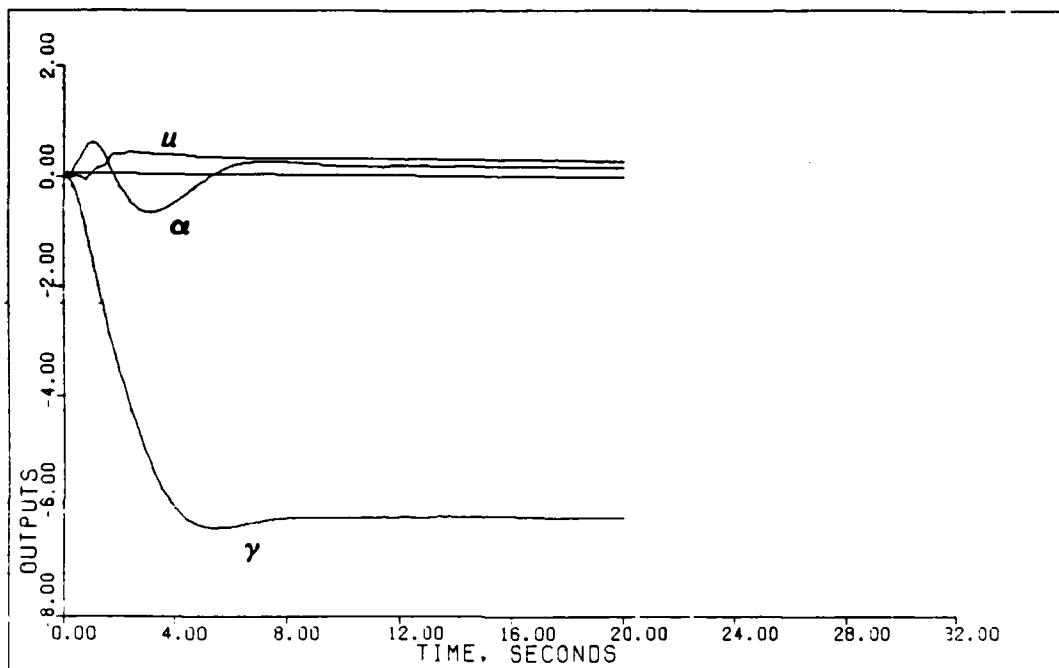


Fig. 5.76. Outputs, Flight Path Noise, Simulation Mean

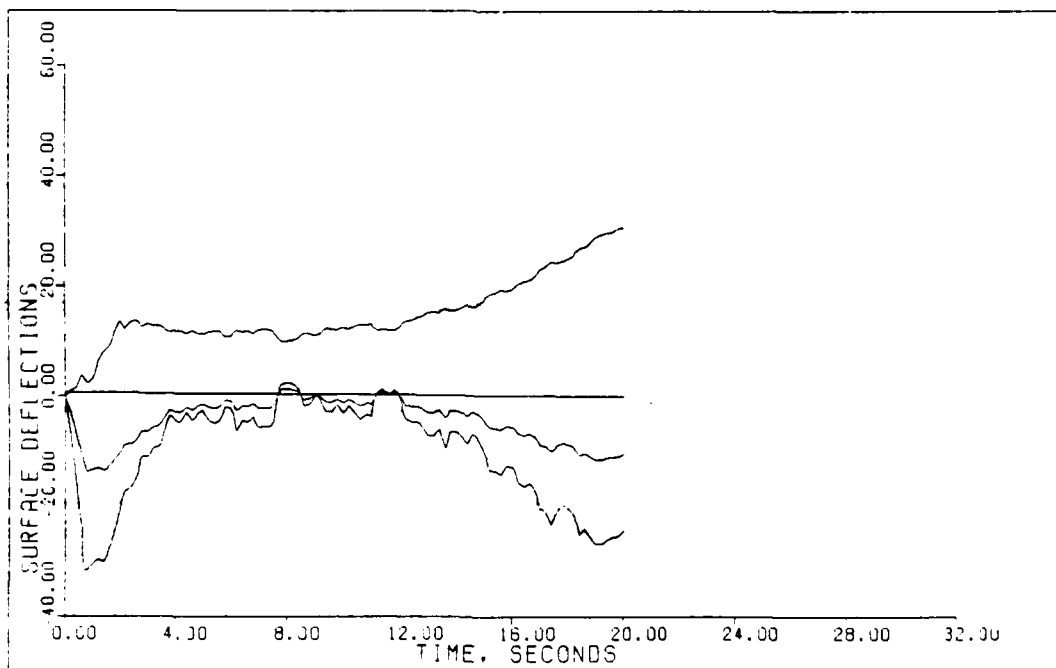


Fig. 5.77. Surface Deflections, Flight Path Noise, Simulation Mean

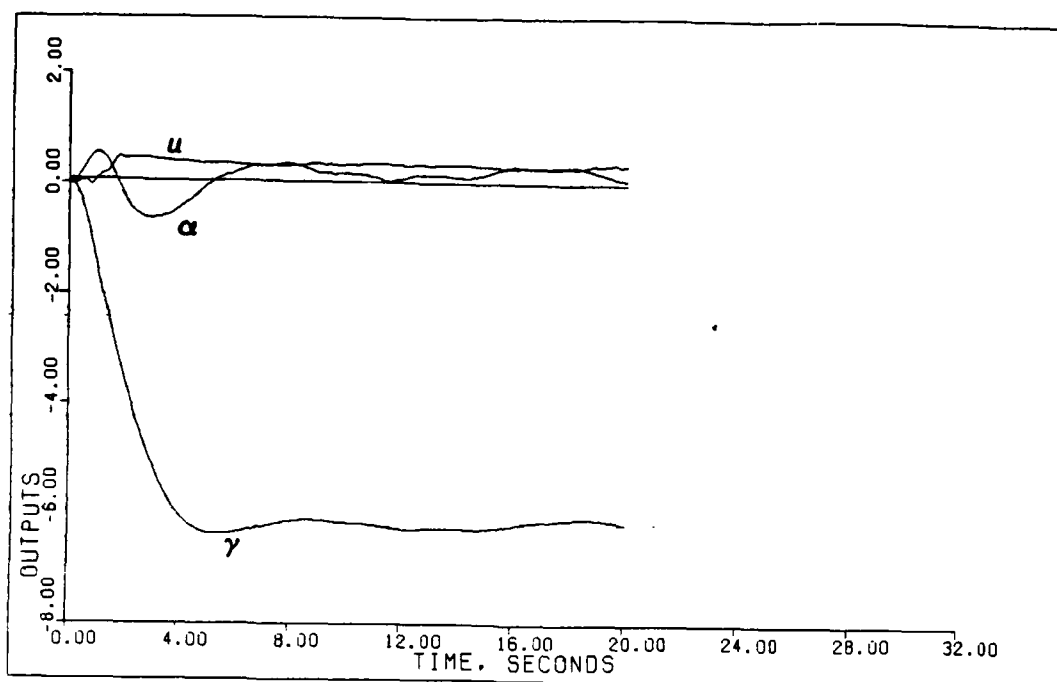


Fig. 5.78. Outputs, Pitch Rate Noise, Simulation 1

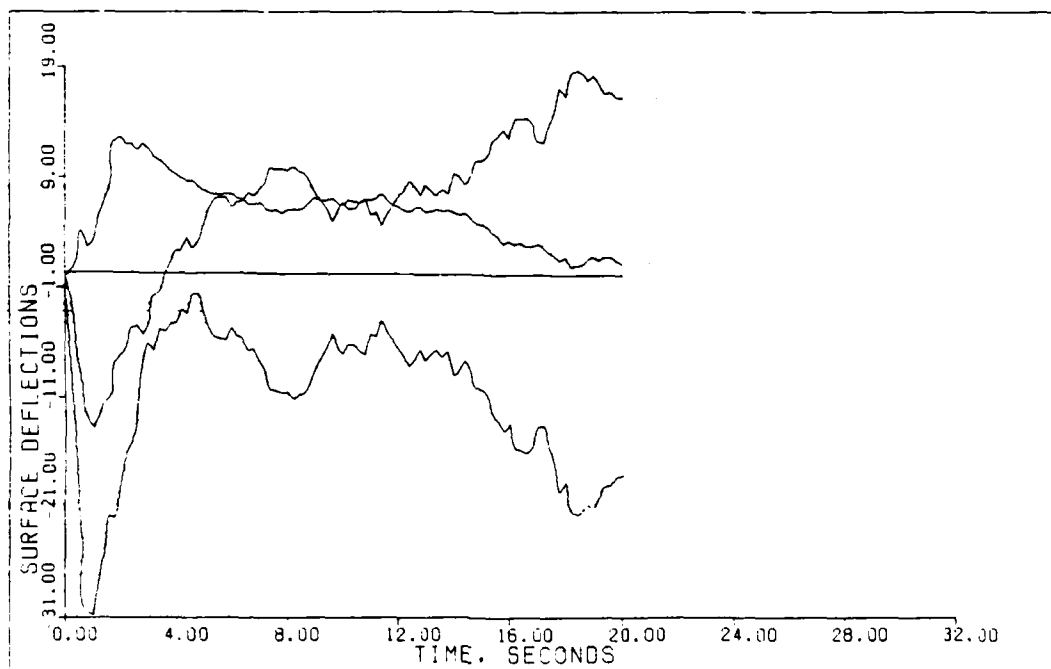


Fig. 5.79. Surface Deflections, Pitch Rate Noise, Simulation 1

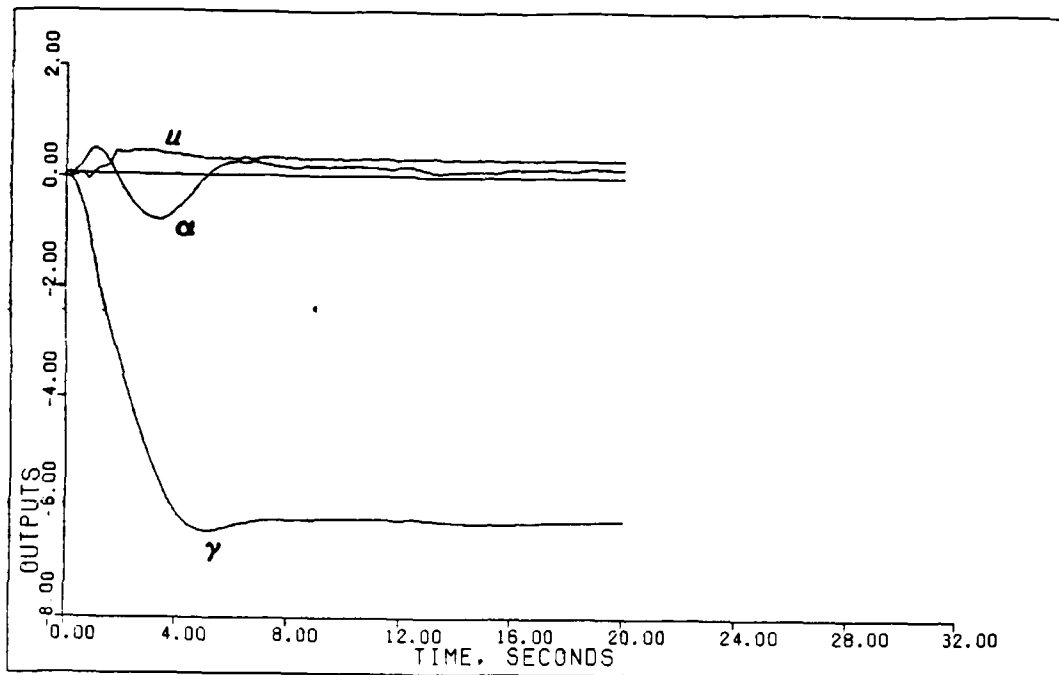


Fig. 5.80. Outputs, Pitch Rate Noise, Simulation 2

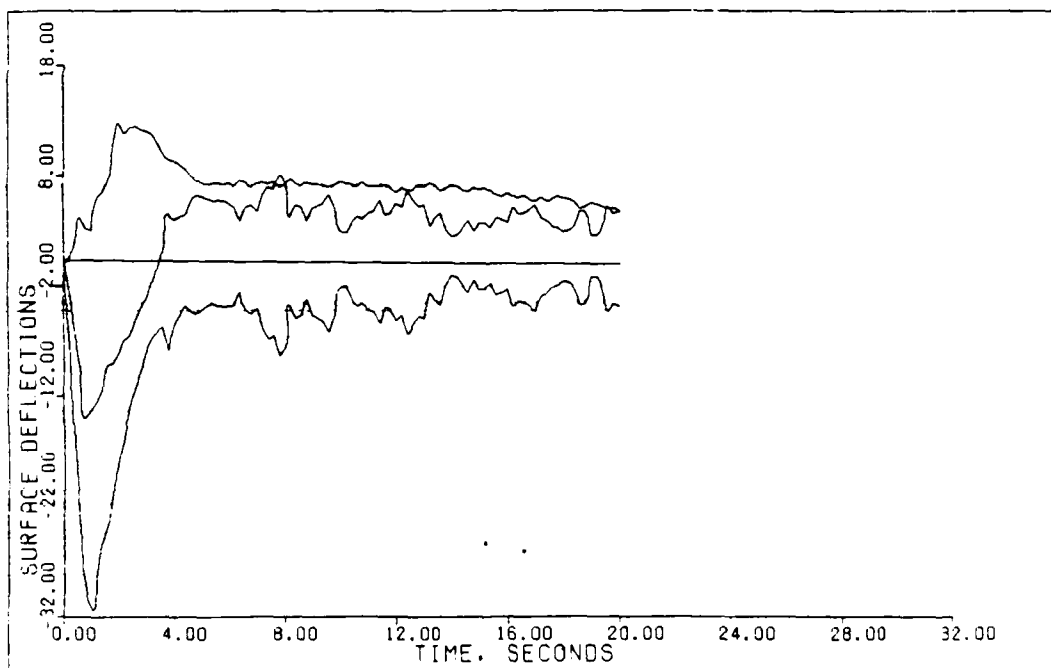


Fig. 5.81. Surface Deflections, Pitch Rate Noise, Simulation 2

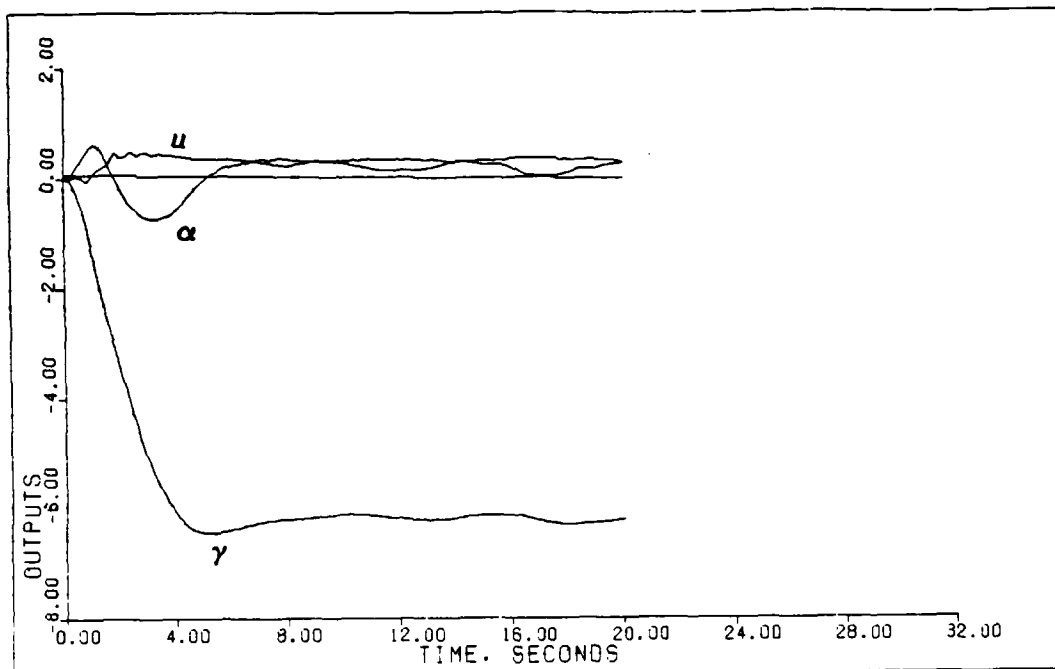


Fig. 5.82. Outputs, Pitch Rate Noise, Simulation 3

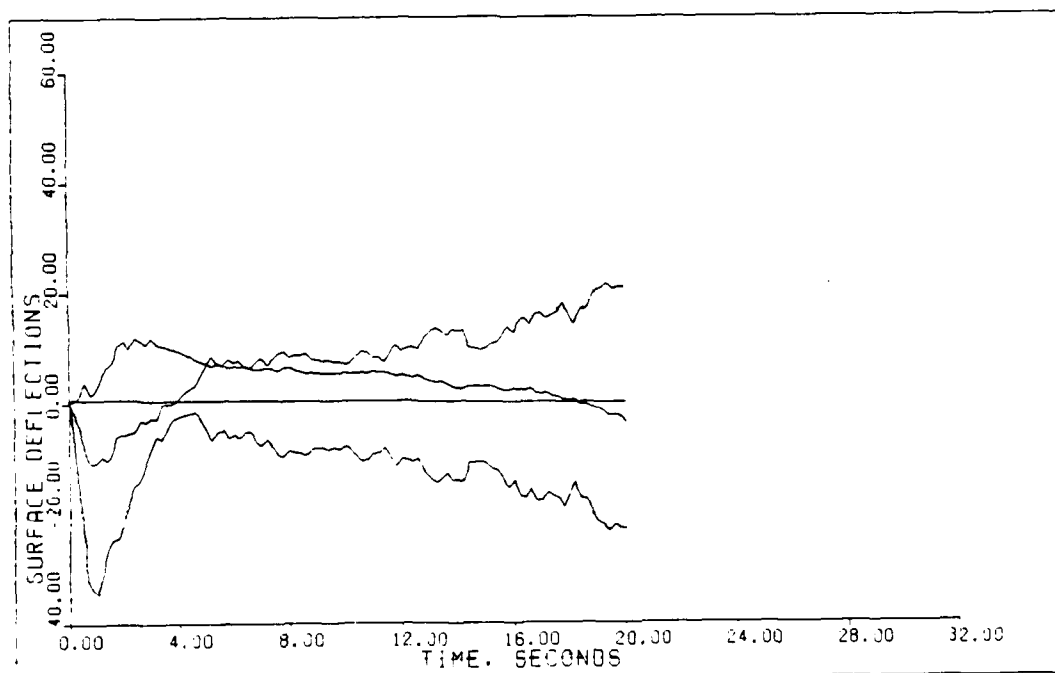


Fig. 5.83. Surface Deflections, Pitch Rate Noise, Simulation 3

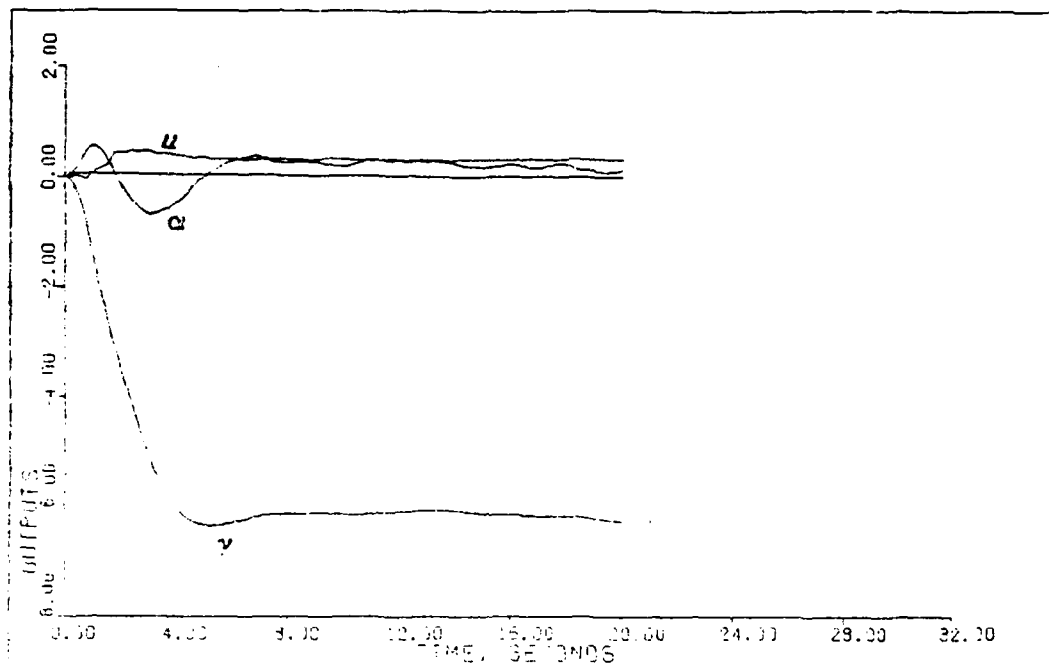


Fig. 5.84. Outputs, Pitch Rate Noise, Simulation 4

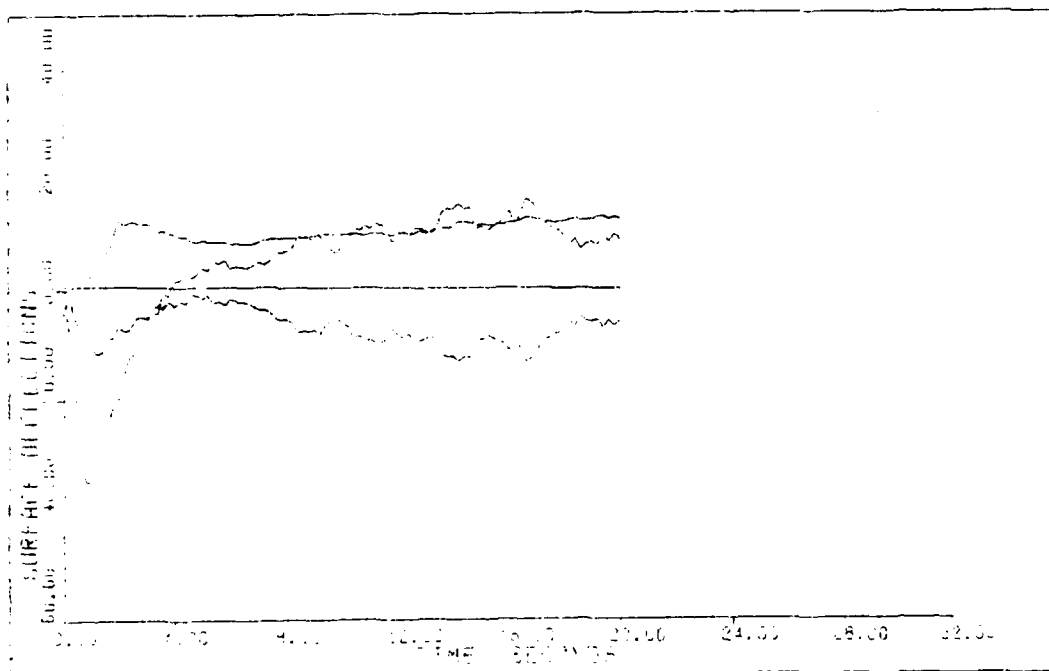


Fig. 5.85. Surface Deflections, Pitch Rate Noise, Simulation 4

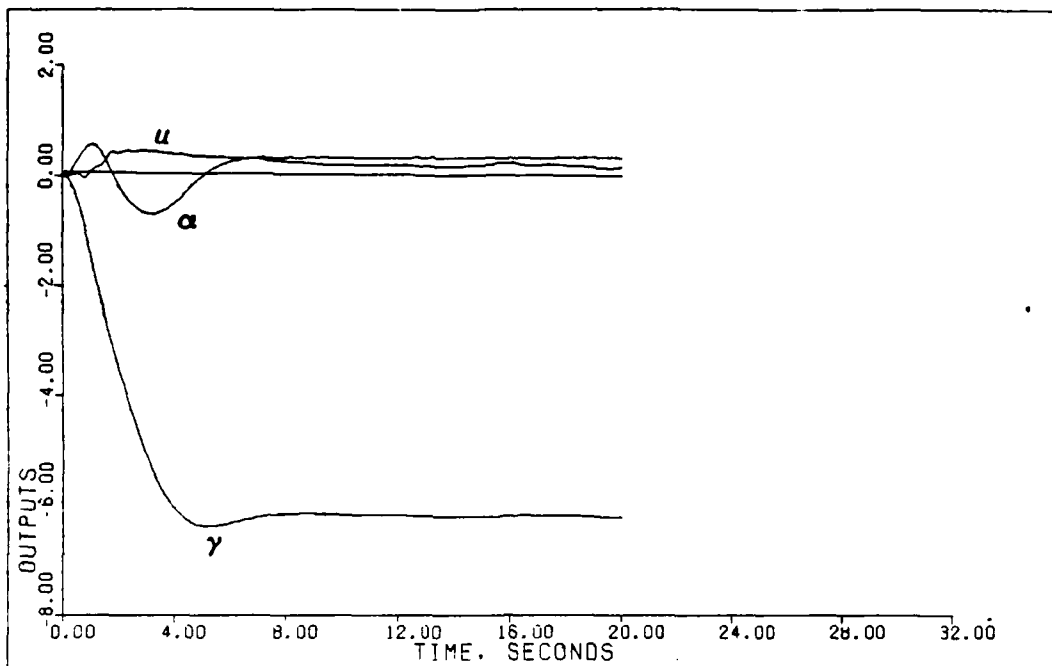


Fig. 5.86. Outputs, Pitch Rate Noise, Simulation Mean

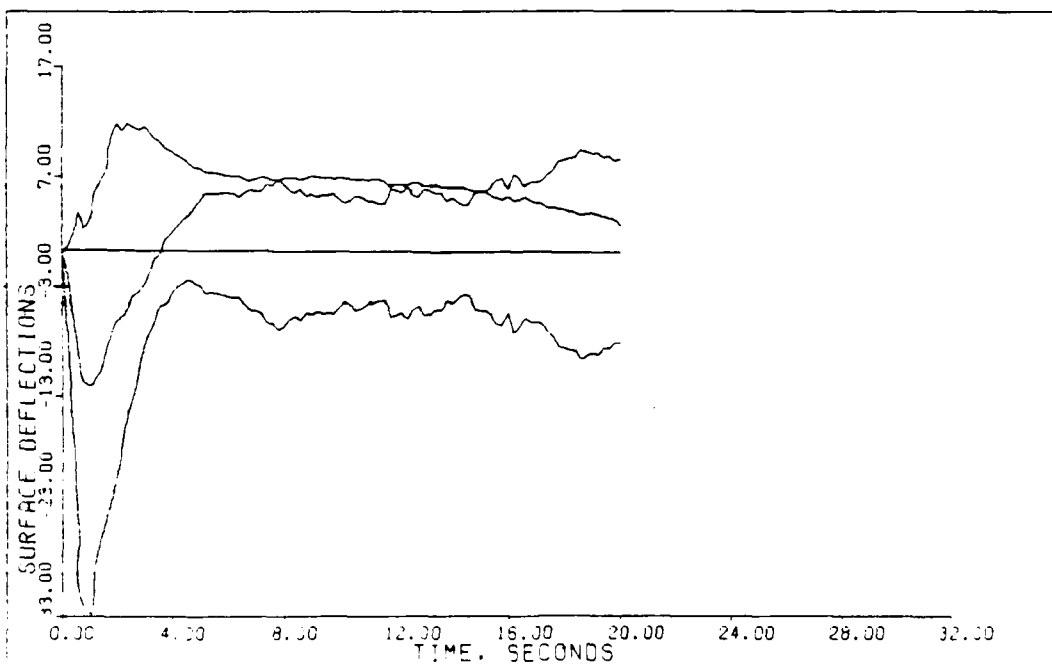


Fig. 5.87. Surface Deflections, Pitch Rate Noise, Simulation Mean

in the mean response because of the effect of averaging. It would be desirable to compute the variance of the responses as a function of time in future noise investigations to aid in the analysis of noise effects. In any case, the plots of the effect of high levels of noise are presented to demonstrate their effects on the linear model and it should be noted that in many cases the surface deflection rate limits are exceeded, thereby invalidating the linear model. The significance of this result is that in general it is not advisable to drive an integral controller with unfiltered noise. A practical solution is to place a cascade low pass filter between the noise source and the controller; however, this thesis does not pursue solutions to the problems associated with noisy measurements.

5.7 Parameter Variation

To establish the robustness of the designed controllers with respect to plant parameter variation, the control matrices, K_0 and K_1 , from each flight condition are used to control the plants of the other five flight conditions. Naturally, not all of these simulations are successful and in fact some are unstable. Table 5.9 indicates which controllers are satisfactory at the various flight conditions. The simulations that are stable are plotted in Figures 5.88 through 5.111. The unstable responses are not presented because they quickly exceed the boundaries of

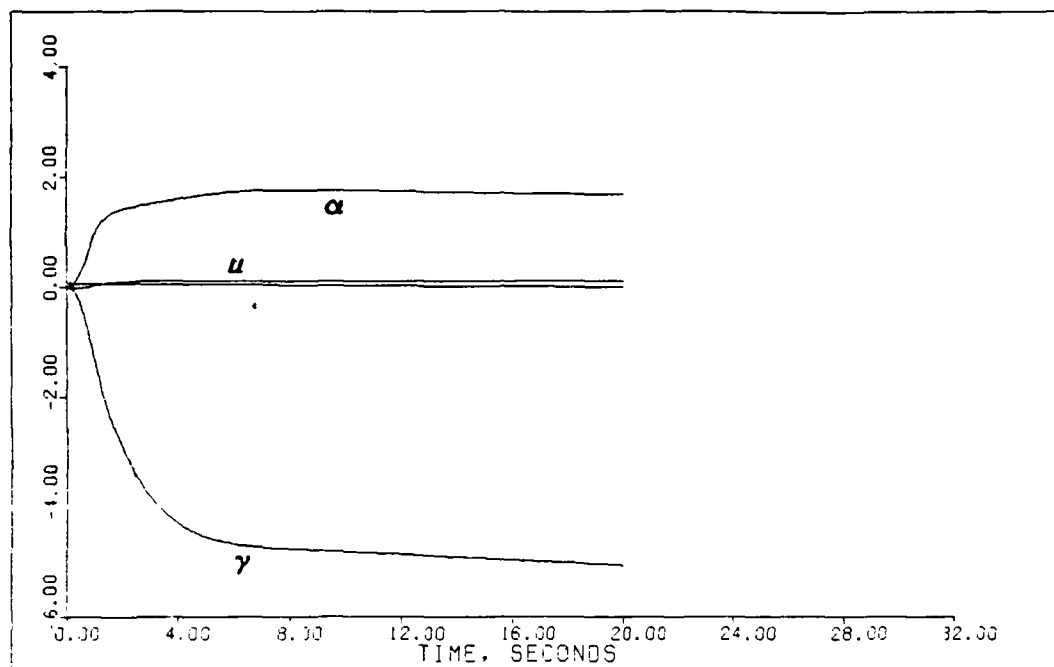


Fig. 5.88. Outputs, Controller 1, Flight Condition 2

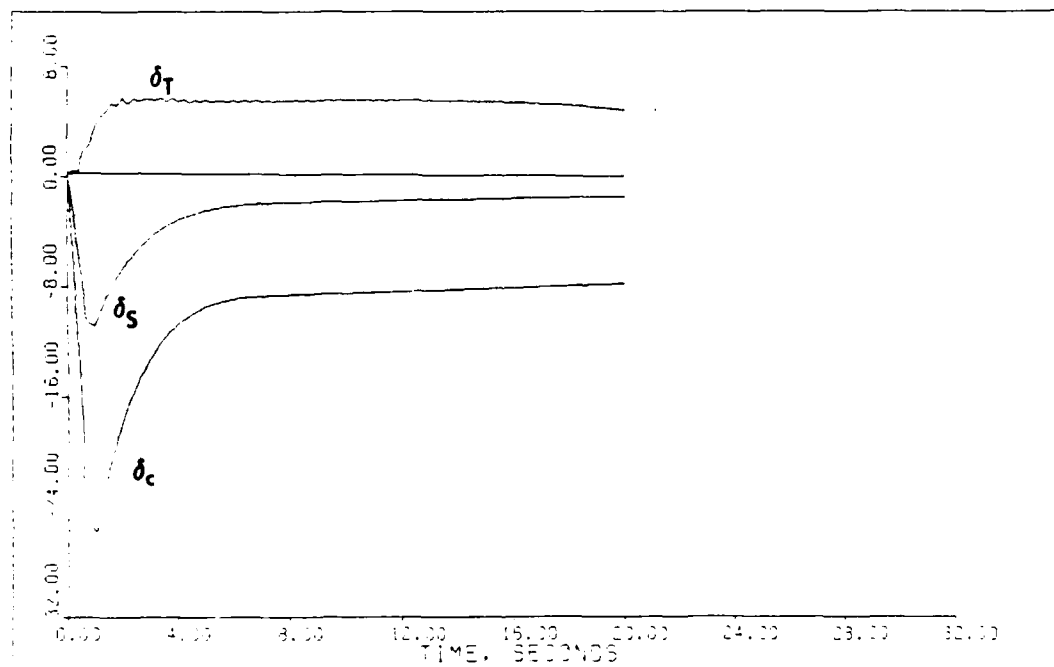


Fig. 5.89. Surface Deflections, Controller 1, Flight Condition 2

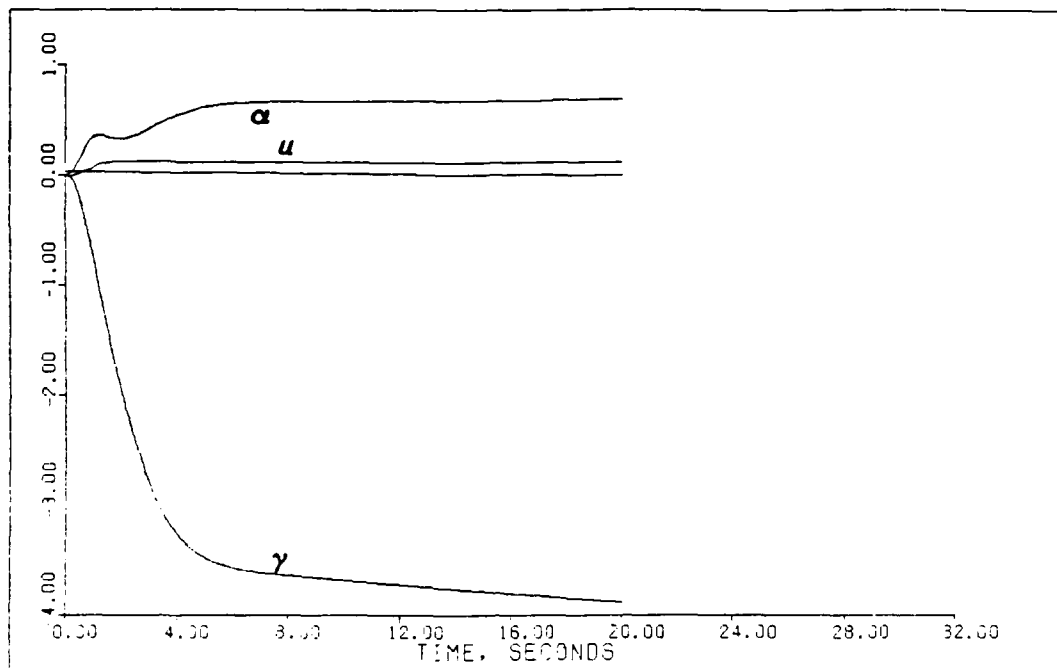


Fig. 5.90. Outputs, Controller 1, Flight Condition 3

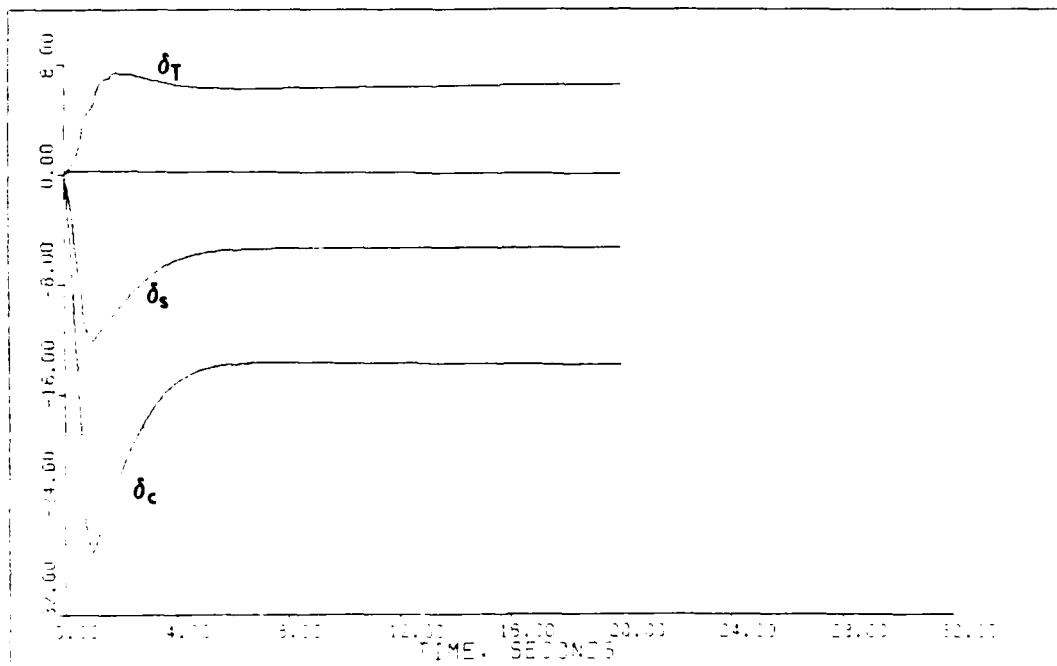


Fig. 5.91. Surface Deflections, Controller 1, Flight Condition 3

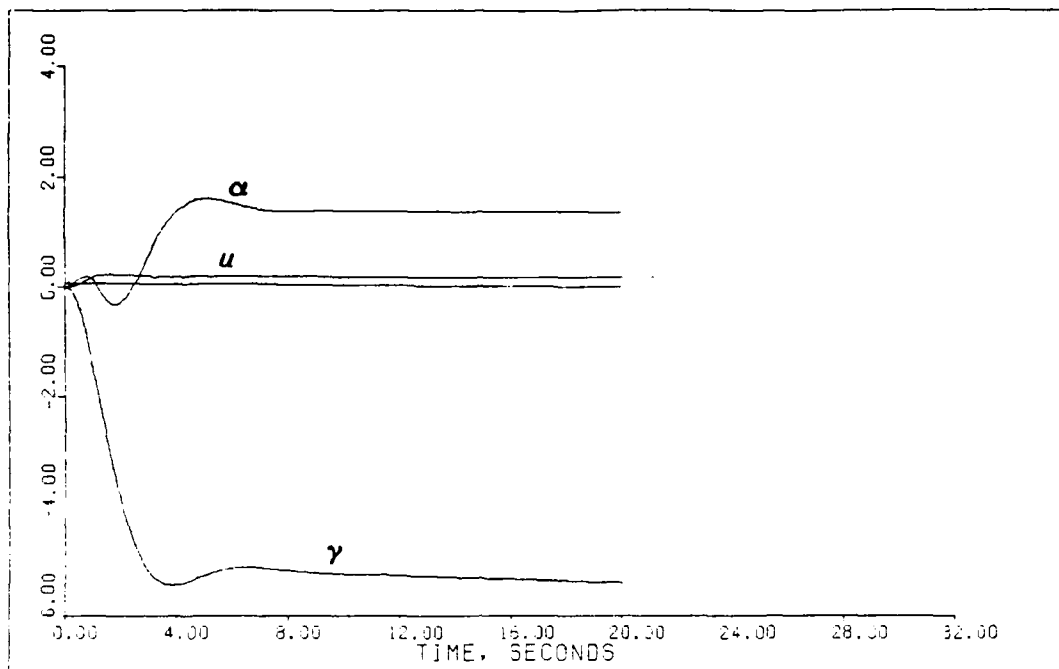


Fig. 5.92. Outputs, Controller 1, Flight Condition 4

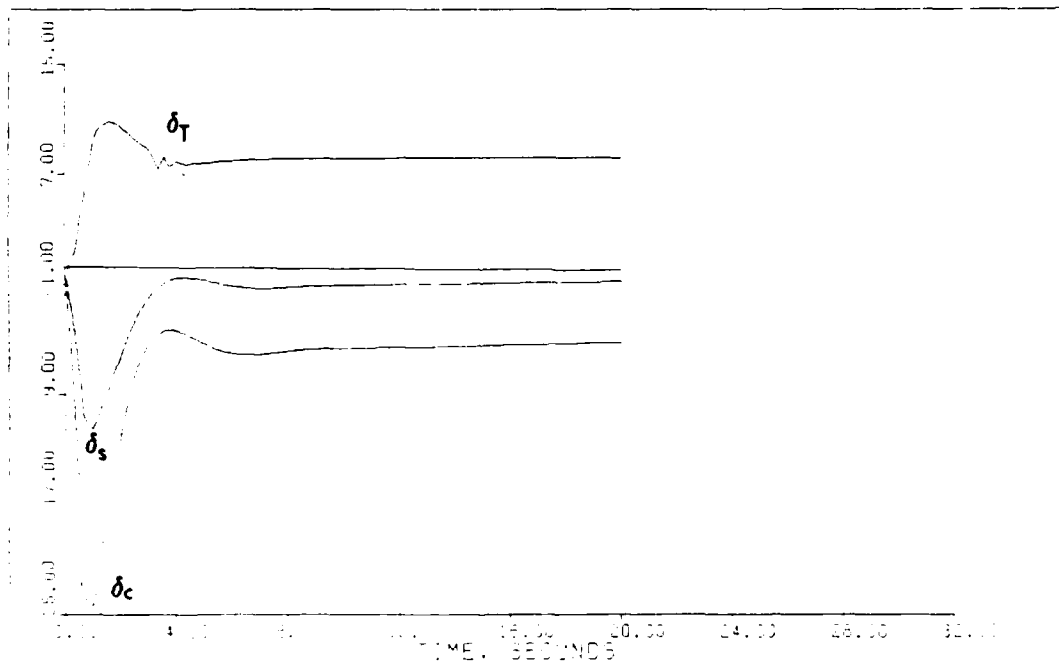


Fig. 5.93. Surface Deflections, Controller 1, Flight Condition 4

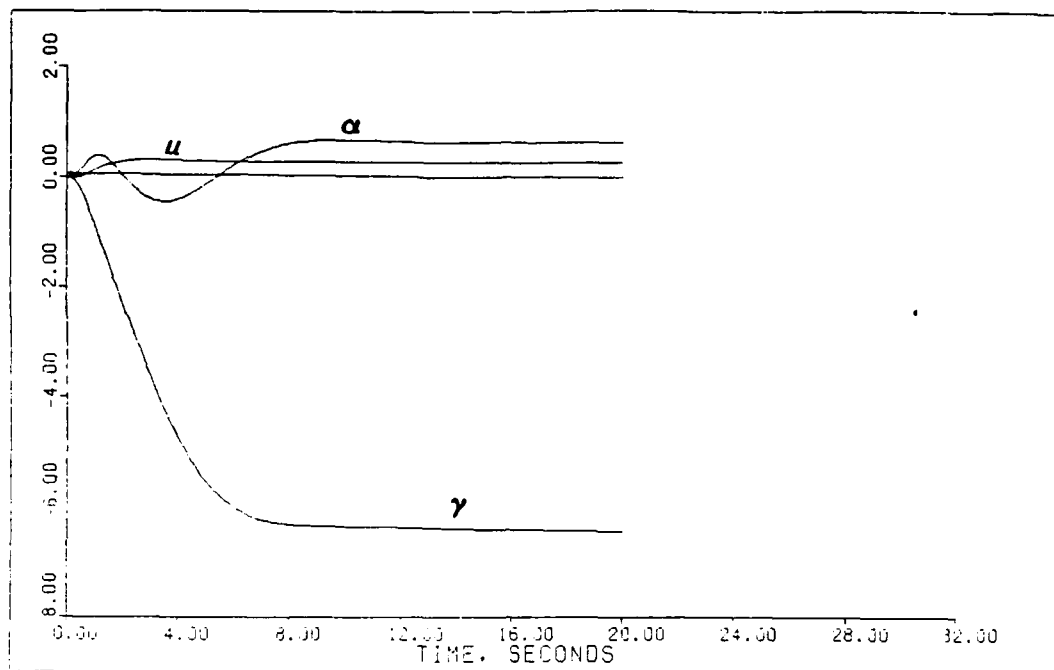


Fig. 5.94. Outputs, Controller 1, Flight Condition 6

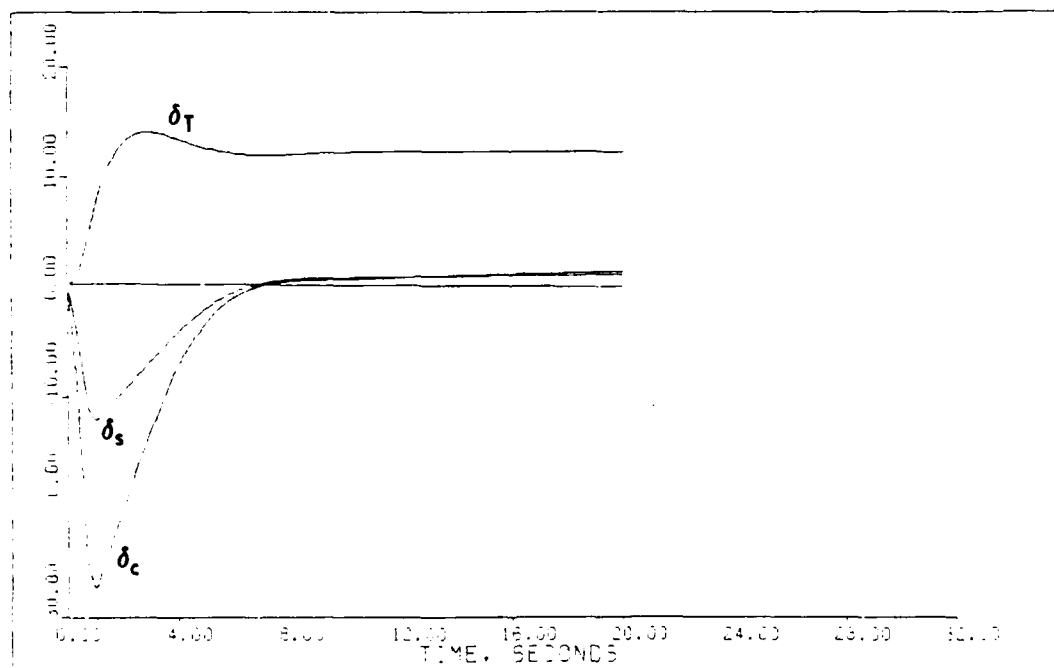


Fig. 5.95. Surface Deflections, Controller 1, Flight Condition 6

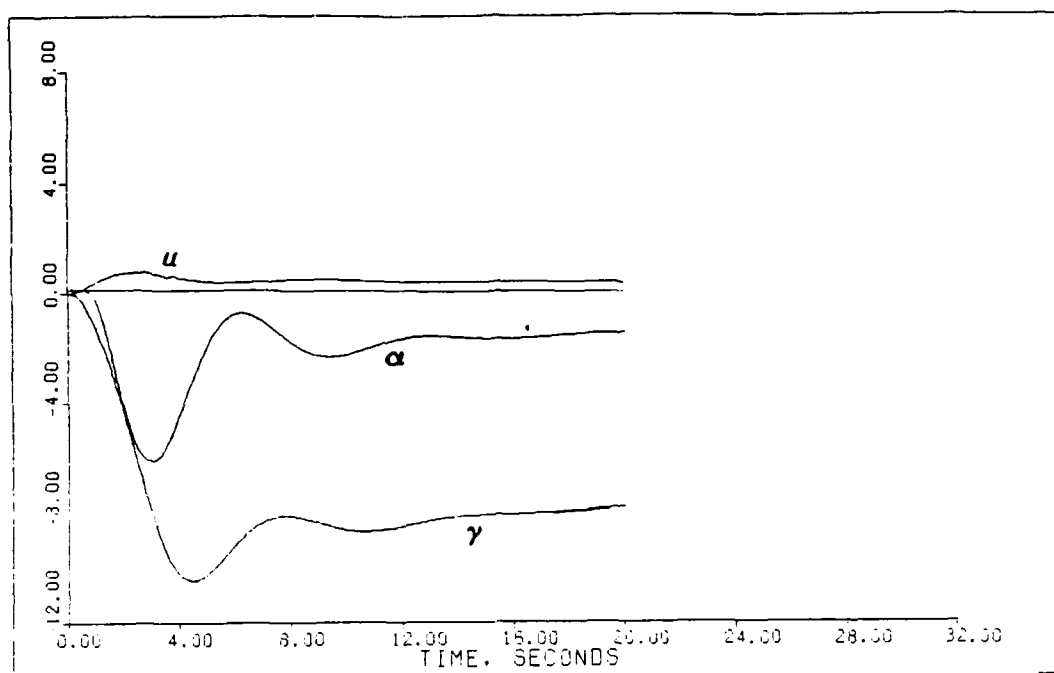


Fig. 5.96. Outputs, Controller 2, Flight Condition 1

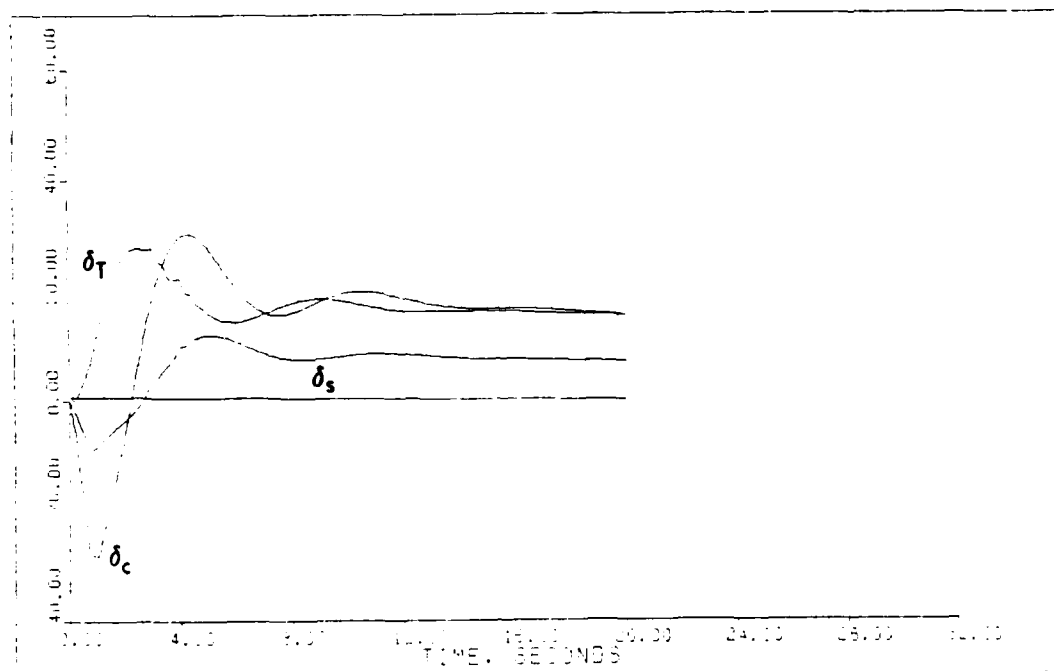


Fig. 5.97. Surface Deflections, Controller 2, Flight Condition 1

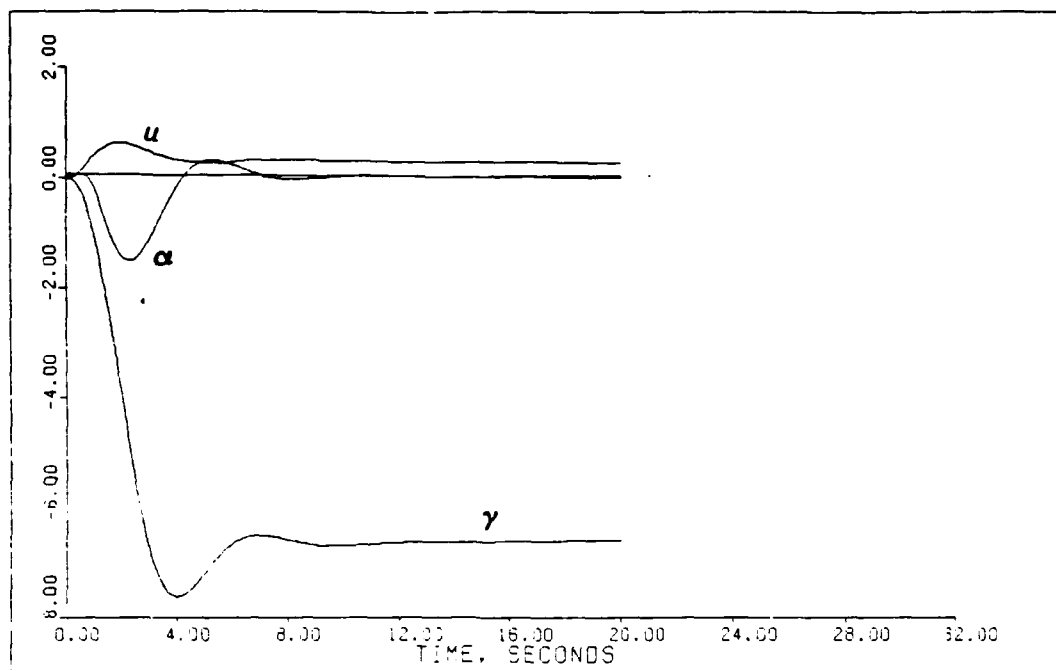


Fig. 5.98. Outputs, Controller 2, Flight Condition 3

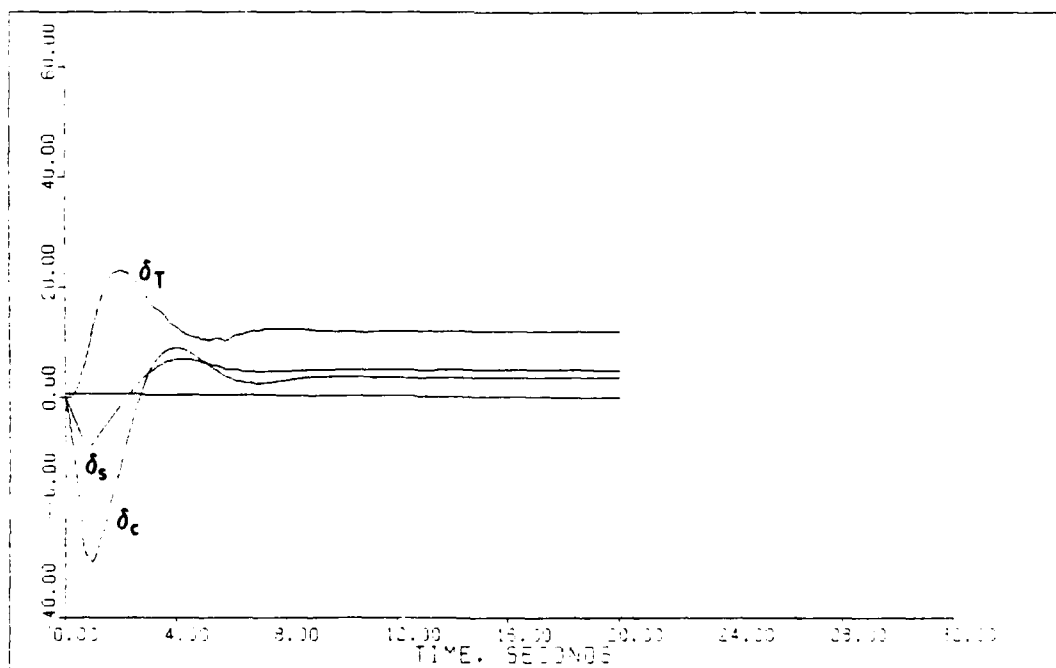


Fig. 5.99. Surface Deflections, Controller 2, Flight Condition 3

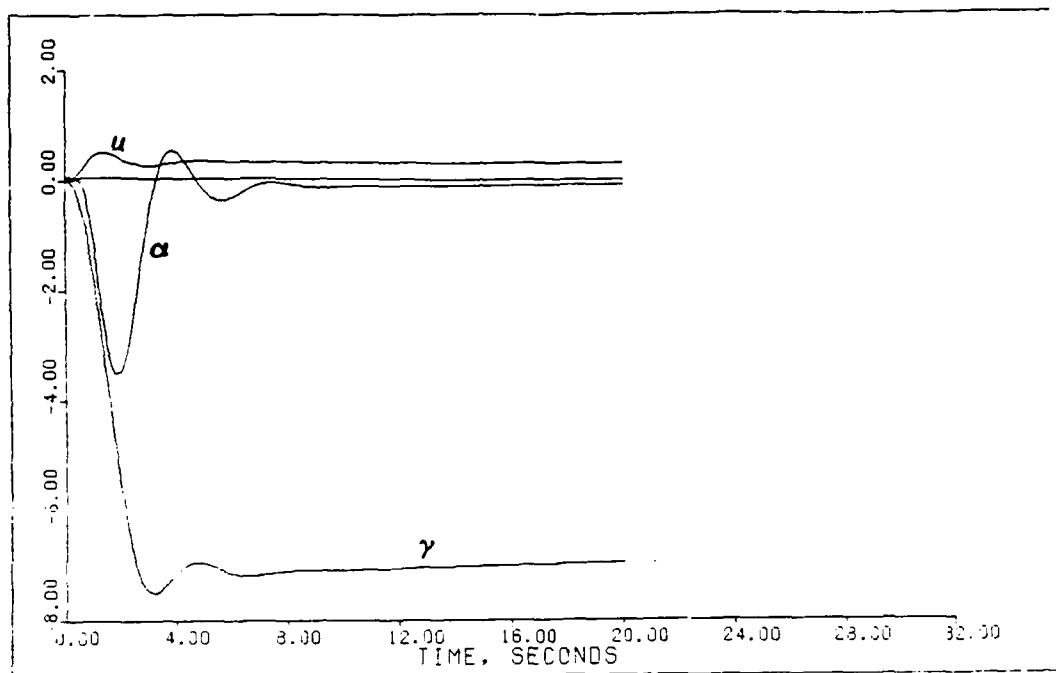


Fig. 5.100. Outputs, Controller 2, Flight Condition 4

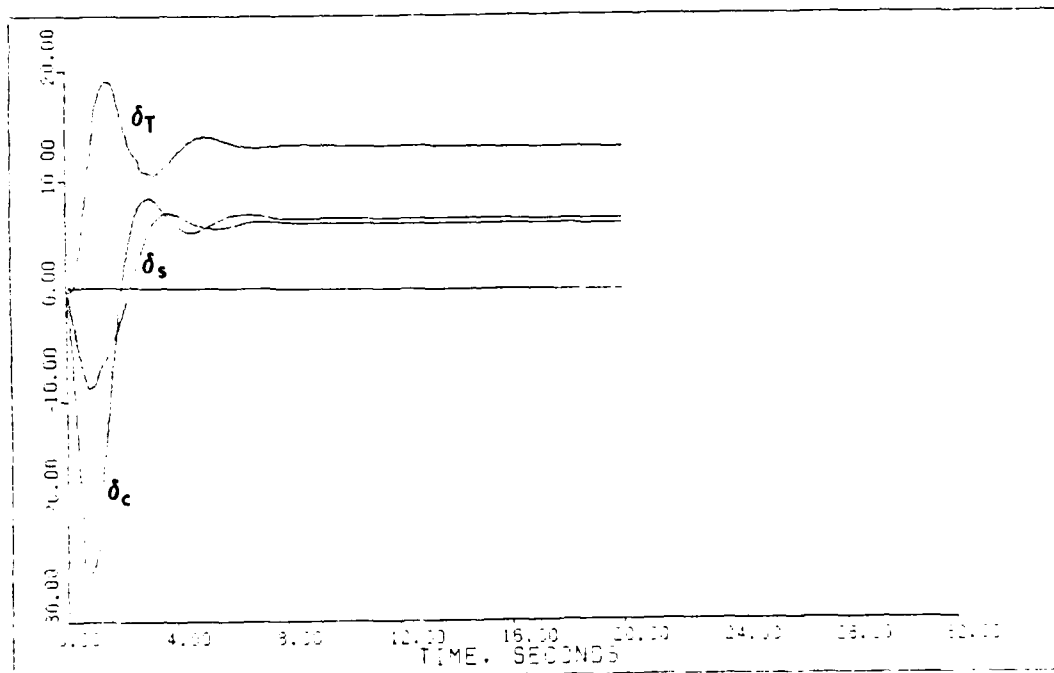


Fig. 5.101. Surface Deflections, Controller 2
Flight Condition 4

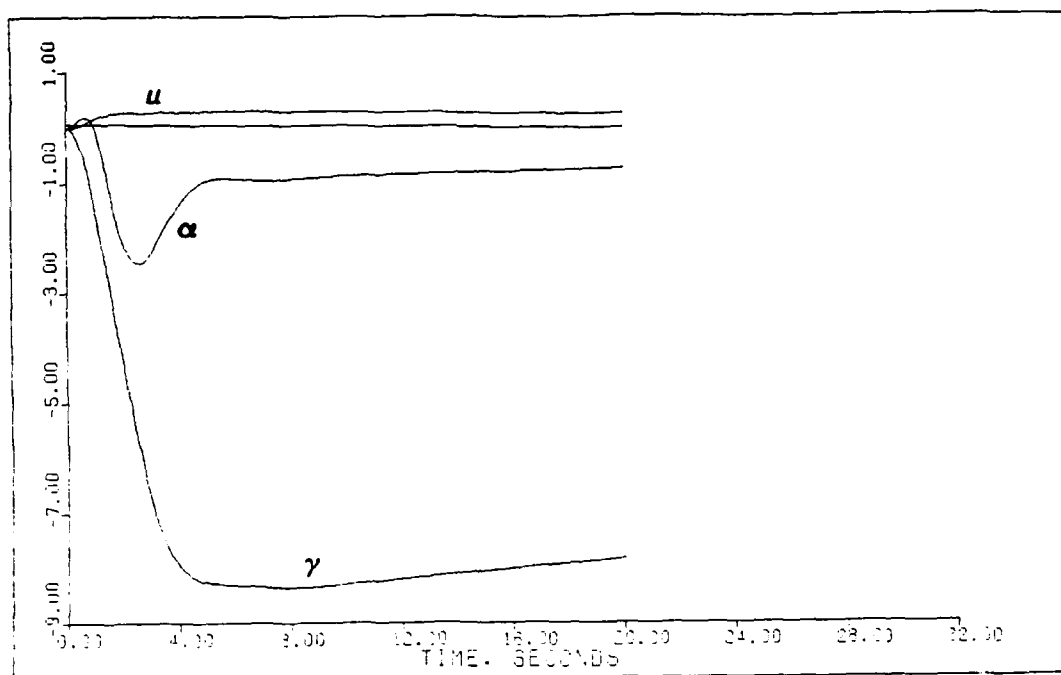


Fig. 5.102. Outputs, Controller 3, Flight Condition 4

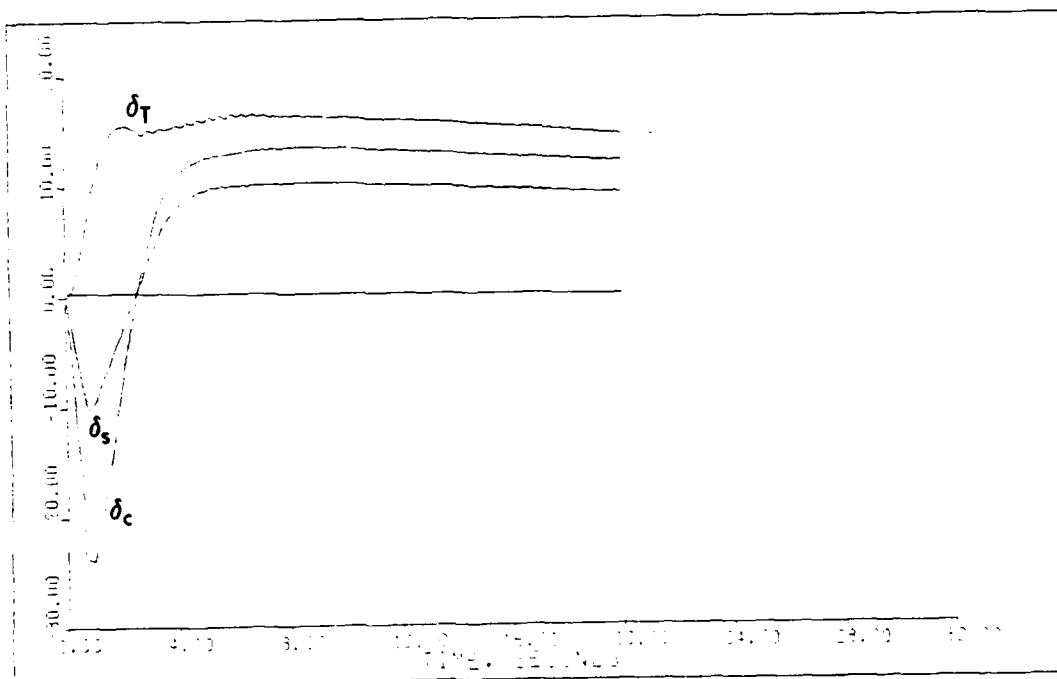


Fig. 5.103. Surface Deflections, Controller 3
Flight Condition 4

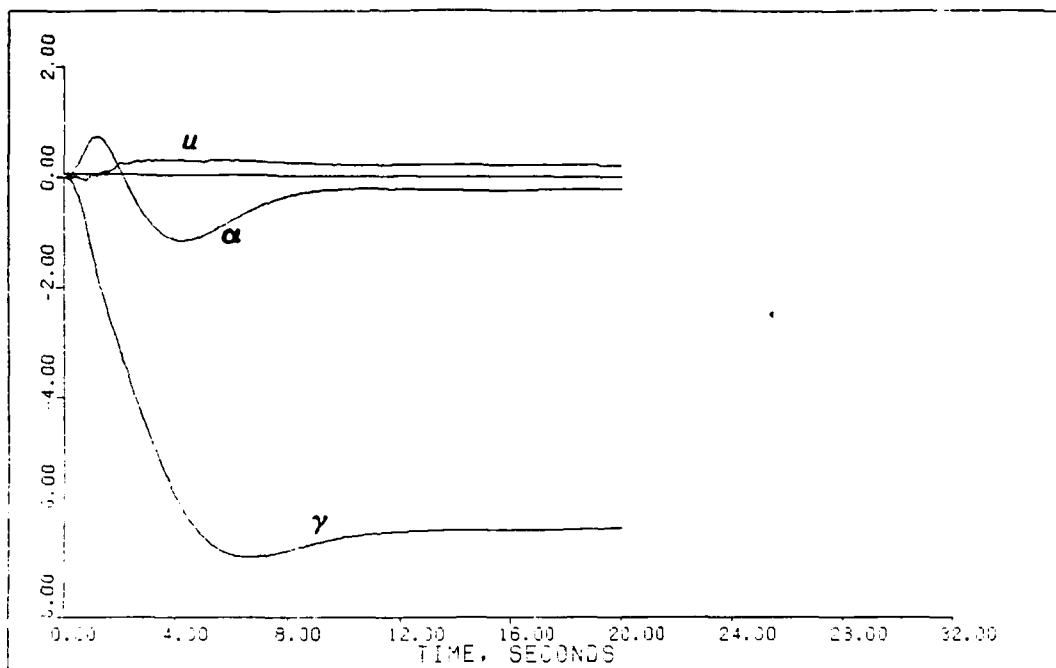


Fig. 5.104. Outputs, Controller 6, Flight Condition 1

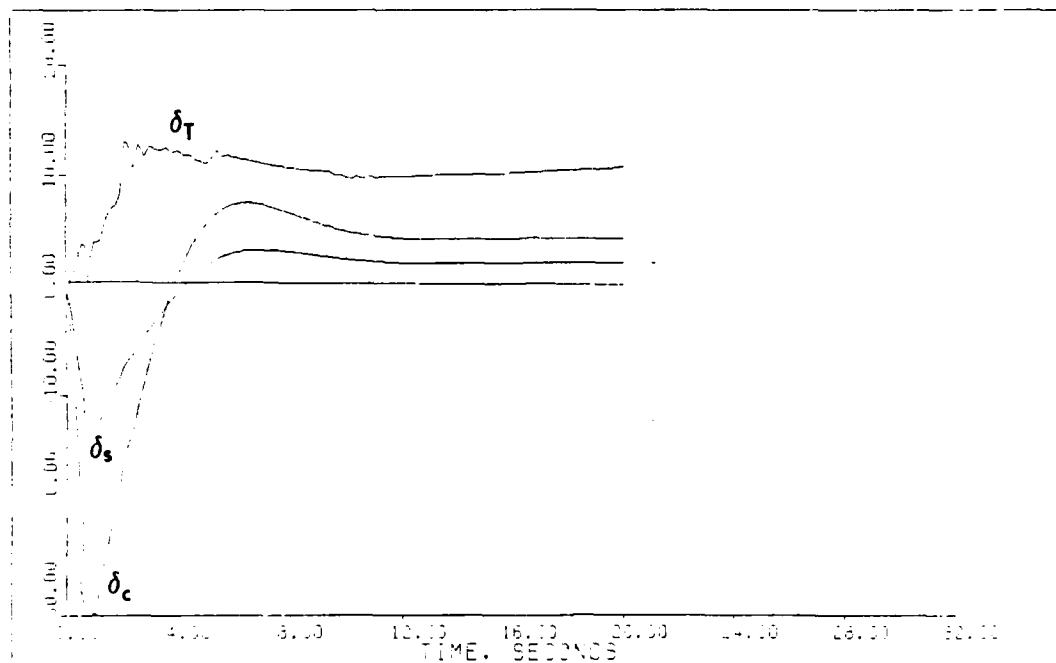


Fig. 5.105. Surface Deflections, Controller 6
Flight Condition 1

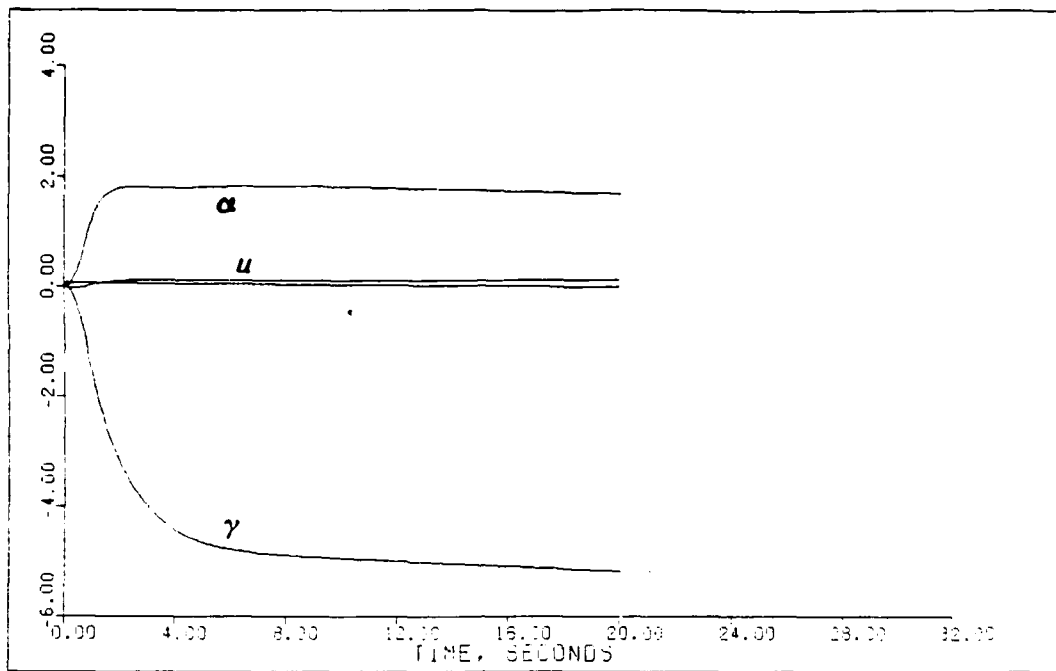


Fig. 5.106. Outputs, Controller 6, Flight Condition 2

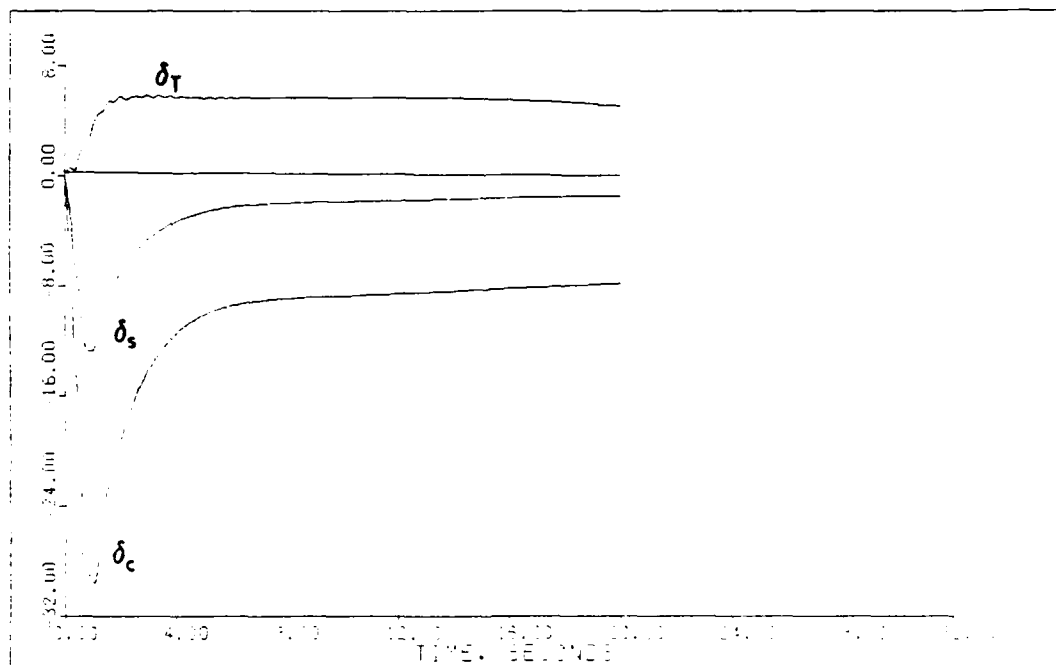


Fig. 5.107. Surface Deflections, Controller 6
Flight Condition 2

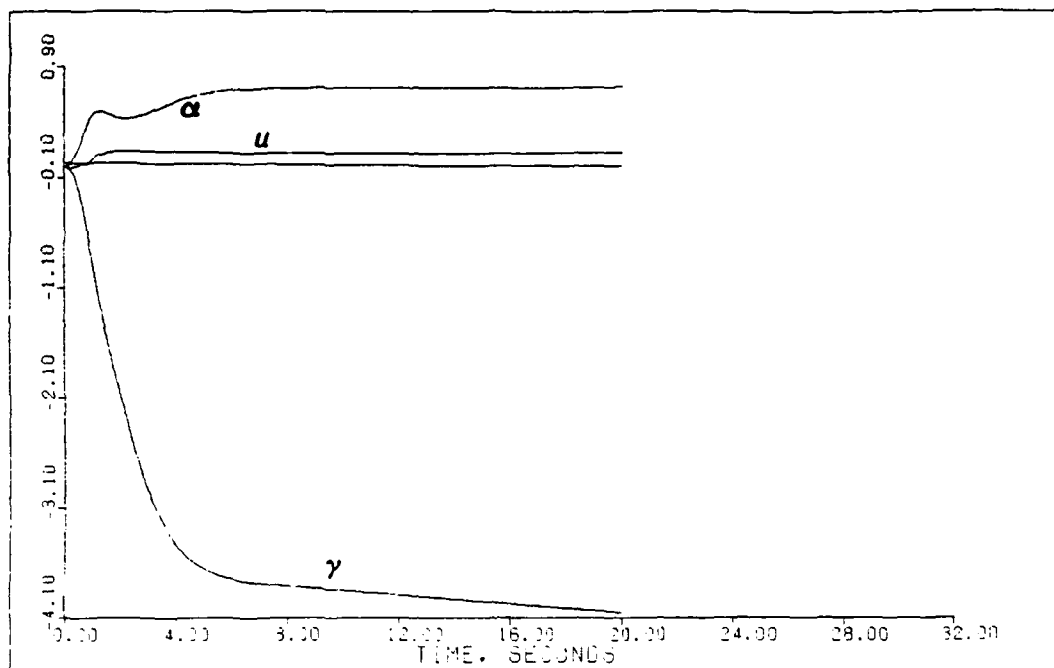


Fig. 5.108. Outputs, Controller 6, Flight Condition 3

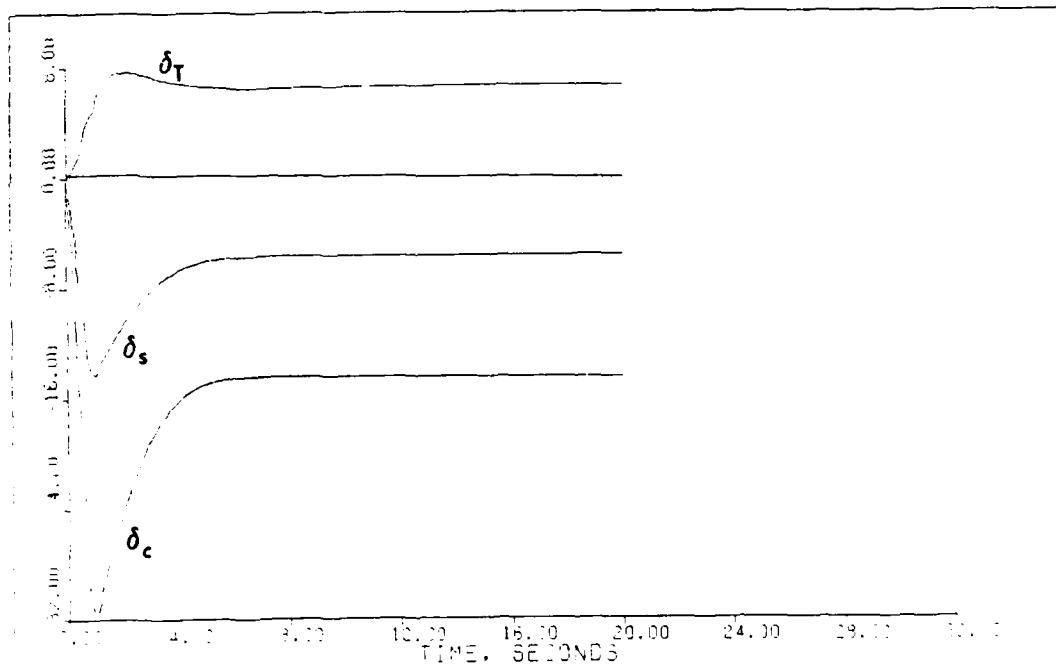


Fig. 5.109. Surface Deflections, Controller 6
Flight Condition 3

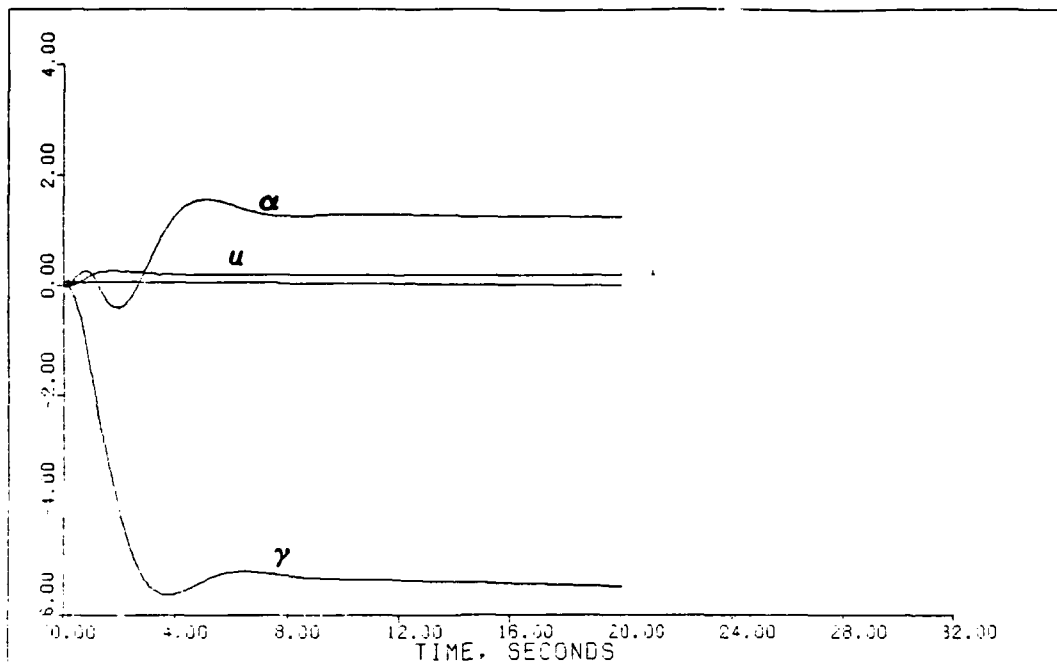


Fig. 5.110. Outputs, Controller 6, Flight Condition 4

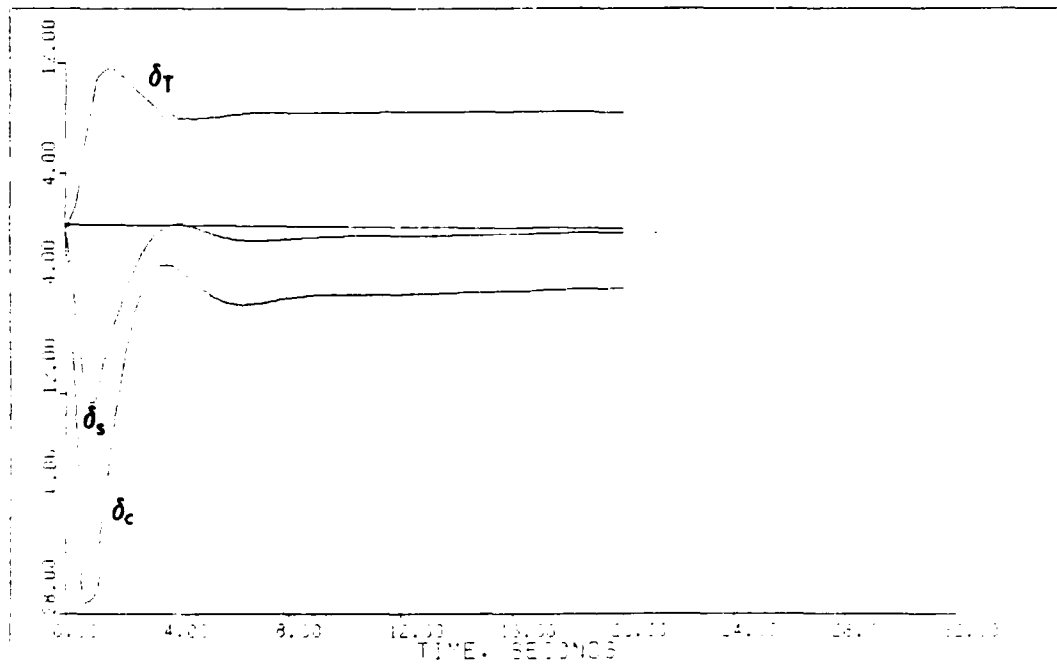


Fig. 5.111. Surface Deflections, Controller 6
Flight Condition 4

TABLE 5.9
PARAMETER VARIATION RESULTS

Flight Condition	Controller					
	1	2	3	4	5	6
1	Good	Stable	Stable	Unstable	Unstable	Stable
2	Stable	Good	Unstable	Unstable	Unstable	Stable
3	Stable	Stable	Good	Unstable	Unstable	Stable
4	Stable	Stable	Stable	Good	Unstable	Stable
5	Unstable	Unstable	Unstable	Unstable	Good	Unstable
6	Stable	Unstable	Unstable	Unstable	Unstable	Good

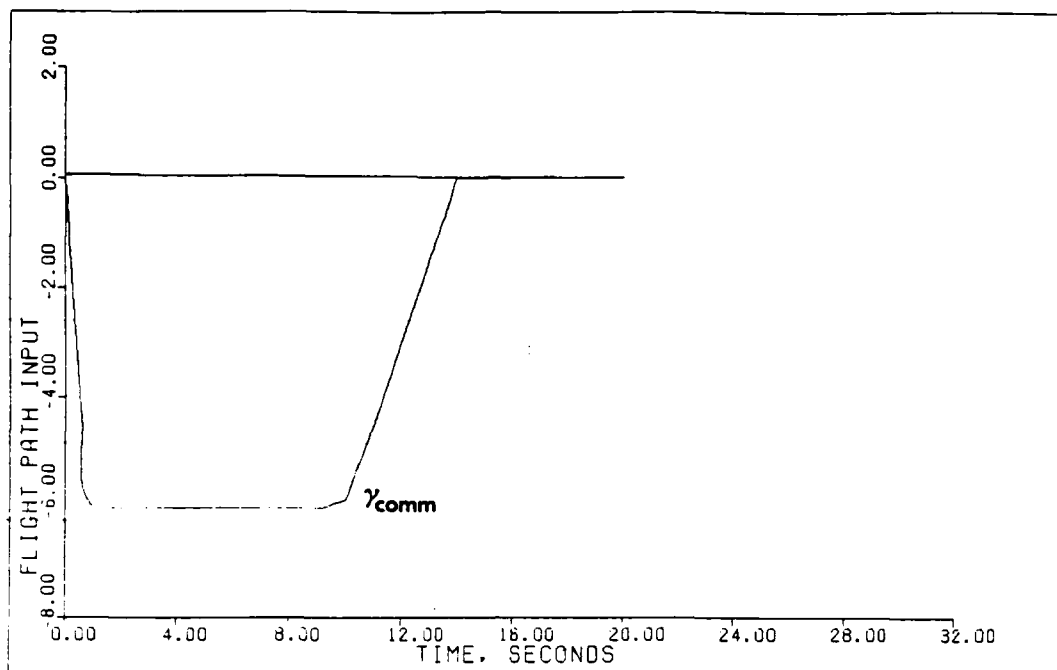
a valid linear model and are meaningless other than to establish that the response is divergent. All of the stable responses contain a lingering transient error in the angle of attack, the principal reason only the diagonal entries in Table 5.8 are considered "Good." In all of the stable simulations the surface deflection limits are within limits and only two responses (Figures 5.94 and 5.98) exhibit objectionable oscillatory characteristics. In a practical system, it is often convenient to use one controller at a variety of flight conditions to avoid the complications of gain scheduling. These results indicate that either of two controllers (those designed for flight conditions 1 and 6) provide acceptable control over all but one of the remaining flight conditions (flight condition 5). The

only satisfactory controller for flight condition 5 is the one designed at that condition.

5.8 Special Maneuvers

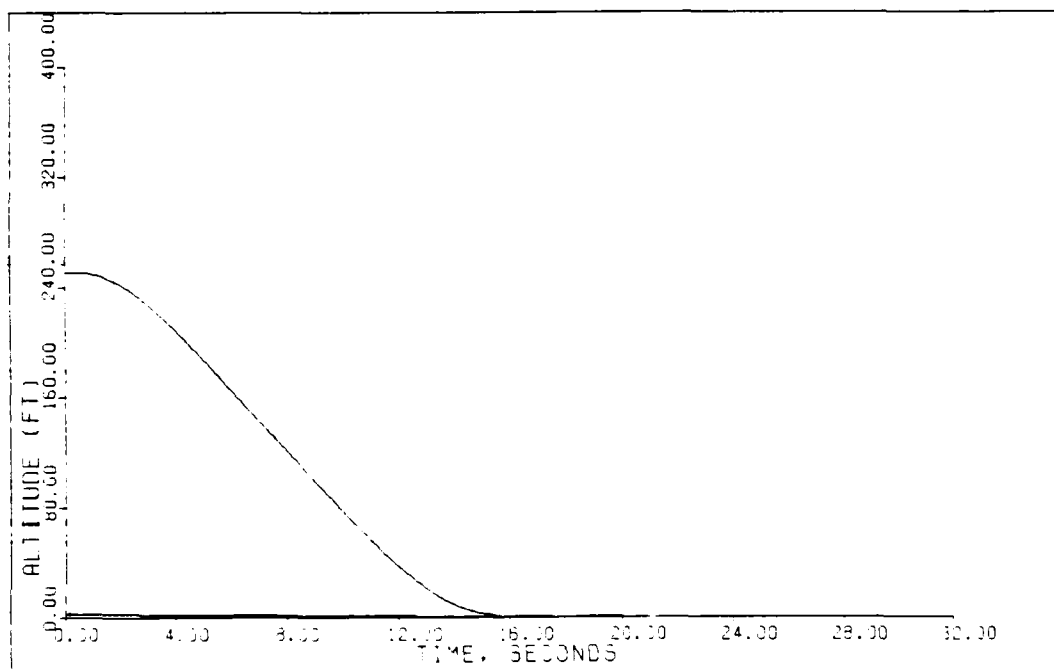
For the reasons outlined in Chapter IV, two additional maneuvers are simulated to demonstrate the system's ability to perform other maneuvers that are representative of the landing flight condition. Both of these maneuvers are demonstrated at flight condition 1 with actuators, computational time delay, sensor dynamics, and surface nonlinearities included. The first maneuver simulated is that of an approach and flare as the aircraft nears the ground. The commanded input (Figure 5.112) begins with a command identical to the input of the previous section. After the aircraft has sufficient time to establish a steady-state descent (ten seconds) the flight path is ramped back to zero over four seconds to simulate the roundout and flare. A profile of the resultant flight path response (altitude vs time) is shown in Figure 5.113. Figures 5.114 and 5.115 contain the outputs and surface deflections during the maneuver and demonstrate smooth performance of the intended maneuver.

The second maneuver performed simulates an aborted landing in which the initial descent is commanded, followed by a return to level flight, and finally the initial descent is resumed (Figure 5.116). Figures 5.117 and 5.118 contain



SIMULATED APPROACH AND FLARE COMMAND INPUT

Fig. 5.112. Flare Command Input



SIMULATED APPROACH AND FLARE

Fig. 5.113. Attitude for Flare Maneuver

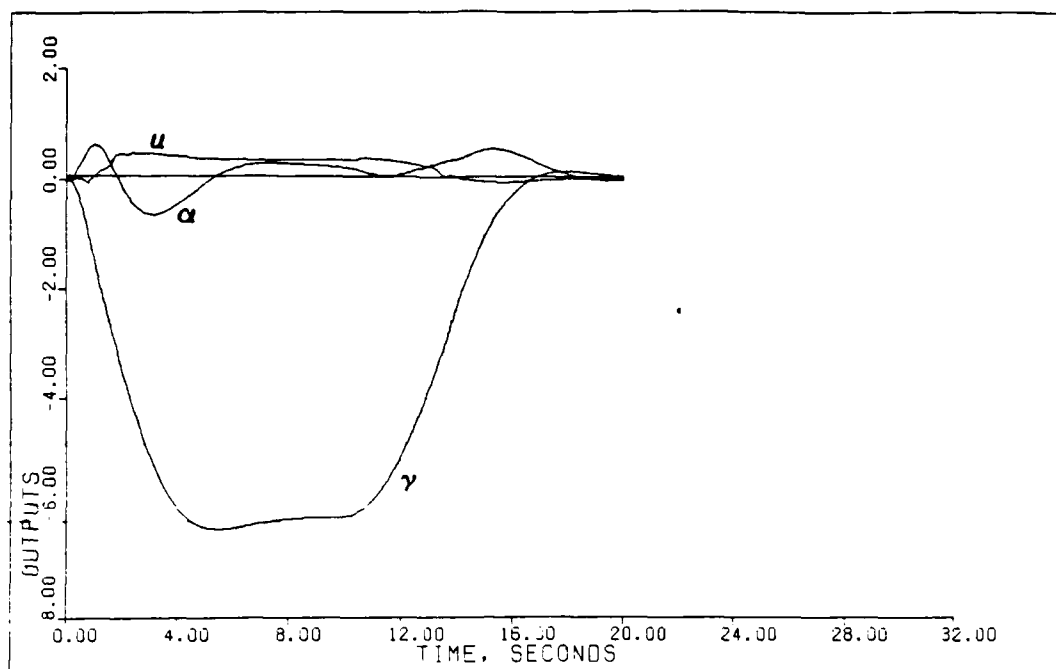


Fig. 5.114. Outputs for Flare Maneuver

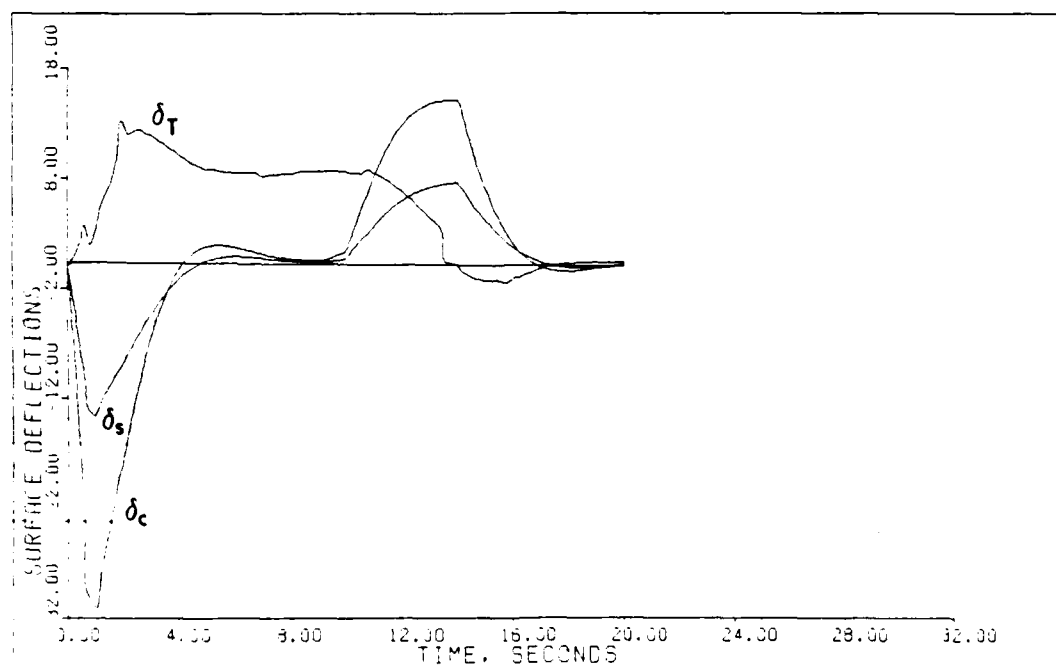


Fig. 5.115. Surface Deflections for Flare Maneuver

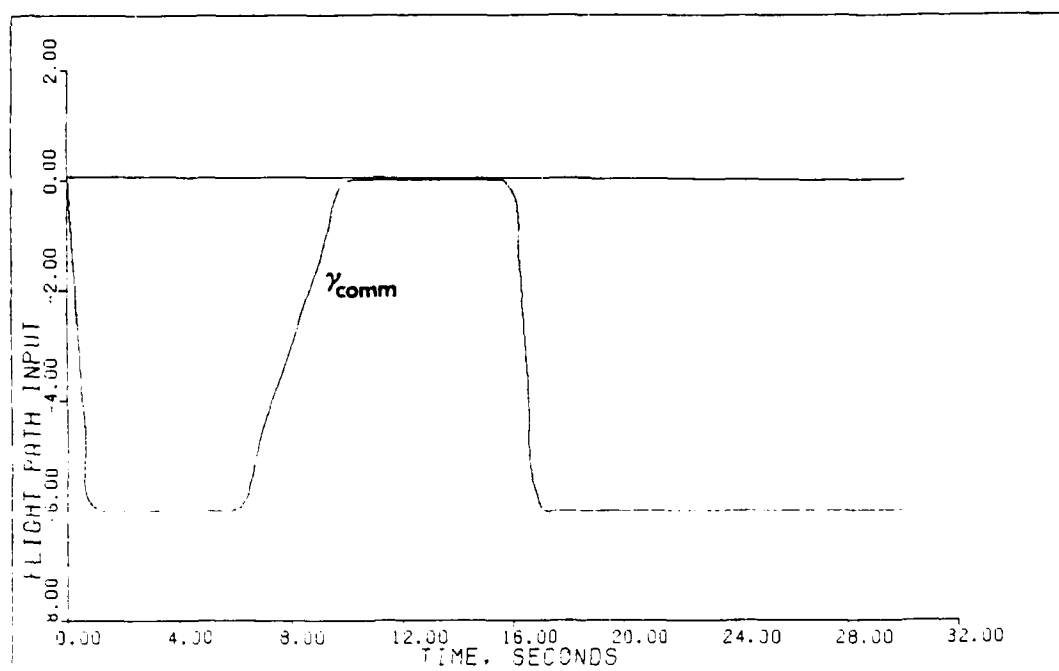


Fig. 5.116. Flight Path Command Input

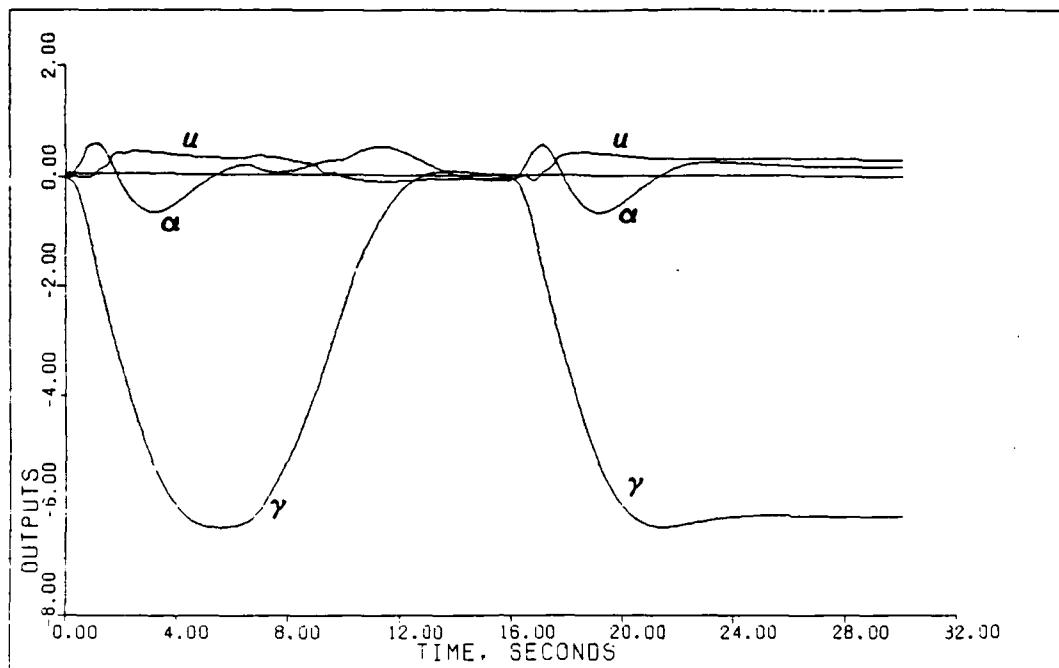


Fig. 5.117. Outputs for Flight Path Change

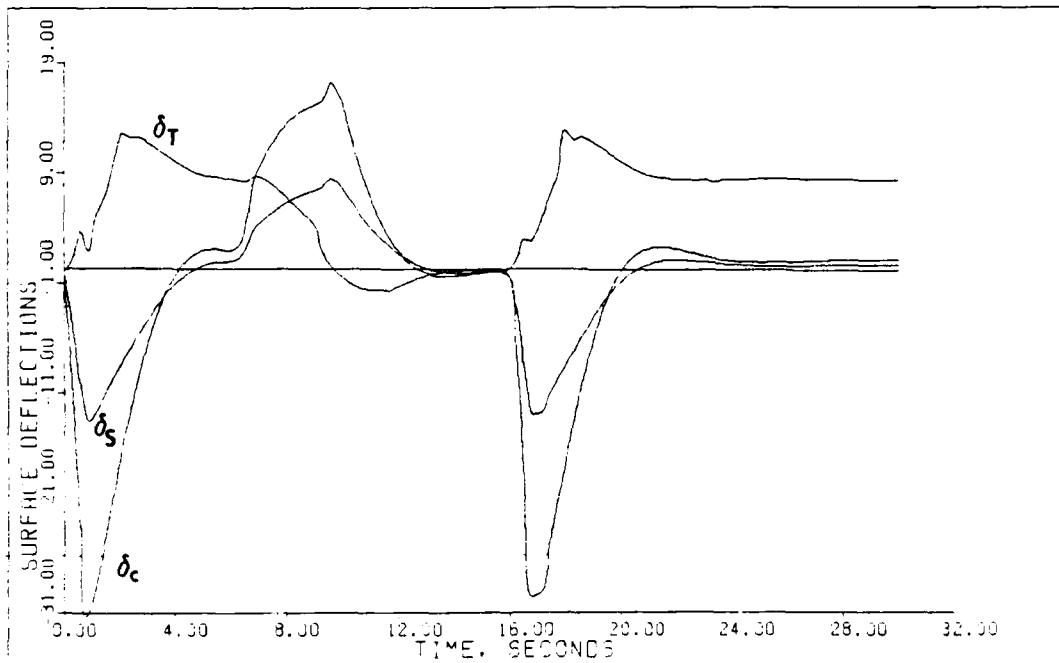


Fig. 5.118. Surface Deflections for Flight Path Change

the system response to this maneuver and demonstrate the controller's ability to satisfactorily respond to sequential inputs with only a minimum time to respond between inputs.

5.9 Summary

The results contained in this chapter demonstrate the application of the design procedure of Chapter IV to the aircraft model of Chapter III. The unstable open loop plants of six different flight conditions are stabilized and satisfactory results are obtained despite the simulation of the destabilizing effects of actuators, computational time delay, sensor dynamics and control surface nonlinearity. The effect of measurement noise is simulated and the responses are found to be unaffected by realistic values of noise. Also, threshold values of noise are determined and indicate that the controlled system at flight condition 1 is most sensitive to noise in the velocity measurement. The controllers at two flight conditions are found to be sufficiently insensitive to plant parameter variation to provide satisfactory control at all but one of the remaining flight conditions. Finally, two additional maneuvers representative of the landing scenario are satisfactorily performed.

VI. Conclusions and Recommendations

6.1 Design Results

Chapter V presents results that achieve the objective of demonstrating successful control of the STOL/F-15 using a proportional plus integral controller designed through the techniques developed by Professor Porter. Although no quantitative performance criteria are specified, the output responses are smooth and relatively fast and uncoupled. Good performance is demonstrated for a very well developed aircraft model that includes actuator dynamics, sensor dynamics, computational time delay, a specific surface nonlinearity, and sensor noise. Furthermore, it is shown that the controllers are robust to very challenging plant parameter variations arising from changing flight conditions.

6.2 Comments on the Design Method

In general, the design method allows rapid calculation of controller matrices based solely on the first Markov parameter and the user definable weighting constants Σ and $\bar{\alpha}$. Using experience gained from trial designs and the insight available from the well defined asymptotic properties of closed loop systems designed by these methods, weighting constants that achieve the design objectives are

readily chosen. Early in the design process it may be difficult to obtain user definable parameters that yield stable results, particularly in the case of unstable open loop plants. However, after some experimentation it soon becomes apparent what measures must be taken to stabilize the plant. For this aircraft, reducing all of the elements of the diagonal weighting matrix and the ratio of integral to proportional gain ($\bar{\alpha}$) is necessary to achieve closed loop stability. However, different plants may well have different requirements for obtaining stability. The design method lacks an algorithmic approach to initial stabilization, but since controller design is a simple calculation, an iterative approach using simulation results is acceptable. Therefore, recommendations for improvement are concerned exclusively with the simulation program MULTI.

6.3 Improvements to MULTI

There are several recommendations for improving the design process through the expansion of the capabilities of the computer aided design and simulation program MULTI. The previous section points out that the design procedure relies on the repetitive use of MULTI design and simulation features to achieve the desired control design. The options in MULTI that perform design calculations are relatively fast and use computer time sparingly. These calculations include the computation of continuous closed loop

roots, provided actuator and sensor dynamics are not included in the simulation. Inspection of these roots provides an initial evaluation of stability prior to a complete simulation, an option that requires considerable central processor time. Since actuator and sensor dynamics are assumed linear, their effects should be included in the calculation of closed loop transfer functions, allowing the rapid identification of unstable designs.

Currently, the control surface deflection data is inaccessible for plotting when actuator dynamics are included. Rather, the data plotted data is the input to the surface actuators. The algorithm that creates the plot file data should be modified to obtain the actual surface deflections. Also, control surface rate limits should be implemented in the program. However, position and rate saturations often result in instability with integral controllers and it is recommended that the implementation of a compensating algorithm be considered.

MULTI features algorithms that smooth the commanded inputs prior to comparing them with the feedback signal. Often this type of smoothing is accomplished by passing the input signal through a linear low pass filter. Implementation of this type of filter in addition to the smoothing may help to reduce the high initial surface deflections and deflection rates.

It is further recommended that the simulation of noise be expanded to include a Monte Carlo evaluation of the variance as a function of time, as well as an option to include filtering of the measurement noise.

Finally, the recently developed methods of Professor Porter et al. (17) for designing proportional plus integral plus derivative control should be added as an option to MULTI.

6.4 Proposed Future Work

This thesis presents an initial evaluation of the effects of sensor noise on the longitudinal control of the STOL/F-15 in landing configuration. To completely evaluate the noise effects and practical implementations of the controllers, it is necessary to implement filter algorithms and quantitatively determine the variance of the output signals. Furthermore, the ability to simulate noise in the form of disturbance inputs exists in MULTI, but disturbance effects on the STOL/F-15 with output control are currently untested. Further study of this aircraft and design method should include both of these evaluations.

Longitudinal control of the F-15/STOL using the Porter techniques of multivariable output control is investigated in this thesis as well as in a parallel effort using the combat configuration of the F-15/STOL (16). It

is recommended that the Porter methods be applied to the lateral control of the STOL/F-15.

Finally, recent improvements to the Porter method allow control of systems with rank deficient first Markov parameters without the use of the measurement matrix (17). As a result, there is no fundamental finite limit to either the speed or decoupling of the responses. It is recommended that these methods of proportional plus integral plus derivative control be applied to the STOL/F-15.

Index for Appendix A

	Page
Introduction	162
List of Changes and Additions	162
A. Gaussian Noise Option	162
1. Description	162
2. User's Guide	163
3. Programmer's Guide	169
B. Custom Input Option	177
1. Description	177
2. User's Guide	177
3. Programmer's Guide	182
C. Suppression of Actuators and Sensors	196
1. Description	196
2. User's Guide	196
3. Programmer's Guide	197
D. Saving Memory Files Without Exit	198
1. Description	198
2. User's Guide	198
3. Programmer's Guide	199
E. Convert Input Vector "U" From Radians to Degrees	200
1. Description	200
2. User's Guide	201
F. Plot Combination of States and Inputs	201
1. Description	201
2. User's Guide	201
3. Programmer's Guide	204

	Page
G. Simulation of Nonlinearities Peculiar to Aircraft	206
1. Description	206
2. User's Guide	207
3. Programmer's Guide	208
H. Calculate Initial Integrator State Vector Z0	211
1. Description	211
2. User's Guide	212
3. Programmer's Guide	213
I. Program Outline	214
1. Introduction	214
2. List and Description of Major Program Elements	214
3. Memory Files	219

Appendix A: Additions to MULTI

Introduction

During the course of this thesis, a number of changes and additions were made to the computer program MULTI to facilitate current and future research efforts. This appendix describes each of these changes and additions, as well as providing an outline of the entire program for the benefit of future programmers.

List of Changes and Additions

- A. Gaussian noise option
- B. Custom input option
- C. Suppression of actuators and sensors
- D. Saving memory files without exit
- E. Convert input vector "u" from radians to degrees
- F. Plot combination of states and inputs
- G. Simulation of nonlinearities peculiar to aircraft
- H. Calculate initial integrator state $Z(0)$ vector
- I. Program outline

A. Gaussian Noise Option

1. Description. This addition gives the user the option of simulating zero and non-zero mean, white,

gaussian, noise inputs to the system during execution of option 26. There are three types of noise inputs available, distinguished by the place in which the noise is injected into the linearized model. The first type, output measurement noise, is that noise which is introduced by the sensors used to measure the output variables being fed back to the controller. The second, measurement matrix noise, is identical to output measurement noise, except that it is the noise associated with measuring the quantities required to augment a rank defective CB matrix. The third type of noise, disturbance noise, allows the user to add disturbance inputs directly into the state equations in the form

$$\dot{\underline{x}} = \underline{A}\underline{x} + \underline{B}\underline{u} + \underline{G}\underline{w} \quad (\text{A-1})$$

where \underline{w} is a vector of random variables representing the disturbance input and \underline{G} is a matrix that governs the distribution of the noise into the state equations.

This addition also provides the user the option of making multiple simulations to statistically determine the influence of noise through the use of a Monte Carlo analysis.

2. User's Guide. Option 25 is selected to enter the data for the simulation of noise. Prior to entry into option 25 the user must have provided the number of states, outputs and inputs, by option 2, 9, or 199. In this case there are 3 states, 2 inputs, and 2 outputs. The following

prompt appears upon selection of option 25:

OPTION, PLEASE > #

? 25

THIS OPTION ALLOWS SIMULATION OF INDEPENDENT GAUSSIAN
DISTURBANCES AND SENSOR NOISE.

ENTER YOUR CHOICE OF THE FOLLOWING OPTIONS:

ENTER,SUPPRESS OR RESET DISTURBANCE INPUT....."0"

ENTER,SUPPRESS OR RESET OUTPUT MEASUREMENT NOISE..."1"

ENTER,SUPPRESS OR RESET MEASUREMENT MATRIX NOISE..."2"

DEFINE MONTE CARLO SIMULATION....."3"

TO QUIT OPTION 25....."4"

? 0

At the prompt the user selects "0" to operate on the disturbance noise. In this case the user desires to enter new noise data, makes the proper selection, and enters the data at the prompts.

THIS OPTION ALLOWS SIMULATION OF A DISTURBANCE OF THE
FORM $\dot{X} = AX + BU + GW$, WHERE W IS A VECTOR OF N
INDEPENDENT GAUSSIAN RANDOM VARIABLES.

G IS A MATRIX THAT IS N BY N WHERE N IS THE NUMBER OF
STATES, FORMING A LINEAR COMBINATION OF THE RANDOM
VARIABLES.

ENTER YOUR CHOICE OF THE FOLLOWING OPTIONS:

ENTER NEW DISTURBANCE PARAMETERS....."0"

SUPPRESS DISTURBANCE INPUT....."1"

RESET DISTURBANCE INPUT....."2"

? 0

ENTER THE MEAN AND STANDARD DEVIATION OF $W(1)$

? 2.3

$W(2)$

? 2.3

$W(3)$

? 2.3

ENTER THE G MATRIX BY ROW, 3 ELEMENTS PER ROW

```

ROW 1
? 1,2,3
ROW 2
? 2,3,1
ROW 3
? 3,1,2

```

Upon completion of the disturbance noise input, the program returns to the main menu for option 25 and awaits further input. At this point the user proceeds to input measurement matrix noise, output measurement noise, and define the size of the Monte Carlo analysis.

ENTER YOUR CHOICE OF THE FOLLOWING OPTIONS:

```

ENTER.SUPPRESS OR RESET DISTURBANCE INPUT....."0"
ENTER.SUPPRESS OR RESET OUTPUT MEASUREMENT NOISE..."1"
ENTER.SUPPRESS OR RESET MEASUREMENT MATRIX NOISE..."2"
DEFINE MONTE CARLO SIMULATION....."3"
TO QUIT OPTION 25....."4"

```

THIS OPTION ALLOWS SIMULATION OF NOISY OUTPUT SENSORS, CORRUPTING THE SIGNAL BEING FED BACK. INDEPENDENT GAUSSIAN NOISE IS ADDED TO EACH ELEMENT OF THE OUTPUT VECTOR WITH MEAN AND STANDARD DEVIATION OF YOUR CHOICE

ENTER YOUR CHOICE OF THE FOLLOWING OPTIONS:

```

TO ENTER NEW OUTPUT NOISE PARAMETERS....."0"
TO SUPPRESS OUTPUT SENSOR NOISE....."1"
TO RESET OUTPUT SENSOR NOISE....."2"

```

ENTER THE MEAN AND STANDARD DEVIATION OF THE NOISE ASSOCIATED WITH MEASURING OUTPUT 1:

```

? 2,3
OUTPUT2
? 1,2

```

ENTER YOUR CHOICE OF THE FOLLOWING OPTIONS:

ENTER,SUPPRESS OR RESET DISTURBANCE INPUT....."0"
 ENTER,SUPPRESS OR RESET OUTPUT MEASUREMENT NOISE..."1"
 ENTER,SUPPRESS OR RESET MEASUREMENT MATRIX NOISE..."2"
 DEFINE MONTE CARLO SIMULATION....."3"
 TO QUIT OPTION 25....."4"

? 2

THIS OPTION ALLOWS SIMULATION OF A NOISY MEASUREMENT OF
 THE STATE DERIVATIVES IN THE CASE OF AN IRREGULAR PLANT
 THE NOISE IS MODELLED AS INDEPENDENT GAUSSIAN RANDOM
 VARIABLES WITH MEAN AND VARIANCE OF YOUR CHOICE ADDED TO
 ANY OR ALL OF THE DERIVATIVES OF THE X2 VECTOR

ENTER YOUR CHOICE OF THE FOLLOWING OPTIONS:

TO ENTER NEW MEASUREMENT NOISE PARAMETERS....."0"
 TO SUPPRESS MEASUREMENT MATRIX NOISE....."1"
 TO RESET MEASUREMENT MATRIX NOISE....."2"

? 0

ENTER THE MEAN AND STANDARD DEVIATION OF THE NOISE
 ASSOCIATED WITH MEASURING STATE DERIVATIVE 1

? 5,4

STATE DERIVATIVE 2?

? 6,5

ENTER YOUR CHOICE OF THE FOLLOWING OPTIONS:

ENTER,SUPPRESS OR RESET DISTURBANCE INPUT....."0"
 ENTER,SUPPRESS OR RESET OUTPUT MEASUREMENT NOISE..."1"
 ENTER,SUPPRESS OR RESET MEASUREMENT MATRIX NOISE..."2"
 DEFINE MONTE CARLO SIMULATION....."3"
 TO QUIT OPTION 25....."4"

? 3

ENTER NUMBER OF SIMULATION RUNS DESIRED FOR MONTE CARLO
 ANALYSIS.....>

? 5

The user has selected a Monte Carlo simulation that is to
 be comprised of five independent noise simulations. Now,
 every time the simulation option (option 26) is selected
 the user will be asked if that simulation is to be included
 in the Monte Carlo analysis. The user may exit MULTI,
 log off, or run as many "non-Monte Carlo" simulations as

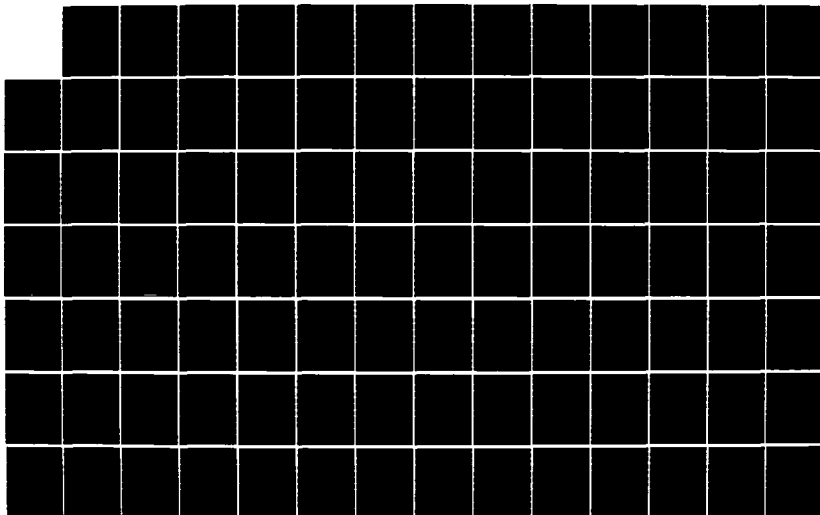
AD-A164 516

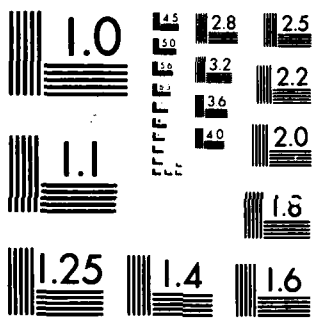
MULTIVARIABLE OUTPUT CONTROL LAW DESIGN FOR THE STOL
(SHORT TAKEOFF AND L... (U) AIR FORCE INST OF TECH
WRIGHT-PATTERSON AFB OH SCHOOL OF ENGI... B H ACKER
DEC 85 AFIT/GE/ENG/85D-1 F/G 1/2

3/24

UNCLASSIFIED

NL





MICROCOPY RESOLUTION TEST CHART
NATIONAL BUREAU OF STANDARDS-1963-A

he chooses. Once five Monte Carlo simulations have been executed the program returns to normal. To avoid unnecessary expenditure of computer resources, the total number of Monte Carlo simulations is limited to twenty-five. Finally, the user decides that the output measurement noise should be suppressed temporarily. This allows the noise to be eliminated without having to re-enter the noise parameters when the noise input is required. Entering a "1" at the prompt suppresses the noise, entering a "2" will reset suppressed noise. After suppressing the noise the user exits to the main program.

ENTER YOUR CHOICE OF THE FOLLOWING OPTIONS:

ENTER,SUPPRESS OR RESET DISTURBANCE INPUT....."0"
 ENTER,SUPPRESS OR RESET OUTPUT MEASUREMENT NOISE..."1"
 ENTER,SUPPRESS OR RESET MEASUREMENT MATRIX NOISE..."2"
 DEFINE MONTE CARLO SIMULATION....."3"
 TO QUIT OPTION 25....."4"

THIS OPTION ALLOWS SIMULATION OF NOISY OUTPUT SENSORS. CORRUPTING THE SIGNAL BEING FED BACK. INDEPENDENT GAUSSIAN NOISE IS ADDED TO EACH ELEMENT OF THE OUTPUT VECTOR WITH MEAN AND STANDARD DEVIATION OF YOUR CHOICE

ENTER YOUR CHOICE OF THE FOLLOWING OPTIONS:

TO ENTER NEW OUTPUT NOISE PARAMETERS....."0"
 TO SUPPRESS OUTPUT SENSOR NOISE....."1"
 TO RESET OUTPUT SENSOR NOISE....."2"

ENTER YOUR CHOICE OF THE FOLLOWING OPTIONS:

```

ENTER,SUPPRESS OR RESET DISTURBANCE INPUT....."0"
ENTER,SUPPRESS OR RESET OUTPUT MEASUREMENT NOISE..."1"
ENTER,SUPPRESS OR RESET MEASUREMENT MATRIX NOISE..."2"
DEFINE MONTE CARLO SIMULATION....."3"
TO QUIT OPTION 25....."4"
? 4

```

At this point the user desires to verify the inputs he made in option 25. This is accomplished with option 125, which displays the current noise parameters. Notice under the data for output measurement noise the word "(SUPPRESSED)", indicating that this noise is not currently being used.

```

OPTION, PLEASE > #
? 125

```

DISTURBANCE NOISE PARAMETERS
3 MATRIX

.1000E+01	.2000E+01	.3000E+01
.2000E+01	.3000E+01	.1000E+01
.3000E+01	.1000E+01	.2000E+01

NOISE MEANS AND STANDARD DEVIATIONS
.2000E+01 .3000E+01
.2000E+01 .3000E+01
.2000E+01 .3000E+01

OUTPUT MEASUREMENT NOISE
MEAN AND STANDARD DEVIATION
.2000E+01 .3000E+01
.1000E+01 .2000E+01
(SUPPRESSED)

```

MEASUREMENT MATRIX NOISE
MEAN AND STANDARD DEVIATION
.5000E+01    .4000E+01
.6000E+01    .5000E+01

```

3. Programmer's Guide. The following FORTRAN code is located in PROGRAM OPT20, a subprogram of the executive program MULTI. This portion of the noise option addition is an interactive routine in which the user enters the desired noise, associated parameters, and the number of runs desired in the Monte Carlo analysis. The following variables have been introduced in this section of code:

<u>Variable</u>	<u>Description</u>
WRMEAN(I)	Vector containing the means of each disturbance to be added to the state equations.
WSIGMA(I)	Vector containing standard deviations of disturbances.
G(I,J)	Matrix distributing disturbances into state equation.
DISTURB	Integer flag indicating existence of disturbance noise.
PG(I,J)	Matrix where G(I,J) is permanently stored when the disturbance noise is suppressed.

RMEAN(I)	Vector of output measurement noise means.
RSIGMA(I)	Vector of output measurement noise standard deviations.
PRMN(I)	Vector where RMEAN(I) is permanently stored when the output measurement noise is suppressed.
PSIG(I)	Vector where RSIGMA(I) is permanently stored.
NOISE	Integer flag indicating existence of output measurement noise.
MRMEAN(I)	Vector of measurement matrix noise means.
MSIGMA(I)	Vector of measurement matrix noise standard deviations.
PMRMN(I)	Vector where MRMEAN(I) permanently stored when measurement matrix noise is suppressed.
PMSIG(I)	Vector where MSIGMA(I) is permanently stored.
MNOISE	Integer flag indicating existence of measurement matrix noise.
MONTC	Integer indicating number of Monte Carlo simulations desired.
DAT4	=80, output device assignment for local file MEM30, the file that contains the running sum of the simulation data.
MCOUNT	Integer counter indicating the number of Monte Carlo simulations already run. This variable is only initialized and stored in this part of the code.

```

*****
C***** OPTION 25 IS THE NOISE INPUT OPTION*****
C*****
2025 PRINT*, 'THIS OPTION ALLOWS SIMULATION OF INDEPENDENT GAUSSIAN'
      PRINT*, 'DISTURBANCES AND SENSOR NOISE.'
      PRINT*, ' '
      IF (IFLAG(2).EQ.0) THEN
        PRINT*, '# OF STATES, INPUTS & OUTPUTS MISSING...SEE OPTION #2'
        GO TO 8007
      ENDIF
5000 PRINT*, 'ENTER YOUR CHOICE OF THE FOLLOWING OPTIONS:'
      PRINT*, ' '
      PRINT*, ' '
      PRINT*, 'ENTER,SUPPRESS OR RESET DISTURBANCE INPUT....."0"'
      PRINT*, 'ENTER,SUPPRESS OR RESET OUTPUT MEASUREMENT NOISE..."1"'
      PRINT*, 'ENTER,SUPPRESS OR RESET MEASUREMENT MATRIX NOISE..."2"'
      PRINT*, 'DEFINE MONTE CARLO SIMULATION....."3"'
      PRINT*, 'TO QUIT OPTION 25....."4"'
      READ*,ISKIP
      IF (ISKIP.EQ.4) GO TO 8007
      IFLAG(25)=1
      IF (ISKIP.EQ.0) THEN
        PRINT*, 'THIS OPTION ALLOWS SIMULATION OF A DISTURBANCE OF THE'
        PRINT*, 'FORM  $\dot{X} = AX + BU + GW$ , WHERE W IS A VECTOR OF N'
        PRINT*, 'INDEPENDENT GAUSSIAN RANDOM VARIABLES.'
        PRINT*, 'G IS A MATRIX THAT IS N BY N WHERE N IS THE NUMBER OF'
        PRINT*, 'STATES, FORMING A LINEAR COMBINATION OF THE RANDOM'
        PRINT*, 'VARIABLES.'
        PRINT*, ' '
        PRINT*, 'ENTER YOUR CHOICE OF THE FOLLOWING OPTIONS:'
        PRINT*, ' '
        PRINT*, ' '
        PRINT*, 'ENTER NEW DISTURBANCE PARAMETERS....."0"'
        PRINT*, 'SUPPRESS DISTURBANCE INPUT....."1"'
        PRINT*, 'RESET DISTURBANCE INPUT....."2"'
        READ*, ISKIP
        IF (ISKIP.EQ.0) THEN
          3-----ENTER DISTURBANCE PARAMETERS-----
          PRINT*, 'ENTER THE MEAN AND STANDARD DEVIATION OF W(1)'
          READ*, WRMEAN(1),WSIGMA(1)
          IF (N.EQ.1) GO TO 5002
          DO 5001 I=2,N
            PRINT*, 'W(',I,')'
5001   READ*, WRMEAN(I),WSIGMA(I)
5002   PRINT*, 'ENTER THE G MATRIX BY ROW, ',N,' ELEMENTS PER ROW'
          DO 5004 I=1,N
            PRINT*, 'ROW ',I
            READ*, (G(I,J),J=1,N)
            DO 5003 J=1,N

```

```

5003 PG(I,J)=G(I,J)
5004 CONTINUE
      DISTURB=1
      GO TO 5000
ENDIF
C *****
C*****SUPPRESS DISTURBANCE PARAMETERS*****
      IF (ISKIP.EQ.1) THEN
        DO 5007 I=1,N
          DO 5006 J=1,N
5006   G(I,J)=0
5007   CONTINUE
          DISTURB=0
          GO TO 5000
        ENDIF
C*****RESET DISTURBANCE PARAMETERS*****
      IF (ISKIP.EQ.2) THEN
        DO 5010 I=1,N
          DO 5009 J=1,N
5009   G(I,J)=PG(I,J)
5010   CONTINUE
          DISTURB=1
        ENDIF
        GO TO 5000
      ENDIF
C*****
C****          OUTPUT MEASUREMENT NOISE          ****
C*****
      IF (ISKIP.EQ.3) THEN
        PRINT*, 'THIS OPTION ALLOWS SIMULATION OF NOISY OUTPUT SENSORS.'
        PRINT*, 'CORRUPTING THE SIGNAL BEING FED BACK. INDEPENDENT'
        PRINT*, 'GAUSSIAN NOISE IS ADDED TO EACH ELEMENT OF THE OUTPUT'
        PRINT*, 'VECTOR WITH MEAN AND STANDARD DEVIATION OF YOUR CHOICE'
        PRINT*,
        PRINT*, 'ENTER YOUR CHOICE OF THE FOLLOWING OPTIONS:'
        PRINT*,
        PRINT*,
        PRINT*, 'TO ENTER NEW OUTPUT NOISE PARAMETERS....."0"'
        PRINT*, 'TO SUPPRESS OUTPUT SENSOR NOISE....."1"'
        PRINT*, 'TO RESET OUTPUT SENSOR NOISE....."2"'
        READ*, ISKIP
C*****
C***** ENTER OUTPUT NOISE*****
      IF (ISKIP.EQ.3) THEN
        PRINT*, 'ENTER THE MEAN AND STANDARD DEVIATION OF THE NOISE'
        PRINT*, 'ASSOCIATED WITH MEASURING OUTPUT 1:'
        READ*, RMEAN(1),RSIGMA(1)
        PRMN(1)=RMEAN(1)
        PSIG(1)=RSIGMA(1)

```

```

        DO 5012 I=2,P
        PRINT *, 'OUTPUT',I
        READ*, RMEAN(I),RSIGMA(I)
        PRMN(I)=RMEAN(I)
        PSIG(I)=RSIGMA(I)
5012    CONTINUE
        NOISE=1
        GO TO 5000
    ENDIF
C***** SUPPRESS OUTPUT NOISE *****
    IF (ISKIP.EQ.1) THEN
        DO 5014 I=1,P
        RMEAN(I)=0
5014    RSIGMA(I)=0
        NOISE=0
        GO TO 5000
    ENDIF
C***** RESET OUTPUT NOISE *****
    IF (ISKIP.EQ.2) THEN
        DO 5016 I=1,P
        RMEAN(I)=PRMN(I)
5016    RSIGMA(I)=PSIG(I)
        NOISE=1
    ENDIF
    GO TO 5000
ENDIF

C*****
C**** MEASUREMENT MATRIX NOISE ****
C*****
    IF (ISKIP.EQ.2) THEN
    PRINT*, 'THIS OPTION ALLOWS SIMULATION OF A NOISY MEASUREMENT OF '
    PRINT*, 'THE STATE DERIVATIVES IN THE CASE OF AN IRREGULAR PLANT'
    PRINT*, 'THE NOISE IS MODELLED AS INDEPENDENT GAUSSIAN RANDOM'
    PRINT*, 'VARIABLES WITH MEAN AND VARIANCE OF YOUR CHOICE ADDED TO'
    PRINT*, 'ANY OR ALL OF THE DERIVATIVES OF THE X1 VECTOR'
    PRINT*, ' '
    PRINT*, 'ENTER YOUR CHOICE OF THE FOLLOWING OPTIONS: '
    PRINT*, ' '
    PRINT*, 'TO ENTER NEW MEASUREMENT NOISE PARAMETERS....."0"'
    PRINT*, 'TO SUPPRESS MEASUREMENT MATRIX NOISE....."1"'
    PRINT*, 'TO RESET MEASUREMENT MATRIX NOISE....."2"'
    READ*, ISKIP
C***** ENTER MEASUREMENT MATRIX NOISE*****
    IF (ISKIP.EQ.0) THEN
        PRINT*, 'ENTER THE MEAN AND STANDARD DEVIATION OF THE NOISE'
        PRINT*, 'ASSOCIATED WITH MEASURING STATE DERIVATIVE 1'
        READ *, MRMEAN(1), MSIGMA(1)

```

```

        PMRMN(1)=MRMEAN(1)
        PMSIG(1)=MSIGMA(1)
        DO 5018 I=2,P
        PRINT*, 'STATE DERIVATIVE ',I,'?'
        READ*, MRMEAN(I),MSIGMA(I)
        PMRMN(I)=MRMEAN(I)
5018    PMSIG(I)=MSIGMA(I)
        MNOISE=1
        GO TO 5000
    ENDIF
C***** SUPPRESS MEASUREMENT NOISE *****
    IF (ISKIP.EQ.1) THEN
        DO 5020 I=1,P
        MRMEAN(I)=0
        MSIGMA(I)=0
5020    CONTINUE
        MNOISE=0
        GO TO 5000
    ENDIF
C***** RESET MEASUREMENT NOISE *****
    IF (ISKIP.EQ.2) THEN
        DO 5022 I=1,P
        MRMEAN(I)=PMRMN(I)
        MSIGMA(I)=PMSIG(I)
5022    CONTINUE
        MNOISE=1
    ENDIF
    GO TO 5000
ENDIF
C ***** DEFINE MONTE CARLO ANALYSIS *****
    IF (ISKIP.EQ.3) THEN
5023    PRINT*, 'ENTER NUMBER OF SIMULATION RUNS DESIRED FOR MONTE CARLO'
        PRINT*, 'ANALYSIS.....>'
        READ*, MONTC
        IF (MONTC.GT.25) THEN
            PRINT*, 'YOU HAVE GOT TO BE JOKING. OBVIOUSLY YOU'RE NOT PAYING'
            PRINT*, 'FOR THIS. THE OUTPUT WILL BE ROUTED TO THE IG FOR '
            PRINT*, 'FRAUD, WASTE & ABUSE INVESTIGATION.'
            PRINT*, ' '
            GO TO 5023
        ENDIF
        DAT4=80
        OPEN (DAT4,FILE='MEM30')
        REWIND DAT4
        MCOUNT = 0
        WRITE (DAT4,*) MCOUNT
        CLOSE (DAT4,STATUS='KEEP')
        GO TO 5000
    ENDIF

```

The noise described by the entries in option 25 is entered into the simulation in option 26 by means of several subroutine calls to SUBROUTINE GPNML (listed below). This subroutine generates a seed and then makes a call to the IMSL Library routine GGNMC which returns the random vector RDEV(I). Variables introduced here are:

<u>Variable</u>	<u>Description</u>
DSEED	Real seed for IMSL routine GGNML.
RDEV(I)	Vector, random and zero-mean, returned by GGNML.
NR	Integer dimension of RDEV(I).

```

      SUBROUTINE GPNML (RMEAN,RSIGMA,N,RDEV)
C  DEVIATES RETURNED FROM IMSL IN RDEV(I)
      INTEGER NR
      REAL MRMEAN,MSIGMA
      COMMON /B 27/ MONTC,MCOUNT
      DIMENSION RMEAN(15),RSIGMA(15),RDEV(15)
      DOUBLE PRECISION DSEED
      DATA DSEED /2001.D0/
      NR=N
C  REPETITIVE CALLS TO GGNMC (IMSL) WILL AUTOMATICALLY CHANGE DSEED
C  GGNML RETURNS A NORMALIZED ZERO MEAN GAUSSIAN N(0,1)
      DSEED = DSEED + (1000 + MCOUNT)
      CALL GGNML (DSEED,NR,RDEV)
      DO 5025 I=1,N
5025 RDEV(I)=RDEV(I)*RSIGMA(I) + RMEAN(I)
C  TRANSFORM THE NORMALIZED VECTOR TO MRMEAN,RSIGMA
      RETURN
      END

```

A number of minor changes were made throughout MULTI to accommodate the noise input option. Previously, the calculation step size was entered in option 25. This function is now accomplished in option 24. Option 125 now

prints out the current values of the noise parameters. All noise data entered in option 25 is stored in local file MEM20, and as a result the options which affect the reading and writing of MEM20 (options 29, 99, and 199) are changed accordingly. Finally, option 26 includes a section of code that reads, operates on, and writes to local file MEM30 to keep a running total of the simulation data needed to perform the Monte Carlo analysis. During each simulation the current data is added to the values stored in MEM30 from previous simulations, creating a running total at each time increment. When the last run is complete, the running totals are divided by the total number of runs to obtain an "average" run. This data can then be plotted in the same manner as the results of any other simulation. Currently this code, listed below, only calculates the mean value of multiple simulation runs. It is recommended that in the future this be expanded to include a calculation of the standard deviation as well. The new variables in this section are:

<u>Variable</u>	<u>Description</u>
MONTY	Logical character indicating whether user wishes current simulation to be included in the Monte Carlo analysis.
DATD	=90, input device assignment for local file MEM30.

DAT4 =80, output device assignment for local file
MEM30.

MYP(IJ,I) Matrix containing a running sum of output
data.

MUP(IJ,I) Matrix containing a running sum of input (U)
data.

MVP(IJ,I) Matrix containing a running sum of input (V)
data.

MXP(IJ,I) Matrix containing a running sum of state data.

B. Custom Input Option

1. Description. This option expands the input alternatives to include a wide variety of possibilities as defined by the user. By selecting the custom input feature of option 22, the user can select ten points that define the input magnitude as a function of time. The points are connected with straight lines by the program and if desired the corners are smoothed. The option of using the original input routine is retained and its use is recommended whenever possible, since it is easier to use.

2. User's Guide. To select a custom input, the user enters "22" at the option prompt. Following is a sample of the interactive prompts and inputs.

OPTION, PLEASE > #
? 22

THIS OPTION SETS THE INPUT COMMAND VECTOR, V

DO YOU WANT THE STANDARD OR CUSTOM INPUT?
ENTER S OR C >

? C

THIS PORTION OF THE PROGRAM ALLOWS THE USER
TO DEFINE 10 POINTS ALONG A CUSTOM INPUT THAT
ARE TO BE CONNECTED BY STRAIGHT LINES AND
THEN SMOOTHED IF SO DESIRED.

ENTER INPUT 1: TIME, MAGNITUDE>

PT. 1>>

? 1,1

PT. 2>>

? 2,2

PT. 3>>

? 3,3

PT. 4>>

? 4,4

PT. 5>>

? 5,5

PT. 6>>

? 6,6

PT. 7>>

? 7,7

PT. 8>>

? 8,8

PT. 9>>

? 9,9

PT. 10>>

? 10,10

ENTER INPUT 2: TIME, MAGNITUDE>

PT. 1>>

? 1,3

PT. 2>>

? 2,3

PT. 3>>

? 3,4

PT. 4>>

? 4,3

TIME FOR PT. 4 MUST BE GREATER THAN
OR EQUAL TO PT. 3. TRY AGAIN.

ENTER INPUT 2: TIME, MAGNITUDE>

PT. 1>>

? 2,3

PT. 2>>

? 3,4

PT. 3>>

? 5,5

PT. 4>>

? 7,3

```

PT. 5>>
? 9,10
PT. 6>>
? 11,12
PT. 7>>
? 13,14
PT. 8>>
? 15,16,
PT. 9>>
? 17,18
PT. 10>>
? 19,20
DO YOU WANT TO SMOOTH THE INPUTS? Y OR N
? Y

```

Notice that if the user attempts to enter the data in other than sequential or chronological order, the program interprets this as going backward in time and requests corrected data. Like most of the data options in MULTI, the values may be verified in its corresponding 100-series option.

```

OPTION. PLEASE #
? 122

(10). INITIAL STATES...

.0000E+00 .0000E+00 .0000E+00

2(0). INITIAL STATES...

.0000E+00 .0000E+00
CUSTOM INPUT
INPUT 1
PT. TIME MAG
1 1. 1.
2 2. 2.

```

3	3.	3.
4	4.	4.
5	5.	5.
6	6.	6.
7	7.	7.
8	8.	8.
9	9.	9.
10	10.	10.

INPUT 2

PT.	TIME	MAG
1	2.	3.
2	3.	4.
3	5.	6.
4	7.	8.
5	9.	10.
6	11.	12.
7	13.	14.
8	15.	16.
9	17.	18.
10	19.	20.

INPUT IS SMOOTHED

OPTION. PLEASE > #

In order to make effective use of the custom input feature it is imperative that the user understand the mathematical foundations of the smoothing routine and the assumptions made in implementing the option. The specifics of the smoothing algorithm are discussed in the programmer's guide. Following is a summary of features and limitations that the user may find useful.

a. Step inputs cannot be smoothed. It is assumed that if a smoothed input is desired a ramp would be selected for the initial step up or down. The program defines a step input as any two consecutive points having the same time axis coordinate. If any part of any of the

inputs is a step, then none of the inputs can be smoothed. If the user desires smoothed step inputs within the custom input, it is recommended that a ramp with a duration of less than a sample period be entered. It is very likely that a ramp of such short duration cannot be smoothed with the polynomial techniques used, but even if unable to smooth the step the algorithm will continue to smooth the remainder of the input normally.

b. It is important that the input be defined for at least the longest simulation time anticipated. In most cases, failure to do so will result in the value of the magnitude of the last point being held throughout the undefined region. Obviously, points beyond the simulation time will never be encountered in option 26 but they may be useful for shaping the input prior to the end of the simulation.

c. All ten points must be defined. Note that there are no trivial inputs. If no input to a particular channel is desired, then an input that is specified as zero magnitude for the entire simulation time is required, that is, at each of the ten points. (Simply entering zeros at both the time and magnitude prompts will result in an input which is only defined at the origin.)

d. The input always begins at the origin. Unless a step is desired, the time at point 1 should be

greater than zero. If, however, the time at point 1 is chosen to be zero, the magnitude should be non-zero.

e. Clever application of the mathematical principles used for the smoothing algorithm can produce nearly any input desired. The duration and amount of smoothing can be varied without changing the basic input by inserting extra points along straight line segments. A sample input, both smoothed and unsmoothed, is shown in Figures A.1 and A.2.

3. Programmer's Guide. The bulk of the code to accomplish this feature is located in one of two places--in PROGRAM OPT20 under option 22, and in PROGRAM OPT26. The code in option 22 is where the data is entered for the custom input feature, and where the parameters for the smoothing curve are calculated. The basic structure of the algorithm, as shown in Figure A.3, is to first establish the unsmoothed, "dot-to-dot" input curve. Then, if smoothing is desired, a third order polynomial is chosen such that the slope and magnitude of the polynomial match the basic curve at the beginning and end of smoothing. Smoothing occurs in the last 20 percent of the line segment before the point of interest and the first 20 percent of the line segment following the point. Often, the curve to be smoothed changes slope too rapidly to be adequately smoothed by a third order polynomial.

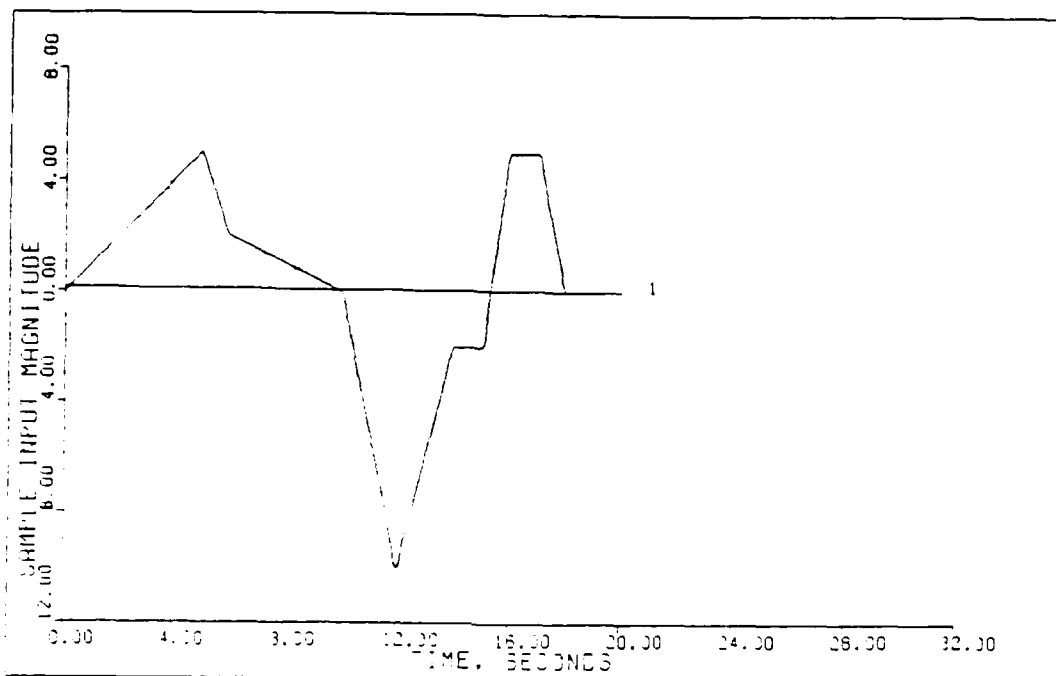


Fig. A.1. Sample Custom Input--Unsmoothed

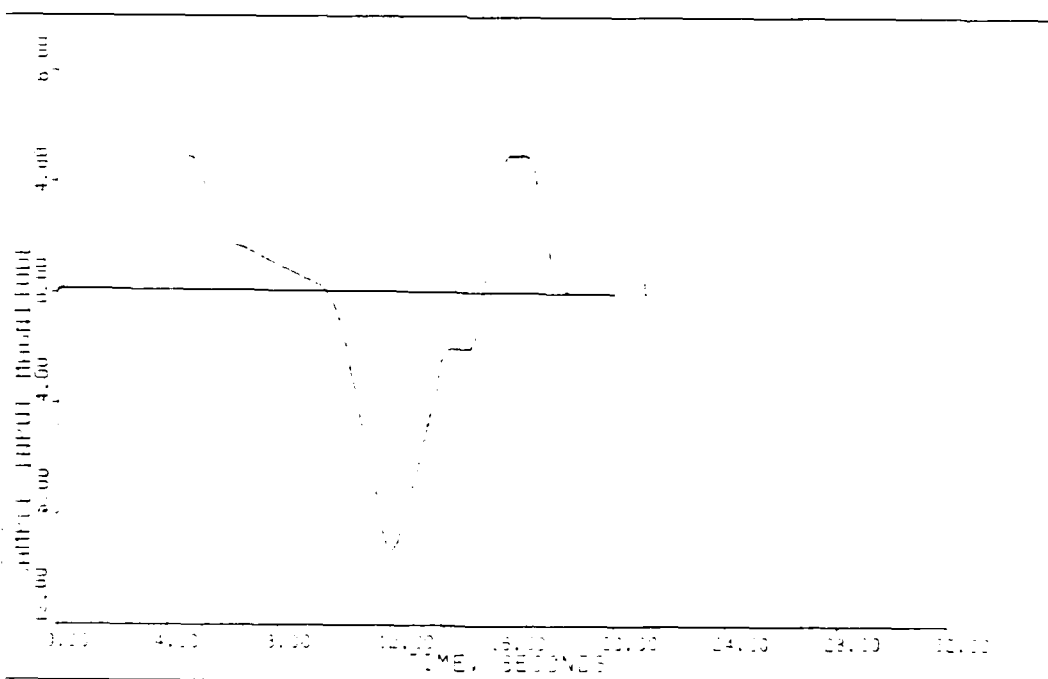


Fig. A.2. Sample Custom Input--Smoothed

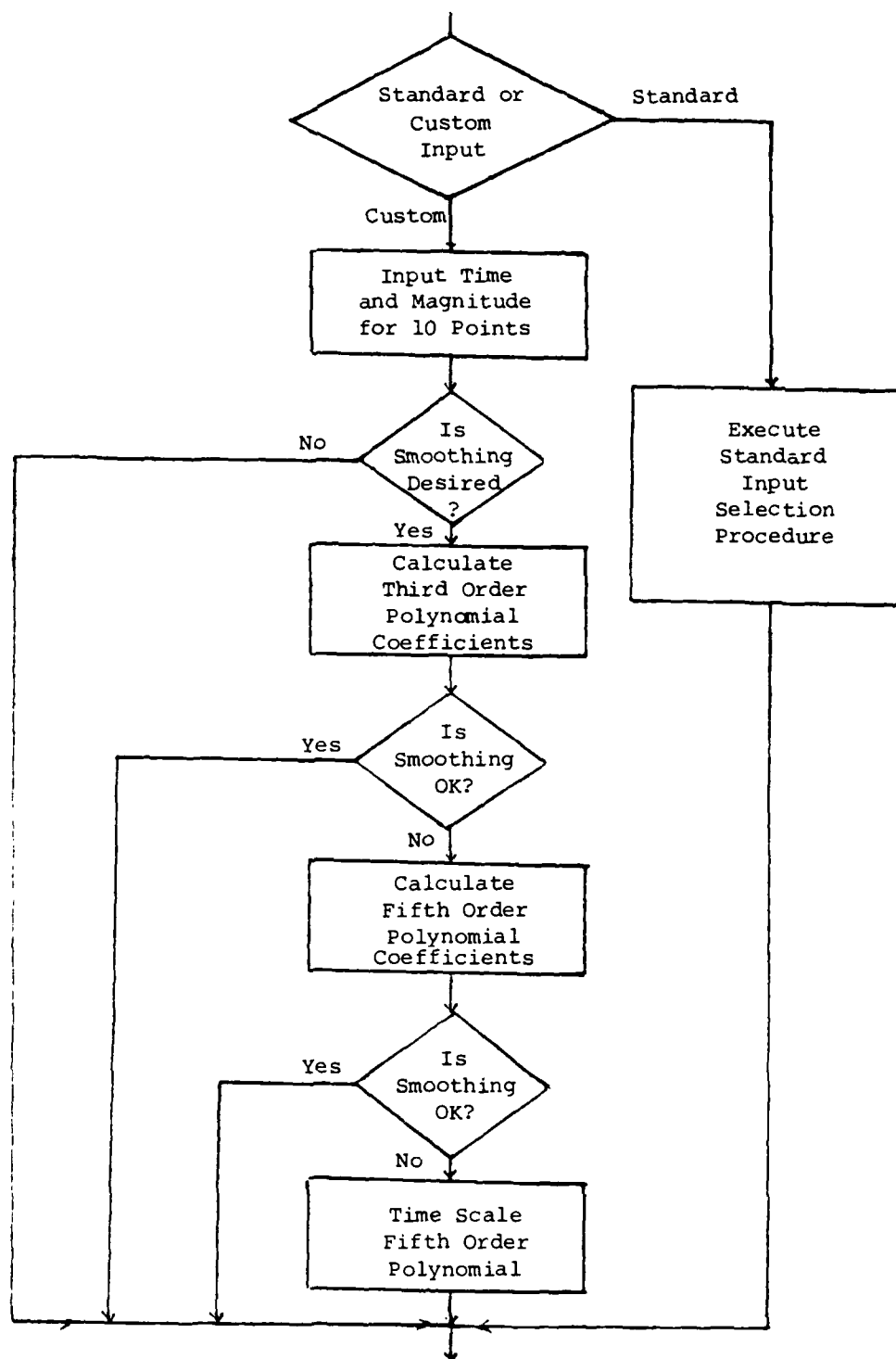


Fig. A.3. Option #22 Algorithm Outline
184

This condition is indicated by the second derivative of the polynomial at the beginning and end of smoothing being opposite in sign from the desired slope change. This situation can sometimes be corrected by using a fifth order polynomial and improving two more conditions; specifically that the acceleration at the beginning and end of smoothing be continuous (i.e., zero). Even fifth order polynomials can have unacceptable smoothing characteristics if the third derivative at the beginning or end of smoothing is of opposite sign of the desired acceleration change. In this event the algorithm attempts to time scale the fifth order polynomial to satisfy these conditions. If the user attempts to smooth an input that has large slope changes with short line segments the smoothing will be unsatisfactory. The only way to identify inadequate smoothing is to plot the inputs (V vector) using a calcomp plot option (34 or 35). The astute programmer will find that the routine used to find an acceptable time scaling factor is an unsophisticated, brute force sequential search. It was found that determining that the current value does not satisfy the required conditions yields no information on which direction to search, rendering a more efficient approach, like a binary search, impossible. If no solution is found, eventually a matrix that must be inverted becomes singular, and the program returns a message to that effect and does not smooth that particular point. The math used

to solve these problems is not complex, but is difficult to follow from the code alone. The key equations are developed below to facilitate understanding of the program. The variables used in this development are as follows:

t independent variable, time
 h dependent variable, input magnitude
 t_0 time at previous input point
 t_1 time at current point
 t_2 time at next point
 \hat{t} time smoothing begins
 $\hat{\Delta t}$ duration of smoothing
 a_n ($n=0,5$) coefficients of smoothing polynomial
 h_0 magnitude of previous input point
 h_1 magnitude of current point
 h_2 magnitude of next point
 s_1 slope before current point
 s_2 slope after current point
 f time scaling factor

a. Third order smoothing. If a third order polynomial is to be used, the general form of the input between \hat{t} and $(\hat{t} + \hat{\Delta t})$ is:

$$h(t) = a_0 + a_1(t - \hat{t}) + a_2(t - \hat{t})^2 + a_3(t - \hat{t})^3 \quad (A-2)$$

To solve for the four unknowns (a_0 , a_1 , a_2 , and a_3), four constraints must be satisfied. In this case, the conditions

are chosen in order to match the magnitude and slope of the straight-line input at the beginning and end of smoothing ($t = \hat{t}$, and $t = \hat{t} + \hat{\hat{t}}$). Applying these conditions to the polynomial and its derivative (slope) and then solving the four simultaneous equations yields:

$$a_0 = h_0 + s_1(\hat{t} - t_0) \quad (A-3)$$

$$a_1 = s_1 \quad (A-4)$$

$$a_2 = [3(h_1 + .2t_2s_2 - .2t_1s_2 - a_0 - a_1\hat{t}) - s_2\hat{t} + a_1\hat{t}]/\hat{t}^2 \quad (A-5)$$

$$a_3 = (s_2 - a_1 - 2a_2\hat{t})/3\hat{t}^2 \quad (A-6)$$

b. Fifth order smoothing. The general form of the fifth order polynomial used to smooth more difficult inputs is:

$$h(t) = a_0 + a_1(t - \hat{t}) + a_2(t - \hat{t})^2 + a_3(t - \hat{t})^3 + a_4(t - \hat{t})^4 + a_5(t - \hat{t})^5 \quad (A-7)$$

Since there are now six unknowns, two more constraints must be applied to find a unique solution for each of the coefficients. These conditions are chosen so that the second derivative of the input is zero at the beginning and end of smoothing. These constraints result in the following equations:

$$a_0 = h_0 + s_1(\hat{t}-t_0) \quad (A-8)$$

$$a_1 = s_1 \quad (A-9)$$

$$a_2 = 0 \quad (A-10)$$

$$a_3 + a_4\hat{t} + a_5\hat{t}^2 = \{h_1 + s_2[.2(t_2-t_1)] - a_0 - a_1\hat{t}\}/\hat{t}^3 \quad (A-11)$$

$$a_3 + (4/3)a_4\hat{t} + (5/3)a_5\hat{t}^2 = (s_2 - a_1)/3\hat{t}^2 \quad (A-12)$$

$$a_3 + 2a_4\hat{t} + (20/6)a_5\hat{t}^2 = 0 \quad (A-13)$$

For programming convenience, since a_2 is always zero, a_3 , a_4 , and a_5 are changed to a_2 , a_3 , and a_4 respectively. Equations (A-11), (A-12), and (A-13) are solved as simultaneous equations by MULTI in PROGRAM OPT20 under option #22.

c. Time scaled fifth order polynomial. The general form of the time scaled fifth order polynomial is the same except for the independent variable:

$$h(t) = a_0 + a_1\bar{t} + a_2\bar{t}^3 + a_3\bar{t}^4 + a_4\bar{t}^5 \quad (A-14)$$

$$\bar{t} = (t - \hat{t})/f \quad (A-15)$$

The conditions of the fifth order polynomial are again applied with the additional constraint that the third derivative at the beginning of the smoothing be the same

sign as the change in slope desired and of opposite sign at the end of smoothing. The program calculates the polynomial coefficients and executes an iterative search for a value of "f" that will satisfy these constraints.

d. FORTRAN code. The equations presented in the last three paragraphs are only the basic framework for the custom input routine. The programmer will also notice a number of conditional statements in both option 22 and option 26 to avoid overflow conditions that result from dividing by zero and other discontinuities. The variables introduced in these sections of code are contained in the comment statement preceding option 22.

```

ELSEIF (OPTINP.EQ. 22) THEN
  PRINT*, 'THIS PORTION OF THE PROGRAM ALLOWS THE USER
  PRINT*, 'TO DEFINE 10 POINTS ALONG A CUSTOM INPUT THAT
  PRINT*, 'ARE TO BE CONNECTED BY STRAIGHT LINES AND
  PRINT*, 'THEN SMOOTHED IF SO DESIRED.'
  DO 1350 K=1,10
1351  PRINT*, 'ENTER INPUT (K,1: TIME, MAGNITUDE)'
    DO 1352 I=1,10
      PRINT*, 'PT. ', I, ' '
      F=1
      READ*, (INPRT(K,I,J),J=1,2)
      IF (INPRT(K,I,1).LT.0, INPRT(K,I,1), AND, F.EQ.1) THEN
        PRINT*, 'TIME FOR PT. ', I, ' MUST BE GREATER THAN '
        PRINT*, 'OR EQUAL TO PT. ', I-1, ' TRY AGAIN.'
        GO TO 1351
      ENDIF
    DO 1352 CONTINUE
  DO 1350 CONTINUE
  PRINT*, 'DO YOU WANT TO SMOOTH THE INPUTS? Y OR N'
  READ*, A(1), SMOPT
  C*****
  C   THE CODE THAT FOLLOWS COMPUTES THE COEFFICIENTS OF THE
  C   POLYNOMIALS THAT ARE USED AS SMOOTHING CURVES BETWEEN LINE SEGMENTS
  C   IN EACH INPUT. THE POLYNOMIALS ARE INITIALLY CHOSEN AS THIRD ORDER

```

```

C POLYNOMIALS SUCH THAT THEIR MAGNITUDE AND SLOPE MATCH THE LINE *
C SEGMENT VALUES AT THE POINTS WHERE THE SMOOTHING STARTS AND STOPS. *
C OFTEN, HOWEVER, THE INPUT CHANGES SLOPE TOO RAPIDLY TO BE SMOOTHED *
C BY A THIRD ORDER POLYNOMIAL. MATHEMATICALLY IT IS POSSIBLE TO MEET *
C ANY BOUNDARY CONDITIONS (OTHER THAN INFINITE SLOPES) WITH ONLY A *
C THIRD ORDER POLYNOMIAL BUT THE CURVE SOMETIMES INITIALLY TURNS IN *
C THE WRONG DIRECTION. THIS PHENOMENON IS EVIDENT IN THE SECOND *
C DERIVATIVE OF THE FUNCTION, WHICH SHOULD AT LEAST BE THE SAME SIGN *
C AS THE CHANGE IN SLOPE AT THE POINT OF INTEREST. THE CODE TESTS FOR *
C THIS CONDITION AND CALCULATES COEFFICIENTS FOR FIFTH ORDER POLYS *
C IF NECESSARY. THIS ALLOWS TWO MORE CONDITIONS TO BE IMPOSED ON THE *
C SMOOTHING CURVE, AND THEY ARE CHOSEN SUCH THAT THE ACCELERATION IS *
C CONTINUOUS AND ZERO AT THE START AND STOP OF THE SMOOTHING. IT IS *
C POSSIBLE IN EXTREMELY DIFFICULT SMOOTHING SITUATIONS (LIKE LARGE *
C SLOPE CHANGES IN VERY SHORT TIME PERIODS) THAT THE SAME PROBLEM WILL *
C ARISE IN THE THIRD DERIVATIVE (JERK) OF THE FIFTH ORDER POLYNOMIAL. *
C THIS CONDITION IS TESTED AS WELL AND IF NECESSARY THE FIFTH ORDER *
C POLYNOMIAL IS TIME SCALED BY A FACTOR  $F_1$ . SINCE THE SCALE FACTOR *
C RESULTS IN NON-LINEAR SIMULTANEOUS EQUATIONS A SOLUTION (NOT UNIQUE) *
C IS FOUND THROUGH AN ITERATIVE SEARCH. A SOLUTION MAY NOT EXIST IN *
C THE REGION SEARCHED ( $F > .01$ ). *
C IN THIS EVENT THAT PARTICULAR POINT IS NOT SMOOTHED. NOTE THAT AS *
C THE ORDER OF THE POLYNOMIAL INCREASES IT APPROACHES A TAYLOR *
C SERIES REPRESENTATION OF THE INPUT, AND LESS SMOOTHING OCCURS. *
C AFTER SMOOTHING THE INPUT SEGMENTS ARE STRAIGHT IN THE MIDDLE 50% *
C OF THEIR LENGTH. AT EACH POINT THE INPUT IS SMOOTHED FOR 20% OF THE *
C LINE SEGMENT BEFORE AND 30% OF THE LINE SEGMENT FOLLOWING THE POINT *
C
C VARIABLES IN THIS SECTION OF CODE ARE: *
C
C   K.....COUNTER, USUALLY THE CURRENT INPUT *
C   I.....COUNTER, USUALLY THE CURRENT PT. IN INPUT *
C   J.....COUNTER, INTERNAL TO ARRAY INPPT *
C   INPPT(K,I,J).....ARRAY, CONTAINING INPUT PTS, POLYNOMIAL *
C   COEFFICIENTS, AND A SMOOTHING FLAG  $J=9$  *
C   T0.....INPPT(K,I-1,1), TIME AT LAST INPUT PT. *
C   T1.....INPPT(K,I,1), TIME AT CURRENT INPUT PT. *
C   T2.....INPPT(K,I+1,1), TIME AT NEXT INPUT PT. *
C   H0.....INPPT(K,I-1,2), MAG. AT LAST INPUT PT. *
C   H1.....INPPT(K,I,2), MAG. AT CURRENT INPUT PT. *
C   H2.....INPPT(K,I+1,2), MAG. AT NEXT INPUT PT. *
C   S1.....SLOPE UP TO CURRENT INPUT PT. *
C   S2.....SLOPE AFTER CURRENT INPUT PT. *
C   TH.....TIME SMOOTHING STARTS. *
C   TTH.....DURATION OF SMOOTHING *
C   XDDTH.....VALUE OF SMOOTHED ACCELERATION AT  $T=(TH+TTH)$  *
C   XJDT.....VALUE OF SMOOTHED JERK AT  $T=(TH+TTH)$  *
C   F.....TIME SCALING FACTOR  $F = .01$  *
C   A0,A1,A2,A3,A4.....INPPT(K,I,3)  $J=3,7$ , POLYNOMIAL COEFFICIENTS *

```

```

C      INPPT(K,I,8).....= 0, WHEN UNABLE TO SMOOTH      *
C      = 3, WHEN THIRD ORDER SMOOTHING USED              *
C      = 5, WHEN FIFTH ORDER SMOOTHING USED              *
C      = F, WHEN FIFTH ORDER IS TIME SCALED              *
C*****
      IF (SMOPT.EQ.'Y') THEN
        DO 1855 K=1,P
        DO 1854 I=1,9
          IF (I.EQ.1) THEN
            H0=0
            T0=0
          ELSE
            H0=INPPT(K,I-1,2)
            T0=INPPT(K,I-1,1)
          ENDIF
          H1=INPPT(K,I,2)
          H2=INPPT(K,I+1,2)
          T1=INPPT(K,I,1)
          T2=INPPT(K,I+1,1)
          IF (T1.EQ.T2.OR.T0.EQ.T1) THEN
            PRINT*, 'YOU HAVE A STEP IN INPUT ',K,' THAT'
            PRINT*, 'CANNOT BE SMOOTHED. DO YOU WISH TO <A>BORT'
            PRINT*, 'THE SMOOTHING ROUTINE, OR <E>NTER NEW'
            PRINT*, 'INPUT DATA? ENTER <A> OR <E>'
            READ '(A)',SMOPT
            IF (SMOPT.EQ.'A') THEN
              SMOPT='Y'
              GO TO 1855
            ELSEIF (SMOPT.EQ.'E') THEN
              GO TO 2022
            ELSE
              GO TO 2022
            ENDIF
          ELSE
            S1=(H1-H0)/(T1-T0)
            S2=(H2-H1)/(T2-T1)
            ENDIF
            TH=.3*T1 + .2*T0
            THH=.2*T2 + .2*T0
            A0=H0+S1*(TH-T0)
            A1=S1
            A2= H1 + .2*T2*S2 + .2*T1*S2 - A0 - THH*A1
            A2= A2*3 - S2*THH + A1*THH
            A2= A2/THH**2
            A3=(S2 - A1 - 2*A2*THH)/(3*THH**2)
            ADDTH=2*A2+3*A3*THH
            INPPT(K,I,8)=3
            IF (S1.S2).AND.(A2.LT.0) INPPT(K,I,8)=5

```

```

      IF (S1.LT.0.AND.A2.GT.0) INPPT(K,I,8)=5
      IF (S2.GT.0.AND.XDDTH.LT.0) INPPT(K,I,8)=5
      IF (S2.LT.0.AND.XDDTH.GT.0) INPPT(K,I,8)=5
      IF (INPPT(K,I,8).EQ.5) THEN
        POLYMAT(1,1)=1.
        POLYMAT(1,2)=THH
        POLYMAT(1,3)=THH**2
        POLYMAT(2,1)=1.
        POLYMAT(2,2)=(4./3.)*THH
        POLYMAT(2,3)=(5./3.)*THH**2
        POLYMAT(3,1)=1.
        POLYMAT(3,2)=2.*THH
        POLYMAT(3,3)=(20./6.)*THH**2
        HH=H1+S2*(THH-T1+TH)
        CA2=(HH-A1*THH-A0)/THH**3
        CA3=(S2-A1)/(3*THH**2)
        CA4=0.
        CALL INVERT(POLYMAT,IPOLY,3,3,*1261)
        A2=CA2*IPOLY(1,1)+CA3*IPOLY(1,2)+CA4*IPOLY(1,3)
        A3=CA2*IPOLY(2,1)+CA3*IPOLY(2,2)+CA4*IPOLY(2,3)
        A4=CA2*IPOLY(3,1)+CA3*IPOLY(3,2)+CA4*IPOLY(3,3)
        XDT=6.*A2+24.*A3*THH+60.*A4*THH**2
        INPPT(K,I,8)=5
        IF (S2-S1).LT.0.AND.A2.GT.0) INPPT(K,I,8)=1
        IF (S2-S1).GT.0.AND.A2.LT.0) INPPT(K,I,8)=1
        IF (A2.GT.0.AND.XDT.GT.0) INPPT(K,I,8)=1
        IF (A2.LT.0.AND.XDT.LT.0) INPPT(K,I,8)=1
        IF (INPPT(K,I,8).EQ.5) THEN
          INPPT(K,I,3)=A0
          INPPT(K,I,4)=A1
          INPPT(K,I,5)=A2
          INPPT(K,I,6)=A3
          INPPT(K,I,7)=A4
          GO TO 1262
        ELSE
          GO TO 1262
        ENDIF
1261 INPPT(K,I,8)=0
      PRINT*, 'UNABLE TO SMOOTH INPUT (K,I) AT PT. ',I
      INPPT(K,I,3)=A0
      INPPT(K,I,4)=A1
1262 IF (INPPT(K,I,8).EQ.1) THEN
      F=.01
1263 F1=0
      HH=H1+S2*(THH-T1+TH)
      CA2=(HH-A1*THH/F-A0)/(THH/F)**3
      CA3=(S2-A1)/(3*(THH/F)**2)
      CA4=0.
      POLYMAT(1,1)=1.

```

```

POLYMAT(1,2)=THH/F
POLYMAT(1,3)=(THH/F)**2
POLYMAT(2,1)=1.
POLYMAT(2,2)=(4./3.)*THH/F
POLYMAT(2,3)=(5./3.)*(THH/F)**2
POLYMAT(3,1)=1.
POLYMAT(3,2)=2.*THH/F
POLYMAT(3,3)=(10./3.)*(THH/F)**2
CALL INVERT(POLYMAT,IPOLY,3,3,*1261)
A2=CA2*IPOLY(1,1)+CA3*IPOLY(1,2)+CA4*IPOLY(1,3)
A3=CA2*IPOLY(2,1)+CA3*IPOLY(2,2)+CA4*IPOLY(2,3)
A4=CA2*IPOLY(3,1)+CA3*IPOLY(3,2)+CA4*IPOLY(3,3)
XTDT=6.*A2+24.*A3*(THH/F)+60.*A4*(THH/F)**2
IF ((S2-S1).LT.0.AND.A2.GT.0) FI=1
IF ((S2-S1).GT.0.AND.A2.LT.0) FI=1
IF (A2.GT.0.AND.XTDT.GT.0) FI=1
IF (A2.LT.0.AND.XTDT.LT.0) FI=1
IF (FI.EQ.1) THEN
    F=F*1.02
    GO TO 1263
ELSE
    INPPT(K,I,3)=A0
    INPPT(K,I,4)=A1
    INPPT(K,I,5)=A2
    INPPT(K,I,6)=A3
    INPPT(K,I,7)=A4
    INPPT(K,I,8)=F
ENDIF
ENDIF
ELSE
    INPPT(K,I,3)=A0
    INPPT(K,I,4)=A1
    INPPT(K,I,5)=A2
    INPPT(K,I,6)=A3
    INPPT(K,I,7)=0.
    INPPT(K,I,8)=3
ENDIF
1854    CONTINUE
1855    CONTINUE
ENDIF
ENDIF
IFLAG(22)=1
GO TO 3007

```

The following code is located in PROGRAM OPT26.

```

DO 1861 K=1,P
C*****
C   THIS IS THE CODE WHERE THE INPUT IS GENERATED WHEN      *
C   A CUSTOM INPUT HAS BEEN SELECTED. A0,A1,A2,A3,A4 ARE     *
C   COEFFICIENTS OF THE THIRD OR FIFTH ORDER POLYNOMIAL USED *
C   TO SMOOTH THE CURVE. T0,T1,H0,H1 ARE THE TIMES AND       *
C   MAGNITUDES AT THE BEGINNING AND END OF THE LINE SEGMENT  *
C   RESPECTIVELY AND S1 (=A1) IS THE SLOPE OF THE LINE.      *
C   THE VALUE CONTAINED IN INPPT(K,I,8) DETERMINES WHETHER  *
C   THE CURVE IS SMOOTHED BY A THIRD ORDER POLY, FIFTH ORDER *
C   POLY, OR A TIME SCALED FIFTH ORDER POLY. OPTION #22      *
C   CONTAINS A DETAILED DESCRIPTION OF THE SMOOTHING METHODS *
C   AND THE DEFINITION OF THE SMOOTHING VARIABLES IN A COMMENT *
C   STATEMENT PRIOR TO THE SMOOTHING ALGORITHM.              *
C*****
      IF (SMOPT.EQ.'N') THEN
        I=1
1401      IF (I.LT.10) THEN
          IF (T.GT.(INPPT(K,I,1))) THEN
            I=I+1
            GO TO 1401
          ENDIF
          ELSE
            I=10
          ENDIF
          IF (I.EQ.1) THEN
            IF (INPPT(K,I,1).EQ.0) THEN
              V(K)=INPPT(K,I,2)
            ELSE
              S1=INPPT(K,I,2)-INPPT(K,I,1)
              V(K)=S1*T
            ENDIF
          ELSE
            IF ((INPPT(K,I,1).EQ. INPPT(K,I-1,1))) THEN
              V(K)=INPPT(K,I,2)
            ELSE
              S1=INPPT(K,I,2)-INPPT(K,I-1,2)
              S2=S1*(INPPT(K,I,1)-INPPT(K,I-1,1))
              V(K)=INPPT(K,I-1,2)-S1*T-INPPT(K,I-1,1)
            ENDIF
          ENDIF

```

```

ELSE
  I=1
1402 IF (I.LT.10) THEN
      IF (T.GE. (.8*INPPT(K,I,1)+.2*INPPT(K,I+1,1))) THEN
          I=I+1
          GO TO 1402
      ENDIF
      ELSE
          I=10
      ENDIF
      IF (I.EQ.1) THEN
          T0=0
          H0=0
      ELSE
          T0=INPPT(K,I-1,1)
          H0=INPPT(K,I-1,2)
      ENDIF
      T1=INPPT(K,I,1)
      TH=.3*T1+.2*T0
      H1=INPPT(K,I,2)
      A0=INPPT(K,I,3)
      A1=INPPT(K,I,4)
      A2=INPPT(K,I,5)
      A3=INPPT(K,I,6)
      A4=INPPT(K,I,7)
      IF (T.GT.TH.AND.I.LE.9) THEN
          IF (INPPT(K,I,8).EQ.3) THEN
              V(K)=A0+A1*(T-TH)+A2*(T-TH)**2+A3*(T-TH)**3
          ELSEIF (INPPT(K,I,8).EQ.3) THEN
              V(K)=A0+A1*(T-TH)+A2*(T-TH)**3+A3*(T-TH)**4
              +A4*(T-TH)**5
          ELSEIF (T.GE.T1.AND.INPPT(K,I,8).EQ.0) THEN
              S2=INPPT(K,I+1,2)-INPPT(K,I,2)
              S2=S2/(INPPT(K,I-1,1)-INPPT(K,I,1))
              V(K)=H1 + S2*(T-T1)
          ELSEIF (INPPT(K,I,8).NE.0) THEN
              F=1./INPPT(K,I,8)
              V(K)=A0+A1*(T-TH)+F*A2*((T-TH)+F)**3
              +A3*((T-TH)+F)**4+A4*((T-TH)+F)**5
          ENDIF
      ELSE
          V(K)=H0+A1*(T-T0)
      ENDIF
      ENDIF
1861 CONTINUE
ENDIF

```

C. Suppression of Actuators and Sensors

1. Description. It is sometimes convenient to eliminate actuator and or sensor dynamics from the simulation. Previously, this would involve destroying the actuator and sensor data and then re-entering the same data when the dynamics are desired. The actuator and sensor data is now stored in permanent variable locations, while temporary variables can be suppressed and reset in option 4 or option 5.

2. User's Guide. The interactive prompts are self-explanatory for this change and are listed below.

OPTION, PLEASE > #

1

THIS OPTION ENTERS THE ACTUATOR STATE EQUATION DATA

ENTER "0" TO SUPPRESS ACTUATORS
ENTER "1" TO GET ACTUATOR VALUES...>
ENTER "2" TO USE STORED ACTUATOR VALUES...>
)

OPTION, PLEASE > #

3

THIS OPTION ENTERS THE SENSOR STATE EQUATION DATA

ENTER "0" TO SUPPRESS SENSORS
ENTER "1" TO GET SENSOR VALUES...>
ENTER "2" TO USE STORED SENSOR VALUES...>
)

It is important to note that if the actuator or sensor dynamics are suppressed, they will not be saved in MEM0 when exiting the program. A warning message to this effect has been added to the exit routine and is shown in the "Saving Memory Files Without Exiting" section of this appendix.

3. Programmer's Guide. The code to accomplish this option is very simple but is spread out in options 4, 5, 9, 99, 104, and 105. For these two reasons it is not repeated here. The following variables are added for this feature:

<u>Variable</u>	<u>Description</u>
PNA(I)	Vector of "m" integers (m = number of inputs), each being the number of states in the actuator for that input. This variable is a permanent storage location for the vector variable NA(I), the quantity used by the simulation for actuator state data. NA(I) is set to zero when the actuators are suppressed and is set equal to PNA(I) when the actuators are reset.
PNS(I)	Vector analagous to PNA(I) containing the number of states for each output sensor. NS(I) is the local variable used by the simulation.

D. Saving Memory Files Without Exit

1. Description. Upon selection of option 99, MULTI will save all pertinent data in local files MEM0, MEM10, MEM20, and MEM30 and then the program will either return to normal execution or exit according to the user's desires.

2. User's Guide. Option 99 allows graceful termination of MULTI and automatically saves all plant, actuator, sensor, design and simulation data in local files prior to exiting the program. However, as all MULTI users will inevitably discover, there are a number of ways to exit MULTI involuntarily, leaving the user with the irritating task of re-entering all data that had not been saved. The most commonly encountered inadvertent termination of MULTI occurs when the user enters a "RETURN" at the prompt without any data preceding the "RETURN". The computer program has interrupted execution at a read statement and is expecting input from the terminal. If no input is provided, an "END OF FILE" is encountered and the program aborts execution. Naturally, this phenomenon is accompanied by the loss of all volatile data, which may have taken hours to generate. This problem has not been corrected, but if the user is cautious to save data regularly, the frustration of re-entering data can be avoided and one is likely to stay motivated toward the ultimate objective for a considerably longer time. The

procedure for saving data is quite simple as is demonstrated below:

```
OPTION, PLEASE > #  
? 99
```

```
ALL PLANT INPUT DATA HAS BEEN SAVED IN A LOCAL FILE  
CALLED "MEM0"
```

```
ALL DESIGN DATA HAS BEEN SAVED IN A LOCAL FILE  
CALLED "MEM10"
```

```
ALL SIMULATION DATA HAS BEEN SAVED IN A LOCAL FILE  
CALLED "MEM20"
```

```
ALL MONTE CARLO SIMULATION DATA HAS BEEN SAVED  
IN A LOCAL FILE CALLED "MEM30"
```

```
*****
```

```
* ACTUATORS AND SENSORS WERE NOT SAVED *
```

```
*****
```

```
DO YOU WANT TO EXIT MULTI: Y OR N ?
```

```
? N
```

```
OPTION, PLEASE > #
```

3. Programmer's Guide. The code changes required to accomplish the desired changes to option 99 consist of several conditionals to determine whether sensors and actuators have been suppressed, generation of a warning based on that determination and finally a question asking the user if termination is desired. The only variable introduced is a logical character "EXIT", depending on the user's desires. The exit routine code reads as follows:

```

C -----ROUTING FOR OPTION #99-----
  ELSEIF (NOPT.EQ.99) THEN
    IF (IPLOT.GT.0) THEN
      CALL PLOTE (BLK)
      PRINT '(A/)', ' REMINDER: ROUTE 'PLOT(S)' BEFORE LOGOUT!'
    ENDIF
    CALL OVERLAY (MULTI,12,0)
    IF (ACT.EQ.'N'.OR.SEN.EQ.'N') THEN
      PRINT*, '*****'
      IF (ACT.EQ.'Y') THEN
        PRINT*, '* NOTE: SENSOR DYNAMICS WERE NOT SAVED *'
      ELSEIF (SEN.EQ.'Y') THEN
        PRINT*, '* NOTE: ACTUATOR DYNAMICS WERE NOT SAVED *'
      ELSE
        PRINT*, '* ACTUATORS AND SENSORS WERE NOT SAVED *'
      ENDIF
      PRINT*, '*****'
    ENDIF
    PRINT*, 'DO YOU WANT TO EXIT MULTI: Y OR N ?'
    READ '(A)', EXIT
    IF (EXIT.EQ.'N') THEN
      GO TO 9000
    ENDIF
    PRINT '(A/)', ' HAVE A NICE DAY!'
    STOP

```

E. Convert Input Vector "U"
From Radians to Degrees

1. Description. After completion of option 26 the user is given the option of converting several of the data arrays from radians to degrees prior to plotting the data. Previously this option did not include the control input vector "U". The routine now includes this conversion as well, to account for plants in which the input matrix is given in terms of radians. The original code is the work of Major Terry L. Courtheyn (5:C-1). Courtheyn's work is merely copied to accomplish the additional conversion.

2. User's Guide. The prompts for this option are identical to the prompts originally programmed by Courtheyn with the addition of a similar prompt for the conversion of the "U" vector. Both the use and programming of this change are self-explanatory and the programmer's guide is omitted.

F. Plot Combination of States and Inputs

1. Description. Often it is desired to plot not only a state but its derivative as well. In the case of an aircraft, it is often convenient to plot the normal acceleration as a function of time, requiring a combination of states and state derivatives. Since in a linear system of equations any state derivative can be described in terms of the states and inputs, all that is required is to be able to combine state and input data to obtain any function of states and state derivatives as a function of time. This change expands the existing capability of plotting combinations of states to the option of plotting a user definable combination of states and inputs.

2. User's Guide. Following is the interactive dialog that the user will encounter after selecting one of the six plotting options (31-36). This particular example is a terminal plot option (31). To obtain a plot of some combination of states and inputs, the user selects plot choice "4" at the prompt.

THIS OPTION PRODUCES A PLOT AT YOUR TERMINAL

PLEASE CHOOSE ONE OF THE FOLLOWING:

FOR A SINGLE SAMPLING TIME

- 1...A PLOT OF UP TO 2 INPUT AND OUTPUT PAIRS
- 2...A PLOT OF UP TO 4 INPUTS OR OUTPUTS OR STATES
- 3...A PLOT OF UP TO 4 DIFFERENT SIMULATIONS
(FOR ANY SINGLE INPUT OR OUTPUT)

OR 4...A PLOT OF UP TO 4 COMBINATIONS OF STATES

ENTER CHOICE DESIRED >

? 4

CHOICE #4...YOU'VE CHOSEN TO PLOT COMBINATION OF STATES
ENTER THE NUMBER OF COMBINATIONS
OF STATES AND INPUTS.....>

? 1

ENTER "Z" MATRIX....1 ROWS WITH 4 ELEMENTS EACH
ROW 1 >

? 1,2,3,4

COMBO MATRIX Z...

.1000E-01 .2000E-01 .3000E-01 .4000E-01

IS THIS CORRECT...YES,NO,\$...>

? Y

Up to this point, the user sees no change in the interactive prompts. Now the program requires entry of the inputs to be included in the combination. As with states, the user enters the matrix which adds the weighted inputs into the desired combination.

? Y

ROW 1 >

COMBO MATRIX ZU...

.1000E+01 .2000E+01 .3000E+01

Y

7 1

[illegible]

Q.

20.)

CURVE X ABOVE IS COMBO 1

DO YOU WANT A LIST OF POINTS USED IN PLOTTING?

ENTER...YES OR NO...>

? N

OPTION, PLEASE > #

3. Programmer's Guide. All of the code to produce plots, either at the terminal or files for CALCOMP plotting, is located in three overlays: OPTPLOT, OPT31, and OPT34. Although there are six options (31-36) that require the combining of states and inputs for plotting, there is only one routine to accomplish the calculations and it is located in OPTPLOT. The code to combine the inputs is nearly identical to the code to combine the states that was originally in MULTI. This code, listed below, requires the addition of two variables.

<u>Variable</u>	<u>Description</u>
CO(I,J)	Array containing the coefficients used to combine (I) inputs into (J) combinations.
IINP	Logical character indicating the presence of inputs in the combination to be plotted.

```

1486 PRINT '(A)', ' ENTER THE NUMBER OF COMBINATIONS'
PRINT*, 'OF STATES & INPUTS.....>'
READ*, K
DO 1499 I=1,K
DO 1497 J=1,M
1497 Z(I,J)=0
DO 1498 L=1,INPS
1498 ZU(I,L)=0
1499 CONTINUE
PRINT*, '
PRINT*, 'ENTER "Z" MATRIX... ',K, ' ROWS WITH ',M, ' ELEMENTS EACH
DO 1490 I=1,K
PRINT*, 'ROW ',I, ' >'
1490 READ*, (Z(I,J),J=1,M)
PRINT*, '
GO TO 190
1495 CALL FIX (Z,K,M)
190 PRINT*, 'COMBO MATRIX Z...'
CALL MATPR (Z,K,M)
CALL ANSWER (*1495,*8010)
PRINT*, '
PRINT*, ' DOES THE COMBO INCLUDE INPUTS?.....Y OR N'
READ '(A)',IINP
IF (IINP.EQ.'Y') THEN
GO TO 1502
ELSE
GO TO 1503
ENDIF
] *****
] ***** ZU MATRIX FORMS THE COMBO OF INPUTS *****
] *****
1502 PRINT*, '
PRINT*, ' ENTER "ZU" MATRIX... ',K, ' ROWS WITH ',INPS, ' ELEMENTS
DO 1491 I=1,K
PRINT*, 'ROW ',I, '
1491 READ*, (ZU(I,J),J=1,INPS)
PRINT*, '
GO TO 191
1492 CALL FIX (ZU,K,INPS)
191 PRINT*, ' COMBO MATRIX ZU...'
CALL MATPR (ZU,K,INPS)
CALL ANSWER (*1492,*8010)
1503 DO 1510 I=1,N
DO 1505 J=1,K
1505 B = B + J*(I-1)*ZU(I,J)
DO 1506 L=1,M

```

```

1501 S = S + X(I,L+1)*Z(J,L)
1505 PLMAT(I,J)=S
1510 CONTINUE
      ICLM=K
      CHOICE=' COMBO'

```

```

C -----
1515 IF (IFLTEN.EQ.0) IFLTEN=1
      IFLTEN=IFLTEN-1
      IF (IFLTEN.NE.0) GO TO 1520
      IF (ICODE.EQ.3) ICLM=LINES
      GO TO 8010

```

G. Simulation of Nonlinearities Familiar to Aircraft

1. Description. Linear models of aircraft are usually quite accurate, provided, of course, the assumptions made in obtaining the linear model are not violated in the simulation. One of the key assumptions is that the forces and moments on the aircraft are linear with control surface deflection. If control surface deflections are large, as in maximum performance maneuvers, or in the case of inherently nonlinear control surfaces like vectored, variable thrust, a linear model is inadequate. For the reasons described in Chapter III the principal nonlinearity of large longitudinal control surface deflections is the reversal of the sign of the partial derivative of velocity with respect to the deflection when the surface passes through zero angle of attack. This phenomenon is easily modeled in the simulation and is implemented in a special version of MULTI customized for aircraft models. In the case of vectored, variable thrust and nonlinearities are

more complex. A rigorous development of the nonlinear effects of this type of input is contained in Reference 15. These effects are also simulated, at the user's option, in the customized version of MULTI.

2. User's Guide. Unfortunately, to implement these two features it is necessary to place additional requirements on the allowable form of the model used in the customized version of MULTI. These constraints are as follows:

a. The plant must be longitudinal, body axis, linearized model of an aircraft.

b. The states are defined as THETA (pitch angle), U (X-axis velocity), Q (pitch rate), and ALPHA (angle of attack). These are all perturbation values and must be arranged in that order. Additional states are allowed but must be after ALPHA in the state vector.

c. The first two inputs must be aerodynamic surfaces, like stabilators or canards. The third input must be a variable thrust input like a throttle or reverser vanes. If a two-dimensional nozzle is desired, its deflection angle must be the fourth input.

d. The equilibrium angle of attack for each of the aerodynamic surfaces, and the equilibrium deflection of the two-dimensional nozzle must be known and entered in option #3.

It is important to note that when a two-dimensional nozzle is used, not only is the simulation nonlinear, but the solution is not unique. This of course means that there are an infinite number of steady state solutions and it may be difficult to obtain one that is satisfactory. It is left to the user to determine how one finds a satisfactory solution. A sample of the interactive prompts for option #3 follows:

```

OPTION, PLEASE > #
? 3
ENTER EQUILIBRIUM VALUE FOR EACH INPUT
INPUT 1
? -.01
INPUT 2
? .2
INPUT 3
? .1
IS THERE A TWO-DIMENSIONAL NOZZLE INPUT ON THIS
AIRCRAFT? (Y OR N)
? Y
ENTER THE NOZZLE MOMENT ARM FROM CG (FT)
? .25
ENTER PITCH MOMENT OF INERTIA IYY (SLUG*FT**2)
? 1255489
ENTER THE AIRCRAFT MASS (SLUGS) >
? 1437.2
ENTER THE EQUILIBRIUM VELOCITY (FT/SEC) >
? 201.5
ENTER THE DERIVATIVE Z-ALPHA-DOT (FT/SEC) >
? 1.256

OPTION, PLEASE > #

```

3. Programmer's Guide. There are two blocks of code added to MULTI for this feature. The first block is

located in PROGRAM OPTO under option #3 and is the interactive portion where the user enters the necessary data. The second block of code is located in PROGRAM OPT26 and is where the nonlinearities are actually computed during the simulation.

<u>Variables</u>	<u>Description</u>
EV(I)	Vector containing the equilibrium angles of attack for aerodynamic surfaces and initial nozzle and thrust input values.
EVA(I)	Vector containing time varying angles of attack for the aerodynamic surfaces.
NOZ2D	Logical character indicating presence of a two-dimensional nozzle.
LX	Local real variable, nozzle moment arm.
IYY	Local real variable, aircraft pitch moment of inertia.
MASS	Local real variable, aircraft mass.
UEQ	Local real variable, equilibrium velocity.
ZAD	Local real variable, body axis coefficient of force in the z direction with respect to the time derivative of the angle of attack.
BNOZ1	Real variable, nonlinear input matrix coefficient.
BNOZ2	Real variable, nonlinear input matrix coefficient.

BNL(K,J) Array containing original input matrix plus
 the nonlinear effects of BNOZ1, BNOZ2, and
 sign change.

The following code is located in PROGRAM OPTO:

```

PRINT*, 'ENTER EQUILIBRIUM VALUE FOR EACH INPUT'
DO 311 I=1,M
PRINT*, 'INPUT ',I
READ*, EV(I)
311 CONTINUE
PRINT*, 'IS THERE A TWO-DIMENSIONAL NOZZLE INPUT ON THIS
PRINT*, 'AIRCRAFT? (Y OR N)'
READ*(A),NOZ2D
IF (NOZ2D.EQ.'Y') THEN
PRINT*, 'ENTER THE NOZZLE MOMENT ARM FROM CG (FT)'
READ*, LX
PRINT*, 'ENTER PITCH MOMENT OF INERTIA (YY SLUG*FT**2)'
READ*, IYY
BNOZ1=LX/IYY
PRINT*, 'ENTER THE AIRCRAFT MASS (SLUGS)'
READ*, MASS
PRINT*, 'ENTER THE EQUILIBRIUM VELOCITY (FT/SEC)'
READ*, UEQ
PRINT*, 'ENTER THE DERIVATIVE Z-ALPHA-DOT (FT/SEC)'
READ*, ZAD
BNOZ2=1./(MASS*(UEQ-ZAD))
ELSE
NOZ2D='N'
ENDIF
IFLAG(3)=1
IPLANT=1
GO TO 9001

```

The remaining code for this feature is located in PROGRAM

OPT26:

```

C*****
C** CODE TO HARDWIRE NONLINEARITIES FOR STOL F-15      ****
C*****
      EVA(1)=EV(1)+X(4)
      EVA(2)=EV(2)+X(4)
      EVA(3)=EV(3)
      IF(NDZ2D.EQ.'Y') EVA(4)=EV(4)
      DO 1204 I=1,N
      BNL(1,3)=B(I,3)
      DO 1203 J=1,2
      BNL(1,J)=B(I,J)
      IF EVA(J).GE.0) THEN
        IF((U(J) + EVA(J)).LT.0) THEN
          BNL(2,J)=-B(2,J)
        ENDIF
      ELSE
        IF((U(J) + EVA(J)).GT.0) THEN
          BNL(2,J)=-B(2,J)
        ENDIF
      ENDIF
      1203 CONTINUE
      1204 CONTINUE
      IF NDZ2D.EQ.'Y') THEN
        BNL(3,3)=B(3,3)+BNZ11*X(5)
        BNL(4,3)=B(4,3)+BNZ12*X(5)
      ENDIF
C*****      END NON-LINEARITIES *****

```

H. Calculate Initial Integrator State Vector ZO

1. Description. MULTI requires two vectors of initial conditions to specify an initial system state. The first is the initial conditions desired on each of the plant states. In the case of an aircraft this specifies the initial orientation and motion of the aircraft. The second vector is the initial conditions imposed by the integral of the error vector $Z(0)$. If initial control

surfaces deflections are desired they must be specified by the $Z(0)$ vector. The relationship between $Z(0)$ and $U(0)$ is given by:

$$Z(0) = g K1^{-1} U(0)$$

g = forward loop gain (1/SAMPT)

$K1$ = controller integral gain matrix

$U(0)$ = initial control surface deflections

Option #6 now includes a routine that calculates the $Z(0)$ vector using the current values of $K1$ and g as well as a user specified $U(0)$.

2. User's Guide. This feature is invoked by selecting option 6 and making the appropriate choice from the menu (shown in the example below). The program requests the desired initial control inputs, calculates the $Z(0)$ vector and stores it in the appropriate memory location.

THIS OPTION COMPUTES THE TRANSFER FUNCTIONS OF THE SYSTEM

FOR OPEN-LOOP TRANSFER FUNCTION ENTER 1,

FOR CLOSED-LOOP TRANSFER FUNCTION ENTER 2 >

FOR $S(0)$ AND $S(0)$ INVERSE MATRICES ENTER 3 >

TO CALCULATE $Z(0)$ VECTOR ENTER 4 >

1

ENTER THE 3 ELEMENTS OF THE DESIRED $U(0)$ VECTOR

2,3,-5

THE INITIAL CONDITION $Z(0)$ HAS BEEN SET TO:

624.0088399888 -200.7108585859 49.21010101011

OPTION, PLEASE 4

3. Programmer's Guide. The code for this feature resides in PROGRAM XFERFN, the overlay for computing the system transfer functions.

```

362 PRINT '(A)', ' FOR OPEN-LOOP TRANSFER FUNCTION ENTER 1,'
PRINT*, 'FOR CLOSED-LOOP TRANSFER FUNCTION ENTER 2 > '
PRINT*, 'FOR G(O) AND G(O) INVERSE MATRICES ENTER 3 > '
PRINT*, 'TO CALCULATE Z(O) VECTOR ENTER 4 > '
READ*, TTYPE
*****
C* THIS SECTION CALCULATES THE NECCESARY INITIAL CONDITION VECTOR Z(O) *
C* TO SPECIFY A VECTOR OF INITIAL CONTROL INPUTS U(O). THE EQUATION *
C* USED FOR THIS CALCULATION IS: *
C*       $U(O) = G \cdot K1 \cdot Z(O) + G \cdot K0 \cdot ZDOT(O)$  *
C* ASSUMING THAT THESE INITIAL CONDITIONS ARE IMPOSED TO ESTABLISH AN *
C* EQUILIBRIUM CONDITION WITH NON-ZERO CONTROL SURFACE DEFLECTIONS. *
C*  $ZDOT(O) = 0$ , AND THE EQUATION REDUCES TO: *
C*       $U(O) = G \cdot K1 \cdot Z(O)$  *
C* *
C*       $Z(O) = (K1 \text{ INVERSE}) \cdot U(O) / G$  *
C* *****
IF (TTYPE.EQ.4) THEN
PRINT*, 'ENTER THE 'M' ELEMENTS OF THE DESIRED U(O) VECTOR'
READ*, U(I), I=1,M)
CALL MATPR(K1,P,P)
CALL INVERT(K1,K1I,P,PD,*4569)
DO 4568, I=1,P
  Z(O)=0.
DO 4567, J=1,P
  Z(O)=Z(O)+K1I(I,J)*U(J)*SAMPT
4567 CONTINUE
4568 CONTINUE
PRINT*, 'THE INITIAL CONDITION Z(O) HAS BEEN SET TO:
PRINT*, (Z(O), I=1,P)
GO TO 4570
4569 PRINT*, 'K1 MATRIX IS SINGULAR AND CANNOT BE INVERTED'
4570 GO TO 9017
ENDIF

```

I. Program Outline

1. Introduction. The intent of this section is to provide a programmer's guide for the entire MULTI program. A copy of this outline can be found on the magnetic tape containing the master copy of MULTI. Additions and revisions by future users is highly encouraged and will eventually result in thorough documentation.

2. List and Description of Major Program Elements. Following is a list and brief description of all of the overlays and subroutines contained in MULTI. The program elements are listed in the order that they occur in the program listing.

a. PROGRAM EXEC. This overlay is the master program for MULTI and organizes its execution. After printing the beginning message, EXEC requests the user's choice of options and routes execution to one of the other seventeen overlays depending on the response. The exit routine is also contained in EXEC.

b. SUBROUTINE MATPR. This subroutine is used to print matrices.

c. SUBROUTINE QPRINT. This subroutine asks the user if a particular set of data should be printed at the terminal.

d. SUBROUTINE ANSWER. After printing data, ANSWER asks if the data is correct as printed.

e. SUBROUTINE INVERT. This subroutine formats a matrix and its associated parameters for inversion by the IMSL routine, LINV2F.

f. SUBROUTINE FIX. If, in SUBROUTINE ANSWER, the user desires to change a matrix, this subroutine accepts the changes and updates the matrix.

g. PROGRAM OPT0. This overlay contains the routines for the plant input options (options 0 through 9). However, option 6 is a separate overlay called XFERFN.

h. PROGRAM OPT10. This overlay contains all the design parameter routines (options 10 through 19) with the exception of options 14 and 18.

i. PROGRAM OPT14U. OPT14U calculates the controller matrices K0 and K1 for designs in which the plant parameters are unknown.

j. PROGRAM OPT14R. K0 and K1 are calculated in OPT14R for regular plants (first Markov parameter non-zero).

k. PROGRAM OPT14I. Irregular plant controller matrices are calculated in this overlay.

l. PROGRAM OPT18. In the case of an irregular plant, a measurement matrix is required. Option 18 (contained in OPT18) provides several utility routines that can be useful in choosing an appropriate measurement matrix.

m. PROGRAM OPT20. With the exception of options 26 and 28, all simulation options (20 through 29) are contained in OPT20.

n. PROGRAM OPTPLT. OPTPLT is the first of four routines (three overlays and a subroutine) written to generate plots. OPTPLT is the interactive portion in which the user selects the type of plot and the necessary parameters (options 30 through 39).

o. PROGRAM OPT31. Upon selection of one of the terminal plot options (31-33), OPT31 interactively asks for data specifically required for terminal plots. The data is then formatted for use by the terminal plot subroutine PLOTIT.

p. SUBROUTINE PLOTIT. This subroutine is an adaptation of the generalized routine used to produce plots on the line printer. It produces a plot at the user's terminal using non-graphics characters.

q. PROGRAM OPT34. OPT34 transforms the data for plotting into the form required by the CALCOMP plotting routine.

r. PROGRAM ERROR. This overlay contains all messages that result from errors that are neither fatal nor terminal. These errors are usually a result of attempting to perform calculations requiring data that has not yet been entered.

s. PROGRAM MEMORY. Upon selection of option 99, EXEC routes execution to MEMORY for generation of memory files MEM0, MEM10, MEM20. Section 3 contains the format of the files generated.

t. PROGRAM PRINT. PRINT contains all of the 100 series options that print the current values of the data generated in any of the input options.

u. PROGRAM OPT14B. This overlay computes the controller matrices when the BSTAR method is chosen in option 14.

v. PROGRAM XFERFN. This is the overlay that executes option 6. This option includes computation of any open or closed loop transfer function, steady state transfer functions, and initial controller integrator states.

w. SUBROUTINE PHOFS. This subroutine, called by XFERFN, calculates the transfer function denominator polynomials.

x. SUBROUTINE CADJB. CADJB is also called by XFERFN and computes the transfer function numerator polynomials.

y. SUBROUTINE POLYRT. POLYRT calculates the roots of the polynomials generated by PHOFS and CADJB.

z. SUBROUTINE CLMAT. This subroutine calculates the closed loop matrix used by XFERFN to compute the closed loop transfer functions.

aa. PROGRAM OPT26. OPT26 is the overlay that performs the simulation. It is important to note that the simulation integrates one calculation step at a time, allowing the introduction of noise, nonlinear effects like control surface saturation, and data packing for plotting.

bb. SUBROUTINE CLPASS. CLPASS is the first of four subroutines called by OPT26 to form the differential equations prior to invoking the library routine ODE to solve them. CLPASS is used to form the equations when both actuator and sensor dynamics are present.

cc. SUBROUTINE CLPSS1. CLPSS1 is used to form the differential equations when only actuator dynamics are present.

dd. SUBROUTINE CLPSS2. CLPSS2 is used to form the differential equations when only sensor dynamics are present.

ee. SUBROUTINE CLPSS3. CLPSS3 is used to form the differential equations when neither actuator nor sensor dynamics are present.

ff. SUBROUTINE GPNML. This subroutine uses the IMSL library routine GGNML to produce a zero mean, gaussian random vector with a standard deviation of 1. GPNML uses this normalized random vector to obtain a random vector with the mean and standard deviation required by the various noise inputs.

0. 1. 0. 0.	:
0. 0. 0. 1.	: C Matrix
1. 0. 0. -1.	:
Y	: Is there a D Matrix?
1. 2. 3.	:
2. 3. 1.	: D Matrix
3. 1. 2.	:
1. 2.5 3.	: Equilibrium surface position **
Y	: Is there a 2-d nozzle? **
1.234 1.345	: Nozzle effect on B Matrix **
Y	: Are there actuator dynamics?
2. 3. 1.	: #states in each actuator
0. 1.	: Actuator 1: A Matrix
-8755.198 -300.52	:
0. 3055.198	: Actuator 1: B Matrix
1. 0.	: Actuator 1: C Matrix
0. 1.	:
-8755.198 -300.52	: Actuator 2: A, B,
0. 3055.198	and C Matrices
1.25 1.	:
-99.	:
39.	: Actuator 3: A, B,
1.	and C Matrices
Y	: Are there sensor dynamics?
2. 3. 1.	: #states in each sensor
0. 1.	: Sensor 1: A Matrix
-123. 123.	:
0. 123.	: Sensor 1: B Matrix
1. 0.	: Sensor 1: C Matrix
0. 1.	:
-123. 123.	: Sensor 2: A, B,
0. 123.	and C Matrices
0. 1.	:
-123. 123.	: Sensor 3: A, B,
0. 123.	and C Matrices
0. 1.	:

** These entries are found only in MEMO files intended for use in the MULTI version designed for aircraft.

b. MEM10. This file contains the design data.

I	:	Type of design (R,I,O,B)
.01	:	Alpha
15. .4 .4	:	Sigma matrix diagonal elements
.05	:	Epsilon
-.000444086307 .0411717192 .252760573	:	
.000301990284 -.0279978440 .0892128160	:	K0 Matrix
-.0344416265 .00205523127 -.0261815938	:	
-.0000044408630 .0004117171 .0025276057	:	
.00000301990284 -.0002799784 .0008921281	:	K1 Matrix
-.00024441626 .00002055231 -.0002618159	:	
0.	:	
.25	:	Measurement Matrix
0.	:	
0. 1. 0. 0.	:	
0. 0. .25 1.	:	F Matrix
1. 0. 0. -1.	:	

c. MEM20. This file contains the simulation data.

0. 0. 0. 0.	:	Initial state vector
0. 0. 0.	:	Initial integrator vector (0)
0.	:	Custom or Standard Input
0. 0. 0. 0.	:	
0. 0.	:	
0. 0. 0. 0.	:	Data for state and output
0. 0.	:	
.3 -.1047 25. 25.	:	
1. 0.	:	
-1.E-10 1.E-10	:	
-1.E-10 1.E-10	:	Control surface limits
-1.E-10 1.E-10	:	
.025	:	Sample Time
20.	:	Total simulation time
.025	:	Calculation step size
1	:	Computational delay
0. 0. 0.	:	Output noise means
0. 0. 0.	:	Output noise standard deviation
0. 0. 0. 0.	:	Disturbance noise means
0. 0. 0. 0.	:	Disturbance noise deviations
0. 0. 0.	:	Measurement noise means

0. 0. 0.	_: Measurement noise deviations
0. 0. 0. 0.	_:
0. 0. 0. 0.	: Disturbance Noise
0. 0. 0. 0.	: G Matrix
0. 0. 0. 0.	_:
1 1 1	_: Noise flags

d. MEM30. This file contains the data used in the Monte Carlo noise simulation. It is recommended that the user not tamper with this file since it contains a great deal of raw plot data with little apparent meaning. Thus, an example is not shown here.

Appendix B: Multivariable Control Theory

(Edited and reproduced from Reference 2)

This thesis uses the multivariable design method of Professor Brian Porter of the University of Salford, England (13). The design method employs output feedback with high-gain error-actuated controllers. Output feedback is advantageous since state variables may be difficult to measure while system response data are more readily available.

System State Equations

Porter's method works equally well for either continuous or discrete systems, but it is often easier to first examine a system in the continuous time domain. This is because of the numerical accuracy problem with designing in the z-plane. A continuous time system is represented by the state space model:

$$\begin{aligned}\dot{\underline{x}} &= \underline{A}\underline{x} + \underline{B}u \\ \underline{y} &= \underline{C}\underline{x}\end{aligned}\tag{B-1}$$

where

\underline{A} = continuous plant matrix (n x n)

\underline{B} = continuous input control matrix (n x m)

\underline{C} = continuous output matrix (l x n)

\underline{x} = state variable vector with n states

\underline{u} = input vector with m inputs

\underline{y} = output vector with ℓ outputs

The system inputs for an aircraft are the control deflections or actuator input commands, and the system outputs are aircraft responses affected by the inputs.

The method does not allow for a feedforward, \underline{D} , matrix. If such a matrix is present in the original state space model, the control inputs must be redefined as states so that the \underline{D} matrix is absorbed into the \underline{C} matrix. This can be accomplished by incorporating the actuator dynamics into the plant model. Actuator inputs then become control inputs.

To employ Porter's method, it is desirable (but not necessary) to partition the system state equations as follows:

$$\begin{bmatrix} \dot{\underline{x}}_1 \\ \dot{\underline{x}}_2 \end{bmatrix} = \begin{bmatrix} \underline{A}_{11} & \underline{A}_{12} \\ \underline{A}_{21} & \underline{A}_{22} \end{bmatrix} \begin{bmatrix} \underline{x}_1 \\ \underline{x}_2 \end{bmatrix} + \begin{bmatrix} \underline{B}_1 \\ \underline{B}_2 \end{bmatrix} \underline{u} \quad (\text{B-2a})$$

$$\underline{y} = \begin{bmatrix} \underline{C}_1 & \underline{C}_2 \end{bmatrix} \begin{bmatrix} \underline{x}_1 \\ \underline{x}_2 \end{bmatrix} \quad (\text{B-2b})$$

The equations are partitioned so that \underline{B}_2 and \underline{C}_2 are square ($m \times m$) and ($\ell \times \ell$) matrices, respectively. The method requires that the number of inputs to the system equals

the number of outputs which means $m = l$, and therefore the dimension of \underline{B}_2 equals the dimension of \underline{C}_2 . It is always possible to form the state equations so that $\underline{B}_1 = \underline{0}$. Sometimes, however, a transformation matrix \underline{T} is necessary to achieve $[0, \underline{B}_2]$ form. In this case, the transformed states no longer have the same physical significance that the original states once had.

For the discrete case the system equations are written as follows:

$$\begin{aligned}\underline{x}[(k+1)T] &= \underline{\phi}\underline{x}(kT) + \underline{\psi}u(kT) \\ \underline{y}(kT) &= \underline{\Gamma}\underline{x}(kT)\end{aligned}\tag{B-3}$$

where

$\underline{\phi} = \exp(\underline{A}T)$ = discrete plant matrix

$\underline{\psi} = \int_0^T \exp(\underline{A}(T-t))\underline{B}dt$ = discrete input control matrix

$\underline{\Gamma} = \underline{C}$ = discrete output matrix

In the above equations T is the sampling period, and k takes on integer values from zero to plus infinity.

System With Output Feedback

Figure B.1 shows the block diagram for a continuous output feedback system, where \underline{v} is the command input vector, and \underline{y} is the desired output vector. The blocks for the plant are derived directly from the system state equations,

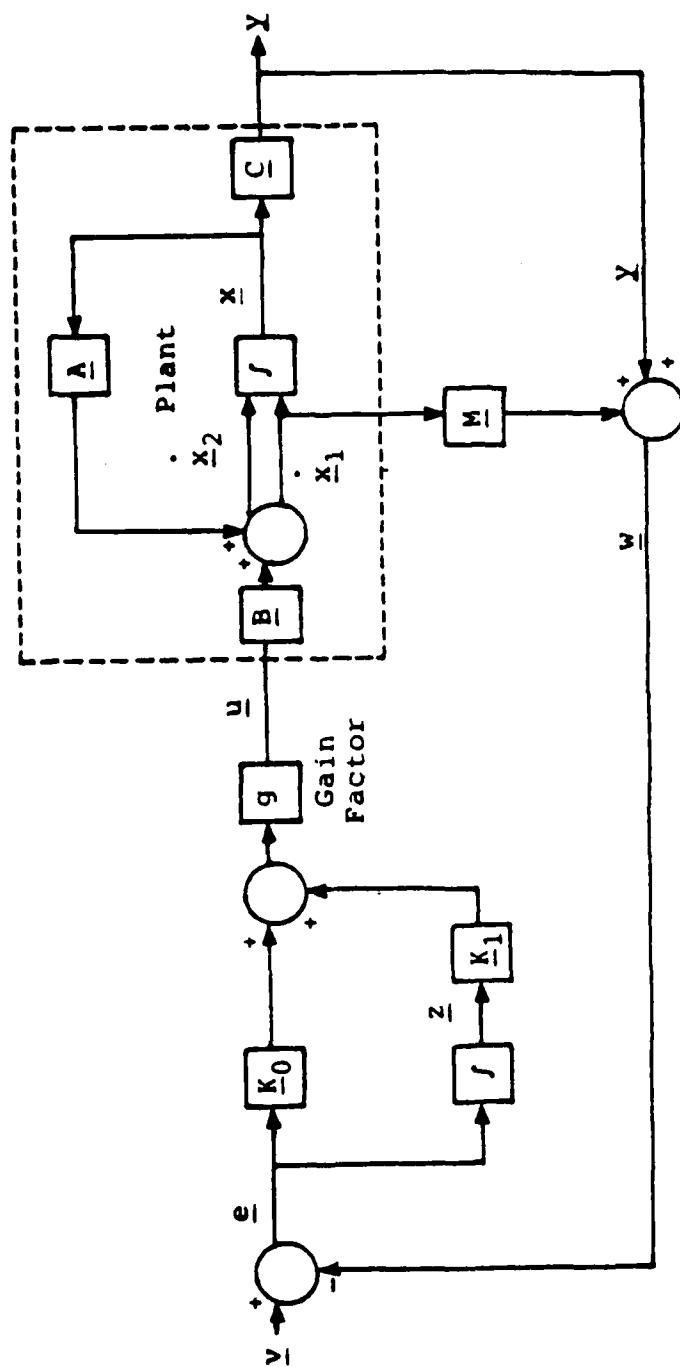


Fig. B.1. System Block Diagram--Continuous Case

Equation (B-1). The proportional plus integral controller has three parameters, \underline{K}_0 , \underline{K}_1 , and g , which must be determined by the designer. The output signal of the controller, \underline{u} , is given in the following control law equation:

$$\underline{u} = g(\underline{K}_0 \underline{e} + \underline{K}_1 \int \underline{e} dt) \quad (\text{B-4})$$

where

\underline{u} is the output signal of the controller

\underline{e} is the error signal at the input of the controller

\underline{K}_0 is the proportional gain matrix

\underline{K}_1 is the gain matrix for the integral term

g is the scalar forward path gain

Figure B.1 is the depiction of a system with only first-order integration in the controller design. The theory allows for a q -dimensional bank of integrators in which case the controller is made up of $(q + 1)$ \underline{K} matrices, \underline{K}_0 thru \underline{K}_q . A measurement matrix \underline{M} is included in the system if the plant is irregular. Regular and irregular plants are discussed later.

The discrete system block diagram, shown in Figure B.2, is similar to the continuous system, but Equation (B-4) becomes

$$\underline{u}(kT) = (1/T) [\underline{K}_0 \underline{e}(kT) + \underline{K}_1 \underline{z}(kT)] \quad (\text{B-5})$$

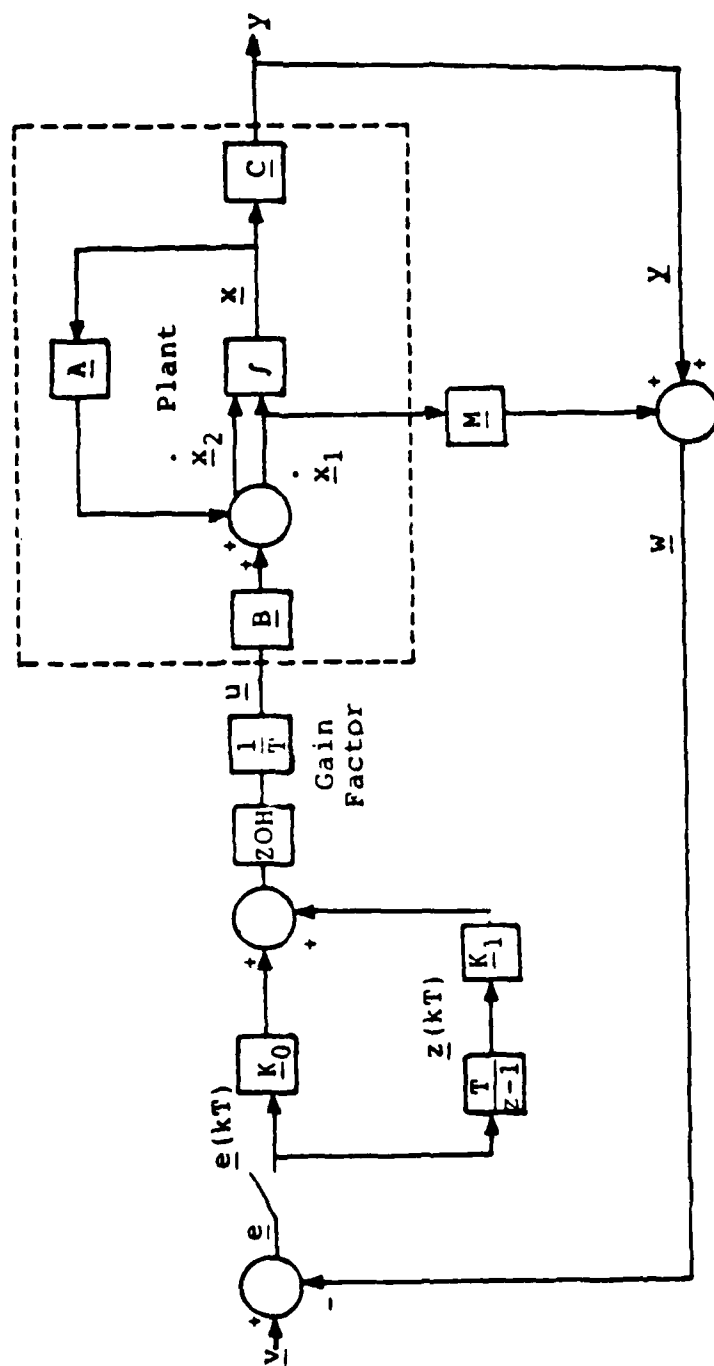


Fig. B.2. System Block Diagram--Discrete Case

where the forward path gain g equals the sampling frequency, $(1/T)$. The $\underline{z}(kT)$ matrix is derived from the backward difference equation,

$$\underline{z}[(k+1)T] = \underline{z}(kT) + T\underline{e}(kT) \quad (B-6)$$

The steps to be taken next in the design method depend on whether or not the first Markov parameter $[\underline{CB}]$, has full rank, i.e., does it have an inverse. If the matrix $[\underline{CB}]$ has full rank, the plant is called "regular" and no measurement matrix \underline{M} is needed. However, if $[\underline{CB}]$ does not have full rank, the plant is called "irregular" and \underline{M} is needed to form a new matrix $[\underline{FB}]$ (See Equations (B-12) through (B-14)) which does have an inverse. This is explained in more detail in the next sections. When the partitioned \underline{B} matrix in Equation (B-2a) has the form

$$\begin{bmatrix} \underline{0} \\ \underline{B}_2 \end{bmatrix} \quad (B-7)$$

then

$$[\underline{CB}] = [\underline{C}_2 \underline{B}_2] \quad (B-8)$$

$$[\underline{FB}] = [\underline{F}_2 \underline{B}_2] \quad (B-9)$$

As in the continuous case, a q -dimensional bank of integrators applies equally well to the discrete design (Figure B.2).

Asymptotic Characteristics

As the gain factor of the system, g (or $1/T$ for the discrete case), approaches infinity, the system transfer function matrix $G(s)$ assumes the asymptotic form

$$\underline{\Gamma}(\lambda) = \underline{\tilde{\Gamma}}(\lambda) + \underline{\hat{\Gamma}}(\lambda) \quad (\text{B-10})$$

where

$\underline{\tilde{\Gamma}}(\lambda)$ is the slow transfer function matrix

$\underline{\hat{\Gamma}}(\lambda)$ is the fast transfer function matrix

The roots of the asymptotic closed-loop transfer function may be grouped into three sets: \underline{z}_1 , \underline{z}_2 , and \underline{z}_3 . Table B.1 gives the equations for finding these asymptotic roots. Sets \underline{z}_1 and \underline{z}_2 correspond to the slow modes of the system, where the modes associated with the roots in \underline{z}_1 become uncontrollable, and, for regular designs, the modes associated with the roots in \underline{z}_2 become unobservable as the gain increases. Set \underline{z}_3 , the infinite roots, are associated with the fast modes of the system which become dominant as the gain increases.

The roots in set \underline{z}_2 correspond to the transmission zeros of the system which are not altered by output feedback. As the gain is increased, the closed-loop roots of the system tend to migrate toward the transmission zeros. This may adversely affect the system stability if the location of these zeros is in the unstable region.

TABLE B.1

ASYMPTOTIC EQUATIONS FOR ZERO- \underline{B}_2 FORM

System represented by:

$$\begin{bmatrix} \dot{x}_1 \\ \dot{x}_2 \end{bmatrix} = \begin{bmatrix} \hat{A}_{11} & \hat{A}_{12} \\ \hat{A}_{21} & \hat{A}_{22} \end{bmatrix} \begin{bmatrix} x_1 \\ x_2 \end{bmatrix} + \begin{bmatrix} 0 \\ \hat{B}_2 \end{bmatrix} u \quad \text{and} \quad y = \begin{bmatrix} \hat{C}_1 & \hat{C}_2 \end{bmatrix} \begin{bmatrix} x_1 \\ x_2 \end{bmatrix}$$

Continuous Case
(s-plane)Gain Factor = g

$$\hat{I}(\lambda) = \underline{C}_0 (\lambda \underline{I}_n - \underline{A}_0)^{-1} \underline{B}_0$$

$$\hat{I}(\lambda) = (\lambda \underline{I}_m + g \hat{C}_2 \hat{B}_2 K_0)^{-1} g \hat{C}_2 \hat{B}_2 K_0$$

Finite Roots

$$\underline{z}_1 = \{ (\lambda K_0 + K_1) = 0 \}$$

$$\underline{z}_2 = \{ (\lambda \underline{I}_{n-m} - \hat{A}_{11} + \hat{A}_{12} \hat{C}_2^{-1} \hat{C}_1) = 0 \}$$

Infinite Roots

$$\underline{z}_3 = \{ (\lambda \underline{I}_m + g \hat{C}_2 \hat{B}_2 K_0) = 0 \}$$

where

$$\underline{A}_0 = \begin{bmatrix} -K_0^{-1} K_1 & 0 \\ \hat{A}_{12} \hat{C}_2^{-1} K_0^{-1} K_1 & \hat{A}_{11} - \hat{A}_{12} \hat{C}_2^{-1} \hat{C}_1 \end{bmatrix}$$

$$\underline{B}_0 = \begin{bmatrix} 0 \\ \hat{A}_{12} \hat{C}_2^{-1} \end{bmatrix}$$

Regular Design

$$\underline{C}_0 = \begin{bmatrix} K_0^{-1} K_1 & 0 \end{bmatrix}$$

Discrete Case
(z-plane)Gain Factor = $1/T$

$$\hat{I}(\lambda) = \underline{C}_0 (\lambda \underline{I}_n - \underline{A}_0)^{-1} \underline{B}_0$$

$$\hat{I}(\lambda) = (\lambda \underline{I}_m - \underline{I}_m + \hat{C}_2 \hat{B}_2 K_0)^{-1} \hat{C}_2 \hat{B}_2 K_0$$

$$\underline{z}_1 = \{ (\lambda \underline{I}_m - \underline{I}_m + T K_0^{-1} K_1) = 0 \}$$

$$\underline{z}_2 = \{ (\lambda \underline{I}_{n-m} - T \hat{A}_{11} + \hat{A}_{12} \hat{C}_2^{-1} \hat{C}_1) = 0 \}$$

$$\underline{z}_3 = \{ (\lambda \underline{I}_m - \underline{I}_m + \hat{C}_2 \hat{B}_2 K_0) = 0 \}$$

Irregular Design

$$\underline{C}_0 = \begin{bmatrix} \hat{C}_2 \hat{E}_2^{-1} K_0^{-1} K_1 & \hat{C}_1 - \hat{C}_2 \hat{E}_2^{-1} \hat{E}_1 \end{bmatrix}$$

Reference 15 gives a procedure for locating the transmission zeros of a system.

For a regular design, as the gain increases, the system output responses become increasingly decoupled and dominated by the infinite root characteristics. The asymptotic closed-loop transfer function for the continuous case has the form

$$\underline{\Gamma}(\lambda) = \text{diag} \left\{ \frac{g^{\sigma_1}}{\lambda + g^{\sigma_1}}, \frac{g^{\sigma_2}}{\lambda + g^{\sigma_2}}, \dots, \frac{g^{\sigma_\ell}}{\lambda + g^{\sigma_\ell}} \right\} \quad (\text{B-11})$$

For the discrete case the form is

$$\underline{\Gamma}(\lambda) = \text{diag} \left\{ \frac{\sigma_1}{\lambda - 1 + \sigma_1}, \frac{\sigma_2}{\lambda - 1 + \sigma_2}, \dots, \frac{\sigma_\ell}{\lambda - 1 + \sigma_\ell} \right\} \quad (\text{B-12})$$

where the σ_i ($i=1, \dots, \ell$) are determined by the weighting matrix, $\underline{\Sigma}$.

For certain irregular designs where the structure of the output vector creates a diagonal Γ matrix, the system will exhibit increasingly decoupled behavior (Chapter IV). In other cases, the Γ matrix contains off-diagonal terms which prevent full output decoupling as the gain approaches infinity. In all irregular designs, the transmission zero always appears as a finite asymptotic root in at least one position on the diagonal of Γ and may appear on the off-diagonal. This characteristic places an upper bound on the time responses of these particular outputs (13).

Regular Plant

For the system to be classified as "regular" the first Markov parameter $[CB]$ must have full rank. If this is true, the gain matrices can be found from

$$\underline{K}_0 = [CB]^{-1} \underline{\Sigma} \quad (B-13)$$

and

$$\underline{K}_1 = \bar{\alpha} [CB]^{-1} \underline{\Sigma} \quad (B-14)$$

where

$\bar{\alpha}$ is a constant which assigns the ratio of proportional to integral control

$\underline{\Sigma}$ is the diagonal weighting matrix

The diagonal weighting matrix, $\underline{\Sigma} = \text{diag} \{ \sigma_1, \sigma_2, \dots, \sigma_\ell \}$, is specified by the designer. Each σ_i ($i=1, \dots, \ell$) determines the weighting of the effect of a particular error signal on each control input. This is the methodology used in the MULTI design program and is a simplified version of the complete Porter method. In theory, the total number of finite (slow) roots of the system is equal to:

$$Z_f = n + q\ell - \ell \quad (B-15)$$

which also equals $\underline{Z}_1 + \underline{Z}_2$ (Table B.1).

The \underline{Z}_1 roots, equal to $(q\ell)$ in number, are assigned by the relationship between the proportional and integral matrices. If the matrices differ by a simple

Proportionality constant, $\bar{\alpha}$, then all of the \underline{z}_1 roots are assigned, under conditions of infinite gain (asymptotically), to the value of $-\bar{\alpha}$ in the s-plane. By replacing $\bar{\alpha}$ with a diagonal matrix, these roots can be individually assigned as the negative value of its diagonal elements.

Irregular Plant

If the first Markov parameter $[\underline{CB}]$ is rank deficient, then the plant is called "irregular." In this case, the \underline{C} matrix must be replaced by

$$\underline{F} = [\underline{F}_1 \mid \underline{F}_2] \quad (\text{B-16})$$

where

$$\underline{F}_1 = [\underline{C}_1 + \underline{MA}_{11}] \quad (\text{B-17})$$

$$\underline{F}_2 = [\underline{C}_2 + \underline{MA}_{12}] \quad (\text{B-18})$$

The matrix \underline{M} in the above equations is a measurement matrix which is chosen such that the matrix $[\underline{FB}]$ has full rank. The designer chooses the measurement matrix so that it is as sparse as possible, thus the smallest number of additional measurements are required. Reference 18 gives an approach for selecting the measurement matrix to achieve optimal decoupling. Once \underline{M} is formed, \underline{K}_0 and \underline{K}_1 are computed by

$$\underline{K}_0 = [\underline{FB}]^{-1} \underline{\Sigma} \quad (\text{B-19})$$

$$\underline{K}_1 = \overline{\alpha}[\underline{FB}]^{-1}\underline{\Sigma} \quad (\text{B-20})$$

which are similar to Equations (B-13) and (B-14). As in the regular design case, the same conditions of \underline{Z}_1 root assignment apply here.

For irregular plants the error vector \underline{e} is defined as

$$\underline{e} = \underline{v} - \underline{w} \quad (\text{B-21})$$

where

$$\underline{w} = \underline{y} + \underline{M}\dot{\underline{x}}_1 \quad (\text{B-22})$$

For step inputs the values of the rates, $\dot{\underline{x}}_1$, become zero in the steady state because they represent kinematic variables (no \underline{B} matrix entries).

The computer program MULTI greatly reduces the time required to achieve a satisfactory design. The MULTI User's Manual (9) describes the program and its operation.

Appendix C: Actuator and Sensor Data

Introduction

This appendix contains the data provided by MCAIR for modeling the actuator and sensor dynamics for the STOL/F-15 (10), and the simplifying assumptions made in the course of the thesis. Also the data used for the sensor noise model is presented.

Actuator Models

The following linear actuator transfer functions are provided by MCAIR as models of the actuator dynamics:

Stabilator/Canard

$$\frac{(30.62)(272.9)^2}{(s + 30.62)[s^2 + 2(.502)(272.9)s + (272.9)^2]} \quad (C-1)$$

Aileron/Flaperon

$$\frac{(40.37)(322.2)^2}{(s + 40.37)[s^2 + 2(.371)(322.3)s + 322.3)^2]} \quad (C-2)$$

Rotating Vanes

$$\frac{89}{s + 89} \quad (C-3)$$

With the exception of the rotating vanes (C-3) the actuator dynamics are third order in "s." The current version of MULTI has provisions for no more than two actuator states and therefore Equations (C-1) and (C-2) must be reduced in to second order approximation of these equations. The approximations used retain the slowest root and model the complex pair as a single real root located at the natural frequency of the original poles. This results in the following second order transfer functions:

Stabilator/Canard (Approx.)

$$\frac{(30.62)(272.9)}{(s + 30.62)(s + 272.9)} \quad (C-4)$$

Aileron/Flaperon (Approx.)

$$\frac{(40.37)(322.3)}{(s + 40.37)(s + 322.3)} \quad (C-5)$$

The validity of these approximations is demonstrated by comparing the low frequency characteristics and step responses of corresponding third order transfer functions. It is apparent in Figures C.1 through C.4 that the dynamics are reasonably well modeled by second order transfer functions.

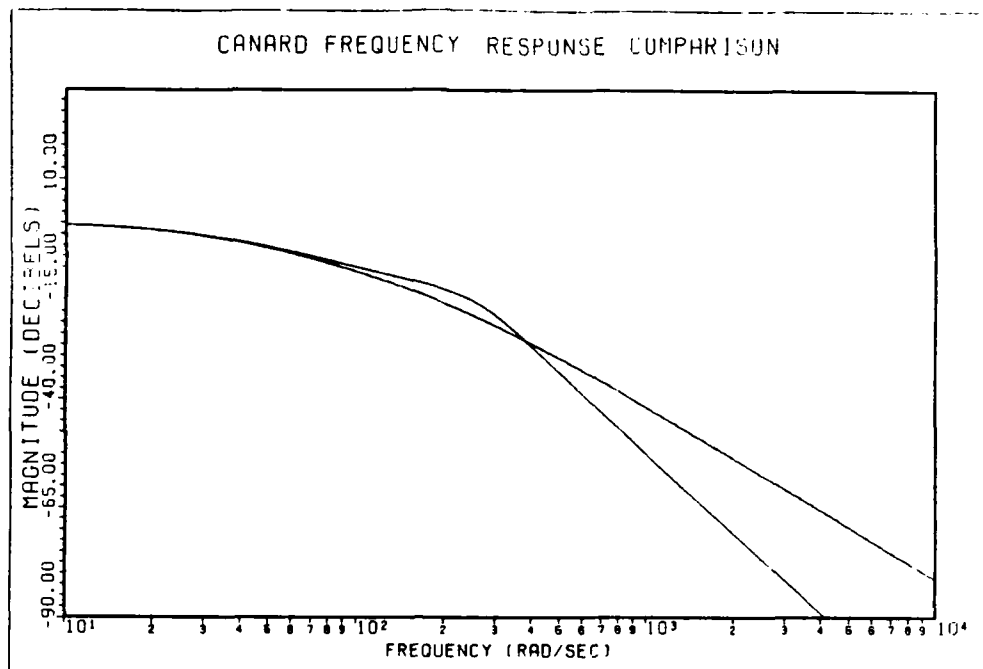


Fig. C.1. Second and Third Order Canard Actuator Frequency Response

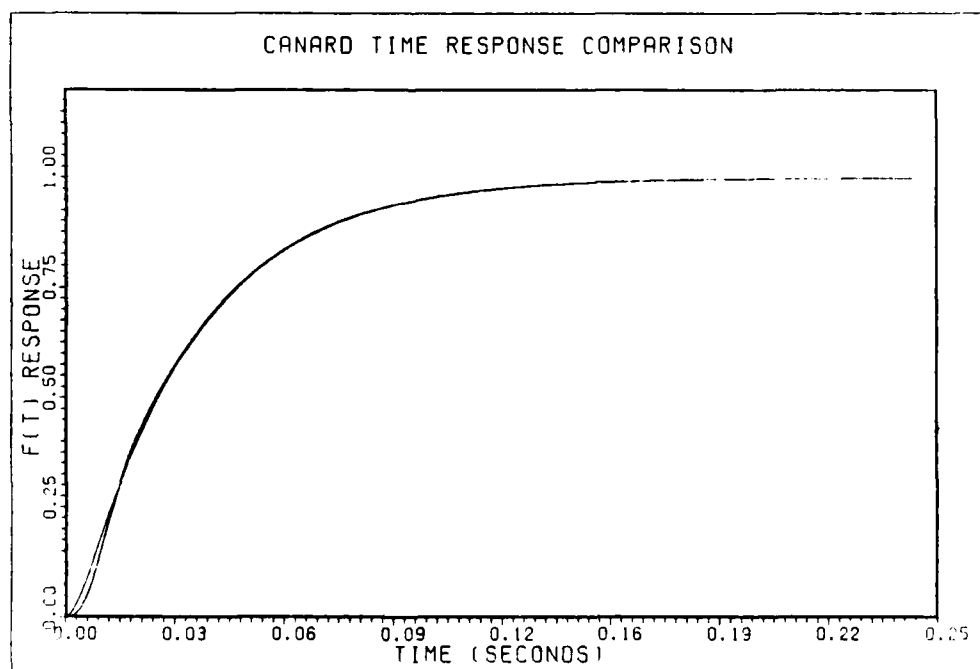


Fig. C.2. Second and Third Order Canard Actuator Step Response

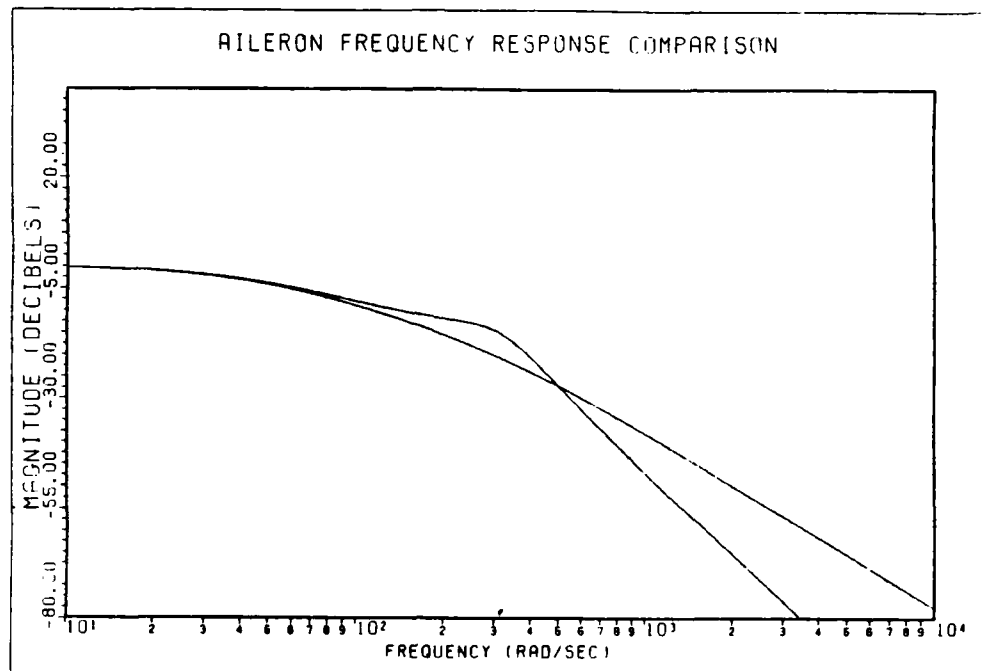


Fig. C.3. Second and Third Order Aileron Actuator Frequency Response

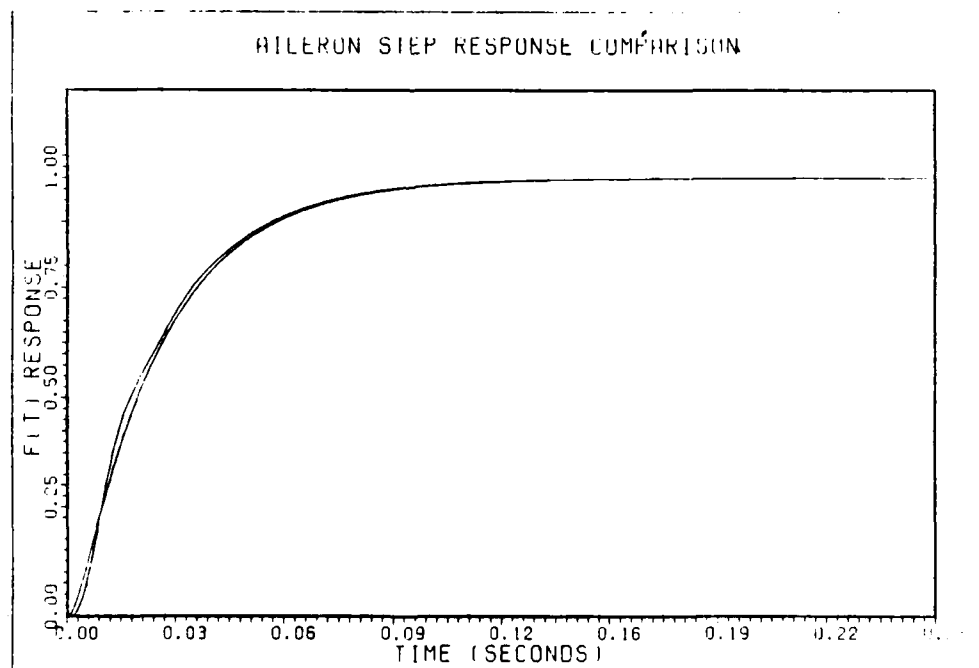


Fig. C.4. Second and Third Order Aileron Actuator Step Response

Combination of Surfaces

As discussed in Chapter III, it is necessary to combine mathematically the ailerons, flaps, and canards into one equivalent surface. The method used is to weigh the contributions of each of the surfaces (B matrix entries) according to their respective deflection limits and summing their effects to obtain a single column in the B matrix. Since the deflection limits are not symmetric about the equilibrium position, the negative limit is used for the weighting calculations. Following is an example of the calculations for flight condition 1:

	<u>B Matrix Element</u>	<u>Deflection Limit (-)</u>
Canard	$u/\delta_c = -2.45679$	-30 deg
Aileron	$u/\delta_u = 2.192$	-15 deg
Flaperon	$u/\delta_f = 1.486$	-5 deg

$$u/\delta_c = -2.45679 + (15/30)(2.192) + (5/30)(1.486) = -1.1142$$

(C-6)

This weighting is performed for each of the affected elements in the B matrix for flight condition 1. For simplicity, the same relationships are used for all of the flight conditions. The data presented in Appendix D contains the resulting B matrices for each flight condition. There is no accurate method of combining actuator dynamics since the output signals are not electrical and are physically separated. As an approximation, the slowest actuator (that

of the canard) is used for the combined canard, flap, and aileron surface.

Sensor Dynamics

The sensor dynamics provided by MCAIR include the dynamics of measurement as well as an aliasing filter.

Airspeed Sensor

$$\frac{1200}{(s + 30)(s + 40)} \quad (C-7)$$

Angle of Attack Sensor

$$\frac{(14)(209)^2}{(s + 14)[s^2 + 2(.74)(209)s + (209)^2]} \quad (C-8)$$

In MULTI, sensor dynamics are also restricted to second order transfer functions so the angle of attack sensor model is reduced by the same procedure used for the actuators. The resulting transfer function is given by Equation (C-9) and Figures C.5 and C.6 demonstrate the validity of the approximation.

Angle of Attack Sensor (Approx.)

$$\frac{(14)(209)}{(s + 14)(s + 209)} \quad (C-9)$$

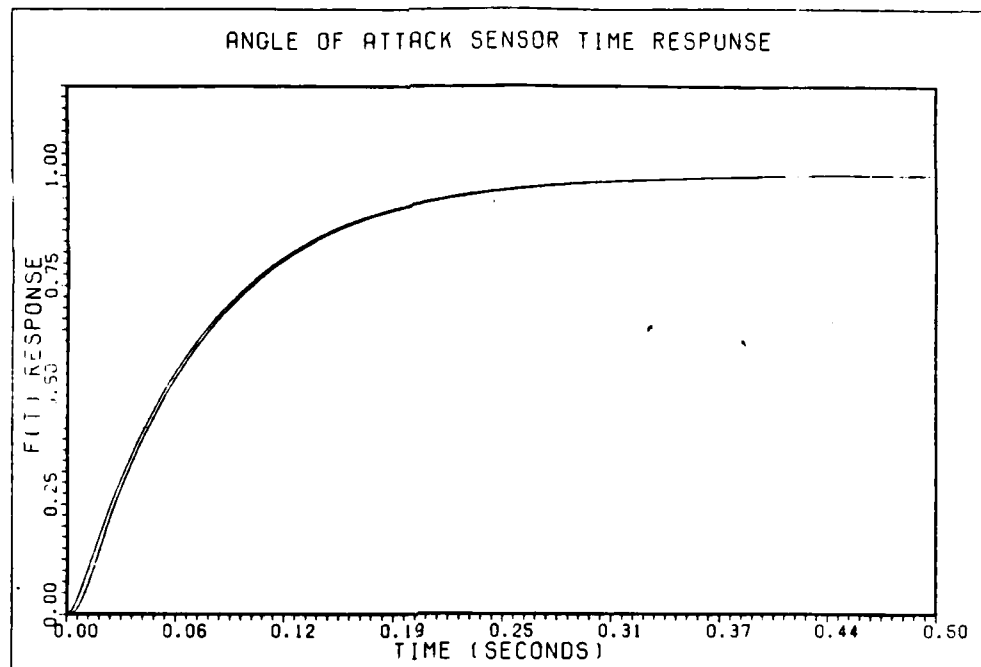


Fig. C.5. Second and Third Order Angle of Attack Sensor Step Response

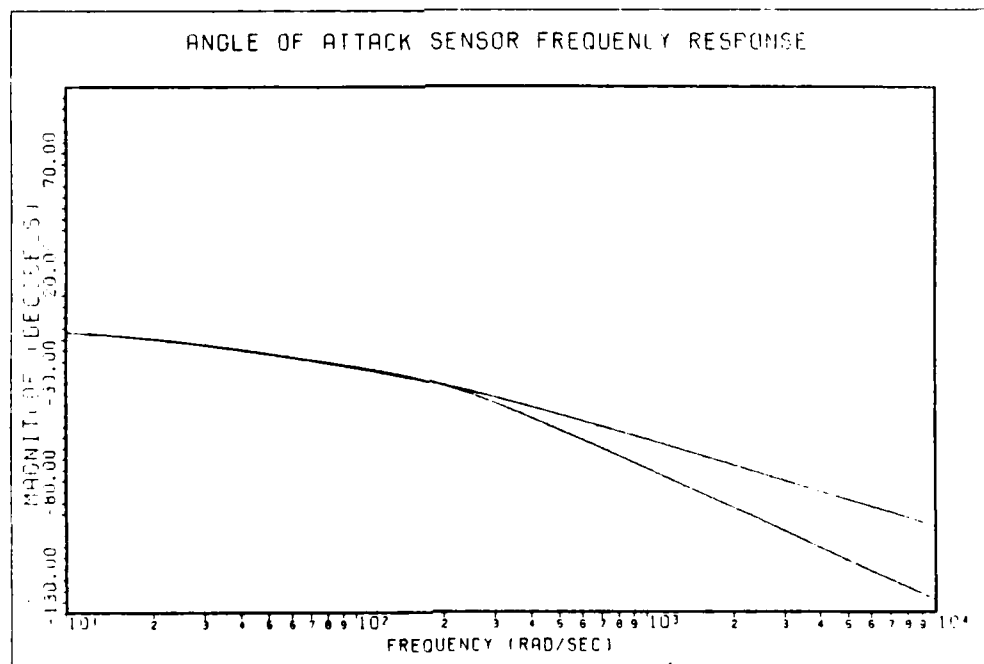


Fig. C.6. Second and Third Order Angle of Attack Sensory Frequency Response

Also, since no data is available for the flight path angle sensor dynamics, the transfer function is arbitrarily chosen to include the slowest root of the angle of attack sensor and the pitch rate sensor dynamics. The resulting transfer function is shown in Equation (C-10).

Flight Path Sensor

$$\frac{(14)(80)}{(s + 14)(s + 80)} \quad (C-10)$$

Sensor Noise

The noise associated with measuring the outputs is assumed to be zero mean, independent, white, gaussian noise injected into each of the measurement channels, including the minor loop pitch rate feedback measurement. Realistic values for the standard deviations for the various measurements are obtained from Mosley (12) and are presented in Table C.1.

TABLE C.1
REALISTIC NOISE VALUES

Measured Quantity	Standard Deviation
θ	0.476E-5
α	1.220E-5
γ	1.309E-5
q	3.220E-5

Note that the flight path angle noise is not provided and is obtained from the combined noise for pitch angle and angle of attack (square root of the sum of the squares). No noise value is provided for the velocity measurement.

Appendix D: Aircraft Data

Introduction

This appendix contains the original data obtained from MCAIR (10), a brief discussion of the conversion to linearized body axis state space form, lists the longitudinal state space models obtained for each flight condition and finally the resulting open loop transfer functions.

MCAIR Data

The following computer products (Tables D.1 through D.6) are listings of nondimensional body axis stability derivatives provided by MCAIR and the dimensional equivalent of that data. The variables are defined as follows:

$CZA = C_{z_{\alpha}}$	$CMA = C_{m_{\alpha}}$	$CXA = C_{x_{\alpha}}$
$CZQ = C_{z_q}$	$CMQ = C_{m_q}$	$CXQ = C_{x_q}$
$CZH = C_{z_h}$	$CMH = C_{m_h}$	$CXH = C_{x_h}$
$CZDn = C_{z_{\delta_n}}$	$CMDn = C_{m_{\delta_n}}$	$CXDn = C_{x_{\delta_n}}$
$ZA = Z_{\alpha}$	$MA = M_{\alpha}$	$XA = X_{\alpha}$
$ZQ = Q_q$	$MQ = M_q$	$XQ = X_q$
$ZH = Z_h$	$MH = M_h$	$XH = X_h$
$ZDn = Z_{\delta_n}$	$MDn = M_{\delta_n}$	$XDn = X_{\delta_n}$

TABLE D.1
FLIGHT CONDITION 1 AERO DATA

AIRCRAFT PARAMETERS

Q (DYNAMIC PRESSURE - LBS/FT**2) = 48.0600
S (WING REFERENCE AREA - FT**2) = 608.000
C (WING MEAN AERODYNAMIC CORD - FT) = 15.9399
B (WING SPAN - FT) = 42.7000
VT (TRIM VELOCITY - FT/SEC) = 200.000
THETA = 11.5840
W (WEIGHT - LBS) = 33576.0
IXX (SLUG-FT**2) = 23634.0
IYY (SLUG-FT**2) = 181837.
IZZ (SLUG-FT**2) = 199674.
IXZ (SLUG-FT**2) = -3086.00

ALPHA = 11.5840

LONGITUDINAL NON-DIM BODY AXIS COEFFICIENTS(1/DEG)

CZA = -.796233E-01	CMA = .931356E-02	CXA = .208763E-03
CZQ = 0.	CMQ = -.169490	CXQ = 0.
CZH = -.181866E-04	CMH = -.388591E-04	CXH = .681123E-03
CZU = .658418E-02	CMU = -.140683E-01	CXU = -.246580
CZD1 = -.257164E-02	CMD1 = .572880E-02	CXD1 = -.153014E-02
CZD2 = -.955232E-02	CMD2 = -.107546E-01	CXD2 = -.201656E-02
CZD3 = -.488427E-02	CMD3 = .112899E-02	CXD3 = .136541E-02
CZD4 = -.451559E-02	CMD4 = -.214211E-02	CXD4 = .925632E-03
CZD5 = .135028E-02	CMD5 = .129075E-02	CXD5 = -.340353E-02
CZD6 = -.135028E-02	CMD6 = -.137616E-02	CXD6 = -.340353E-02
CZD7 = .135028E-02	CMD7 = .129075E-02	CXD7 = -.340353E-02
CZD8 = -.135028E-02	CMD8 = -.137616E-02	CXD8 = -.340353E-02

LONGITUDINAL AXIS DIMENSIONAL DERIVATIVES

BODY AXIS (1/RAD)

ZA = -127.843	MA = 1.36688	XA = .335190
ZQ = 0.	MQ = -.991250	XQ = 0.
ZH = -.254821E-05	MH = -.497684E-06	XH = .954355E-04
ZU = .184508E-02	MU = -.360356E-03	XU = -.690991E-01
ZD1 = -4.12902	MD1 = .840770	XD1 = -2.45679
ZD2 = -15.3372	MD2 = -1.57837	XD2 = -3.23779
ZD3 = -7.84218	MD3 = .165693	XD3 = 2.19230
ZD4 = -7.25022	MD4 = -.314380	XD4 = 1.48619
ZD5 = 2.16801	MD5 = .189433	XD5 = -5.46470
ZD6 = -2.16801	MD6 = -.201968	XD6 = -5.46470
ZD7 = 2.16801	MD7 = .189433	XD7 = -5.46470
ZD8 = -2.16801	MD8 = -.201968	XD8 = -5.46470

TABLE D.2
FLIGHT CONDITION 2 AERO DATA

AIRCRAFT PARAMETERS

Q (DYNAMIC PRESSURE - LBS/FT**2) = 39.6400
S (WING REFERENCE AREA - FT**2) = 808.000
C (WING MEAN AERODYNAMIC CHORD - FT) = 15.9400
B (WING SPAN - FT) = 42.7000
VT (TRIM VELOCITY - FT/SEC) = 168.000
THETA = 17.3952
W (WEIGHT - LBS) = 33576.0
IXX (SLUG-FT**2) = 23644.0
IYY (SLUG-FT**2) = 181847.
IZZ (SLUG-FT**2) = 199674.
IXZ (SLUG-FT**2) = -3086.00

LONGITUDINAL NON-DIM BODY AXIS COEFFICIENTS (1/DEG)

CZA = -.866000E-01	CMA = .845000E-02	CXA = .168000E-01
CZD = 0.	CMD = -.177000	CXD = 0.
CZH = -.211000E-03	CMH = .200000E-03	CXH = .105000E-02
CZU = -1.47000	CMU = .864000E-01	CXU = .438000E-01
CZD1 = -.408000E-02	CMD1 = .615000E-02	CXD1 = -.131000E-02
CZD2 = -.114000E-01	CMD2 = -.114000E-01	CXD2 = .159700E-03
CZD3 = -.561000E-02	CMD3 = .431000E-03	CXD3 = .176000E-02
CZD4 = -.409000E-02	CMD4 = -.142000E-02	CXD4 = .128000E-02
CZD5 = .290000E-02	CMD5 = .204000E-02	CXD5 = -.420000E-02
CZD6 = -.157000E-02	CMD6 = -.242000E-02	CXD6 = -.488000E-02
CZD7 = .290000E-02	CMD7 = .204000E-02	CXD7 = -.420000E-02
CZD8 = -.157000E-02	CMD8 = -.242000E-02	CXD8 = -.488000E-02

LONGITUDINAL AXIS DIMENSIONAL DERIVATIVES
BODY AXIS (1/RAD)

ZA = -88.1985	MA = 1.02025	XA = 22.2483
ZD = 0.	MU = -1.01130	XU = 0.
ZH = -.290294E-04	MH = .250870E-05	XH = .141707E-03
ZU = -.404485	MU = .216752E-02	XU = .120520E-01
ZD1 = -5.40315	MD1 = .742550	XD1 = -1.73483
ZD2 = -15.0970	MD2 = -1.37643	XD2 = .211491
ZD3 = -7.42933	MD3 = .520389E-01	XD3 = 2.33077
ZD4 = -5.41639	MD4 = -.171451	XD4 = 1.69511
ZD5 = 3.84047	MD5 = .485641	XD5 = -5.56207
ZD6 = -2.07915	MD6 = -.292191	XD6 = -6.46259
ZD7 = 3.84047	MD7 = .485641	XD7 = -5.56207
ZD8 = -2.07915	MD8 = -.292191	XD8 = -6.46259

TABLE D.3
FLIGHT CONDITION 3 AERO DATA

AIRCRAFT PARAMETERS

Q (DYNAMIC PRESSURE - LBS/FT**2) = 48.8700
S (WING REFERENCE AREA - FT**2) = 608.000
C (WING MEAN AERODYNAMIC CORD - FT) = 15.9390
B (WING SPAN - FT) = 42.7000
VT (TRIM VELOCITY - FT/SEC) = 201.100
THETA = 15.4400
W (WEIGHT - LBS) = 43511.0
IXX (SLUG-FT**2) = 35215.0
IYY (SLUG-FT**2) = 190800.
IZZ (SLUG-FT**2) = 219105.
IXZ (SLUG-FT**2) = -2881.00

LONGITUDINAL NON-DIM BODY AXIS COEFFICIENTS(1/DEG)

CZA = -.784900E-01	CMA = .957400E-02	CXA = .150900E-02
CZQ = 0.	CMQ = -.169000	CXQ = 0.
CZH = -.167600E-03	CMH = .176600E-03	CXH = .666200E-03
CZU = -1.06500	CMU = .639400E-01	CXU = -.619300E-02
CZD1 = -.263600E-02	CMD1 = .557600E-02	CXD1 = -.155200E-02
CZD2 = -.831500E-02	CMD2 = -.102000E-01	CXD2 = -.274900E-03
CZD3 = -.559100E-02	CMD3 = .852100E-03	CXD3 = .115700E-02
CZD4 = -.450800E-02	CMD4 = -.211100E-02	CXD4 = .942100E-03
CZD5 = .189600E-02	CMD5 = .255400E-02	CXD5 = -.312000E-02
CZD6 = -.742200E-03	CMD6 = -.130100E-02	CXD6 = -.359500E-02
CZD7 = .189600E-02	CMD7 = .255400E-02	CXD7 = -.312000E-02
CZD8 = -.742200E-03	CMD8 = -.130100E-02	CXD8 = -.359500E-02

LONGITUDINAL AXIS DIMENSIONAL DERIVATIVES

BODY AXIS (1/RAD)

ZA = -98.8871	MA = 1.36158	XA = 1.90114
ZQ = 0.	MQ = -.952482	XQ = 0.
ZH = -.183259E-04	MH = .217975E-05	XH = .728443E-04
ZU = -.232900	MU = .157841E-02	XU = -.135432E-02
ZD1 = -3.32101	MD1 = .793002	XD1 = -1.95532
ZD2 = -10.4758	MD2 = -1.45061	XD2 = -.346338
ZD3 = -7.04393	MD3 = .121183	XD3 = 1.45767
ZD4 = -5.67949	MD4 = -.300220	XD4 = 1.18692
ZD5 = 2.38871	MD5 = .363222	XD5 = -3.93079
ZD6 = -.935075	MD6 = -.185024	XD6 = -4.52923
ZD7 = 2.38871	MD7 = .363222	XD7 = -3.93079
ZD8 = -.935075	MD8 = -.185024	XD8 = -4.52923

TABLE D.4

FLIGHT CONDITION 4 AERO DATA

AIRCRAFT PARAMETERS

Q (DYNAMIC PRESSURE - LBS/FT**2) = 109.970
 S (WING REFERENCE AREA - FT**2) = 608.000
 C (WING MEAN AERODYNAMIC CORD - FT) = 15.9390
 B (WING SPAN - FT) = 42.7000
 VT (TRIM VELOCITY - FT/SEC) = 304.000
 THETA = 5.04000
 W (WEIGHT - LBS) = 43511.0
 IXX (SLUG-FT**2) = 35215.0
 IYY (SLUG-FT**2) = 190800.
 IZZ (SLUG-FT**2) = 219105.
 Ixz (SLUG-FT**2) = -2881.00

LONGITUDINAL NON-DIM BODY AXIS COEFFICIENTS(1/DEG)

CZA = -.690500E-01	CMA = .733300E-02	CXA = .854200E-02
CZQ = 0.	CMQ = -.157000	CXQ = 0.
CZH = -.106400E-03	CMH = .149500E-03	CXH = .290600E-03
CZU = -.477000	CMU = .358200E-01	CXU = -.354400E-01
CZD1 = -.234500E-02	CMD1 = .562100E-02	CXD1 = -.692400E-03
CZD2 = -.792100E-02	CMD2 = -.887400E-02	CXD2 = -.434000E-04
CZD3 = -.546300E-02	CMD3 = .698900E-03	CXD3 = .305800E-03
CZD4 = -.482800E-02	CMD4 = -.258900E-02	CXD4 = .328300E-03
CZD5 = .824600E-03	CMD5 = .112400E-02	CXD5 = -.148600E-02
CZD6 = -.174800E-03	CMD6 = -.409300E-03	CXD6 = -.170000E-02
CZD7 = .824600E-03	CMD7 = .112400E-02	CXD7 = -.148600E-02
CZD8 = -.174800E-03	CMD8 = -.409300E-03	CXD8 = -.170000E-02

LONGITUDINAL AXIS DIMENSIONAL DERIVATIVES

BODY AXIS (1/RAD)

ZA = -195.759	MA = 2.34674	XA = 24.2168
ZQ = 0.	MQ = -1.31717	XQ = 0.
ZH = -.173182E-04	MH = .274681E-05	XH = .472995E-04
ZU = -.155278	MU = .131626E-02	XU = -.115368E-01
ZD1 = -6.64814	MD1 = 1.79886	XD1 = -1.96297
ZD2 = -22.4563	MD2 = -2.83990	XD2 = -.123040
ZD3 = -15.4878	MD3 = .223665	XD3 = .866951
ZD4 = -13.6875	MD4 = -.828543	XD4 = .930739
ZD5 = 2.33776	MD5 = .359707	XD5 = -4.21285
ZD6 = -.495563	MD6 = -.130986	XD6 = -4.81955
ZD7 = 2.33776	MD7 = .359707	XD7 = -4.21285
ZD8 = -.495563	MD8 = -.130986	XD8 = -4.81955

TABLE D.5
FLIGHT CONDITION 5 AERO DATA

AIRCRAFT PARAMETERS

Q (DYNAMIC PRESSURE - LBS/FT**2) = 81.1400
S (WING REFERENCE AREA - FT**2) = 608.000
C (WING MEAN AERODYNAMIC CORD - FT) = 15.9390
B (WING SPAN - FT) = 42.7000
VT (TRIM VELOCITY - FT/SEC) = 304.000
THETA = 8.07600
W (WEIGHT - LBS) = 43511.0
IXX (SLUG-FT**2) = 35215.0
IYY (SLUG-FT**2) = 190800.
IZZ (SLUG-FT**2) = 219105.
IXZ (SLUG-FT**2) = -2881.00

LONGITUDINAL NON-DIM BODY AXIS COEFFICIENTS(1/DEG)

CZA = -.740500E-01	CMA = .859500E-02	CXA = .828500E-02
CZQ = 0.	CMQ = -.162000	CXQ = 0.
CZH = -.946800E-04	CMH = .162800E-03	CXH = .386600E-03
CZU = -.657000	CMU = .363200E-01	CXU = -.122200E-01
CZD1 = -.199400E-02	CMD1 = .586000E-02	CXD1 = -.108900E-02
CZD2 = -.870000E-02	CMD2 = -.955500E-02	CXD2 = -.452800E-03
CZD3 = -.525200E-02	CMD3 = .773900E-03	CXD3 = .554600E-03
CZD4 = -.464600E-02	CMD4 = -.262200E-02	CXD4 = .507400E-03
CZD5 = .900700E-03	CMD5 = .122300E-02	CXD5 = -.157800E-02
CZD6 = -.257300E-03	CMD6 = -.518700E-03	CXD6 = -.180700E-02
CZD7 = .900700E-03	CMD7 = .122300E-02	CXD7 = -.157800E-02
CZD8 = -.257300E-03	CMD8 = -.518700E-03	CXD8 = -.180700E-02

LONGITUDINAL AXIS DIMENSIONAL DERIVATIVES
BODY AXIS (1/RAD)

ZA = -154.897	MA = 2.02950	XA = 17.3305
ZQ = 0.	MQ = -1.00280	XQ = 0.
ZH = -.113705E-04	MH = .220700E-05	XH = .464284E-04
ZU = -.157804	MU = .984744E-03	XU = -.293510E-02
ZD1 = -4.17103	MD1 = 1.38370	XD1 = -2.27796
ZD2 = -18.1986	MD2 = -2.25618	XD2 = -.947162
ZD3 = -10.9861	MD3 = .182738	XD3 = 1.16011
ZD4 = -9.71845	MD4 = -.619123	XD4 = 1.06137
ZD5 = 1.88407	MD5 = .288782	XD5 = -3.30084
ZD6 = -.538217	MD6 = -.122479	XD6 = -3.77986
ZD7 = 1.88407	MD7 = .288782	XD7 = -3.30084
ZD8 = -.538217	MD8 = -.122479	XD8 = -3.77986

TABLE D.6
FLIGHT CONDITION 6 AERO DATA

AIRCRAFT PARAMETERS

Q (DYNAMIC PRESSURE - LBS/FT**2) = 81.1400
S (WING REFERENCE AREA - FT**2) = 608.000
C (WING MEAN AERODYNAMIC CORD - FT) = 15.9390
B (WING SPAN - FT) = 42.7000
VT (TRIM VELOCITY - FT/SEC) = 304.000
THETA = 6.23200
W (WEIGHT - LBS) = 33576.0
IXX (SLUG-FT**2) = 23644.0
IYY (SLUG-FT**2) = 181847.
IZZ (SLUG-FT**2) = 199674.
IXZ (SLUG-FT**2) = -3086.00

LONGITUDINAL NON-DIM BODY AXIS COEFFICIENTS(1/DEG)

CZA = -.740500E-01	CMA = .859500E-02	CXA = .828500E-02
CZQ = 0.	CMQ = -.162000	CXQ = 0.
CZH = -.946800E-04	CMH = .162800E-03	CXH = .386600E-03
CZU = -.657000	CMU = .363200E-01	CXU = -.122200E-01
CZD1 = -.199400E-02	CMD1 = .586000E-02	CXD1 = -.108900E-02
CZD2 = -.870000E-02	CMD2 = -.955500E-02	CXD2 = -.452800E-03
CZD3 = -.525200E-02	CMD3 = .773900E-03	CXD3 = .554600E-03
CZD4 = -.464600E-02	CMD4 = -.262200E-02	CXD4 = .507400E-03
CZD5 = .900700E-03	CMD5 = .122300E-02	CXD5 = -.157800E-02
CZD6 = -.257300E-03	CMD6 = -.518700E-03	CXD6 = -.180700E-02
CZD7 = .900700E-03	CMD7 = .122300E-02	CXD7 = -.157800E-02
CZD8 = -.257300E-03	CMD8 = -.518700E-03	CXD8 = -.180700E-02

LONGITUDINAL AXIS DIMENSIONAL DERIVATIVES

BODY AXIS (1/RAD)

ZA = -200.730	MA = 2.12942	XA = 22.4585
ZQ = 0.	MQ = -1.05218	XQ = 0.
ZH = -.147350E-04	MH = .231566E-05	XH = .601664E-04
ZU = -.204497	MU = .103323E-02	XU = -.380358E-02
ZD1 = -5.40522	MD1 = 1.45182	XD1 = -2.95200
ZD2 = -23.5835	MD2 = -2.36726	XD2 = -1.22742
ZD3 = -14.2368	MD3 = .191735	XD3 = 1.50338
ZD4 = -12.5941	MD4 = -.649604	XD4 = 1.37543
ZD5 = 2.44157	MD5 = .303000	XD5 = -4.27755
ZD6 = -.697474	MD6 = -.128509	XD6 = -4.89831
ZD7 = 2.44157	MD7 = .303000	XD7 = -4.27755
ZD8 = -.697474	MD8 = -.128509	XD8 = -4.89831

where n is an integer corresponding to a particular control surface as defined below:

- 1 = Canard
- 2 = Stabilator
- 3 = Trailing edge flaps
- 4 = Ailerons
- 5 = Right top vane
- 6 = Right bottom vane
- 7 = Left top vane
- 8 = Left bottom vane

State Space Models

The nondimensional body axis stability derivatives are converted to dimensional state space form first by calculating the dimensional derivatives and then the state space elements by the equations contained in References 2 and 10. These calculations are performed by the Program STOLCAT, an adaptation of the Conversion and Transformation (CAT) program written by Finley Barfield (2). The resulting state space models are contained in Tables D.7 through D.12.

Open Loop Transfer Functions

The open loop LaPlace transfer functions for the state models at each flight condition are listed in Tables D.13 through D.18.

TABLE D.7
FLIGHT CONDITION 1 STATE MODEL

<u>A (Plant Matrix)</u>			
0	0	1	0
-31.55	-.06909	-40.161	.33519
0	-3.603E-4	-.9913	1.3668
-3.233E-2	9.225E-6	.97963	-.6392

<u>B (Input Matrix)</u>		
0	0	0
-1.1142	-3.238	-21.79
.81	-1.57837	-.02507
-.0521	-.0766	0

<u>C (Output Matrix)</u>			
0	1	0	0
0	0	0	1
1	0	0	-1

$$\mathbf{x} = \begin{bmatrix} \theta \\ u \\ q \\ \alpha \end{bmatrix} \quad \mathbf{y} = \begin{bmatrix} u \\ \alpha \\ \gamma \end{bmatrix} \quad \mathbf{u} = \begin{bmatrix} \delta_C \\ \delta_S \\ \delta_T \end{bmatrix}$$

TABLE D.8
FLIGHT CONDITION 2 STATE MODEL

<u>A (Plant Matrix)</u>			
0	0	1	0
-30.72	.0120	-50.22	22.20
0	2.160E-3	-1.011	1.020
-5.730E-2	-2.410E-3	.9540	-.5249

<u>B (Input Matrix)</u>		
0	0	0
-.2829	.21149	-24.049
.7399	-1.376	.3430
-.0596	-.0898	.0210

<u>C (Output Matrix)</u>			
0	1	0	0
0	0	0	1
1	0	0	-1

$$\mathbf{x} = \begin{bmatrix} \theta \\ u \\ q \\ \alpha \end{bmatrix} \quad \mathbf{y} = \begin{bmatrix} u \\ \alpha \\ \gamma \end{bmatrix} \quad \mathbf{u} = \begin{bmatrix} \delta_C \\ \delta_S \\ \delta_T \end{bmatrix}$$

TABLE D.9
FLIGHT CONDITION 3 STATE MODEL

<u>A (Plant Matrix)</u>			
0	0	0	0
-31.038	-1.354E-3	-53.53	1.9011
0	1.578E-3	-9.524	1.3615
-4.263E-2	-1.158E-3	.9639	-1.492

<u>B (Input Matrix)</u>		
0	0	0
-1.208	-.3463	-16.92
.803	-1.4506	.356
-.03868	-.05208	.0144

<u>C (Output Matrix)</u>			
0	1	0	0
0	0	0	1
1	0	0	-1

$$x = \begin{bmatrix} \theta \\ u \\ q \\ \alpha \end{bmatrix} \quad y = \begin{bmatrix} u \\ \alpha \\ \gamma \end{bmatrix} \quad u = \begin{bmatrix} \delta_C \\ \delta_S \\ \delta_T \end{bmatrix}$$

TABLE D.10
FLIGHT CONDITION 4 STATE MODEL

<u>A (Plant Matrix)</u>			
0	0	1	0
-32.07	-.0115	-26.70	24.21
0	-1.31E-2	-1.317	2.347
-9.305E-2	-5.107E-4	.9961	-.6439

<u>B (Input Matrix)</u>		
0	0	0
-1.517	-.123	-18.06
1.773	-2.839	.4562
-.0672	-.07386	.01212

<u>C (Output Matrix)</u>			
0	1	0	0
0	0	0	1
1	0	0	-1

$$\mathbf{x} = \begin{bmatrix} \theta \\ u \\ q \\ \alpha \end{bmatrix} \quad \mathbf{y} = \begin{bmatrix} u \\ \alpha \\ \gamma \end{bmatrix} \quad \mathbf{u} = \begin{bmatrix} \delta_C \\ \delta_S \\ \delta_T \end{bmatrix}$$

TABLE D.11
FLIGHT CONDITION 5 STATE MODEL

<u>A (Plant Matrix)</u>			
0	0	1	0
-31.88	-2.930E-3	-42.71	17.33
0	9.847E-4	-1.003	2.029
-.01488	-5.191E-4	.9901	-.50953

<u>B (Input Matrix)</u>		
0	0	0
-1.52	-.9471	-14.16
1.51	-2.256	-.3300
-.0323	-.0597	8.84E-3

<u>C (Output Matrix)</u>			
0	1	0	0
0	0	0	1
1	0	0	-1

$$\mathbf{x} = \begin{bmatrix} \theta \\ u \\ q \\ \alpha \end{bmatrix} \quad \mathbf{y} = \begin{bmatrix} u \\ \alpha \\ \gamma \end{bmatrix} \quad \mathbf{u} = \begin{bmatrix} \delta_C \\ \delta_S \\ \delta_T \end{bmatrix}$$

TABLE D.12
FLIGHT CONDITION 6 STATE MODEL

<u>A (Plant Matrix)</u>			
0	0	1	0
-30.88	1.007E-2	-56.56	21.01
0	1.167E-3	-.7558	.7577
-4.533E-2	-1.465E-3	.9591	-.3034

<u>B (Input Matrix)</u>		
0	0	0
-1.482	-.4642	-15.35
.6499	-1.227	0
-.0245	-.0679	9.863E-3

<u>C (Output Matrix)</u>			
0	1	0	0
0	0	0	1
1	0	0	-1

$$\mathbf{x} = \begin{bmatrix} \theta \\ u \\ q \\ \alpha \end{bmatrix} \quad \mathbf{y} = \begin{bmatrix} u \\ \alpha \\ \gamma \end{bmatrix} \quad \mathbf{u} = \begin{bmatrix} \delta_C \\ \delta_S \\ \delta_T \end{bmatrix}$$

TABLE D.13
FLIGHT CONDITION 1 TRANSFER FUNCTIONS

$$CE = (s + 1.998)(s - .3468)(s + .02428 \pm .0715j)$$

$$u/\delta_C = -1.11(s + 31.76)(s + .6421 \pm .1493j) / C.E.$$

$$u/\delta_S = -.052(s - 15.35)(s - .038)(s + .0657) / C.E.$$

$$u/\delta_T = .052(s + .6661 \pm 3.068j)(s + .0690) / C.E.$$

$$\alpha/\delta_C = -3.24(s - 19.49)(s + .9976)(s + .556) / C.E.$$

$$\alpha/\delta_S = -.0766(s + 21.21)(s - .0394)(s + .0754) / C.E.$$

$$\alpha/\delta_T = -.0766(s - 3.627)(s + 4.198)(s + .0695) / C. E.$$

$$\gamma/\delta_C = -21.79(s - .366)(s - .0289)(s + 1.979) / C.E.$$

$$\gamma/\delta_S = -.0247(s - .2343)(s - .0328) / C.E.$$

$$\gamma/\delta_T = -.000309(s + 53.59)(s - .2307) / C.E.$$

TABLE D.14
FLIGHT CONDITION 2 TRANSFER FUNCTIONS

$$C.E. = (s - .2865)(s + 1.728)(s + .04099 \pm .2763j)$$

$$u/\delta_C = -.2829(s + 136.9)(s + .3181 \pm .4282j) / C.E.$$

$$u/\delta_S = -.0596(s - 10.91)(s + .0290 \pm .2795j) / C.E.$$

$$u/\delta_T = .0596(s - .0625)(s + .8106 \pm 2.056j) / C.E.$$

$$\alpha/\delta_C = .2115(s + 318.2)(s + .3051 \pm .4996j) / C.E.$$

$$\alpha/\delta_S = -.0898(s + 15.57)(s + .02635 \pm .2777j) / C.E.$$

$$\alpha/\delta_T = .0898(s + 3.005)(s - 2.648)(s - .0565) / C.E.$$

$$\gamma/\delta_C = -.74.05(s + 2.256)(s - .0118 \pm .3845j) / C.E.$$

$$\gamma/\delta_S = .0210(s + 19.27)(s + .0339 \pm .2701j) / C.E.$$

$$\gamma/\delta_T = -.0210(s + 4.26)(s - 1.402)(s + .1499) / C.E.$$

TABLE D.15

FLIGHT CONDITION 3 TRANSFER FUNCTIONS

$$C.E. = (s - .04311 \pm .2615j)(s + 2.387)(s + .1451)$$

$$u/\delta_C = -1.028(s + 42.4)(s + 1.30)(s + .629) / C.E.$$

$$u/\delta_S = -.0386(s - 19.11)(s - .00964 \pm .1909j) / C.E.$$

$$u/\delta_T = .0386(s - .0217)(s + .8471 \pm 5.346j) / C.E.$$

$$\alpha/\delta_C = -.3463(s - 223.6)(s + 1.494)(s + .6005) / C.E.$$

$$\alpha/\delta_S = -.0521(s + 27.77)(s + .01128 \pm .1939j) / C.E.$$

$$\alpha/\delta_T = .0521(s - 6.522)(s - .02176)(s + 6.485) / C.E.$$

$$\gamma/\delta_C = -16.92(s + 2.832)(s + .3682 \pm 4921j) / C.E.$$

$$\gamma/\delta_S = .0144(s + 26.14)(s + .00127 \pm .1971j) / C.E.$$

$$\gamma/\delta_T = -.0144(s - 5.329)(s - .0502)(s + 6.801) / C.E.$$

TABLE D.16
FLIGHT CONDITION 4 TRANSFER FUNCTIONS

$$C.E. = (s + 2.561)(s - .3744)(s - .1794)(s - .0344)$$

$$u/\delta_C = -1.517(s + 33.47)(s + .3859 \pm .7469j) / C.E.$$

$$u/\delta_S = -.0672(s - 24.89)(s - .0370 \pm .1152j) / C.E.$$

$$u/\delta_T = .0672(s + .00634)(s + .7068 \pm 4.033j) / C.E.$$

$$\alpha/\delta_C = -.1230(s - 600.8)(s + .5005 \pm .8392j) / C.E.$$

$$\alpha/\delta_S = -.0738(s + 39.68)(s - .0324 \pm .1218j) / C.E.$$

$$\alpha/\delta_T = .0738(s + 6.104)(s - 4.933)(s + .00624) / C.E.$$

$$\gamma/\delta_C = -18.06(s + 2.992)(s - .1867 \pm .4983j) / C.E.$$

$$\gamma/\delta_S = .01212(s + 39.67)(s - .0437 \pm .1351j) / C.E.$$

$$\gamma/\delta_T = -.01212(s - 4.467)(s + 6.391)(s + .0186) / C.E.$$

AD-A164 516

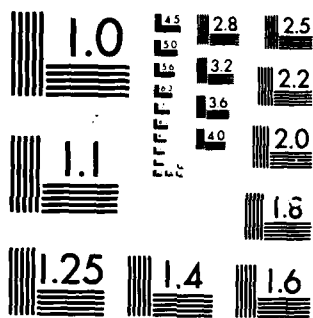
MULTIVARIABLE OUTPUT CONTROL LAW DESIGN FOR THE STOL
(SHORT TAKEOFF AND L. (U) AIR FORCE INST OF TECH
WRIGHT-PATTERSON AFB OH SCHOOL OF ENGI.. B H ACKER
DEC 85 AFIT/GE/ENG/85D-1 F/G 1/2

4/4

UNCLASSIFIED

NL

END
3-16



MICROCOPY RESOLUTION TEST CHART
 NATIONAL BUREAU OF STANDARDS-1963-A

TABLE D.17
FLIGHT CONDITION 5 TRANSFER FUNCTIONS

$$C.E. = (s + 2.183)(s - .663)(s - .00264 \pm .1092j)$$

$$u/\delta_C = -1.52(s + 43.55)(s + .3781 \pm .4502j) / C.E.$$

$$u/\delta_S = -.0323(s - 45.31)(s + .004705 \pm .1278j) / C.E.$$

$$u/\delta_T = .0323(s - .0115)(s + .7282 \pm 4.578j) / C.E.$$

$$\alpha/\delta_C = -.947(s - 100.1)(s + .4659 \pm .4652j) / C.E.$$

$$\alpha/\delta_S = -.0598(s + 38.3)(s + .005473 \pm .1305j) / C.E.$$

$$\alpha/\delta_T = .0598(s - 4.267)(s - .01165)(s + 4.902) / C.E.$$

$$\gamma/\delta_C = -14.16(s - 1.360)(s + 1.732)(s + .1333) / C.E.$$

$$\gamma/\delta_S = .00884(s - 35.15)(s + .01535 \pm .1254j) / C.E.$$

$$\gamma/\delta_T = -.00884(s - .06065)(s + 1.134 \pm 4.058j) / C.E.$$

TABLE D.18
FLIGHT CONDITION 6 TRANSFER FUNCTION

$$C.E. = (s + 1.413)(s - .2945)(s + .01514 \pm .2130j)$$

$$u/\delta_C = -1.482(s + 25.78)(s + .2643 \pm .3803j) / C.E.$$

$$u/\delta_S = -.0245(s - 24.81)(s + .0146 \pm .2176j) / C.E.$$

$$u/\delta_T = .0245(s - .0498)(s + .8948 \pm 2.866j) / C.E.$$

$$\alpha/\delta_C = -.4642(s - 145.9)(s + .3198 \pm .4050j) / C.E.$$

$$\alpha/\delta_S = -.0680(s + 18.01)(s + .01417 \pm .2181j) / C.E.$$

$$\alpha/\delta_T = .0680(s - 2.678)(s - .0510)(s + 2.727) / C.E.$$

$$\gamma/\delta_C = -15.35(s + 1.449)(s - .1515 \pm .1061j) / C.E.$$

$$\gamma/\delta_S = .00986(s + 3.027)(s - .000118 \pm .1982j) / C.E.$$

$$\gamma/\delta_T = -.00986(s - .3757)(s + 2.42)(s + .982) / C.E.$$

Bibliography

1. Abbott, I., and Von Doenhoff, A. Theory of Wing Sections. New York: Dover Publications, Inc., 1959.
2. Barfield, A. Multivariable Control Law Development for the AFTI-F-16. MS thesis, AFIT/GE/EE-84S-4. School of Engineering, Air Force Institute of Technology (AU), Wright-Patterson AFB OH, December 1982.
3. Blakelock, J. Automatic Control of Aircraft and Missiles. New York: John Wiley and Sons, Inc., 1965.
4. "British Harriers Average Six Sorties per Day," Aviation Week and Space Technology, 117 (3): 20 (Jul 19, 1982).
5. Courtheyn, Maj T. Multivariable Control Law Design for the X-29 Aircraft. MS thesis, AFIT/GE/EE/84D-21. School of Engineering, Air Force Institute of Technology (AU), Wright-Patterson AFB OH, December 1984.
6. D'Azzo, J. and C. Houpis. Linear Control Systems Analysis and Design (Second Edition). New York: McGraw-Hill, 1981.
7. Etkin, B. Dynamics of Atmospheric Flight. New York: John Wiley and Sons, Inc., 1972.
8. Masi, A. and D. Russ. Multi User's Manual. AFWAL-TM-83-182-FIGL. Air Force Flight Dynamics Laboratory, Wright-Patterson AFB OH, August 1984.
9. Maybeck, P. Stochastic Models, Estimation and Control, Volume 1. New York: Academic Press, 1979.
10. McDonnell Aircraft Company. Subcontractor Engineering Memorandum, SMTP-HSR-001, 10 Jan 1985.
11. "McDonnell Douglas to Develop F-15/STOL," Aviation Week and Space Technology, 122 (15): 21 (Oct 8, 1984).
12. Moseley, A. Design of Advanced Digital Flight Control Systems via Command Generator Tracker (CGT) Synthesis Methods. Volume 1. MS thesis, AFIT/GE/EE/82D-51. School of Engineering, Air Force Institute of Technology (AU), Wright-Patterson AFB OH, December 1982.

13. Porter, B. and A. Bradshaw. "Design of Linear Multivariable Discrete-Time Tracking Systems Incorporating High-Gain Error Actuated Controllers," International Journal of System Science, 12 (10): 1169-1220 (1981).
14. -----. "Singular Perturbation Methods in the Design of Tracking System Incorporating High-Gain Error Actuated Controllers," International Journal of System Science, 12 (10): 1169-1220 (1981).
15. Pugh, A. "Transmission and System Zeros," International Journal of Control, 26 (2): 315-324 (1977).
16. Sheehan, K. MS thesis, AFIT/GE/EE/85D-38. Multivariable Control Law Design for Enhanced Air Combat Maneuvering: F-15/STOL Derivative Fighter. School of Engineering, Air Force Institute of Technology (AU), Wright-Patterson AFB OH, December 1985.
17. Porter, B, A. Manganas, and T. Manganas. "Design of Fast Non-Interacting Digital Flight-Mode Control Systems for High-Performance Aircraft," AIAA Guidance, Navigation and Control Conference, August 19-21, 1985, Snowmass CO.

VITA

Bruce Acker is a native of Olympia, Washington. He graduated from the United States Air Force Academy, Colorado Springs, Colorado in 1981 with a Bachelor of Science in Engineering Science. He was commissioned in the Air Force upon graduation and assigned to the 475th Test Squadron, 325th Fighter Weapons Wing, Tactical Air Command at Tyndall Air Force Base, Florida. At Tyndall, his work involved the operational test and evaluation of air defense weapons systems, ranging from the modification and flight test of electronic warfare equipped F-106 and F-5 aircraft, to the preliminary ground testing of passive radar tracking capability with the F-16 APG-66 radar.

In 1984 he was assigned to the Air Force Institute of Technology, Wright-Patterson Air Force Base, Ohio where he is currently working toward an advanced degree in guidance and control.

Permanent address: 3125 32nd Court, S.E.
Olympia, Washington 98503

UNCLASSIFIED

SECURITY CLASSIFICATION OF THIS PAGE

REPORT DOCUMENTATION PAGE

1a. REPORT SECURITY CLASSIFICATION UNCLASSIFIED			1b. RESTRICTIVE MARKINGS	
2a. SECURITY CLASSIFICATION AUTHORITY			3. DISTRIBUTION/AVAILABILITY OF REPORT Approved for public release; distribution unlimited	
2b. DECLASSIFICATION/DOWNGRADING SCHEDULE				
4. PERFORMING ORGANIZATION REPORT NUMBER(S) AFIT/GE/ENG/85D-1			5. MONITORING ORGANIZATION REPORT NUMBER(S)	
6a. NAME OF PERFORMING ORGANIZATION School of Engineering		6b. OFFICE SYMBOL (If applicable) AFIT/ENG		7a. NAME OF MONITORING ORGANIZATION
6c. ADDRESS (City, State and ZIP Code) Air Force Institute of Technology Wright-Patterson AFB, OH 45433			7b. ADDRESS (City, State and ZIP Code)	
8a. NAME OF FUNDING/SPONSORING ORGANIZATION Flight Dynamics Lab		8b. OFFICE SYMBOL (If applicable) AFWAL/FIGL		9. PROCUREMENT INSTRUMENT IDENTIFICATION NUMBER
8c. ADDRESS (City, State and ZIP Code) Wright-Patterson AFB, OH 45433			10. SOURCE OF FUNDING NOS.	
11. TITLE (Include Security Classification) See Block 19			PROGRAM ELEMENT NO.	TASK NO.
12. PERSONAL AUTHOR(S) Bruce H. Acker, B.S., Captain, USAF			PROJECT NO.	WORK UNIT NO.
13a. TYPE OF REPORT MS Thesis		13b. TIME COVERED FROM _____ TO _____		14. DATE OF REPORT (Yr., Mo., Day) 1985 December
15. PAGE COUNT 294				
16. SUPPLEMENTARY NOTATION				
17. COSATI CODES			18. SUBJECT TERMS (Continue on reverse if necessary and identify by block number)	
FIELD	GROUP	SUB. GR.		
01	03		Multivariable Control, Output Feedback, Proportional-Integral Control, STOL F-15, Flight Control Systems	
19. ABSTRACT (Continue on reverse if necessary and identify by block number)				
<p>Title: MULTIVARIABLE OUTPUT CONTROL LAW DESIGN FOR THE STOL F-15 IN LANDING CONFIGURATION</p> <p>Thesis Chairman: John J. D'Azzo</p> <p style="text-align: right;">Approved for public release: IAW AFR 190-17. 16 JAN 86 E. E. WOLAVER Dean for Research and Professional Development Air Force Institute of Technology Wright-Patterson AFB OH 45433</p>				
20. DISTRIBUTION/AVAILABILITY OF ABSTRACT UNCLASSIFIED/UNLIMITED <input checked="" type="checkbox"/> SAME AS RPT. <input type="checkbox"/> DTIC USERS <input type="checkbox"/>			21. ABSTRACT SECURITY CLASSIFICATION UNCLASSIFIED	
22a. NAME OF RESPONSIBLE INDIVIDUAL Dr. John J. D'Azzo			22b. TELEPHONE NUMBER (Include Area Code) 513-255-2024	22c. OFFICE SYMBOL AFIT/ENG

UNCLASSIFIED

SECURITY CLASSIFICATION OF THIS PAGE

Multivariable, output feedback digital control laws are designed for the short take-off and landing F-15 aircraft in the landing configuration. The design is based on the methods developed by Professor Brian Porter of the University of Salford, England, and was accomplished using a computer-aided design and simulation program called MULTI.

The STOL F-15 landing configuration includes canards and reversible thrust in addition to the conventional F-15 control surfaces. The additional controls allow decoupling of the output variables in the longitudinal plane. Longitudinal aircraft dynamics are derived from data provided by McDonnell-Douglas, the prime contractor for the STOL F-15, and are presented in linearized state space form for the design procedure.

Control laws are developed to stabilize the aircraft to perform longitudinal landing maneuvers (flight path control and flare) at six flight conditions. The design encompasses actuator dynamics, computational delay, sensor dynamics, sensor noise, and plant nonlinearities. Proportional plus integral controller designs for each of the flight conditions demonstrate good time response characteristics. The designs of two of the flight conditions are sufficiently insensitive to plant variations to be used at all but one of the remaining flight conditions.

The technique of multivariable output feedback, through the use of the program MULTI, is shown to provide good robust designs for the STOL F-15. Additional areas of research on this aircraft are discussed as well as suggested enhancements to the MULTI program:

UNCLASSIFIED